UNIVERSITY OF LIVERPOOL

DEVELOPING A HUMAN CO-CULTURE MODEL OF THE RETINAL DIABETIC MICROVASCULATURE TO STUDY INCORPORATION OF ENDOTHELIAL COLONY FORMING CELLS

Thesis submitted in accordance with the requirements of the
University of Liverpool for the degree of Doctor of Philosophy

By

Jessica Jane Eyre

2019

ABSTRACT

Type II diabetes mellitus (T2DM) is a complex metabolic disorder resulting in chronic hyperglycaemia due to insulin resistance and/or impaired insulin production. A disorder called diabetic retinopathy (DR) occurs when hyperglycaemic damage to the retinal endothelial (REC) and retinal pericyte cells (RP) of the capillary beds leads to leaky vessels, oedema, areas of non-perfusion and ultimately vision loss. Current treatments involve laser therapy and anti-VEGF injections to target the proliferative stage of the disease (PDR), however, an early cellular intervention targeted at repairing the damaged EC layer of the capillary bed could prevent progression of DR to the sight threatening stage.

Modelling DR *in vitro* would provide a tool to further understand changes to the retinal EC and pericytes in diabetic conditions and assess potential cellular therapies. Endothelial colony forming cells (ECFCs) can be isolated from human umbilical cord (UCB) or adult peripheral blood (APB) and are a potential source of cells for this application. Currently, ECFCs are expanded on rat tail type I collagen (col I.), but in order to enable ECFC cell therapy in humans, culture conditions must be xeno-free or good manufacturing practice (GMP) compliant. Poly-ε-lysine (pεK) hydrogels are a promising option as an expansion surface, as they provide a highly controlled peptide surface with amine functionality to allow cell binding, and the mechanical properties of the hydrogel can be tailored to best suit the cell-type of interest.

hREC and hRP were cultured on either side of PET transwell inserts in healthy or diabetic conditions for up to 21 days and hREC were analysed for cell-cell junction formation, angiogenic and oxidative stress response. ECFCs were isolated from the mononuclear fraction of adult peripheral (APB) and umbilical cord blood (UCB) and expanded *in vitro* on either col I. coated tissue culture (TC) plastic or pεK hydrogels. ECFCs were added into the hREC layer of the co-culture model to assess their ability to integrate with mature hREC in healthy and diabetic conditions. pεK microparticles were assessed as a method for controlled delivery of ECFCs to the hREC layer of the co-culture model.

hREC and hRP successfully grew as co-cultures for up to 21 days in healthy and diabetic conditions. The optimised diabetic conditions resulted in significant differences in the secretome of 4 major angiogenic response proteins. The secretion profiles of mono- compared to co-culture hREC and hRP were different. Both APB and UCB-ECFCs incorporated into the co-culture models, in healthy and diabetic conditions. ECFCs grown on pεK hydrogels retained their endothelial progenitor morphology when cultured long term in both healthy and diabetic conditions, whereas some ECFCs grown on rat tail col I. coated TC plastic differentiated or became senescent. Additionally, ECFCs grown on pεK hydrogels remained a homogenous population whereas ECFCs grown on rat tail col I. coated TC plastic were heterogeneous in their expression of EC-phenotypic markers such as CD31. Delivery of ECFCs to vessels using pεk microparticles is not a viable option as ECFCs did not detach from the microparticles.

An *in vitro* model of the retinal capillary structure using human primary, retina-specific hREC and hRP provides tissue and species-specific data on cellular changes in diabetic conditions, highlighting the advantage of co-cultures over monoculture techniques. Both APB and UCB-ECFCs integrated into the hREC layer of the co-culture model, although *in vitro* expansion of APB-ECFCs was found to be limited. pεK hydrogels are a promising new xeno-free surface on which to expand ECFCs *in vitro* whilst retaining their progenitor phenotype.

ACKNOWLEDGEMENTS

Firstly I'd like to say a huge thank you to my supervisors Hannah and Rachel for supporting me through the tough parts of my PhD, and being there to celebrate when things were a success. You've allowed me to shape my own experiments and develop as a scientist, so thank you for giving me that freedom and keeping me on track.

Thank you to Kevin, who always has his door open and often brought things into perspective by making me look at 'the bigger picture'. You have supported me through my MRes and provided advice and support during my PhD.

I'd like to thank everyone in EVS and IACD who has helped me along the way. A special thanks to Lee, Karen, Danielle and Alys, who have not only helped me in the lab, but also been there as friends and made the tough times easier with general encouragement, gossip and the occasional beverage. Thanks to the girls in the write up office who have kept me on track and kept me grounded for the last eight months.

Thank you to my Mum and Dad for being so supportive and always pushing me to achieve more. I would not have been where I am now without your love and guidance. To Shane and Boba for supporting me through my education and always being there for me when after a difficult day in the lab. And finally, to LYS and all their members for giving me much needed time outside of work to keep me happy and healthy.

CONTENTS

LIST OF FIGURES

LIST OF TABLES

ABBREVIATIONS

αSMA- α-smooth muscle actin

AGEs- Advanced glycation end products

AMD- Age-related macular degeneration

Ang-1- Angiopoietin-1

Ang-2- Angiopoietin-1

APB- Adult peripheral blood

APB-ECFC- Adult peripheral blood endothelial colony forming cell

APC- Allophycocyanin

ATP- Adenosine triphosphate

BBB- Blood-brain-barrier

BM- Basement membrane

BRB- Blood-retina-barrier

BS- Blind spot

CD90/Thy-1- Thymocyte differentiation antigen-1

CFU-Hill- Colony forming unit-Hill

col I.- Collagen I

CRP- C-reactive protein

CTGF- Connective tissue growth factor

CTG- CellTracker Green

CTR- CellTracker Red

CVD- Cardiovascular disease

DAPI- 4',6-diamidino-2-phenylindole

ddH_2O- Double-distilled water

DIP- Diabetes in pregnancy

DME- Diabetic macular edema

DMSO- Dimethyl sulfoxide

dPBS- Dulbecco's phosphate buffered saline

DR- Diabetic retinopathy

E-selectin- Endothelial selectin

ECs- Endothelial cells

ECM- Extracellular matrix

ECFC- Endothelial colony forming cells

EGM-2- Endothelial Growth Medium-2

ENA78- Epithelial neutrophil activator

EPC- Endothelial progenitor cell

ER- Endoplasmic reticulum

FACS- Fluorescence-activated cell sorting

FBS- Fetal bovine serum

FITC- Fluorescein isothiocyanate

GD- Gestational diabetes mellitus

GD-UCB-ECFC- Gestational diabetic umbilical cord blood endothelial colony forming cell

GFP- Green fluorescent protein

GJs- Gap junctions

GLUT-1- Glucose transporter-1

GMP- Good Manufacturing Practice

H- hours

HCE-T cells- human corneal epithelial cell line

hREC- Human retinal microvascular endothelial cells

hRP- Human retinal pericytes

HUVECs- Human umbilical vein endothelial cells

HVJ-liposomes- hemagglutinating virus of Japan-liposomes

ICAM-1- Intercellular adhesion molecule-1

IF- Immunofluorescence

IFN-γ- Interferon-γ

IGF-I- Insulin-like growth factor-I

IL-1β- Interleukin-1β

IL-6- Interleukin-6

Il-8- Interleukin-8

MACs- Myeloid angiogenic cells

MCP-1- Monocyte chemoattractant protein-1

MMPs- Matrix metalloproteinases

NF-κB- Nuclear factor kappa-B

NBF- Neutral buffered formalin

NGS- Normal goat serum

NG2- Neuron-glial antigen-2

NPDR- Non-proliferative diabetic retinopathy

P- Passage

PEDF- Pigmented epithelium-derived growth factor

PEGDA- poly(ethylene glycol) diacrylate

PDGFR-β- Platelet derived growth factor receptor-β

PDR- Proliferative diabetic retinopathy

PE- Phycoerythrin

PET- Polyethylene terephthalate

PlGF- Placental growth factor

PRP- Panretinal laser photocoagulation

RAGE- Receptor for advanced glycation end products

RBC- Red blood cell

ROS- Reactive oxygen species

RPE- Retinal pigmented epithelium

RT- Room temperature

SD- Standard deviation

SIRT-1- silent information regulator protein

SOD- Superoxide dismutase

T2DM- Type II diabetes mellitus

TC- Tissue culture

TEER- Trans-endothelial electrical resistance

TGF-β- Transforming growth factor-β

TJs- Tight junctions

TNF-α-Tumor necrosis factor-α

UCB- Umbilical cord blood

UCB-ECFC- Umbilical cord blood endothelial colony forming cell

VE-Cad- Vascular endothelial cadherin

VCAM-1- Vascular cell adhesion molecule-1

VEGF- Vascular endothelial growth factor

VEGFR- Vascular endothelial growth factor receptor

WHO- World Health Organisation

w/p- Well plate

ZO-1- Zonula occuldens-1

1. CHAPTER 1

1.1 INTRODUCTION

1.1.1 OVERVIEW

The work contained in this thesis focuses specifically on the microvessels at the back of the eye that supply blood to the retina. This retinal capillary bed is severely compromised in people with diabetes, leading to a condition called diabetic retinopathy (DR). Vision loss associated with DR is a huge burden to the increasing number of people suffering with diabetes worldwide. Earlier diagnosis could provide the opportunity for either lifestyle change, pharmaceutical intervention, or in the future, cellular based therapies, to either prevent or slow progression of the numerous complications caused by diabetes. Endothelial colony forming cells (ECFCs) are one type of endothelial progenitor cell that can be easily isolated from adult peripheral blood (ABP) or umbilical cord blood (UBC), and have the potential to provide autologous or allogeneic cell therapy for blood vessel repair during chronic diseases such as diabetes. Modelling DR in a co-culture model system will help improve understanding of the cellular changes that occur during the complicated progression of disease, and enable testing of the ability of ECFCs to repair a damaged endothelial layer.

1.2 THE RETINA

1.2.1 STRUCTURE OF THE RETINA

The interior compartment of the eye is divided into the anterior and posterior segments. The retina is the neural portion of the eye, forming part of the central nervous system, lining the surface of the posterior segment (Figure 1.1). In vertebrates, the retina develops as an outgrowth of the brain, turned in on itself to form a cup, which accounts for the inverted structure of the photoreceptors positioned furthest from the light, in the deepest layer of neurons[1]. Along with the retina, the posterior segment of the eye is composed of the optic never head, the choroid and the vitreous humour. Light enters the eye through the transparent cornea and lens, both of which are involved in refracting the light, which then passes through the vitreous humour and is focused on to the retina.

The retina is responsible for converting light into neural signals, which are sent along the optic nerve to the brain for processing. The retina is crudely divided into two parts: the neural retina and the retinal pigmented epithelium (RPE). The retina can be structurally divided into ten layers, composed of multiple different types of neural cells and an outer-most epithelial

layer, illustrated in Figure 1.2. Light passes through the first eight layers to reach the photoreceptor layer, where light rays are processed. The RPE plays a critical role in the physiology of the underlying photoreceptors by: transport of nutrients from the choroid circulation, formation of the outer blood–retinal barrier, absorption of scattered light, phagocytosis of shed membranous photoreceptor discs and release of trophic factors promoting differentiation and survival of photoreceptor cells[2].

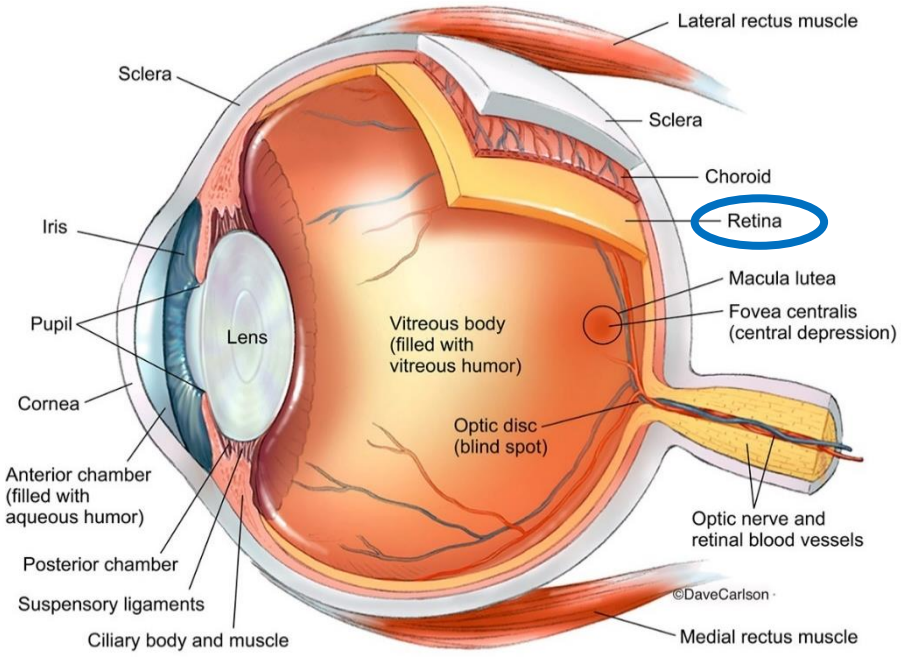

Figure 1.1. Basic anatomy of the different regions of the human eye

Cartoon depicting the basic anatomy of the human eye. The retina (circled blue), is the yellow pseudo-coloured layer lining the posterior chamber, anterior to the choroid [3].

1. **Inner limiting membrane**
2. **Nerve fiber layer**
3. **Ganglion cell layer**
4. **Inner plexiform layer**
5. **Inner nuclear layer**
6. **Outer plexiform layer**
7. **Outer nuclear layer**
8. **External/outer limiting membrane**
9. **Inner & outer segment photoreceptor layer (rods & cones)**
10. **Retinal pigmented epithelium**

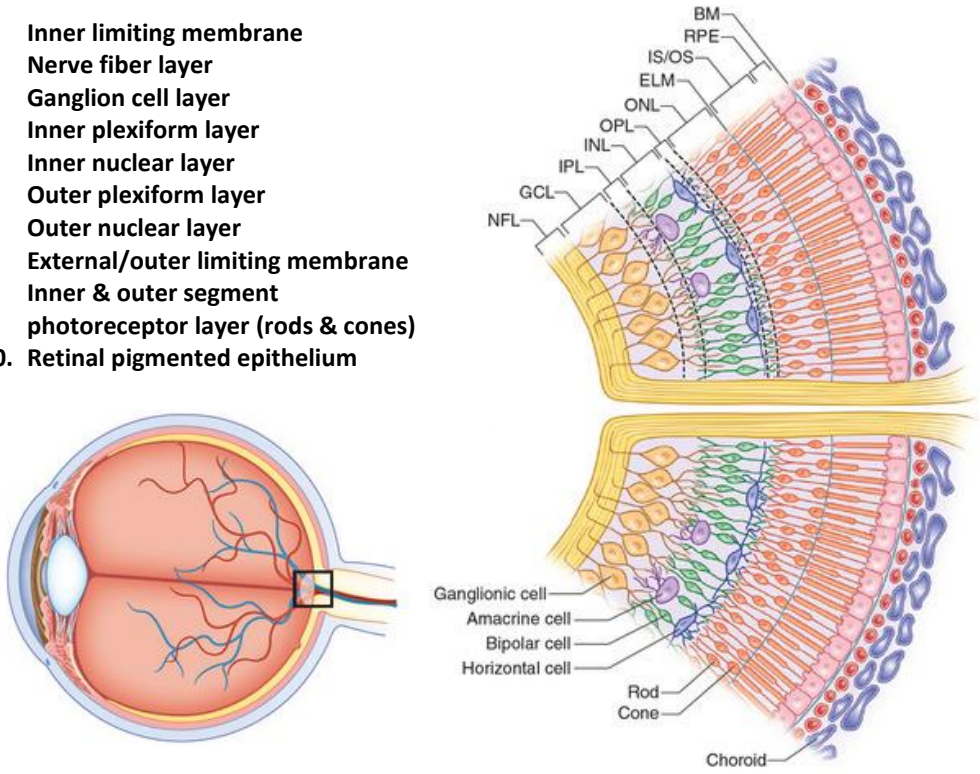

Figure 1.2. The ten layers of the human retina

Proceeding from the vitreous (inner) to the choroid (outer): internal limiting membrane (ILM), nerve fiber layer (NFL), ganglion cell layer (GCL), inner plexiform layer (IPL), inner nuclear layer (INL), outer plexiform layer (OPL), outer nuclear layer (ONL), external limiting membrane (ELM), rod and cone inner and outer segments (IS/OS), and retinal pigment epithelium (RPE). To supply the inner retinal layers with blood, microvessels run on the inner surface of the nerve fibre layer [4].

1.2.2 PHOTORECEPTORS

Although the structure of the eye varies distinctly from species to species, all have in common the molecule rhodopsin, which is responsible for initiating the process of converting light into electrical signals[1]. In humans, ~5 million cones (for sensing fine resolution, spatial resolution, colour and bright light intensity) and ~100 million rods (for sensing, contrast, brightness, motion and low light levels) comprise the photoreceptor layer, which responds to light stimulation[1] . Rods and cones are not evenly distributed across the retina, where the highest density of cones are found in the fovea centralis (150,000/mm^2) and rods are concentrated at the periphery (30,000/mm^2)[5] (Figure 1.3). In humans, the rod and cone cells have

photopigment-bearing regions called outer segments, and these are composed of a large number of disks, with ~150,000 rhodopsin molecules/disc[6]. These membranous outer segment discs undergo daily renewal at the proximal region, and shedding at the distal outer segment region, at a rate of roughly 2µm/day. This enables the outer segment to maintain a constant length while replacing components that have accumulated toxic photo-oxidative compounds[7]. Light photons are absorbed on the highly folded photoreceptor cell membranes, by the photopigment rhodopsin, and photon absorption contributes to the photoreceptor output signal to the optic nerve. Dysfunction or loss of synchronisation of this highly regulated diurnal photoreceptor shedding and renewal process can lead to photoreceptor and RPE degradation and ultimately vision loss. The photoreceptors are the most highly metabolically active cells in the human body[8], and to fulfil this high oxygen demand, strict control of blood flow to the outer retina is imperative. Therefore, the retina is particularly vulnerable to disrupted blood flow and ischemia, which are microvascular complications that can arise in chronic diseases such as diabetes.

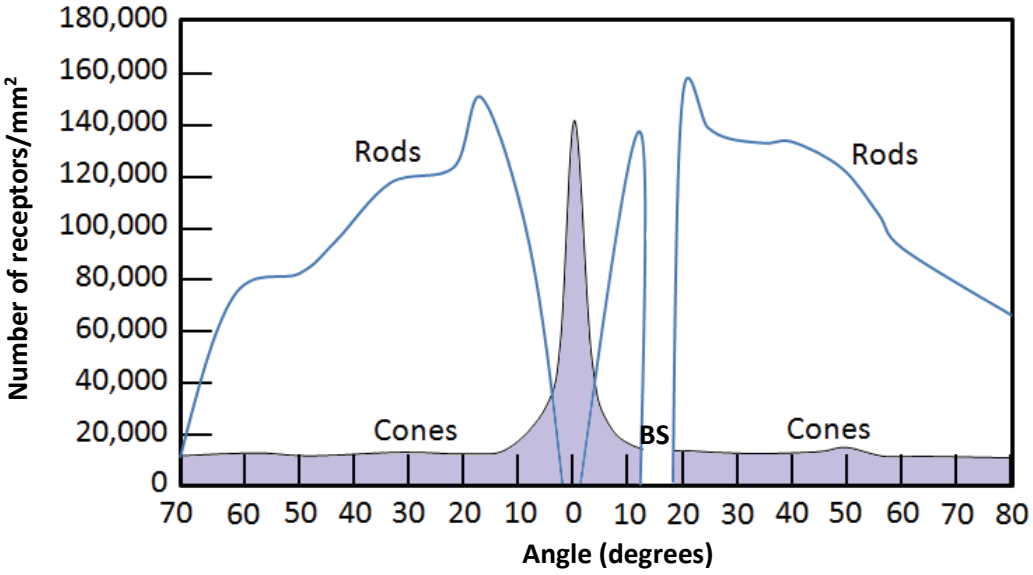

Figure 1.3. Typical distribution of cones and rods in the human retina

0° refers to centre point (fovea) of the central area (macula) of the posterior wall of eye. Cones are concentrated in the fovea centralis and only a small number are found in the periphery (purple). The fovea centralis is rod cell-free and rods are distributed across the periphery of the retina, with the highest amount around the edge of the fovea, radiating out (blue). There are no photoreceptors at the blind spot (BS), where the optic nerve pierces the retina[9].

1.2.3 BLOOD SUPPLY OF THE RETINA

The arterial blood supply to the eye is provided by branches of the ophthalmic artery, including the central retinal artery, the short and long posterior ciliary arteries and the anterior ciliary arteries[10]. Venous outflow is mainly via the central retinal vein and vortex veins, which merge with the superior and inferior ophthalmic veins. In humans, the retina receives a dual blood supply, with the inner 2/3 supplied by branches from the central retinal vessels and the outer 1/3 receiving blood from the choroidal circulation. An outline of the blood vessels supplying the retina is shown in Figure 1.4 [11]. The central retinal circulation (supplying the inner layers) has a low flow rate of 25mm/s and high oxygen exchange whilst the choroidal circulation (supplying the outer layers) has a high flow rate of 150mm/s and low oxygen exchange[5]. The larger vessels supplying the retina lay close to the inner limiting membrane, with vessel walls running in a close spatial relationship with glial cells, mainly astrocytes, and form a plexus of capillaries ~5µm in diameter[12]. This close vascular:glial interaction is illustrated in Figure 1.5.

Two of the main peculiarities of the retinal vasculature include: 1) no autonomic innervation, and 2) a sparse architecture of the inner retinal blood supply. Lack of autonomic nerve supply means the vascular tone is controlled locally. The retinal vasculature must meet the challenging demand of supplying the highly metabolically active tissue, whilst remaining anatomically sparse so as not to interfere with the path of light reaching the photoreceptors[13]. These structural and functional adaptations of the retinal microvasculature advocates the importance of investigating organ or tissue specific vascular endothelial cells (ECs) *in vitro*. In fact, it has been well documented that the ECs possess unique ultrastructural characteristics, and this is microvascular or macrovascular dependant as well as organ-specific, and these characteristics are intrinsic to the cells themselves and not determined by differential culture conditions[14]. Therefore, when studying the microvasculature of the human retina, as far as possible cells sourced specifically from the human retina should be studied *in vitro*, because these cells are structurally and functionally unique from cells sourced from other organs, and other species.

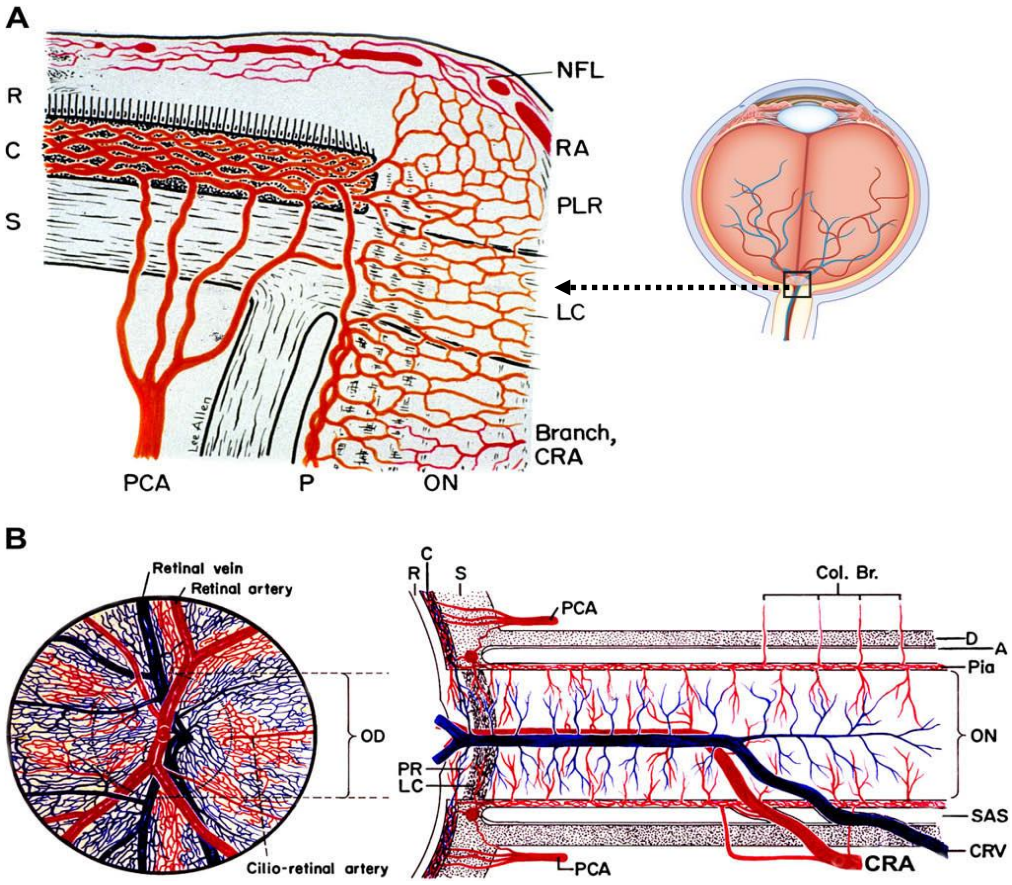

Figure 1.4. Schematic representation of the inner retinal blood supply

Blood supply at: (**A**) the optic nerve head and (**B**) the optic nerve. Red represents arteries, blue represents veins. Abbreviations: A= arachnoid; Ant. Sup. Hyp. Art.= anterior superior hypophyseal artery; C= choroid; CAR and CRA= central retinal artery; Col. Br.= collateral branches; CRV= central retinal vein; CZ= circle of Zinn and Haller; D= dura; ICA= internal carotid artery; LC= lamina cribrosa; LPCA= lateral posterior ciliary artery; Med. Mus.= medial muscular artery; MPCA= medial posterior ciliary artery; NFL= surface nerve fibre layer of the disc; OA= ophthalmic artery; OD= optic disc; ON= optic nerve; P= pia; PCA= posterior ciliary artery; PR and PLR= prelaminar region; R=retina; RA= retinal arteriole; Rec. Br. CZ= recurrent pial branches from peripapillary choroid/CZ; S= sclera; SAS= subarachnoid space[11].

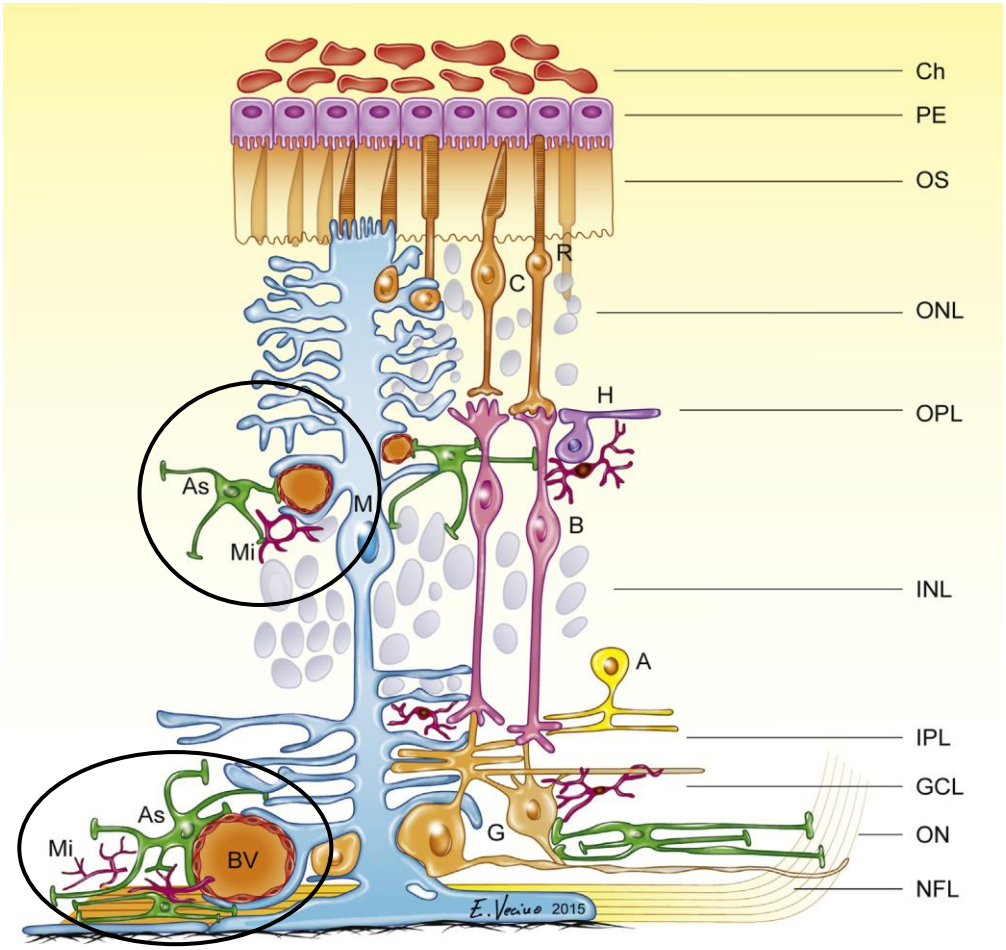

Figure 1.5. Cellular components of the retina: glia and neurons

The different cell-types comprising a standard large mammalian retina. Interactions between the glia and blood vessels (BV) are circled black. Amacrine cells (A), astrocytes in green (AS), bipolar cells (B), cones (C), ganglion cells (G), horizontal cells (H), Müller cells (blue) (M), microglia (red) (Mi), rods (R), cones (C). The different layers of the retina are labelled: optic nerve (ON), nerve fibre layer (NFL), ganglion cell layer (GCL), inner plexiform layer (IPL), inner nuclear layer (INL), outer plexiform layer (OPL), outer nuclear layer (ONL), outer segment layer (OS), pigment epithelium (RPE), choroid (Ch)[15].

1.3 MICROVASCULAR ENDOTHELIAL CELLS

1.3.1 STRUCTURE OF BLOOD VESSELS

In the healthy vasculature, cells comprising the blood vessels are able to respond to changes in: blood pressure, blood sugar levels, flow rate, and temperature fluctuations, in order to maintain homeostasis[16,17]. In the event of vascular wounding, vessels are capable of repair via adult angiogenesis. Blood vessel architecture varies from macro- to microvascular, where larger vessels are surrounded by tunica layers, whilst capillaries lack these extra layers (Figure 1.6). The structure of a blood vessel is directly related to differential function. The larger arteries are under high pressure from the pumping mechanism of the heart and, therefore, their elastic and media layers are thickened to counteract the pulsatile action. However, the blood pressure in veins is much lower, hence valves are located throughout, to prevent backflow of blood. The primary function of the capillary bed of any tissue is nutrient exchange: oxygen and nutrient delivery along with carbon dioxide and toxic metabolite removal, and the single layer EC structure enables this exchange to take place through either a fenestrated, sinusoid or continuous endothelial barrier (Figure 1.7). In the retina, the capillaries maintain a continuous barrier and the diameter of the capillary vessels varies from 3.5-6µm[18].

1.3.2 RETINAL NEUROVASCULAR UNIT

The capillaries supplying the retinal tissue are comprised of two cell-types in close contact with one another; ECs which form the inner lining of the vessel tube surrounded by perivascular pericytes. ECs and pericytes have intimate associations with glial endfeet, astrocytes, Müller cells and neural processes and this has led to the concept of the retinal neurovascular unit[19] (Figure 1.5 and Figure1.8). ECs, pericytes and glial cells send auto- and paracrine factors to maintain vascular and tissue homeostasis, or for adaptation and survival responses during cellular insult or injury. ECs form tight junctions (TJs) with one another forming a continuous capillary bed to enable strictly controlled passages of substances from the blood to the surrounding cells in the retinal tissue. EC and pericytes share a basement membrane (BM) and the pericytes are entirely engulfed within the BM, therefore, dysfunction of either cell-type during injury or disease can result in the breakdown of the highly regulated nutrient exchange mechanism at the vascular bed, causing damage to the underlying tissue.

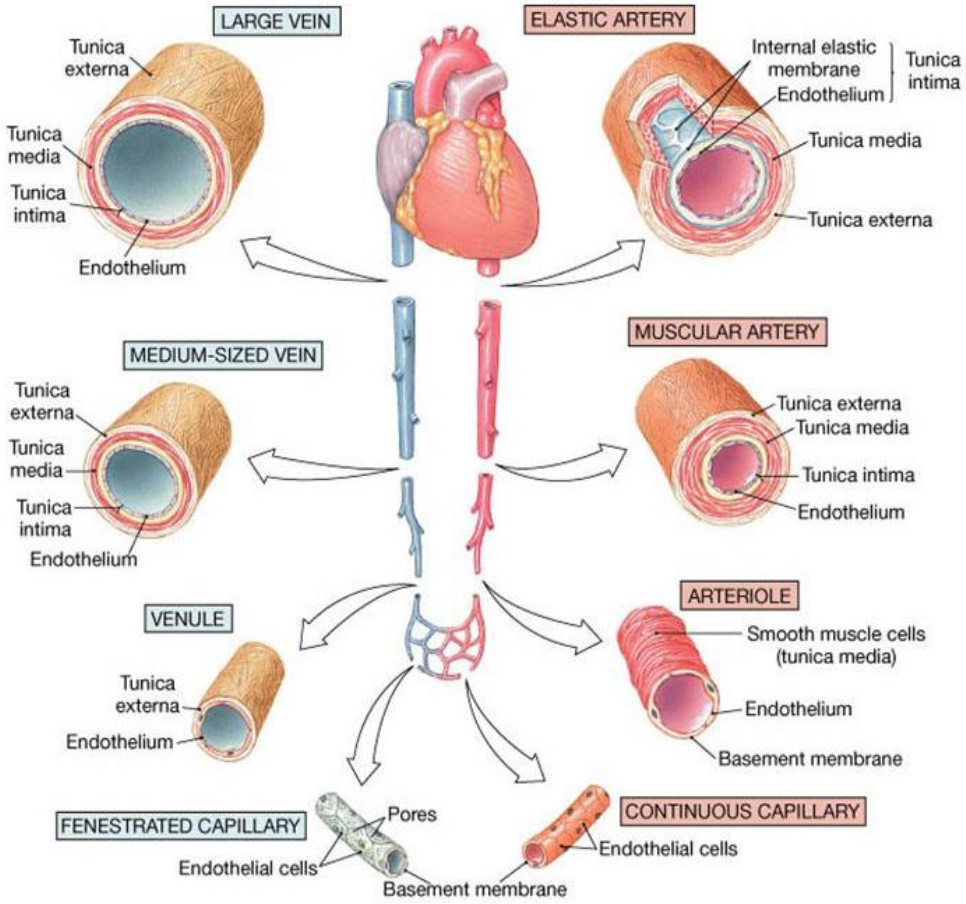

Figure 1.6. Composition of large to small diameter arteries and veins

Their composition directly relates to their function. Thickened tunica layers and an elastic membrane in arteries enable elastic recoil during high pressure pulsatile forces from the heart. Veins have enlarged lumen and valves throughout, to direct low pressure blood back to the heart. Capillaries are one EC layer thick, to enable exchange of oxygen, nutrients and metabolic waste[20].

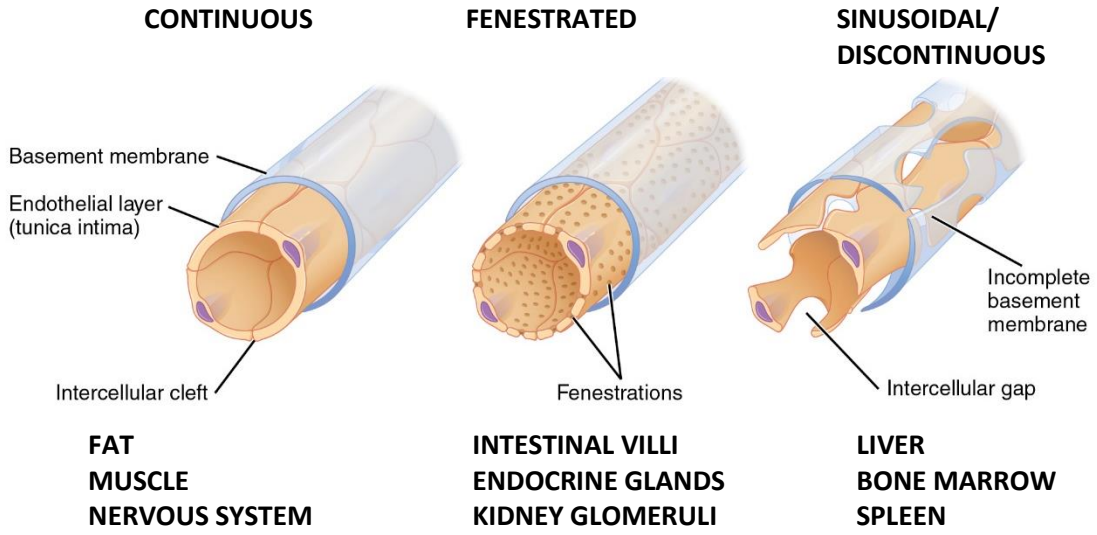

Figure 1.7. The three main types of capillary bed: continuous, fenestrated & sinusoidal

The main locations where each capillary-type is found are listed. The inner retina is supplied by a continuous capillary bed, which forms the inner blood retinal barrier[21].

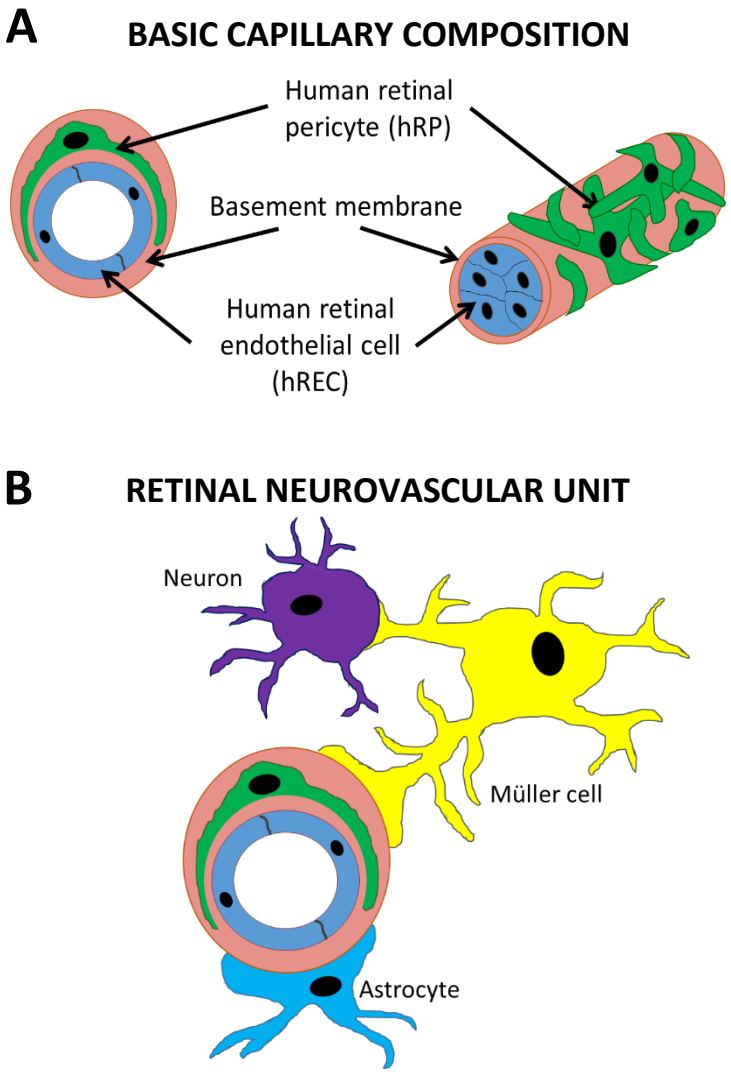

Figure 1.8. Diagram of the simplified structure of the retinal capillary

(**A**) ECs and pericytes with a shared BM, and (**B**) the retinal neurovascular unit, demonstrating the close interaction between vascular cells, glial cells and neural cells of the retina. Each cell type interacts with its neighbour, therefore, dysfunction of one cell has a wide reaching effect if not mitigated during normal homeostasis.

1.3.3 FUNCTION OF THE MICROVASCULAR EC

ECs were first successfully isolated from human umbilical veins (HUVECs) and cultured in the lab in 1973 by Jaffe et al., enabling the study of EC function *in vitro*[22]. The ECs of the blood vessel walls form a semi-permeable barrier which allows controlled passage of oxygen and nutrients from the blood to the surrounding tissues[23]. At the capillary level, the endothelium is just one cell thick. The endothelium is not simply an inert cell layer, as it plays a critical role in controlling homeostatic processes such as: vascular tone, blood fluidity, exchange of nutrients and metabolic waste products, regulating capillary permeability, immune responses and angiogenesis. The endothelium has emerged as the major regulator of vascular homeostasis, as a signal transducer enabling circulating factors to influence the behaviour of the vascular cell wall. ECs produce and release vasoactive mediators such as bradykinin, thrombin and nitric oxide, thereby mediating vessel diameter, in order to balance supply of oxygen according to tissue metabolic demand[24]. Active and passive transport mechanisms involved in EC homeostasis are outlined in (Figure 1.9) [25].

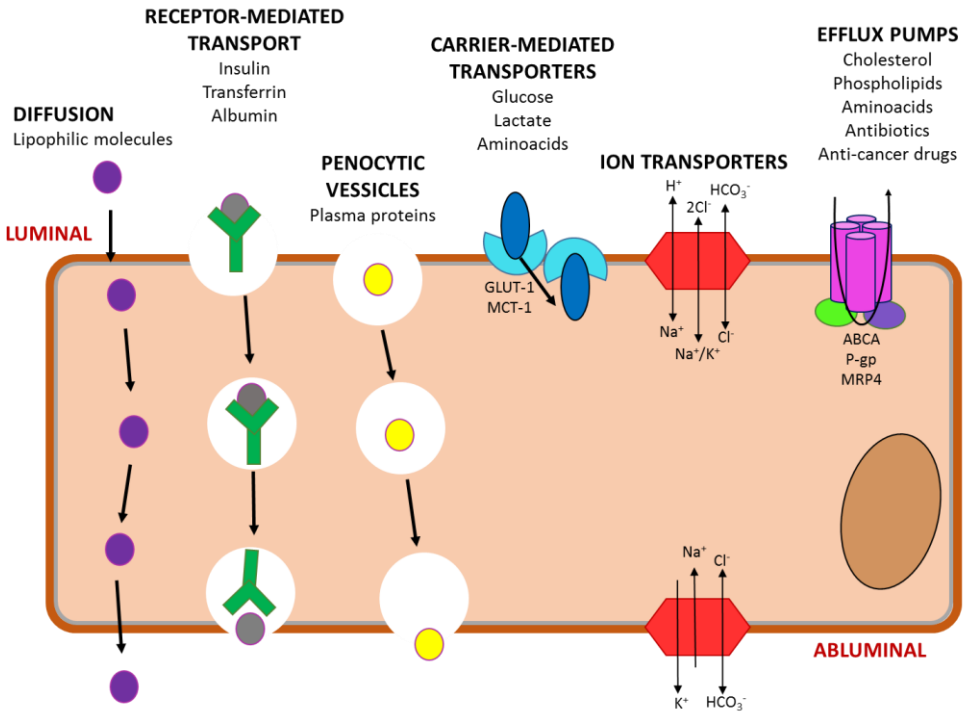

Figure 1.9. Transcellular transport through ECs

Some small molecules can cross by diffusion due to their lipophilic properties. Energy-dependent or receptor-mediated mechanisms include: pinocytosis, carrier-mediated transporters, ion transporters and efflux pumps. Retinal ECs express a low number of these transporter mechanisms[25].

1.3.4 PLATELET ENDOTHELIAL CELL ADHESION MOLECULE-1 (CD31)

Platelet endothelial cell adhesion molecule-1 (PECAM-1/CD31) is crucial for enabling leukocyte transmigration through intercellular junctions on vascular ECs, to reach sites of injury during inflammation or infection[26]. CD31 is expressed constitutively on vascular EC cell-cell junctions and is also present on platelets and leukocytes. As well as its key role in immunomodulation, CD31 also contributes to the barrier properties of the EC layer via homodimeric PECAM-1-PECAM-1 interactions at neighbouring EC contacts[27]. CD31 functions by promoting homo- and heterotypic adhesion by binding to glycosaminoglycans or αvβ3 integrins[28,29]. Subjecting HUVECs to interferon-γ, a pro-inflammatory cytokine, for 24H (hours) resulted in EC transition to a fibroblast-like phenotype, where CD31 was no longer present at cell-cell junctions, and cell growth became disorganised[30]. Therefore, CD31 is a useful cell adhesion molecule to confirm endothelial phenotype *in vitro* and in cell-biomaterial interactions as it remains strongly expressed by ECs grown on various surfaces[31].

1.3.5 THE ANGIOPOIETIN-TIE-2 PATHWAY

The Angiopoietin-Tie-2 pathway is essential for vascular development and plays a role in both healthy and pathological angiogenesis in adulthood. The Tie-2 receptor is a tyrosine kinase receptor expressed selectively by ECs, and both Angiopoietin-1 (Ang-1) and Angiopoietin-2 (Ang-2) proteins bind to the Tie-2 receptor, although Ang-1 binds with stronger affinity. Ang-1 is stored at high levels in platelet granules whilst Ang-2 is stored in intracellular granules (Weibel-Palade bodies)[32,33]. Ang-1 is expressed by perivascular cells (such as pericytes) and Tie-2/Ang-1 binding is affiliated with vessel maturation, stabilisation and homeostasis, whereas Tie-2/Ang-2 binding is upregulated in inflammatory and angiogenic responses[34]. Adding the inflammatory cytokine TNFα or pro-angiogenic vascular endothelial growth factor (VEGF) to cultured ECs or subjecting cultures to hypoxia resulted in upregulation of Ang-2[35,36]. In addition to this, human and mouse pericytes have recently been shown to express functional Tie-2 receptors, challenging current concepts that Tie-2 is EC-specific, which suggests a bidirectional, reciprocal EC-pericyte Tie-2 signalling pathway (Figure 1.10)[37]. This study highlights the role of both ECs and pericytes in adult angiogenesis, therefore, when studying angiogenesis *in vitro*, co-cultures of the two cell types in a contact model would provide more relevant data than each cell-type grown in isolation.

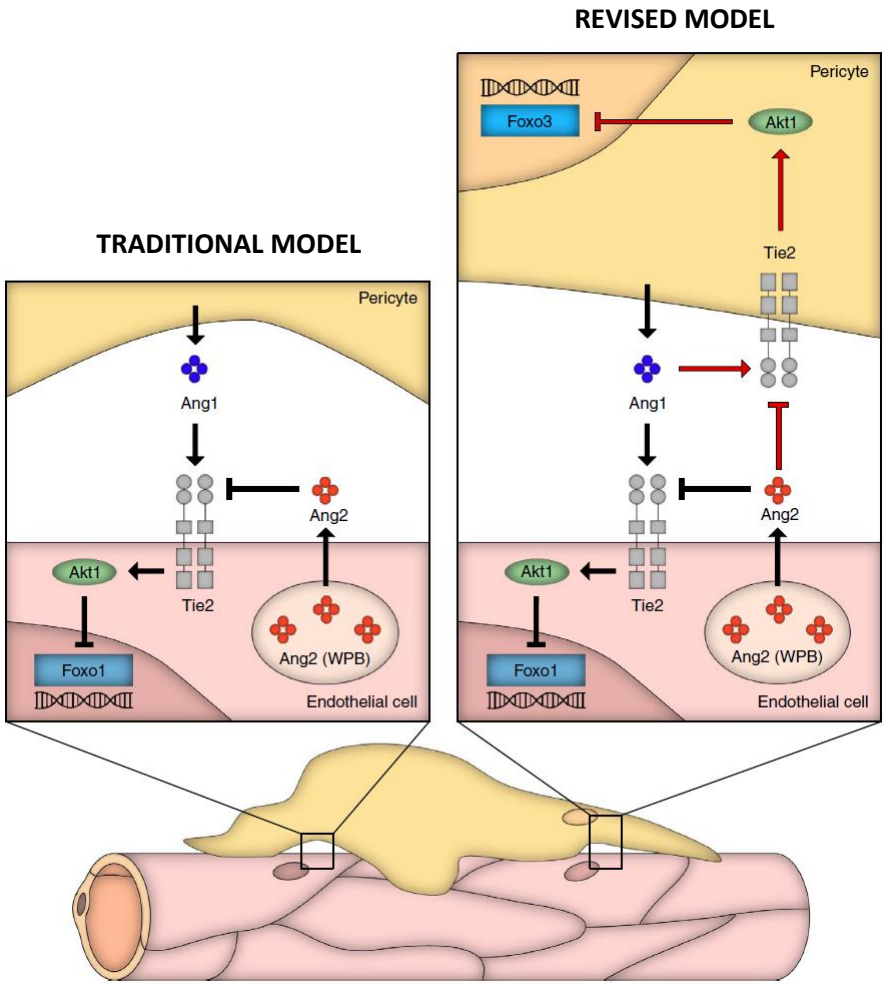

Figure 1.10. Advances in understanding Ang/Tie-2 signalling between ECs and pericytes in the retina

Traditional model of vascular Ang/Tie-2 signalling, outlining the established endothelial-centric model of Ang/Tie-2 signalling (left). The revised bi-directional, reciprocal EC-pericyte model of vascular Tie-2 signalling (right). Red routes represent newly identified pathways. Traditionally, Tie-2 was thought to be expressed only by ECs. Ang-1 is secreted by pericytes and other cells. Ang-2 is almost exclusively secreted by ECs and acts as a dynamic autocrine modulator of Ang-1/Tie-2 signalling. New data demonstrates that Tie-2 receptors are also expressed on pericytes. Therefore, Ang-1 produced by pericytes and other cells can bind to pericyte Tie-2 and drive vessel maturation. Ang-2 produced by ECs acts in a paracrine manner on pericytes, contributing to vascular destabilisation during wound healing, and healthy or pathological angiogenesis[37].

1.3.6 INJURY AND WOUND HEALING

In the event of vascular wounding in the adult, vessels are capable of repair via angiogenesis. The initiation of angiogenesis starts with disruption or loosening of the continuity of the EC cell-cell contacts, enabling ECs to proliferate and migrate to 'fill the gap'. This involves cell-cell and cell-matrix modifications. ECs and their perivascular cells can remodel their surrounding extracellular matrix (ECM) via secretion of proteins such as matrix metalloproteinases (MMPs), which are involved in the enzymatic degradation of most ECM proteins. For successful angiogenesis in the adult, it is crucial that ECs downregulate secretion of MMP-2 and MMP-9 during the maturation phase[38]. During migration and integration at the wound site, vascular endothelial cadherin (VE-Cad), a vascular endothelium-specific adhesion molecule, is upregulated at the cell-cell borders, causing a highly controlled decrease in EC secretion of MMPs allowing the EC barrier to be re-established[39]. VE-Cad is directly involved in control of vascular permeability and leukocyte extravasation and regulates numerous cell functions such as proliferation and apoptosis, and controls vascular endothelial growth factor receptor (VEGF-R) activity[40].

1.3.7 STUDYING ECs *IN VITRO*

Vascular ECs can be isolated from retinal blood vessels, via type II collagenase-dispase digestion and tissue homogenisation and filtration. This is followed by endothelial-specific tissue culture conditions to favour growth of ECs over any contaminating perivascular cells[23]. However, during the characterisation of ECs isolated from different human cadaveric donors, Bhardwaj et al. reported donor variation in global gene expression and adhesion molecule expression, and discussed the importance of investigating multiple EC donors wherever possible to limit the confounding effect of donor-donor variability in studies. EC phenotype can be tested *in vitro* in healthy and pathological conditions, to analyse changes in: proliferative potential, barrier properties and wound healing capabilities, in order to improve understanding of EC function in vascular diseases such as atherosclerosis, cardiovascular disease (CVD) and diabetes.

ECs show remarkable phenotype heterogeneity in different organs and regions of the body, and further phenotype changes can be induced by genetic and environmental factors in both health and disease[13]. By harvesting 'generic' ECs from embryonic stem cells and transplanting grafts of those ECs into regenerating tissues, Nolan et al. reported ECs acquiring organotypic features, providing evidence that ECs within different tissues possess distinct structural, phenotypic and functional characteristics[41]. Microvascular ECs isolated from the retinal

vessels showed upregulation of insulin-like growth factor-1 compared to microvascular ECs isolated from choroidal vessels, demonstrating differences between the ECs comprising the inner vs. outer blood-retinal-barrier[42]. In the same study, unsurprisingly HUVECs showed enrichment for genes involved in embryological development, and therefore are not a suitable substitute for studying ocular disease. In the adult, ECs display enormous phenotypic plasticity, due to their exposure to different environments including varied oxygen levels, mechanical stresses, growth factors and cytokines, and the active process of maintaining tissue-specific EC phenotype is highly regulated[43]. These data highlight the importance of using organ/tissue specific ECs for experimental purposes, but also that ECs showed plasticity and, therefore, their phenotype can be influenced by controlling culture conditions to best mimic the *in vivo*-like environment.

1.4 RETINAL PERICYTES

1.4.1 FUNCTION AND TISSUE-SPECIFICITY

Pericytes were first described over 100 years ago by Charles Rouget, as perivascular cells that wrap around blood capillaries. Pericytes function by wrapping long finger-like projections around the EC layer, with direct contact via gap junctions (GJs) that enable exchange of ions and small molecules. They also display peg-and-socket contacts that penetrate the shared BM and are secured with adhesion plaques, which connect EC:pericyte cytoplasm, enabling transmission of contractile forces[44] (Figure 1.11). Unlike smooth muscle cells, pericytes are embedded and completely surrounded by the EC BM. Pericytes aid in both structural and cell signalling support to the underlying EC, and are involved in regulating vascular permeability as well as preventing neovascularisation, helping to maintain normal capillary function[45].

Pericyte coverage is heterogeneous throughout the vasculature, ranging from 1:100 in skeletal muscle to 1:1 in the brain and retina[46]. Similar to ECs, pericytes from the retina differ from pericytes in other locations in the body[47]. The wrapping pattern of pericytes is also heterogeneous, and this likely represents functional differentiation according to site-specific necessities as opposed to a heterologous subset of pericytes *in vivo*[48]. Pericytes from different species also demonstrated different responses to *in vitro* stress conditions such as hyperglycaemia and low oxygen, compared to human pericytes[49]. An example of this is bovine retinal pericyte sensitivity to apoptosis in sustained hyperglycaemic conditions compared to human pericytes[47]. These studies promote the importance of using human, tissue-specific pericytes to collect more clinically relevant data.

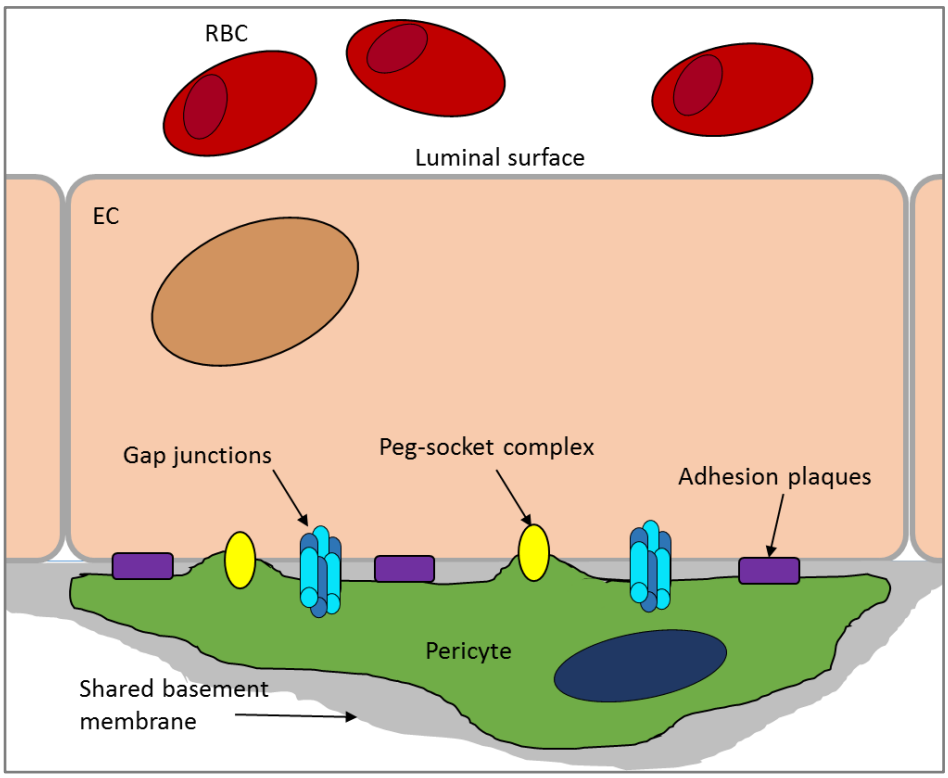

Figure 1.11. EC–pericyte interactions in the retinal capillary

Pericytes wrap around ECs and share the BM. A direct pericyte–EC contact is established via junctional complexes located to peg– socket contacts at sites were the BM is absent. Adhesion plaques connect EC:pericyte cytoplasm, enabling transmission of contractile forces, and GJs enable passage of ions and small molecules[46].

1.4.2 STUDYING PERICYTES *IN VITRO*

Pericytes are relatively straightforward to isolate for use in laboratory experiments and have been isolated from several species: human, monkey, bovine, rat, and been successfully harvested from various tissues: brain, retina, lung, skin and kidney[50]. Freshly isolated pericytes grow from capillary fragments of a mixed population of pericytes and ECs, where in preferential culture conditions pericytes eventually become the dominant cell-type. Pericytes grow as large, irregular, polymorphic-shaped cells, which elongate and narrow as cultures become more confluent. However, Identifying pericytes *in vitro* is not straightforward due to their pluripotent nature and considering there are no definitive pericyte-specific markers. However a general panel of markers commonly used includes: desmin, platelet derived growth factor receptor-β (PDGFR-β), Neuron-glial antigen-2 (NG2), α-smooth muscle actin (αSMA) and Thymocyte differentiation antigen-1 (Thy-1/CD90). Nevertheless, pericytes from venules and arterioles express both αSMA and desmin, whereas pericytes from capillaries typically do not express αSMA, therefore vessel and tissue-specific adjustments to the marker panel need to be considered[51]. Loss of expression of markers such

as desmin during multiple passaging or prolonged experiments may represent dedifferentiation *in vitro*, due to the pluripotent nature of the cells[52].

There is a lot of research interest surrounding pericyte biology, due to the numerous reports of pericyte cell drop-out in microvascular diseases such as DR, tumour-induced angiogenesis and age-related macular degeneration (AMD)[53–55]. To uncover the complicated cell-cell interactions between ECs and pericytes in health and pathology and to investigate the cause-effect relationship, co-culture experiments of ECs and pericytes would provide more valuable data than either cell-type grown alone due to the close structural and signalling association between pericytes and ECs.

1.5 THE BLOOD-RETINAL-BARRIER

1.5.1 STRICTLY REGULATED SEMI-PERMEABLE BARRIER

Blood vessels provide passage of blood throughout the body to deliver oxygen and nutrients via a semi-permeable barrier at the capillary level. The barrier allows passage of nutrients via direct diffusion, intercellular clefts, pinocytotic vesicles or cellular fenestrations (Figure 1.9). There are 3 major types of capillary bed: continuous, fenestrated and discontinuous, at different sites according to local tissue demand (Figure 1.7). The capillaries supplying the retina are continuous in structure, therefore only small molecules such as water and ions pass through intercellular clefts and lipid soluble molecules can passively diffuse along a concentration gradient. ECs in the capillary bed at the retina and in the brain have few vesicles and passage of substances from the blood to the tissue is highly controlled[56]. Similarly, the ECs lining the retinal capillaries must ensure the supply of oxygen and nutrients to the highly metabolically active neural retina, allow access to circulating cells which survey the retina for pathogens or maintain homeostasis, whilst also providing a barrier which protects against circulating toxins, pro-inflammatory leukocytes and microorganisms[23]. This highly regulated barrier is called the blood-retinal-barrier (BRB).

1.5.2 INNER AND OUTER BRB

The BRB has two components: an outer barrier formed by TJs between the RPE, and an inner barrier formed by TJs between ECs lining the inner surface of the retinal capillaries. The outer-BRB regulates transport between the choriocapillaris and the retina, whilst the inner-BRB regulates transport across the retinal capillaries[25]. The BRB is composed of TJs, GJs and adherens junctions (Figure 1.12). Klaassen et al. provide a summary table of molecules identified in retinal endothelial junctions (Table 1.1)[57]. The barrier properties of the inner and

outer BRB means RPE cells and the ECs lining the retinal vessels are impermeable to molecules >20,000-30,000Da in size[5]. Any alteration to the BRB, resulting in increased permeability of blood vessels, can lead to the progressive build-up of fluid within the retina, resulting in diabetic macular edema (DME), and chronic hyperglycaemia-induced damage to the vessel wall is a leading cause of this progressive sight-threatening condition[58].

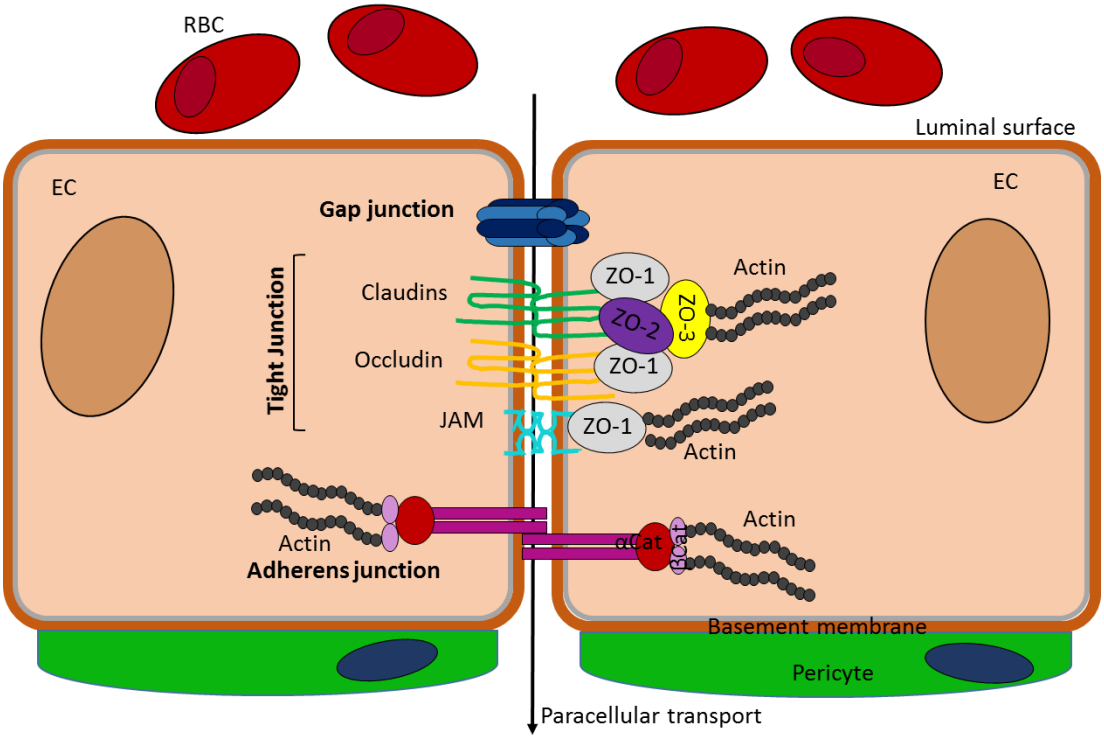

Figure 1.12. Junctions which form the inner blood-retinal-barrier

The inner BRB, formed by GJs, TJs and adherens junctions formed between neighbouring ECs. Major molecules of the TJ proteins include zonula occludens (ZO), occludin, claudins and junctional adhesion molecules (JAMs), while adherens junction proteins include catenins and vinculins. These junctions form interconnections between the actin filaments of the cytoskeleton of neighbouring cells, therefore resulting in tension across the barrier.

Table 1.1. MOLECULES IDENTIFIED IN RETINAL ENDOTHELIAL CELL JUNCTIONS

Category	Name	Gene name
Tight Junctions	Occludin	OCLN
	Claudin 1	CLDN1
	Claudin 2	CLDN2
	Claudin 5	CLDN5
	Claudin 12	CLDN12
	F11 receptor (JAM1)	F11R
	Junction adhesion molecule 2	JAM2
	Junction adhesion molecule 3	JAM3
	Endothelial cell-specific adhesion molecule	ESAM
	Poliovirus receptor-related 1 (Nectin)	PVRL1
	Tight junction protein 1 (zonula occludens 1)	TJP1
	Tight junction protein 2 (zonula occludens 2)	TJP2
Adherens Junctions	VE-Cadherin	CDH5
	β-Catenin	CTNNBIP1
	N-Cadherin	CDH2
Gap Junctions	Gap junction protein, alpha 1, 43 kDa	GJA1

1.5.3 TIGHT JUNCTIONS (TJs)

Zonula occuldens-1 (ZO-1) is a TJ protein involved in monolayer permeability (Figure 1.12). Adherens junction assembly and organisation precedes formation of TJs and in ECs, adherens and TJs are intertwined, whereas in epithelial cells TJs are localised apical to the adherens junctions[59]. ZO-1 TJ protein regulates tension by acting on the VE-Cad junction and as well as its cell-cell adhesive properties, is also involved in cell migration and angiogenesis of primary ECs[60]. Immunofluorescence (IF) imaging of antibodies against ZO-1 provides qualitative data on the presence of TJs, and combined with assessing permeability using dextran and trans-endothelial electrical resistance (TEER), these simple tests can measure EC barrier function *in vitro*.

1.5.4 ADHERENS JUNCTIONS

Vascular endothelial cadherin (VE-Cad) is a vascular endothelial-specific, type II cadherin protein of the adherens junction complex, and cadherins represent one of the major cell adhesion molecules. Cadherins mediate homophilic cell-cell adhesion via calcium-dependent interactions[61]. As well as its cell-cell adhesive properties, VE-Cad is also involved in homeostasis and remodelling via contact inhibition through interfering with VEGFR-2-stimulated cell proliferation, as well as supporting VEGFR-2-stimulated apoptosis[40]. One study showed that external stimuli from growth factors such as VEGF resulted in VE-Cad

translocation from the cell surface to the cell cytoplasm therefore disrupting EC barrier properties *in vitro*[62]. Stimulating ECs with flow *in vitro* has been extensively explored in order to investigate how reduced, increased, or disrupted flow influences EC behaviour, considering ECs would be continually stimulated by flow *in vivo*[63]. Several studies reported flow shear stress-mediated distribution of TJ proteins and a transient decrease or redistribution of VE-Cad and occludin protein expression, caused by flow-stimulated changes in cell shape and alignment[61,64]. Therefore, EC expression of VE-Cad is dynamic and can be altered due to environmental stimuli such as flow and presence of growth factors.

1.6 DIABETES

1.6.1 TYPES OF DIABETES

Diabetes mellitus is a complex metabolic disorder in which the body no longer produces enough insulin, or insulin is no longer effective on target cells. There are two main types: type I, which is caused by autoimmune destruction of the insulin secreting β-cells of the pancreas, and type II, which is a heterogeneous disorder caused predominantly by lifestyle choice, as well as influence from genetic susceptibility, resulting in insulin deficiency and insulin resistance over time[65]. Type II diabetes mellitus (T2DM) accounts for 90% of all diabetes[66]. Another type is gestational diabetes mellitus (GD), which is a hyperglycaemic state first recognised during pregnancy, occurring in 1-14% of pregnancies worldwide[67]. Two of the main pathological components driving T2DM; pancreatic β-cell dysfunction and insulin resistance, are outlined in Figure 1.13.

1.6.2 GESTATIONAL DIABETES (GD)

GD is classified as 'any degree of glucose intolerance with onset or first recognition during pregnancy', however this does not clarify the difference between undiagnosed diabetes pre-pregnancy i.e. diabetes in pregnancy (DIP) compared to GD, and the definition remains an evolving issue[68]. Figure 1.14 provides a guide to current acceptable criteria, however risk factors, age, ethnicity and socioeconomic status also need to be taken into consideration. Offspring from women who had pre-existing diabetes or experienced GD are at increased risk of obesity, glucose intolerance, and T2DM in late adolescence and young adulthood[69]. However, in DIP, the mother has already experienced diabetes for some time, resulting in progressive changes to maternal cells at a molecular level, before falling pregnant. Therefore miscarriage, pre-eclampsia and preterm labour are more common in women with pre-existing diabetes[70]. Although the intrauterine environment will present challenges to the

foetus in both DIP and GD, damage already caused by prolonged DIP results in higher risk pregnancies, compared to the acute onset of GD. Importantly, these differences between DIP and GD explained above, result in different alterations to a population of stem cells called endothelial progenitor cells (EPCs: Section 1:10) where EPCs isolated from GD umbilical cord blood (UCB) showed resistance to hyperglycaemic insult via decreased p38-MAPK activation, whilst EPCs from DIP UCB showed a reduction in colony formation, self-renewal capacity, and capillary-like tube formation[71,72]. As well as exposing clear differences between DIP and GD, these data also highlight the negative effect diabetes has on EC function, which is present from birth.

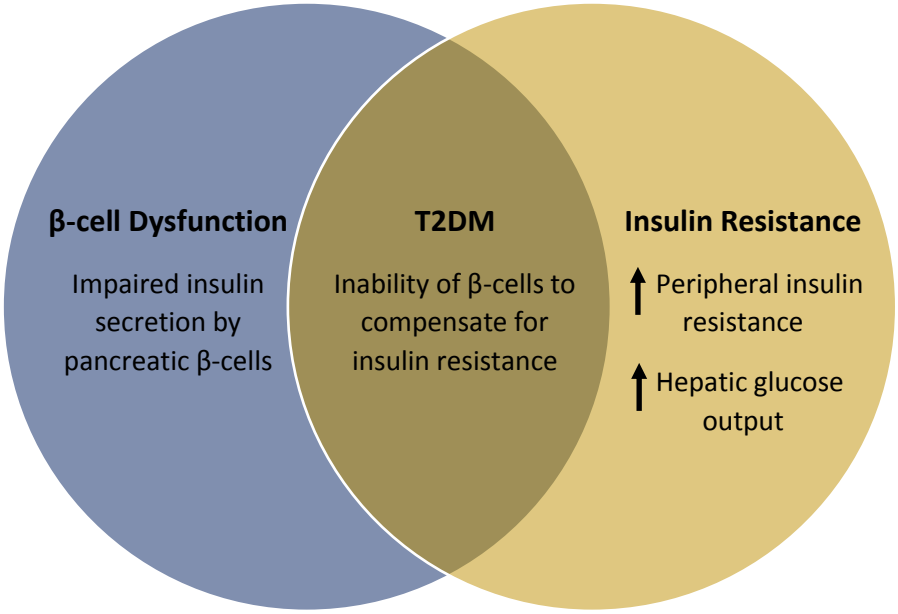

Figure 1.13. The two main pathological components of T2DM

Chronic β-cell dysfunction and insulin resistance combined result in the progression of T2DM. This can be caused by a complex interaction between lifestyle choice: obesity and physical inactivity, as well as genetic predisposition. The Venn diagram is adapted from Holt & Hanley[65].

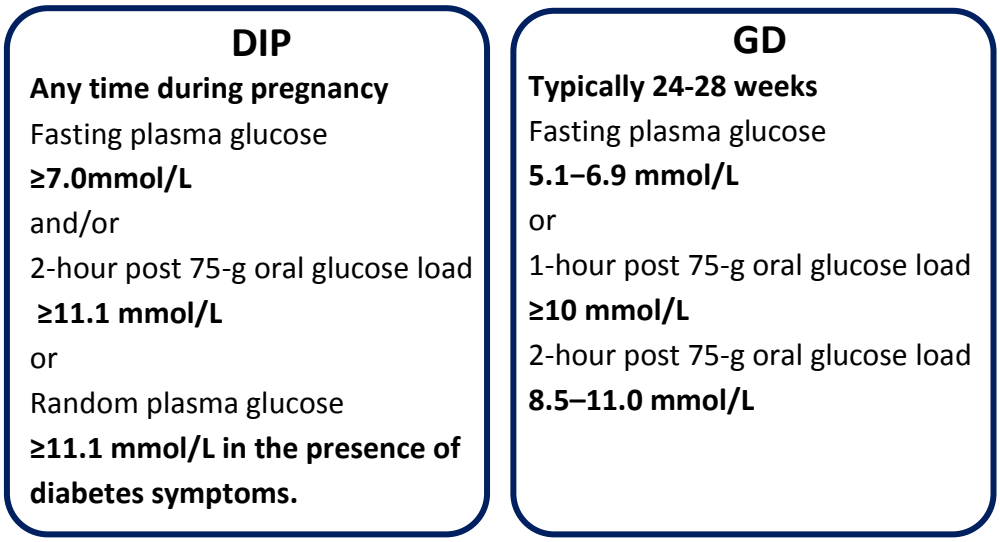

Figure 1.14. Comparison of diabetes in pregnancy (DIP) and gestational diabetes (GD)

Current definitions of DIP compared to GD using the 2-hour, 75-g oral glucose tolerance test threshold values for diagnosis[68].

1.6.3 PREVALENCE OF T2DM

Since 1980, the number of people with diabetes worldwide has quadrupled, particularly in low/middle income countries and although the causes are complex, two major risk factors are rising trends in obesity and physical inactivity[73]. The World Health Organisation (WHO) reports that 422 million adults are currently living with diabetes, with 1.6 million deaths directly attributed to diabetes worldwide each year[74]. Figure 1.15 provides estimates of the projected prevalence of diabetes over the next two decades[75]. According to the American Diabetes Association, In 2015, 9.4% of the population in the USA had diabetes (30.3 million people), and 29 million of those had T2DM (95.8%)[76]. In the UK 1 in 15 people have diabetes, not including one million undiagnosed with T2DM[66].

1.6.4 OBESITY AND DIABETES

Worldwide, 1 in 3 adults are overweight and 1 in 10 are obese[77], and the relationship between obesity and premature insulin resistance/deficiency, has resulted in the term 'diabesity' in the literature[78,79]. Being overweight or obese is one of the highest risk factors for developing T2DM, along with high blood pressure and high cholesterol, and genetic predisposition in 40-80% of cases[65,80]. Adipose tissue-derived factors known as adipokines, are involved in inflammation, mechanical organ protection and thermoregulation, and increased visceral deposits of white adipose tissue during obesity places individuals at risk of

developing insulin resistance, T2DM and cardiovascular disorders[81]. Taken together, these data provide evidence of a spiralling trend of rising levels of diabetes and its closely related co-morbidities worldwide.

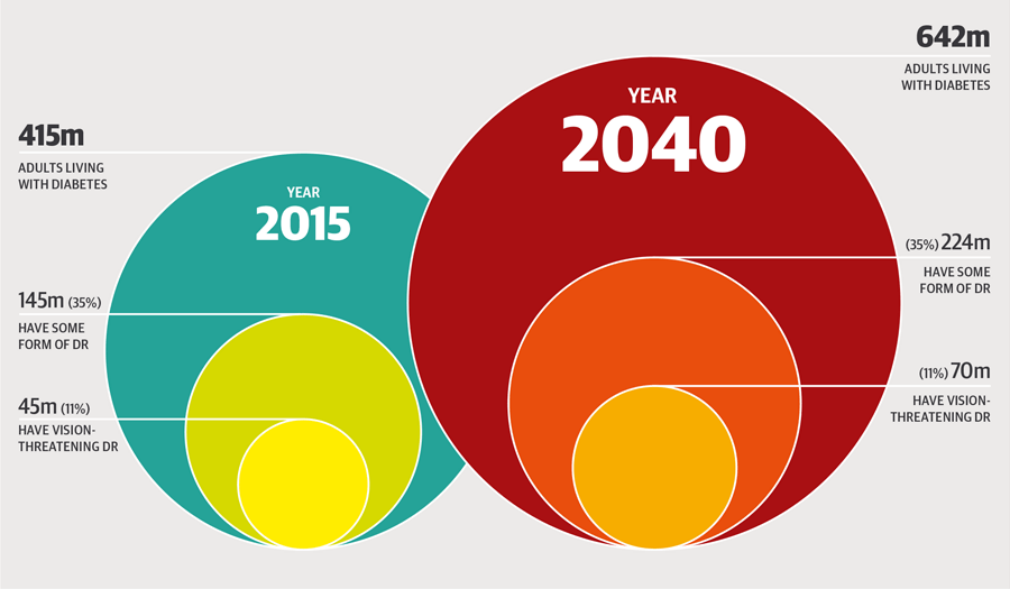

Figure 1.15. Global prevalence of people with diabetes and diabetic retinopathy

Adults with T2DM set to rise by over 200million (m), from ~415m in 2015 to 642m globally in 2040. DR set to remain at roughly 35%, and 11% being sight threatening. The social and economic burden of diabetes and its predicted increase is colossal, and along with an ageing population, will place huge burdens on healthcare facilities worldwide[75].

1.6.5 SOCIAL AND ECONOMIC BURDEN

The social and economic burden of diabetes is colossal, and increasing each year due to a growing ageing population and higher proportion of obesity in modern society. In the UK, 700 new cases of T2DM are diagnosed each day, which is presenting a huge challenge for the NHS to manage[82]. In the UK, over £14 billion/year is spent on treating diabetes and its complications, representing 10% of the NHS budget for England and Wales for 2019[83]. As well as the economic burden, the social burden of diabetes needs to be addressed.

A diagnosis of diabetes can be life changing to patients, who are advised to make major dietary and lifestyle adjustments, face the burden of multiple hospital/clinic visits, and come face-to-face with the realisation that they are living with a disease that will cause detrimental changes to their general health. Metabolic and nutrition-related conditions such as diabetes are also associated with neuropsychiatric disorders, through alteration in microbiota-related

metabolites and signalling molecules, and can lead to mental illness, particularly depression if not managed correctly[84]. The devastating effects of unmanaged T2DM can ultimately involve limb amputation, with people with T2DM 15 times more likely to undergo an amputation[85]. This is due to multiple complications of T2DM including CVD, nephropathy and neuropathy, which in combination can result in wound non-closure, infections and ultimately limb amputation. Included in the myriad of cardiovascular issues, DR is the most common microvascular complication in T2DM which can ultimately lead to impaired vision or sight loss[86]. Overall, treatment and management of T2DM needs to be addressed urgently to provide best quality of life prospects to patients whilst considering the most effective and economically viable treatment options.

1.6.6 DIAGNOSIS

According to the WHO, diabetes can be diagnosed using the oral glucose or HbA1c testing[87,88], and diagnostic criteria are outlined in Table 1.2 and Table 1.3 . HbA1c refers to average plasma glucose concentration of glycated haemoglobin (A1c).

Table 1.2. DIAGNOSISTIC CRITERIA FOR DIABETES & PREDIABETES

Target Levels by Type	Fasting plasma glucose	Oral glucose tolerance test
Non-diabetic*	5.5 mmol/L	<7.8 mmol/L
Prediabetes	5.5 - 7 mmol/L	7.8-11.1mmol/L
Diabetes	> 7 mmol/L	>11.1mmol/L

Table 1.3. HbA1c FOR DIAGNOSIS IN PREDIABETES OR DIABETES

HbA1c	mmol/mol	%
Normal	< 42 mmol/mol	< 6.0%
Prediabetes	42 - 47 mmol/mol	6.0% - 6.4%
Diabetes	> 47 mmol/mol	> 6.4%

1.6.7 OXIDATIVE STRESS & INFLAMMATION

With the onset of insulin resistance and deficiency in the pre-diabetic condition, multiple cell signalling pathways become altered, due to the systemic hyperglycaemic environment. In an attempt to maintain homeostasis and survive in the new, challenging, high glucose environment, ECs become activated. The cellular responses which follow are intrinsically linked with the activation of low-grade inflammation in multiple cell types, but in obese patients this is amplified by hyperglycaemia-induced adipocytes, which produce Tumor necrosis factor-α (TNF-α), interleukin-6 (IL-6), interleukin-1β (IL-1β) and interferon-γ (IFNγ) primarily in visceral, and to a lesser extent, subcutaneous depots[89]. This pro-inflammatory switch and dysfunctional glucose metabolism leads to increased mitochondrial reactive oxygen species (ROS) production and endoplasmic reticulum (ER) stress. Upon activation many immune cells generate free radicals and, in a continuous pathogenic loop, the synthesis of ROS promotes an inflammatory status in the surrounding tissue. Cells have endogenous antioxidant mechanisms, such as superoxide dismutase (SOD), vitamin A, vitamin C, vitamin E and β-carotene, however due to the chronic nature of diabetes, these natural antioxidants become exhausted, leading to redox imbalance and further activation of stress-sensitive intracellular signalling pathways[90–92].

Unlike skeletal muscle cells, hepatocytes and adipocytes, ECs do not require insulin for glucose uptake and, therefore, are a target for glucose-dependent activation of intracellular signalling pathways, several of which have been implicated in EC apoptosis and the microvascular pathogenesis of T2DM[93]. Excess glucose increases the amount of ROS produced by the electron transfer chain during adenosine triphosphate (ATP) production, and this leads to activation of nuclear factor kappa-B (NF-κB) pro-inflammatory pathways and caspase-3-induced EC apoptosis[94,95]. ROS induce the further release of pro-inflammatory cytokines and upregulate expression of adhesion molecules and growth factors such as PDGF, connective tissue growth factor (CTGF), insulin-like growth factor-I (IGF-I), and vascular cell adhesion molecule-1 (VCAM-1), via upregulation of redox-sensitive transcription factors such as NF-κB and the NADPH oxidase pathway[96]. Others have found that subjecting HUVECs to intermittent 'spikes' of hyperglycaemia *in vitro*, mimicking the high blood glucose peaks after glucose intake during diabetes, resulted in increased intercellular adhesion molecule-1 (ICAM-1), VCAM-1, endothelial selectin (E-selectin) and IL-6, through oxidative injuries induced by high glucose[97]. Superoxides are one type of ROS produced during the dysregulation of the biochemical pathways involved in the electron transport chain, and

increased superoxide induces chronic inflammation by upregulation of chemokines and cytokines including IL-1β, ICAM-1, IL-6, monocyte chemoattractant protein-1 (MCP-1), placental growth factor (PlGF) and VEGF[98,99].

1.6.8 ADVANCED GLYCATION END PRODUCTS

As well as the insult caused by ROS, during long term hyperglycaemia and with increased age, glucose forms covalent adducts with the plasma proteins through a non-enzymatic glycation, resulting in advanced glycation end products (AGEs). AGEs are involved in the disease progression of diabetic neuropathy, nephropathy, retinopathy and cardiomyopathy. There is evidence that AGEs interact with their plasma membrane localized receptor (RAGE) to alter intracellular signalling, gene expression and release of pro-inflammatory molecules and free radicals[100]. Therefore, when investigating the disease progression of diabetes; oxidative stress, ROS, inflammation and AGEs add to the myriad of factors which need to be fully elucidated and considered when modelling the disease *in vitro.*

1.7 DIABETIC RETINOPATHY

1.7.1 PREVALENCE AND CLINICAL FEATURES OF DR

DR is the leading cause of vision loss globally in working middle-aged adults[101], and in line with the rising prevalence of T2DM worldwide, this causes huge economic and psychological burden globally. Among diabetic populations, the estimated prevalence of any form of DR is 34.6% (93 million worldwide), and the prevalence of PDR and DME are 6.96% and 6.81%, respectively[86]. Duration of diabetes is a risk factor for developing DR and DR is present in 60% of people 20 years after onset of T2DM; sight-threatening retinopathy is found in 2.0% of people who have had diabetes for more than 5 years and in 15.5% of people who have had diabetes for more than 15 years[102]. DR can be divided into two main categories: the earlier non-proliferative stage (NPDR) and the advanced proliferative stage (PDR). An additional characterisation of DR is the presence of diabetic macular edema (DME), which can occur in both NPDR and PDR, and represents the most common cause of vision loss in patients[19]. Clinical features of NPDR include intra-retinal haemorrhages, microaneurysms, intra-retinal microvascular abnormalities, and cotton wool spots[103]. During PDR, new, leaky vessels form, leading to more microaneurisms which can begin to affect vision. Some of the clinical features of DR are highlighted in Figure 1.16.

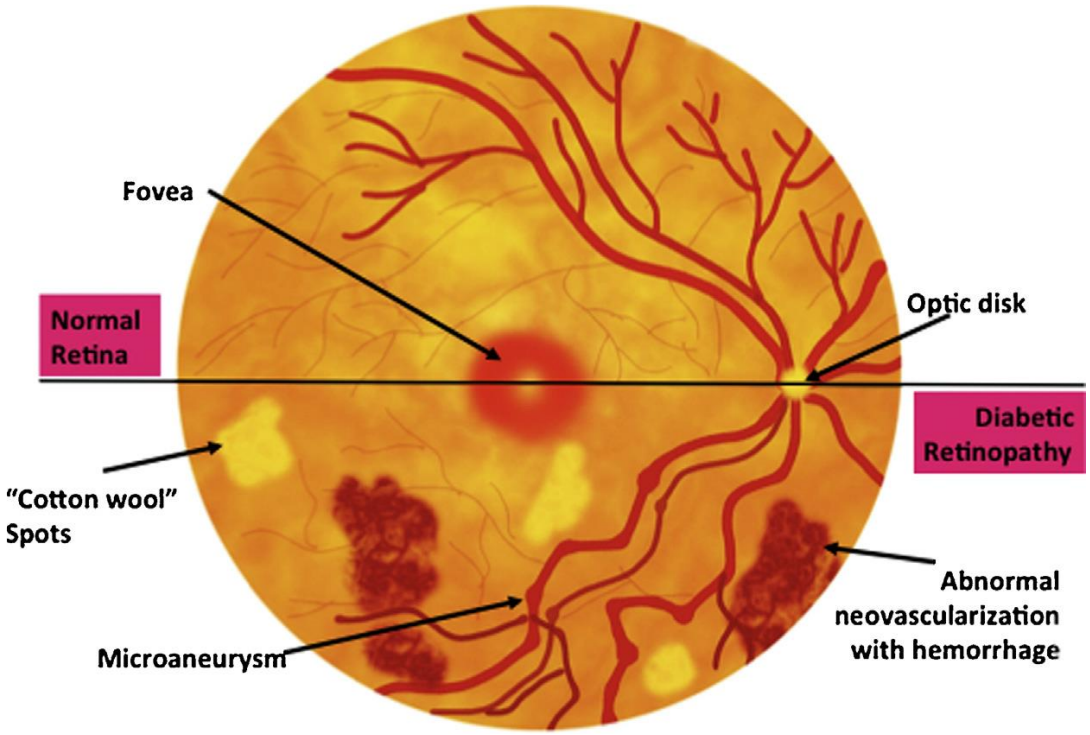

Figure 1.16. Fundus photography for diagnosis of diabetic retinopathy

Diagram illustrating examples of vascular abnormalities which can be detected using fundus photography: abnormal neovascularization, haemorrhages, microaneurysms, and cotton wool spots. Untreated, these will eventually lead to vision loss[104].

1.7.2 SUSCEPTIBILITY TO OXIDATIVE AND HYPERGLYCAEMIC STRESS

The retina is the most metabolically active tissue per weight in the body[105], therefore, the tissue is particularly sensitive to chronic alterations in glucose and oxygen levels. Vascular ECs express high levels of the glucose transporter-1 (GLUT-1), rendering them particularly sensitive to sustained hyperglycaemic conditions, which accounts for the chronic microvascular complications which occur during diabetes[100]. As well as hyperglycaemia, cells of the retina are also insulted with reduced oxygen levels, increased oxidative stress and chronic inflammation, caused by a progressive imbalance of various growth factors such as VEGF and pigmented epithelium-derived growth factor (PEDF), which can ultimately lead to PDR[5]. The changes involved in retinal vascular decline and the order in which they occur is not clearly understood. Further understanding of the progressive decline of cells composing the blood vessels during ageing and diabetes will enable preventative and regenerative strategies to reduce or prevent vision loss.

1.7.3 CHANGES TO THE VESSEL ARCHITECTURE

Changes to the architecture of the retinal capillary include: BM thickening, pericyte loss, endothelial dysfunction and degeneration, leaky blood vessels and loss of barrier function and thus, controlled nutrient exchange. As the capillary bed degenerates, the underlying tissue experiences hypoxia due to insufficient oxygen exchange from the bloodstream to the surrounding cells. As EC death and BM thickening continues, along with increased production of AGEs, BRB breakdown enables water and albumin to pass unregulated into the retinal interstitium. This can lead to edema and build-up of exudates in the retinal tissue that adds to the decline in visual acuity. The choriocapillaris also incurs progressive degeneration under chronic diabetic insult, resulting in thinning of the capillary bed, inflammatory cell invasion and microaneurisms, all of which severely disrupt the underlying RPE and photoreceptors, further exacerbating sight loss[19]. As more vessels of the inner and outer-BRB degenerate, vessel occlusion leads to tissue ischemia, and over time the area of affected retina becomes larger. Vision loss occurs when photoreceptors begin to die, due to the multitude of defects described above.

1.7.4 PERICYTE DROP-OUT

Many studies report pericyte drop-out as an early phenomenon of DR, but it is not clear if this is a cause (or trigger) of disease progression, or a symptom. It is hypothesised that pericyte drop-out leaves the ECs more unstable, leading to leaky blood vessels, and the lack of pericytes could be part of the advance to PDR. ECs secrete PDGF-B, whilst pericytes express the receptor PDGFR-β, and Hammes et al. proved that heterozygous knock-out of PDGF-B in mice resulted in 30% reduction in retinal pericyte number compared to wild-type mice and a small but significant increase in acellular capillaries and microaneurysms[106]. In another study, Ang-2 was found to be upregulated 30-fold in the diabetic rat retina, and injection of Ang-2 into healthy retinae caused Ang-2-induced pericyte drop-out in rat retinae, resulting in avascular capillaries[53], providing evidence that Ang-2/Tie-2 signalling is also involved in pericyte loss and vessel destabilisation. Accumulation of AGEs, polyols and other toxic compounds by pericytes was confirmed in a streptozotocin-induced model of diabetes in rats, where AGEs accumulated first within the shared EC:pericyte BM, and then intracellularly, co-localising with cellular AGE-receptors[107]. Therefore, due to the high coverage of pericytes in the retina, there could be a major hyperglycemia-induced build-up of AGEs in the retinal vasculature throughout progression of diabetes, driving EC and pericyte

cell dysfunction and death. An outline of the involvement of pericyte drop-out in NPDR leading to the progression to PDR is illustrated in Figure 1.17[52].

Pericytes and ECs have different secretomes, and aid one another in maintaining normal vascular function. If pericytes are lost early in diabetes, ECs may lose important pro-survival signals. Taking this into account, it is important to explore the effects of diabetes in a model similar to the *in vivo* environment, which would be ECs and pericytes in close contact. Therefore, an optimised co-culture model of the human retinal microvasculature could provide a very important *in vitro* tool for exploring the cellular changes during diabetes.

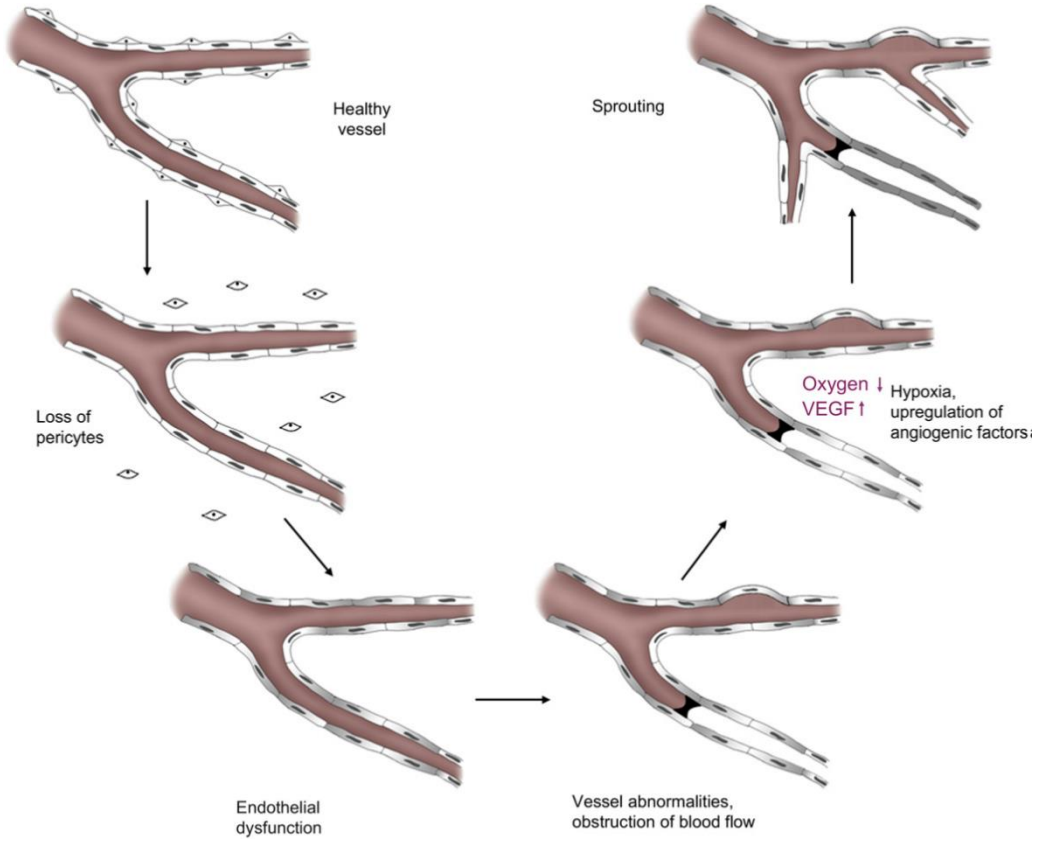

Figure 1.17. Progression of vascular abnormalities in diabetic retinopathy

The diabetic milieu causes pericyte drop-out from retinal blood vessels. Loss of pericytes and diabetic insult causes EC dysfunction. This leads to NPDR with changes to the vessel architecture including: BM thickening, microaneurysms, haemorrhages, and eventually capillary occlusion. This compromises the blood flow in the retina and leads to local hypoxia. Hypoxia induces upregulation of angiogenic factors such as VEGF. As blood vessels with reduced pericyte coverage are more susceptible to angiogenic factors, neovascularization (PDR) is initiated[52].

1.8 CURRENT TREATMENT

1.8.1 TREATMENT OF TYPE II DIABETES

Early detection and lifestyle modification, including diet and exercise management are essential to slow disease progression, and aid in preventing sight loss[108]. According to NICE guidelines 2019, an individualised care approach is recommended, in order to account for multi-morbidities, individual preferences and circumstances. Systemic drugs to lower cholesterol and reduce blood pressure are introduced if a patient remains above NICE guideline levels for over 2 months[109]. Figure 1.18 outlines some of the treatment options for T2DM and its complications. Systemic drugs such as metformin are prescribed to manage blood glucose levels, and these are taken daily, before meals, and combined with lifestyle management have successfully reduced the mean fasting plasma glucose values of T2DM patients[110]. Fenofibrate or simvastatin can be prescribed to lower cholesterol levels and improve the cardiovascular health of patients with T2DM[111,112].

Studies have shown a decrease/disruption to the natural enzymatic and non-enzymatic antioxidant defence mechanism during diabetes, increasing the risk of cellular injury via free-radical damage, therefore, there is scope for antioxidant therapy to slow disease progression[113,114]. Antioxidants such as vitamin C and E have long been investigated as treatment options for various human diseases and overall improvement to general health using animal models[115], however long-term human *in vivo* studies on antioxidants are limited, particularly with regards to the effects seen in diabetes.

1.8.2 CURRENT TREATMENT OF DIABETIC RETINOPATHY

Everyone over the age of 12 years old with diabetes has their eyes screened annually in the UK, using fundus photography[116]. As cameras and software advance each year, the resolution of these images improves and disease can be detected at an earlier stage. Public Health England updates the 'Eye Screening Programme', in line with current grading definitions for referable disease and graders use a feature-based grading form to assess fundus images[117]. Figure 1.16 demonstrates some of the changes occurring in the retinal vasculature during DR, which can be detected using fundus photography[104]. The current treatments for DR are laser photocoagulation, anti-VEGF intravitreal agents, intravitreal corticosteroids, and vitreoretinal surgery, however, these are only offered at late stage of disease, once symptoms have arisen[118]. All these treatments are expensive, require a vitreoretinal specialist and have a number of secondary, or undesirable effects. Other than improvements

to lifestyle and glycaemic control, there remains to be discovered an early stage pharmaceutical or cellular intervention that could prevent or slow progression of DR to sight threatening stage.

EARLY STAGES	ADVANCED STAGES
▪ Control of blood glucose ▪ Control of hypertension ▪ Cholesterol reduction ▪ Antioxidants ▪ Anti-inflammatory therapy ▪ Inhibition of AGEs ▪ Improving oxygen supply ▪ Photobiomodulation ▪ Neuroprotection ▪ Stem cell therapy	▪ Control of blood glucose ▪ Control of hypertension ▪ Cholesterol reduction ▪ Laser photocoagulation ▪ Anti-VEGF injections ▪ Corticosteroid injections ▪ Vitreoretinal surgery ▪ Gene therapy ▪ Antiangiogenic targets ▪ Stem cell therapy

Figure 1.18. Current and future treatments for diabetes and its associated complications

Current treatments **(red)** and potential treatments **(black)**. Tight control of blood glucose, hypertension and cholesterol are for improved systemic health and they should be achieved in all the stages of the disease, but they have a crucial role in early prevention of progression[119].

1.8.2.1 PAN-RETINAL LASER PHOTOCOAGULATION

Pan-retinal laser photocoagulation (PRP) involves creating thermal burns across the peripheral retina, destroying the retinal tissue, with the overall consequence of improved retinal oxygenation. PRP is performed during late-stage PDR, where uncontrolled growth of new, ill-formed, leaky vessels puts a patient's sight at risk. PRP is generally implemented to target leaky vessels in the periphery of the retina and successfully reduces bleeds, although this therapy is inherently destructive[17]. Due to the importance of the structure of the macula to provide central, colour vision and contrast sensitivity, PRP cannot be used in that area, and macular laser techniques are instead performed, although the success rate in preventing vision loss is reduced to 60-70%[120].

1.8.2.2 ANTI-VEGF INJECTIONS

The three main anti-VEGF drugs for treatment of sight-threatening DR with associated DME are ranibizumab (trade name Lucentis), bevacizumab (Avastin) and aflibercept (Eylea) all of which are antibodies against VEGF, but differ in size and structure. Prices range considerably: ranibizumab at ~£742/injection vial, aflibercept at ~£816/injection vial and bevacizumab at

~£12/injection vial, although bevacizumab is not currently licenced for use in the eye in the UK and US and is therefore 'off label'[121]. Often patients require 3-7 injections/year (although this varies markedly according to disease progression), and so these treatments are hugely costly for the NHS[122,123]. Anti-VEGF therapy is also ineffective for ~50% of people, who are unresponsive to treatment[124], therefore exploration of new pharmacological interventions is required.

1.8.2.3 CORTICOSTEROID INJECTIONS

Intravitreal injection of corticosteroids such as triamcinolone have been used off-label and have shown beneficial effects on reducing retinal swelling and vascular leakage, and although the mechanisms involved are not fully understood, steroids may act indirectly by inhibiting inflammatory cells and cytokine function, and directly by inhibiting VEGF, overall reducing BRB breakdown and vascular leakage[125]. However corticosteroids have severe side effects and their benefit is limited when compared to anti-VEGF treatment[57]. Common complications of intravitreal injection of corticosteroids include raised intraocular pressure and cataract formation, therefore long-term studies need to be implemented on the use of corticosteroids in the eye because current data provides mainly 1 year follow up results and the long-term use is underreported[119].

1.9 *IN VITRO* DISEASE MODELLING

1.9.1 MODELLING DIABETES *IN VITRO*

As described previously, diabetes is a multifactorial disease, which leads to hyperglycaemia (due to insulin resistance or impaired production), hypoxia, inflammation and oxidative stress. The first two are casual, whilst the latter are symptoms of the high glucose, low oxygen environment. When investigating cellular responses to diabetes, common *in vitro* conditions include high [D+] glucose, combined with low oxygen. Different groups use various ranges of glucose (15-33mM) and oxygen levels (1-5%) to mimic diabetes, often dependent on the timeframe of experiments and variation in experimental outputs[126,127]. This simple high glucose, low oxygen model can be developed further by introducing flow to mimic the haemodynamic stimulus of circulating blood[16,63], or modifying the properties of the surface which the cells adhere (i.e. mimicking ECM remodelling and BM thickening)[31].

1.9.2 CURRENT CO-CULTURE MODELS

In order to explore changes to the vasculature *in vitro*, studying ECs in isolation, on TC plastic, has been the traditional technique. However, this does not take into account the close

structural and functional relationship of ECs and pericytes *in vivo*. As cell culture techniques have vastly improved over time, it is now possible to grow multiple cell-types together in co- or tri-cultures on transwell inserts, in order to provide data more relevant to the *in vivo* environment. Microporous membranes, attached to cell culture plate inserts (transwell inserts) have been developed over decades by pharmaceuticals companies, in order to offer researchers the opportunity to grow cells together (co/tri-culture) to better mimic the *in vivo* anatomy of e.g. blood vessels, kidney nephrons or germ cell production[128]. Investigating the complex cell-cell interactions involved in co-culture systems will improve knowledge of disease progression at the multicellular or tissue level[129].

Co-culture models to mimic the blood vessel environment have been developed by several groups interested specifically in the pathogenesis of DR[62,130–132], which have greatly contributed to understanding the physiology of the retinal capillaries in healthy and disease. Previous groups have used various combinations of immortalised (cell-line)[131,133], animal[62,132], large vessel[130], or non-site-specific cells in co-culture. It is likely these models made use of these particular cell-types due to accessibility and unlimited expansion rate. Human primary cells can be more challenging to culture, but may be more appropriate as, for example, when immortalized vs. primary hepatocyte cell proteome was analysed, many proteins were downregulated in the immortalised cell-line[134]. Such diversity in the currently published *in vitro* BRB models leads to set-ups with different characteristics, which makes the comparison of results difficult[135]. Similarly, it is well documented that the retina is particularly sensitive to changes in blood glucose and oxygen levels, due to its high metabolic demand[104], therefore, using human, primary cells from the retinal microvasculature would provide data that are species and tissue-specific.

As well as selection of appropriate cell-types, the appropriate layout of the co-culture model and timescale of experiments needs to be considered. Models can be: mono/co/tri-cultures, contact, non-contact, conditioned medium, shared medium etc., as demonstrated in the schematic (Figure 1.19). In order to successfully grow different cell types together in one system, conditioned medium is often used, subjecting cells on either side of the membrane to different growth conditions[131,133]. Considering DR is a progressive disease and patients often present at late stage, it is therefore, important to develop long-term *in vitro* studies, rather than the short time points often used in co-culture studies, such as 8-48H. Developing a 21 day experimental timeframe, with multiple data collection points and repeated measures would enable monitoring of cell behaviour and proteins of interest over time.

These long-term, multiple time point, co-culture model data would fill a gap in the literature, identifying changes over a long time frame.

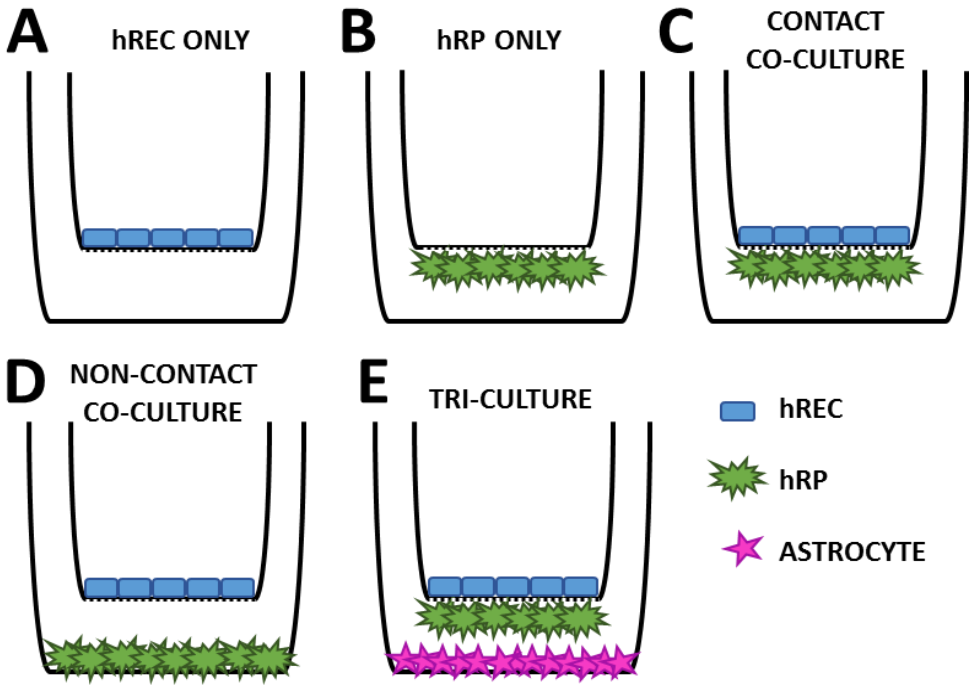

Figure 1.19. Examples of experimental set-up of various mono/co/tri-culture models

Cells were seeded on 24 w/p, polyethylene terephthalate (PET) transwell inserts with 1µm pores. Cells were seeded on either side of the PET membranes, according to the different model configurations (A-E). (A) hREC monoculture, (B) hRP monoculture, (C) contact co-culture, (D) non-contact co-culture and (E) tri-culture. Spatial aspects of cell seeding are dependent on the most appropriate organisation to mimic the tissue. For the retinal capillaries, hREC and hRP are in contact through a shared BM, therefore the contact co-culture (C) is most appropriate. If considering the effect of astrocytes, option (E) would be appropriate. Monocultures enable study of individual cell-types as controls. (D) Non-contact co-culture model allows investigation of the paracrine effect of each cell-type without physical contact.

1.9.3 BARRIER TESTING

When analysing BRB models, it is important to study the barrier function of the ECs, in order to confirm they behave in a similar way to a continuous type capillary *in vivo*. Barrier function can be analysed using simple functional assays. Trans-endothelial electric resistance (TEER) measures the integrity of TJ dynamics in cell culture models of EC layers. TEER is a strong indicator of the integrity of cell-cell barriers and because measurements can be performed in real-time without cell damage, TEER is often assessed before models are evaluated for transport of drugs or chemicals[136]. Dextran permeability assesses the ability of solutes of a particular size to escape through the endothelial layer, considering that selectively

permeable mature capillaries are known to be impermeable to dextrans over a molecular weight of 65 kDa[137]. TJ and adherens junction expression can be assessed using immunofluorescence (IF) labelling of ZO-1 and VE-cadherin proteins, where a functional barrier can be confirmed by continuous expression of junctional proteins at cell-cell borders.

1.10 ENDOTHELIAL PROGENITOR CELLS

1.10.1 HISTORY AND DISCOVERY

For normal maintenance and repair of adult vasculature, ECs need to be available for recruitment to sites of wear and tear and injury. Therefore, it has been postulated that there may be a source of stem cells involved in adult angiogenesis. Following the hypothesis that adult peripheral blood (APB) may contain progenitor cells that can become endothelial upon stimulation, a population of cells with vasoreparative capabilities was first reported in 1997 by Asahara et al.[138]. This groundbreaking study described a CD34 positive subset of putative endothelial progenitor cells (EPCs) which were isolated from human APB, offering the potential of autologous cell therapy for blood vessel repair in adulthood. Over 20 years later these putative EPCs have been investigated by hundreds of researchers, with over 10,766 papers under the search term 'endothelial progenitor cell' in PubMed as of April 2019. Initially, these cells were called EPCs and as the name suggests, were defined as early stage ECs, with higher reparative capabilities than their mature endothelial counterpart[139]. Extensive research has been undertaken to characterise these cells and test their ability to repair vessels damaged by numerous acute and chronic conditions, including; diabetes, retinopathy, peripheral arterial disease, ischemic heart disease and wound healing[140].

The source of EPCs has been debated, questioning if they are resident in the blood vessel wall, or are released from a bone marrow niche. In a study where bone marrow recipient blood was analysed, it was reported that donor genotype was detected in late outgrowth, highly proliferative EC populations, which suggests bone marrow may have an enriched population of EPCs, compared to APB[141]. Using whole animal tritiated thymidine labelling, researchers discovered that EPCs are not uniformly distributed throughout the vasculature, and are higher in number at areas were endothelial turnover is higher, to meet repair demand[142]. EPCs have been isolated from various sites in the body including adipose tissue, foetal liver tissue and adult bone marrow, and their organ-specific vasoreparative capability has been assessed in order to address organ-specific diseases[140,143].

It has been widely reported and is universally accepted that more EPCs can be isolated from same volume of umbilical cord blood (UCB) compared to APB, and also that UCB-EPCs possess a much higher proliferative capacity than APB-EPCs[144]. In fact, Ingram et al. reported a complete hierarchy of EPCs from APB and UCB, suggesting a heterogeneous population of cells involved in EC repair. In order to clarify many contradictory reports from different groups, using different criteria to identify EPCs, several recent reviews have focused on outlining more specific EPC markers and rigorous standards for their *in vitro* expansion and functional testing[145,146]. Efforts in this area should reduce ambiguity when assessing the use of EPCs for human cell therapy in the future.

1.10.2 CURRENT DEFINITION OF ENDOTHELIAL COLONY FORMING CELLS (ECFCs)

The first report of EPCs used cell surface markers for identifying desired cells, and defined the EPC population as: CD34, VEGFR-2, Tie-2 and CD31 positive cells, although these were not CD45 negative, suggesting they were possibly a heterogeneous population of progenitors, some of which had a haematopoietic lineage[138]. Various techniques have been described to isolate EPCs from blood. All include collecting blood and separating and collecting the mononuclear layer using fractionation techniques, but some of the many differences include the use of collagen I coated plates, fibronectin coated plates, re-plating non-adherent cells, disposing of non-adherent cells, culturing for 7 days or culturing for over 21 days, or collecting 'early outgrowth' or 'late outgrowth' endothelial populations. In 2003, Hill et al. attributed the level of circulating EPCs to cardiovascular risk, and from this study, rather than using the earlier ambiguous cell surface markers to identify EPCs, a new assay called the colony forming unit-Hill (CFU-Hill) assay was developed to assess the colony forming capabilities of putative EPCs expanded *in vitro*[147]. EPCs were also reported to have a hierarchy based on their clonogenic and proliferative potential, comparing APB- and UCB-derived EPCs[148].

Concise reviews of the different and evolving techniques to isolate and identify EPCs over time has been provided by Ingram et al. and more recently by Yoder[149,150]. It is now recognised that in early studies, researchers described cells isolated from blood as EPCs, when in fact a heterogeneous population of haematopoietic stem cells as well as putative EPCs were present, and recent advances in monoclonal antibody specificity and flow cytometry have now enabled a much more stringent characterisation of these putative EPCs[150]. Therefore, over time, the requirements to specify EPCs from contaminating cells of a haematopoietic lineage have evolved[151].

1.10.2.1 MYELOID ANGIOGENIC CELLS (MACs) AND ENDOTHELIAL COLONY FORMING CELLS (ECFCs)

Shortly after their discovery in 1997, two distinct populations were recognised when EPCs were expanded *in vitro*: a population which appeared early (less than 7 days), called early EPCs, and a population which appeared late (2-4 weeks) called late EPCs or outgrowth endothelial cells[152,153]. *In vitro* testing of the two sub-populations found the early EPCs were of haematopoietic lineage, did not directly incorporate into damaged vasculature, and were involved in releasing paracrine signalling to encourage the outgrowth population to migrate to sites of vascular damage, where the outgrowth EPCs physically incorporated into the endothelial layer[154]. In line with improvements in flow cytometry, clonogenic assaying and genetic phenotyping, a very recent review by Medina et al. provided clarification on the correct nomenclature regarding the two distinct cell-types present during *in vitro* expansion of the mononuclear fraction of human blood; myeloid angiogenic cells (MACs) and endothelial colony forming cells (ECFCs; outlined in Figure 1.20)[155]. In the review, they explain the term EPC is now outdated and is too vague, and therefore to avoid confusion should no longer be used. This paper was published in a collaboration between three major research groups involved in EPC research, highlighting the recent combined efforts to standardise nomenclature and identification of cells isolated from the mononuclear fraction of human blood. Therefore, following guidelines from Medina et al., ECFCs are defined as CD34 positive/negative, CD31, CD105, and CD146 positive, CD90 negative to confirm they are not fibroblastic, and importantly CD45 and CD14 negative to distinguish them from a haematopoietic lineage. ECFCs appear late in culture (14 days onwards), compared to MACs, which appear early in culture and play an important role in paracrine signalling during vascular repair, rather than physical incorporation into the vascular wall.

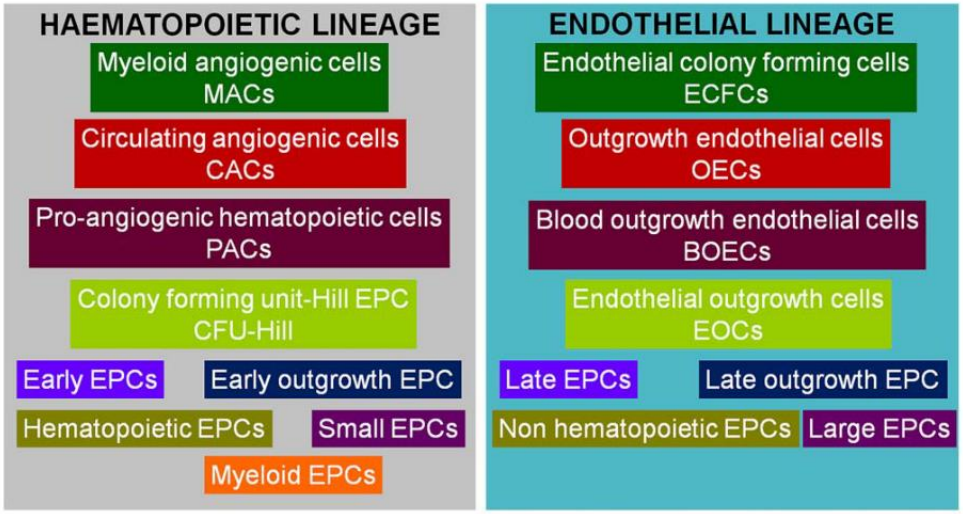

MACs	ECFCs
✓ CD45+ CD14+ CD31+	✓ CD31+ CD105+ CD146+
✓ CD146- CD34-	✓ CD45- CD14-
→ Conditioned media enhances endothelial network formation *in vitro* and *in vivo*.	→ Intrinsic tube forming capacity *in vitro* and *in vivo*.
→ MACs-derived paracrine factors as stimulants of angiogenesis.	→ ECFCs as building blocks for new blood vessel formation or vascular repair

Figure 1.20. Two distinct groups of EPCs according to phenotypic lineage

Nomenclature and minimal criteria for defining MACs (haematopoietic) and ECFCs (endothelial), based on immunophenotype, and function, assessed as a potency assay. Abbreviations: BOECs=blood outgrowth endothelial cells, CAC= circulating angiogenic cells, CFU=colony forming unit, ECFCs=endothelial colony forming cells, EOCs=endothelial outgrowth cells, EPC=endothelial progenitor cell, MACs=myeloid angiogenic cells, PACs=pro-angiogenic hematopoietic cells[155].

1.10.3 ECFCs IN VASCULAR DISEASE

Normal steady-state endothelial turnover is relatively slow, however, in response to injury, EC proliferation rates increase and it is postulated that tissue or vascular wall resident ECFCs may contribute to vascular repair[142]. ECFCs could be a useful tool to repopulate damaged vasculature and ischemic tissues, however, the number and/or function of ECFCs has been reported to be reduced in chronic disease states such as diabetes and CVD[139,156,157]. EPC number has been assessed in various stages of CVD, and have been reported as increased in the early phase of acute myocardial infarction[158], whilst both circulating and bone marrow-derived EPCs were reduced in patients with chronic ischemic heart disease[159], and more CVD EPC studies are summarised in a review by Shantsila et al.[139]. This review highlights the hypothesis that ECFCs are highly dynamic, and respond acutely to environmental changes. This means that depending on disease stage it is very difficult to fully understand the role of

ECFCs in tissue-specific responses to different diseases. The aforementioned studies highlight that, similar to the debate surrounding identification of ECFCs, number and function of ECFCs during disease is also yet to be definitively determined.

1.10.4 ECFCs AS A CELL THERAPY

In order to be useful in human cell therapy, ECFCs isolated from either APB or UCB could be used. APB-ECFCs are easily obtainable from simple venipuncture blood samples, providing an autologous cell therapy. However, as previously mentioned (Section 1.10.1), APB-ECFCs have lower proliferative potential than UCB-sourced ECFCs. UCB-ECFCs could also be utilised and easily expanded *in vitro* due to their higher proliferative potential[144], although they would have to be recipient HLA matched. Several small-scale phase 1 trials transplanting EPCs from peripheral blood and bone marrow into patients to treat acute myocardial infarction and severe ischemic legs, provided preliminary evidence of feasibility and safety[139]. Due to the limited therapeutic options for severe heart failure, bone marrow mononuclear cells and umbilical cord derived mesenchymal stem cells have been used to treat ischemic cardiomyopathy, acute myocardial infarction and non-ischemic cardiomyopathy, although their efficacy remains controversial mainly due to the design of the clinical trials and the need to standardise cell isolation techniques[160]. Due to their superior proliferative potential, UCB-ECFCs could be more useful for engineering of vascularised tissue grafts, and to aid in triggering neovascular events in ischemic disease[145]. ECFCs have also been investigated for tumour targeting, via adenoviral-mediated EPC delivery of soluble CD115, which suppressed growth of prostate tumours *in vitro*, taking advantage of ECFC ability to migrate to areas of ischemia and responsiveness to viral manipulation[161]. ECFCs have also been investigated in tissue engineering, to repair large skin defects, and the highly hypoxic environment of a wound is a major driving force for activating ECFC migration and growth factor cross-talk *in vitro*[162]. Irrespective of which disease ECFCs may be useful to treat, in order for ECFCs to be useful in human trials, their *in vitro* expansion must be xeno-free and compliant with GMP standards[163]. This has been achieved, during a large scale, animal protein free, humanised expansion techniques described by Schallmoser et al., suggesting translation to human trials is possible, although xeno-free cultures are not always used during *in vitro* studies due to the cost implications[164].

1.10.5 ECFCs FOR CELL THERAPY IN DIABETIC RETINOPATHY

The progression of DR involves alteration to a plethora of growth factors, cytokines and chemokines, induced by chronic hyperglycaemia, leading to EC and pericyte dysfunction, cell

loss, loss of BRB integrity, increased permeability and eventually leaky blood vessels. Capillary repair via an exogenous source of endothelial stem cells delivered to the retina via intravitreal injection, may offer a cell-based therapy to repopulate the depleted retinal vasculature in DR. ECFCs are a good candidate, due to the ability to isolate them in sufficient numbers from UCB and healthy APB[165], their high proliferative potential during *in vitro* expansion[149], and their ability to withstand oxidative stress, through high intrinsic expression of SOD-2[166]. This idea of ECFC cell-based therapy has been explored in *in vitro* and animal models of various aspects of CVD, wound healing and DR[140,167].

Focusing on ECFC cell-therapy targeted specifically for treating DR, Stitt, Medina and colleagues have published techniques for isolation and characterisation of ECFC populations from human UCB and APB, and recently clarified the correct nomenclature in an attempt to standardise ECFC use with the aim of progressing along the translational pipeline to human trials[153,155,157,168,169]. Using an oxygen-induced retinopathy (OIR) mouse model[170], an ischaemic hindlimb mouse model[171], and rigorous individual cell analysis, scratch wound and incorporation experiments[172], this group has produced robust data which strongly imply ECFCs are an appealing candidate for treating early stage DR. Currently, rat tail collagen I coated plates are used to isolate and expand ECFCs from the heterogeneous population of cells in the mononuclear layer of blood, as well as fetal bovine serum (FBS) as a source of growth factors during cell culture[153,173]. However, in order to move ECFC cell-therapy to a translational stage, xeno-free or GMP-compliant culture conditions must be developed[163]. Production of ECM-like synthetic or modified culture surfaces may provide the solution.

1.11 POLY-ε-LYSINE (pεK) HYDROGEL APPLICATIONS

1.11.1 pεK POLYMER

Poly-ε-lysine (pεK) is a naturally occurring biomaterial that is biodegradable, edible, water soluble and non-toxic to humans and the environment. pεK is a cationic homopolyamide made of lysine, formed by amide linkage between ε-amino and α-carboxyl groups (Figure 1.21)[174]. pεK was fortuitously discovered as an ECM produced by filamentous bacterium *Streptomyces albulus* ssp. *Lysinopolymerus* strain 346 over 3 decades ago[175], and has more recently been found to be secreted by various Streptomycetaceae bacteria and a few filamentous fungi[176]. Apart from its predominant use as a preservative in the food industry, derivatives of pεK are used in a wide range of applications including as: emulsifying agents, dietary agents, biodegradable fibres, drug carriers, anticancer agent enhancer, biochip coatings and hydrogels[177].

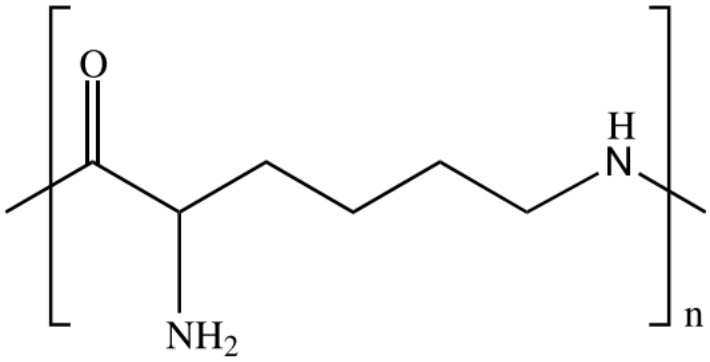

Figure 1.21. Outline of the chemical structure of poly-ε-lysine (pεK)

1.11.2 pεK HYDROGELS

Natural hydrogels are receiving attention as cell culture substrates and scaffolds, due to their mimicry of the *in vivo* ECM composition, inherent biocompatibility and cell adhesiveness and because they possess specific amino acid domains that are recognised by cells[178]. Peptide hydrogels can be synthesised using pεK and cast into gels with handleability and transparency properties similar to contact lenses, when cross-linked with carboxylic acids using carbodiimide chemistry (Figure 1.22, Figure 1.23). The mechanical properties of each gel can be tailored by changing the bis-carboxylic acid (length of carbon chain), density of pεK and the % of cross-linking. Free amine groups allow attachment of bioactive molecules to alter the surface properties of the gel for purposes such as drug carrying, antimicrobial properties and cell attachment (Figure 1.21, Figure 1.23). During gel production, aqueous synthesis allows creation of a porous gel for cell growth, or encapsulation of cells and bioactive molecules, functioning as a potential delivery system[179].

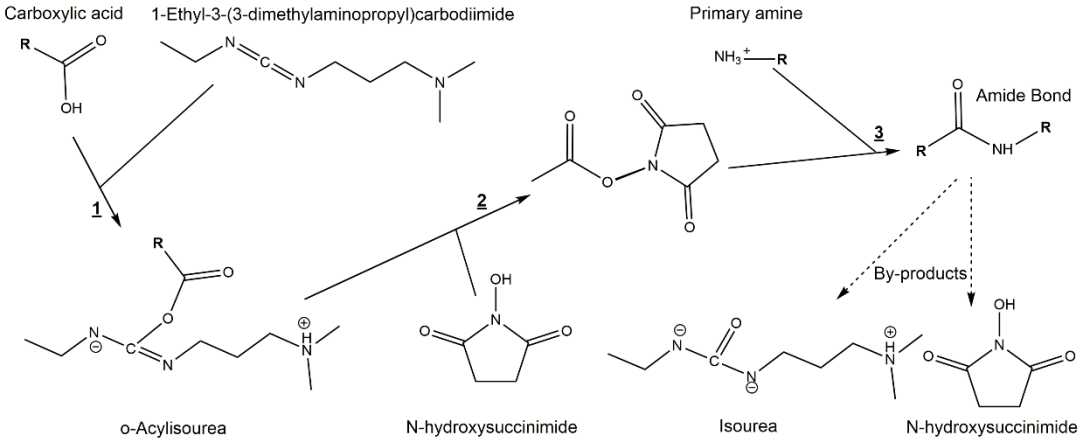

Figure 1.22. Chemistry used for producing pεK

Outline of chemistry used to form an amide bond between pεK and bis-carboxylic acids, using an 1-Ethyl-3-(3-dimethylaminopropyl)carbodiimide (ECDI) and N-hydroxysuccinimide (NHS)-mediated cross-linking technique.

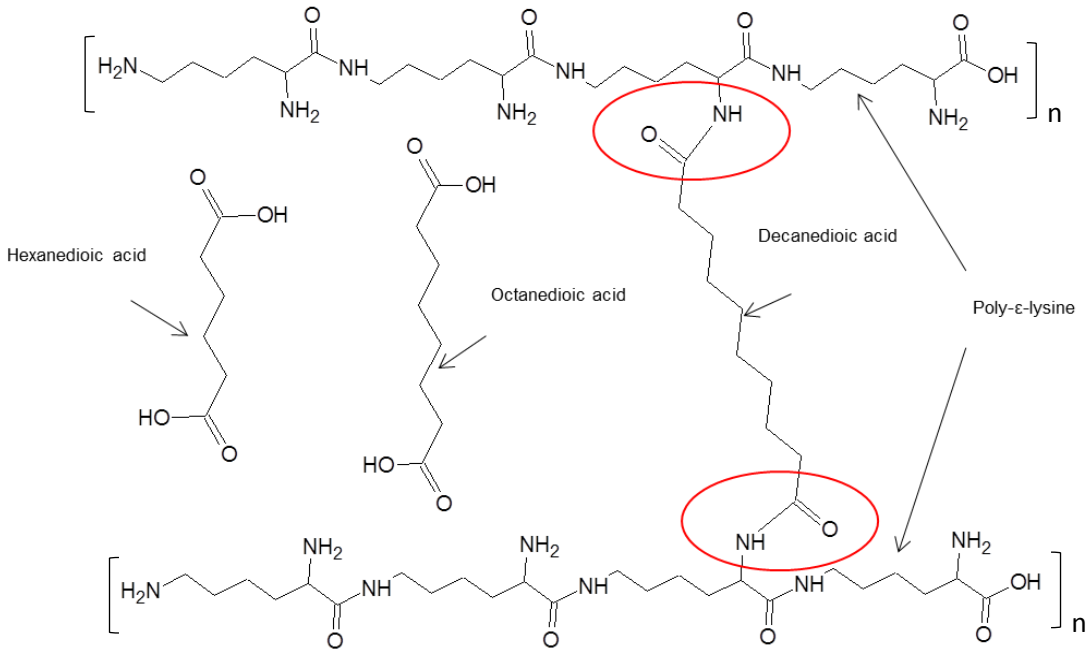

Figure 1.23. Structure of pεK hydrogels cross-linked with carboxylic acid

Outline of pεK cross-linking using carboxylic acids of different chain lengths, where free amine groups react with the carboxylic acid, using EDCI and NHS, via carbodiimide chemistry (**red circles**). The carboxylic acid used and percentage of cross-linking alters the mechanical properties of the gel[179].

1.11.3 PEPTIDE MODIFICATION OF HYDROGELS

The arginine-glycine-aspartic acid (RGD) cell adhesion sequence was discovered in fibronectin in 1984[180]. The RGD motif is not restricted to fibronectin, because it occurs within more than 100 proteins, although its function as a cell adhesion motif is sometimes silent[181]. The RGD sequence is the cell attachment site for a large number of adhesive ECM, blood, and cell surface proteins, and nearly half of the known integrins recognize this sequence in their adhesion protein ligands[182]. Following this discovery, numerous materials have been RGD-functionalised to enhance cell adhesion to otherwise non-adherent surfaces. Traditionally, biomedical devices were coated in proteins such as fibronectin, laminin or collagen, but these had several disadvantages: the proteins have to be isolated from organisms and purified, they may elicit undesirable immune responses, they can be continuously degraded, and may not have proper orientation to elicit cell adhesion. In addition, the properties of the surface, determined by topography, charge and wettability, may influence the orientation or conformation of the protein[183]. Using a small immobilised peptide such as RGD for cell attachment to biomaterials, rather than full length proteins, diminishes all of the aforementioned issues. The coverage and availability of RGD on any material is an important consideration, and ≥1 pmol/mm^2 RGD enabled, for example, human primary saphenous vein cells to establish focal adhesion on RGD modified PET, compared to cells on unmodified PET[184]. Due to the free amine group on pεK hydrogels, RGD can be covalently bound to the surface, with the aim of improving cell adhesion (Figure 1.24).

1.11.4 pεK FOR STEM CELL EXPANSION

To date, expansion of ECFCs has been optimised using rat tail collagen I coated TC plastic[153,173], however there has been minimal focus on the potential influence of the substrate on experimental outcomes, or the fate of the pluripotent nature of the cells[129]. In a study focusing on EPCs as a cell therapy for endothelialising small-diameter vascular grafts to repair areas of the vasculature damaged by atherosclerosis, PEG–peptide grafted poly(ethylene glycol) diacrylate (PEGDA) hydrogels were assessed for their ability to support adherence and expansion of ECFCs[185]. Unmodified gels did not support ECFC adherence, only PEG–REDV, PEG–YIGSRG or PEG–RGDS grafted hydrogels enabled ECFC adhesion, although this study did provide important information on ECFC-specific rolling adhesion. It is well known that biomaterial surfaces directly influence cell attachment, proliferation, phenotype and interaction with the immediate microenvironment[186]. Therefore, when aiming to expand

ECFCs for multiple passages in order to expand numbers for autologous or allogeneic cell therapy, pεK hydrogels are an exciting avenue to investigate.

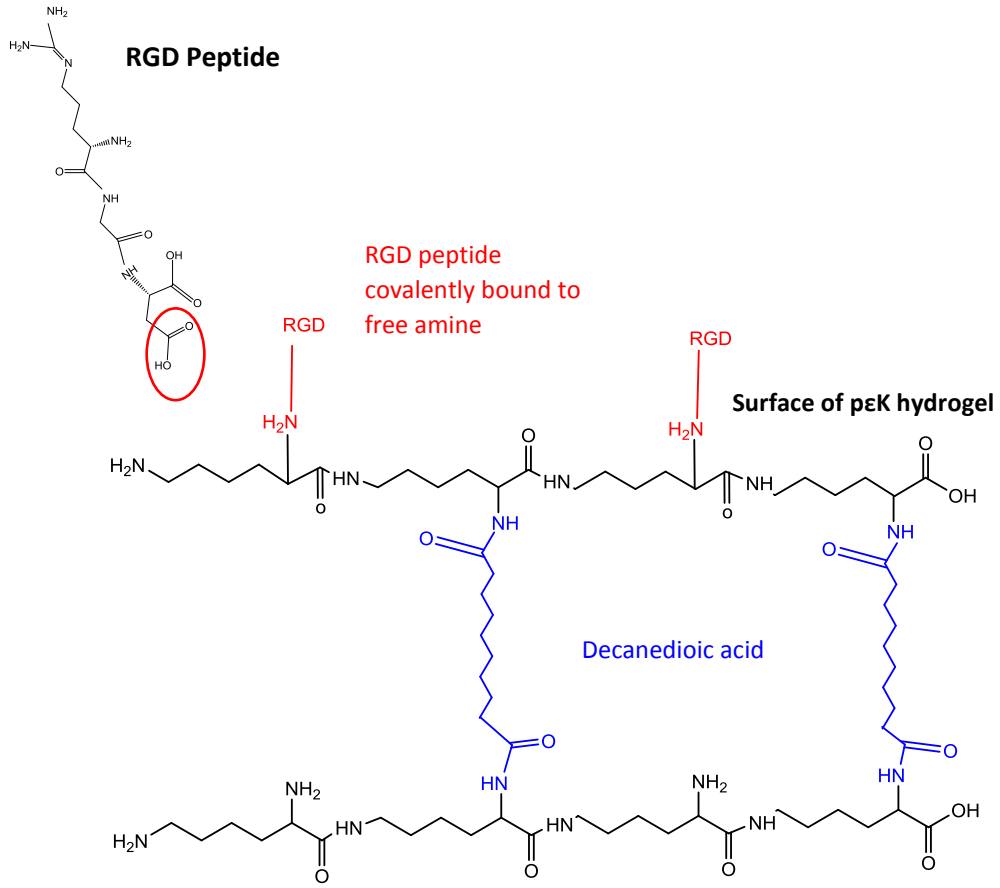

Figure 1.24 RGD binding to free amine group on pεK hydrogel

RGD can bind covalently to the free amine groups available on the surface of the crosslinked pεK gels (blue circles). The RGD motif improves cell attachment via integrin binding.

1.11.5 pεK IN THE EYE

In a review focusing on biomaterials for ocular transplantation, Lace et al. give a concise description of different types of synthetic materials which have been tested for their suitability to delivery cells to the retina[187]. However, it is clear that the focus in this area has been replenishing the specialised cells composing the neural retina and not the retinal microvasculature itself. Biomaterial production and optimisation to deliver cells to the inner BRB to repopulate damaged vasculature remains a major area for development. pεK gels are suitable candidates for delivery of cells to the back of the eye, due to their transparency, non-

toxicity and high water content, which ensures excellent oxygen transmission to any underlying tissues[188]. pεK contact lenses have been investigated for their antimicrobial properties in the cornea, and a study by Gallagher et al. showed the pεK gels supported growth of human corneal epithelial cell line (HCE-T cells) for up to 8 days *in vitro*, with no significant differences in scratch wound closure, compared to TC plastic. The HCE-T cells formed ZO-1 junctions with neighbouring cells, suggesting the pεK gel surface is suitable for epithelial cells to form a functional barrier[179]. As well as casting the gel into lenses, pεK can be formed into microparticles via emulsification polymerisation, providing microparticles ranging in diameter from 1000µm to <150µm[189]. Potentially, these microparticles could be loaded with cells and delivered to the back of the eye via intravitreal injection, although they have not yet been tested for their cell delivery capability.

2 CHAPTER 2

Developing a primary co-culture model of the human retinal microvasculature for use in the development of regenerative medicine strategies for diabetic retinopathy

2.1 OVERVIEW

To investigate the effect of diabetes on the retinal capillaries, co-culture models of ECs and pericytes grown together can be used to examine changes in cell behaviour. Considering their close interaction *in vivo*, through a shared BM, these two cell-types have major structural and paracrine influence on one another. Current co-culture models investigating the retinal capillaries use either non-human, immortalised, or large vessel ECs. This chapter focuses on optimising a human, retina-specific co-culture model using human retinal microvascular endothelial cells (hREC) and human retinal pericytes (hRP) grown together on either side of polyethylene terephthalate (PET) membranes, for an extended period of time (21days). High glucose and low oxygen were used to induce a diabetic phenotype, and cell phenotype, proliferation, metabolic activity, protein expression and angiogenic protein secretion were analysed.

2.2 AIMS & OBJECTIVES

To develop a novel, human, primary, co-culture model of the retinal vasculature to mimic diabetic retinopathy *in vitro*

1. Grow and characterise hREC and hRP in mono- and co-cultures in optimised physiologically healthy or diabetic conditions
2. Explore changes in cell behaviour and protein secretion in healthy compared to diabetic conditions
3. Explore differences in cell behaviour and protein secretion when cells are grown as monoculture compared to co-culture models

2.3 METHODS

2.3.1 hREC CULTURE

Human retinal microvascular ECs (hREC) were purchased from Cell systems *(Cell Systems, ACBRI 181V)*. Cells arrived at passage 3 (P3) and were used in experiments up to P10. hREC were cultured in PromoCell MV medium *(PromoCell, C22020)*, containing 5% fetal bovine serum (FBS), further supplemented with heat inactivated FBS *(Labtech, batch 013BS145)* to final concentration of 10%. Cells were cultured in a T75 flask *(Greiner, 658-175)* with fresh media supplied every 48 hours (H). hREC were sub-cultured at ~90% confluency. A full T75 flask provided approximately 5-6x10^6 cells.

2.3.2 hRP CULTURE

Human retinal pericytes (hRP) were purchased from Cell Systems *(Cell Systems, ACBRI 183V)*. Cells arrived at P3 and were used in experiments at up to P10. hRP were cultured in DMEM *(Life Technologies, 11966-025)* supplemented with 1mM sodium pyruvate *(Life Technologies, 11360-070)*, physiological (5.5mM) [D+] glucose *(Life Technologies, A24940-01)* and 10% FBS. Cells were cultured in a T75 flask with fresh media supplied every 3 days. Allowing cells to become >70% confluence initiated a phenotypic switch to larger, more elongated cells, so to avoid cells transitioning, hRP were sub-cultured at 70-80% confluency. At ~70% confluence, a T75 flask provided approximately 3-4x10^6 cells. Using light microscopy, cell shape, size and number were monitored regularly to ensure cells did not transition during cell culture, over time. At each passage, images were obtained and compared to earlier passage cells.

2.3.3 SUB-CULTURING hREC AND hRP

Once flasks reached appropriate confluence, culture medium was removed and cells were washed with warmed Dulbecco's phosphate buffered saline (dPBS) *(Sigma, D8537)*. dPBS was removed and 1X Trypsin-EDTA *(Sigma, T4174)* was added and incubated at 37°C with cells for 2-4 minutes (mins) or until >90% of the cells had detached. Complete medium was added at double the volume of trypsin, to neutralise the action of the trypsin. Cells suspended in media were spun in a centrifuge at 400xg for 5 mins to form a pellet. For further sub-culture flasks were split 1:3, or for seeding at specific densities, a haemocytometer was used to count cells.

For freezing, cell pellets were re-suspended in 900µl FBS and 100µl of Dimethyl sulfoxide (DMSO) *(Sigma, D2650)* in a 1.8ml cryovial *(STARLAB, E3090-6222)* and transferred into -80°C in a Mr. Frosty *(ThermoFisher, 5100-0001)* containing isopropanol, for freezing at a rate of -

1°C/minute. For long term storage, cells were transferred to liquid nitrogen. To bring cells out of liquid nitrogen, vials were defrosted quickly at 37°C in a water bath over 2-4 mins. The defrosted cell suspension was dispersed into a T75 flask of warmed complete medium and left to adhere overnight. The next morning medium was completely changed to remove remnants of DMSO from the culture flask.

2.3.4 IMMUNOFLUORESCENCE IMAGING

Using human primary cells requires regular testing to ensure cell phenotype remains consistent throughout passaging. To do this, immunofluorescence (IF) imaging of fluorescently labelled antibodies against phenotype-specific proteins and receptors was carried out on hRP and hREC at different passages. Cells were washed 3x 5 mins in warm dPBS to remove remnants of cell culture medium. dPBS was removed and, working inside a fume hood, 10% neutral buffered formalin (NBF) *(Sigma, HT501128)* was added for 9 mins, at room temperature (RT) on a slow rocking platform. NBF was removed and cells were washed 3x 5 mins in dPBS. 0.5% Triton-X *(Sigma, 45H0481)* in dPBS was added for 4 mins at RT on a rocker, to permeabilise the cells. Cells were then washed 3x 5 mins with dPBS. 5% normal goat serum (NGS) *(Sigma, G9023)* in dPBS was added to cells for 1H, at RT on a rocker, to block non-specific binding sites. NGS was removed and primary antibodies, diluted to optimised working concentration in dPBS (Table 2.1), were added to cells and left on a slow rocking platform overnight at 4°C. 3x 5 min 0.1% Tween-20 *(Sigma, P1379)* in dPBS (wash buffer), at RT on a rocker removed any unbound primary antibody.

Secondary antibodies (Table 2.2), were added at 5µg/ml in dPBS for 45 mins at RT on a slow rocking platform, in the dark. Cells were washed 3x 5 mins in wash buffer at RT, in the dark, on a rocking platform, to remove any unbound secondary antibody. 300 nM 4',6-diamidino-2-phenylindole (DAPI) *(Life Technologies, D3571)* in dPBS was added for 20 mins at RT on a slow rocking platform. 1x 5 min wash with wash buffer removed any unbound DAPI. 1x 5 min dPBS wash removed any remnants of Tween-20. 1x 2 min double-distilled water (ddH_2O) wash removed any salt crystals from the cells. When using the 8-well EZ- glass slides *(MERCK, PEZGS0816)*, the plastic frame clips were removed and 1 drop of mounting media *(Agilent, S3023)* was added to each well, and a 22x50mm glass cover slip *(ThermoFisher Scientific, BB02200500AC13MNT0)* gently placed on top. Mounting media was left to set at RT, in the dark for 45 mins before imaging.

Table 2.1. PRIMARY ANTIBODIES FOR IF CHARACTERISATION OF hREC AND hRP

Primary Antibody hRP	Species	Code	Concentration
Alpha-Smooth Muscle Actin (**αSMA**)	Mouse	Abcam ab7817	5µg/ml
Platelet Derived Growth Factor Receptor-β (**PDGFR-β)**	Rabbit	Santa Cruz Biotech. sc-374573	0.8µg/ml
Neural/Glial Antigen-2 (**NG2**)	Rabbit	Merck ab5320	5µg/ml
Desmin	Rabbit	Abcam ab15200	1:200
Thymocyte Antigen (**CD90/Thy-1**)	Mouse	Abcam ab23894	2µg/ml
Primary Antibody hREC	**Species**	**Code**	**Concentration**
Von Willebrand Factor (**vWF**)	Rabbit	Abcam ab6994	21.5µg/ml
Vascular Endothelial Cadherin (**VE-cad**)	Rabbit	Abcam ab33168	1:200
Platelet Endothelial Cell Adhesion Molecule (**CD31/PECAM-1**)	Rabbit	Abcam ab28364	1:20
Zonula Occludens-1 (**ZO-1**)	Rabbit	ThermoFisher Scientific 61-7300	2.5µg/ml
Connexin 43 (**Cx43/GJA1**)	Rabbit	Abcam ab11370	3.5µg/ml
Conjugated Phallotoxin			
Phalloidin-647 (**F-actin**)		ThermoFisher Scientific A22287	0.22µM

Table 2.2. SECONDARY ANTIBODIES FOR IF CHARACTERISATION OF hREC AND hRP

Secondary Antibody	Species	Conjugate	Code	Concentration
Goat anti-	Rabbit	488	Invitrogen A11008	5µg/ml
Goat anti-	Mouse	488	Invitrogen A11029	5µg/ml
Goat anti-	Rabbit	594	Invitrogen A11012	5µg/ml
Goat anti-	Mouse	594	Invitrogen A11005	5µg/ml
Goat anti-	Rabbit	647	Invitrogen A21244	5µg/ml
Goat anti-	Mouse	647	Invitrogen A21235	5µg/ml

2.3.5 FLOW CYTOMETRY

Flow cytometry was performed to explore the different cell surface receptors expressed by hRP and hREC. A panel of cell-surface antigens was selected to distinguish EPCs from mature ECs or cells of haematopoietic origin[153]. Cells from T75 flasks were trypsinised (See section 2.3.3), neutralised using double the amount of complete media, and then spun at 1,200RPM for 8 mins. The cell pellet was re-suspended in 1ml of warmed Fluorescence-activated cell sorting (FACS) buffer (dPBS + 1% FBS) for counting using a haemocytometer. $1x10^5$ cells/tube were re-suspended into 1.5ml Eppendorf tubes *(Starstedt, 72.690.001)* in a total volume of 100µl FACS buffer. Fluorescent conjugated antibodies against 7 proteins of interest and 3 Isotype controls (Table 2.3) were added at 5µl/tube, or 6µl/tube for CD34. Tubes were agitated for 5 seconds using a vortex on high speed, to consistently mix cells into solution with the conjugated antibodies. Cells were incubated with antibodies at 4°C in the dark for 30 mins. FACS buffer was added at 500µl/tube to wash the cells of excess antibody and tubes were spun at 400RCF for 8 mins. Supernatant was gently removed, avoiding disturbing the cell pellet. 300µl FACS buffer was added and each tube was mixed thoroughly by pipetting up and down several times, to disperse cell pellet. Before sampling in the flow cytometer, the contents of each tube was thoroughly mixed again using a high speed vortex.

Flow Cytometry was performed using a BD Accuri 6 machine and Accuri C6 software. Parameters for running flow were $1x10^4$ events, on slow fluidics. Un-labelled cells were used to exclude dead cells/cell debris by gating the population of interest, and all samples were measured against corresponding fluorescent IgG controls for fluorescein isothiocyanate (FITC), phycoerythrin (PE) and allophycocyanin (APC). Steric hindrance was first checked if two antibodies were analysed in the same sample. Results were reported as % of cells positive versus corresponding conjugated IgG control.

Table 2.3. CONJUGATED PRIMARY ANTIBODIES FOR FLOW CYTOMETRY

Primary antibody	Conjugate	Supplier/Code	Volume
IgG 1 kappa	FITC	Fisher Scientific, 15104218	5µl
IgG 1 kappa	PE	Fisher Scientific, 12611959	5µl
IgG 1 kappa	APC	Fisher Scientific, 12642059	5µl
CD34	FITC	Fisher Scientific, 12372223	6µl
CD31	APC	Fisher Scientific, 15577906	5µl
CD146	PE	Fisher Scientific, 15546896	5µl
CD14	APC	Fisher Scientific, 15517886	5µl
CD45	FITC	Fisher Scientific, 15556406	5µl
CD105	PE	Fisher Scientific, 15576846	5µl
CD90	APC	Fisher Scientific,17090942	5µl

2.3.6 GROWTH CURVES

To determine the growth rates of hREC and hRP, growth curves were set up for 21 days. Cells were seeded at $5x10^3$, $1x10^4$, $2x10^4$ and $4x10^4$ cells/well on 24 well plates (w/p) *(Corning, 3524)* , to determine the effect of seeding density and time on cell growth rate. At day 1, 3, 5, 7, 14 and 21 cells were washed and fixed in 10% NBF, permeabilised using 0.5% Triton-X and DAPI stained, and washed in preparation for microscopy (See section 2.3.4). To calculate an average cell number for each well, 5 images/well were captured at x10 magnification; centre, bottom, top, left and right, using the Nikon E-Ti fluorescent microscope. These coordinates were programmed into the Nikon E-Ti NIS Elements AR4.51.01 software to enable consistent imaging of each well across plates. Using ImageJ 1.51K software, a macro was recorded to enable automated counting of DAPI stained cell nuclei in each image (Figure 2.1). In brief, using ImageJ software the raw image was set to auto threshold, using 'Li'. The image was then inverted to black particles on white background, and black nuclei were counted using the 'analyse particles' option with size set to 50-800, to prevent any debris being counted as false positives. An average cell number/well was calculated using Prism 6 software, followed by average cells/cm^2, using cell count divided by the area of the image. At 10x magnification, the field of view of an image using the Nikon E-Ti was 0.0112cm^2.

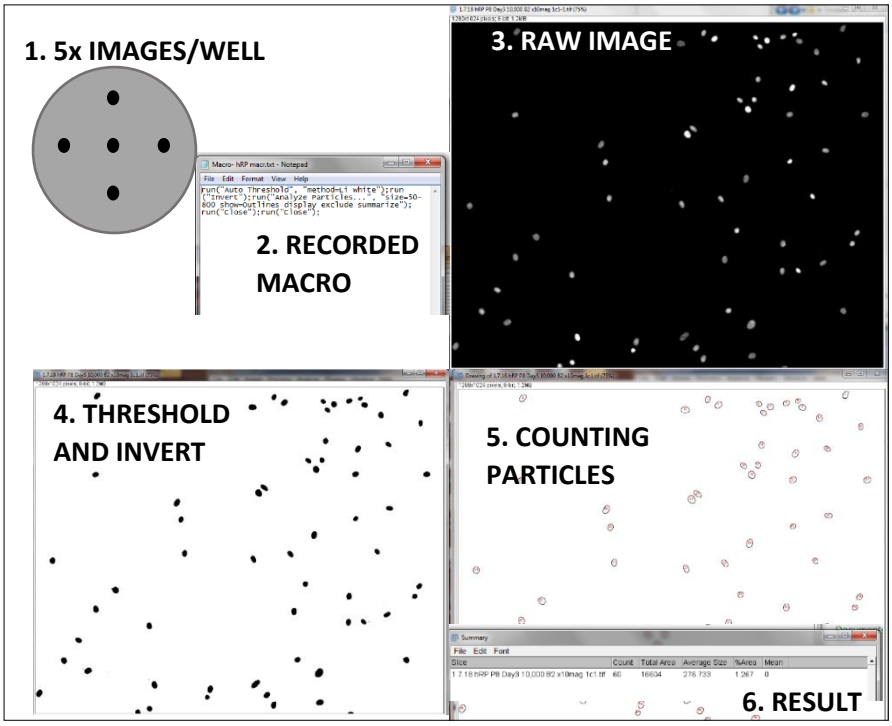

Figure 2.1. Automated cell counting

Screenshots of the process of writing a macro using ImageJ, to run automated cell counting. Images from 5 consistent points/well were taken using a Nikon E-Ti fluorescent microscope, and images were processed using ImageJ 1.51K software.

2.3.7 HEALTHY AND DIABETIC CONDITIONS

For all experiments, healthy conditions were defined as media containing 5.5mM glucose, and incubators set to 37°C, atmospheric oxygen (20%) and 5% CO_2. In order to optimise culture conditions to mimic healthy and diabetic glucose ranges, hRP were grown in 0-35mM [D+] glucose over 14 days, with 35mM mannitol included as an osmotic control. Diabetic conditions were defined as media containing 33mM glucose, and incubators with oxygen reduced to 2%. The diabetic conditions provided a double insult of high glucose with low oxygen, mimicking the *in vivo* environment in DR. However, during early stage disease, the tissue may be subjected to more subtle changes in either glucose and/or oxygen levels, so each parameter was tested individually during optimisation. Therefore, hREC and hRP were also grown in low O_2 (5%) with 5.5mM glucose, and atmospheric O_2 (20%) with 33mM glucose. It was established during optimisation that 5% O_2 had little effect on cell growth and morphology within the experimental time frame, therefore 2% O_2 was chosen for all subsequent diabetic conditions using the transwell inserts. Antibodies used to explore cellular changes in healthy and diabetic conditions are outlined in Table 2.4.

Table 2.4. PRIMARY ANTIBODIES FOR OXIDATIVE STRESS AND ANGIOGENIC RESPONSES

Primary antibody EPC	Species	Code	Concentration
SOD-1	mouse	MABC684	1:200
SOD-2	mouse	A21990	5µg/ml
HIF1-α	mouse	ab199004	1µg/ml
Ang-2	rabbit	ab153934	7.2µg/ml
VEGF-R2	mouse	ab9530	1:200
VEGFA	mouse	ab1316	5µg/ml

2.3.8 METABOLIC ACTIVITY

Cell metabolic activity was measured using resazurin sodium salt *(Sigma, R7017-5G)*. A filtered stock solution of resazurin was made to 0.1mg/ml with dPBS and stored at 4˚C in the dark. For use in assays, stock solution was diluted 1:10 with serum-free culture medium to working concentration of 0.01mg/ml. Growth medium was aspirated from cells and serum-free resazurin medium was added. This procedure was performed in the dark in a sterile hood. Cells were placed back into the incubator, in the dark for 2H for the assay to develop. The incubation time was optimised by initially testing 1-4H for both hREC and hRP. After 2H, 100µl of resazurin media from each well was transferred to a black 96 w/p *(Greiner, 655079)* in duplicate, to account for technical error. Plates were analysed immediately or sealed using para-film and stored at 4˚C in the dark for up to 7 days. Plates were read using a FLUOstar Optima plate reader *(Optima, Serial 413-3363)* with BMG Lab Tech *(Optima, 2.20)* plate reader software, set to excitation 560nm and emission 590nm to measure fluorescence, using endpoint settings with 10 flashes/well. Resazurin media only (blanks) were included on each plate and the average of the blanks was deducted from each reading. Gain was adjusted for each plate to allow comparisons between plates, using a standard curve (Figure 2.2). Assay results were assessed using Optima Data Analysis MARS software and transferred to GraphPad Prism 6 for analysis.

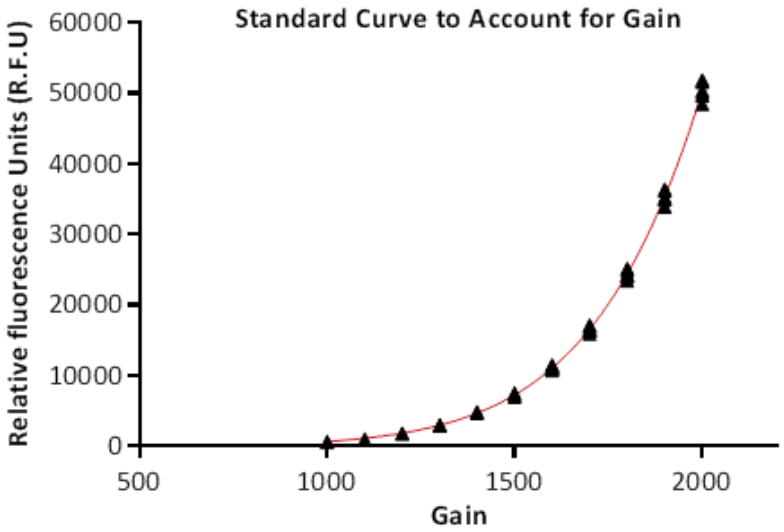

Figure 2.2. Standard curve to adjust for gain

Graph to show how a standard curve was used to allow results from resazurin assays to be adjusted for different gains. This enabled each plate to be read at its optimal range, depending on weak/strong signal, whilst still allowing comparisons across plates. The curve was produced by using the 'fit non-linear regression curve' application on GraphPad Prism 6 software. The equation for the curve is $Y=3E\text{-}17x^{6.4092}$. $R^2=0.9993$.

2.3.9 CO-CULTURE

Transwell inserts with semi-permeable membranes made from polyethylene terephthalate (PET) and polyester, with 0.4µm or 1µm pores were sampled for their suitability for use in the co-culture model. hRP and hREC were seeded individually to assess cell attachment and viability. The inserts which provided superior imaging capabilities, to enable long term monitoring under the light microscope, and sufficient cell attachment and viability were 24 w/p hanging PET transwell membranes with 1µm pores *(MERCK, MCRP24H48)* (Figure 2.3). During optimisation, transwell inserts were coated with collagen IV and laminin III to provide an ECM to aid in initial cell attachment, although this was determined to be unnecessary because cells attached well without protein coating.

A simplified example of the hRP:hREC interaction is shown in Figure 2.4. hRP and hREC were seeded as mono- and co-cultures to enable direct comparisons between cells grown in isolation versus co-cultures. To mimic the ratio of coverage of EC:pericytes in the retina, hRP and hREC were seeded at 1:1 ratio. Inserts were placed upside-down in the inside surface of 60ml pot lids *(Scilabware, 360104)* (Figure 2.5). $2x10^4$ hRP were seeded on the upside-down transwell inserts, in a 50µl bubble of complete DMEM with 10% FBS. A large drop of dPBS was added to each 60ml pot lid for humidity. Pots were loosely screwed on to lids to ensure

sterility when transferring the upside-down inserts into the incubator, at 37°C for 1H to allow hRP to adhere to the PET membrane. Transwell inserts were then gently inverted and placed into 24 w/p's. Each well in the plate was filled with 900µl of MV medium with 10% FBS. hREC were seeded at $2x10^4$ cells/insert in 200µl MV with 10% FBS medium on to the apical surface on the inserts, and plates were moved to the incubator overnight.

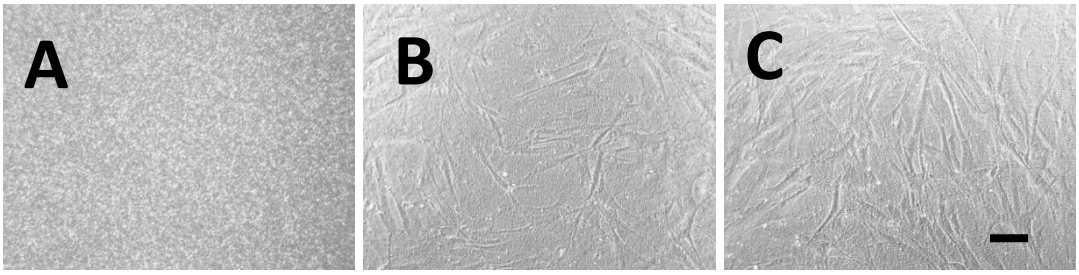

Figure 2.3. Selecting appropriate transwell insert material

Imaging quality of hRP, P10 on underside of different transwell inserts. **A**) 0.4µm pore, MERCK PET 24 w/p transwell insert was opaque, therefore not possible to monitor cells. **B**) 1µm pore, MERCK PET 24 w/p transwell insert provided sufficient cell attachment and was translucent, enabling cell monitoring. **C**) 0.4um pore, Corning Polyester 12 w/p transwell insert provided sufficient cell attachment and was translucent, enabling cell monitoring. **A** and **B** were seeded with $3x10^3$ hRP and grown for 24H. **C** was seeded with $9x10^3$ hRP, and grown for 24H. Scale bar= 200um.

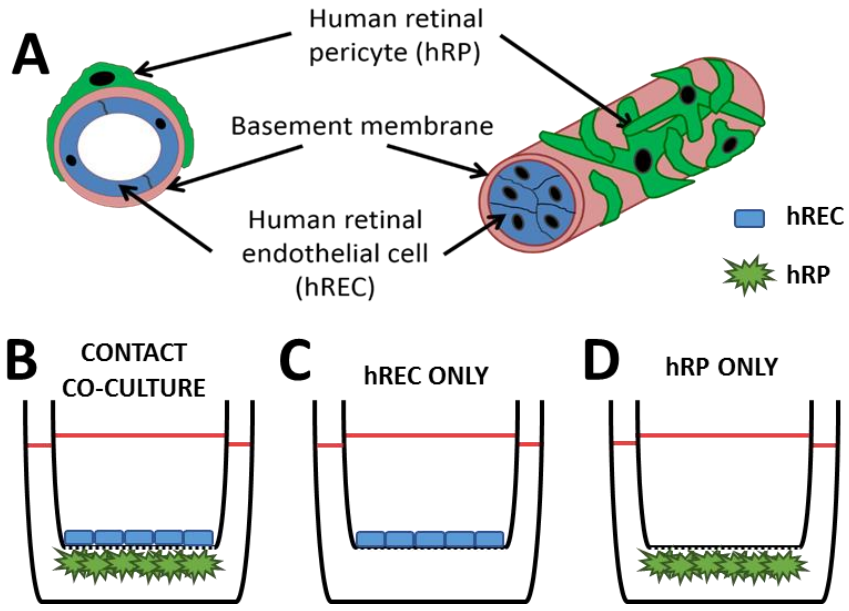

Figure 2.4. Basic anatomy of retinal capillary and mono-/co-culture design

A) Schematic of the basic anatomy of a retinal blood capillary, with hRP wrapping around hREC, sharing a BM. **B**) **Co-Culture:** $2x10^4$ hRP seeded on underside, $2x10^4$ hREC seeded on apical surface of PET membrane. **C**) **hREC only:** $2x10^4$ hREC seeded on the apical surface of the PET membrane. **D**) **hRP only:** $2x10^4$ hRP seeded on the underside of the PET membrane. All models were in MV medium with 5% FBS and either 5.5mM or 33mM glucose for healthy or diabetic conditions.

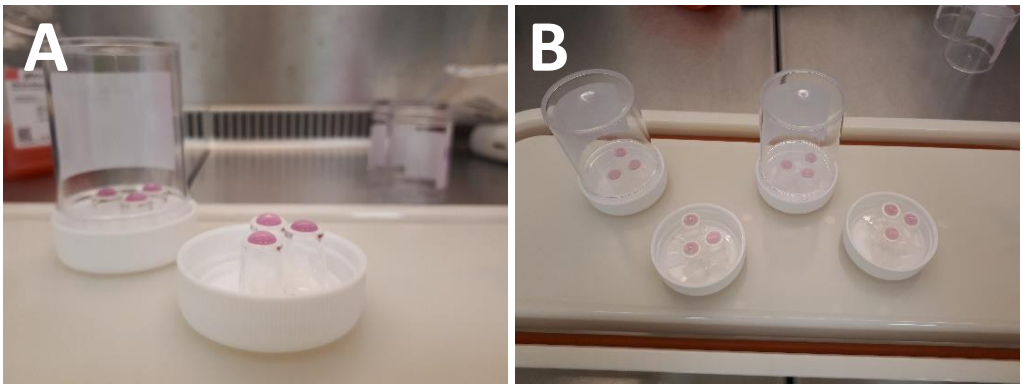

Figure 2.5. Seeding hRP on to the underside of the PET transwell inserts

Transwells were placed upside down in sterile 60ml pot lids with small volume of dPBS on lid. hRP were seeded on upside-down transwell inserts in a 50µl bubble of complete DMEM (**A**). Transwells were transferred to incubator in 60ml pot lids, with 60ml pots loosely secured, on a sterile tray (**B**). hRP required 45 mins to 1H to adhere, before inserts were inverted and hREC were seeded at the same density on the apical side.

The experimental timescale of the mono-/co-culture models is outlined in (Figure 2.6). In brief, after 12-24H, inserts were transferred to a new 24 w/p to prevent any detached hRP (which may re-attach to the TC plastic well) from interfering with the co-culture model. At this point, the whole model was switched to MV medium with 5% FBS. 72H after seeding, inserts either remained in physiological healthy conditions or were transferred to 2% oxygen and 33mM glucose, mimicking a diabetic condition. Cells were cultured for up to 21 days in healthy or diabetic conditions.

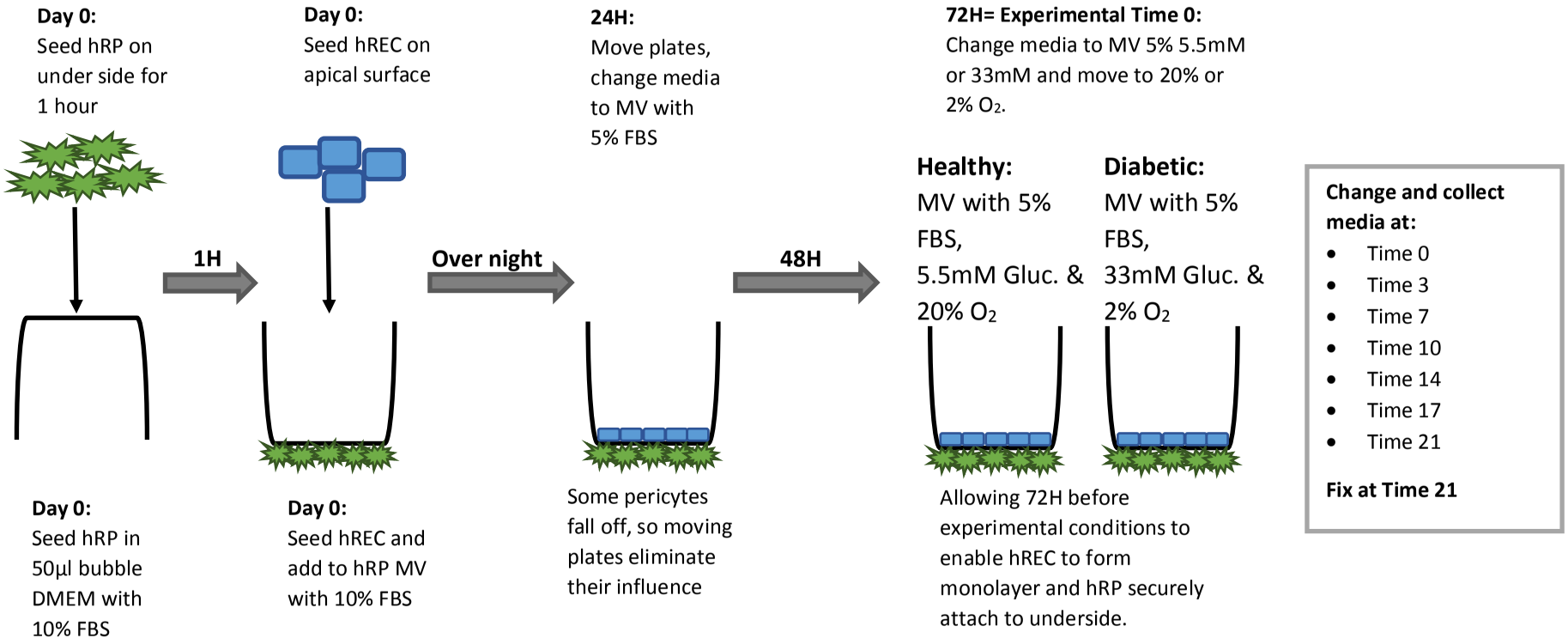

Figure 2.6. Timescale of experimental set-up

Schematic of mono-/co-culture set-up of hREC and hRP, from seeding cells at day 0, transferring cells to diabetic conditions at 72H (experimental time 0), and culturing for a further 21 days.

2.3.10 CELLTRACKER LABELLING

To enable monitoring of attachment and growth of hRP and hREC on the PET membranes, CellTracker dye was used. To aid visualisation of both cell-types in co-culture, two different coloured cell trackers were used. According to manufacturer's instructions, 50µg CellTracker Red (CTR) *(Invitrogen, C34552)* was dissolved in 7.2µl DMSO to make stock concentration of 10mM. 1mg CellTracker Green (CTG) *(Invitrogen, C2925)* was dissolved in 215.1µl DMSO to make stock concentration of 10mM. Confluent cells were trypsinised and spun to form a cell pellet (See section 2.3.3) of ~$1x10^6$. The cell pellet was re-suspended in 1ml serum-free medium. 1µl CTG stock was added to hREC suspension and 1µl CTR stock was added to hRP suspension. After thorough mixing, tubes were placed in the incubator for 30-45 mins for trackers to incorporate into cells. Tubes were spun at 1,200PRM for 5 mins and CellTracker working solution was removed. Cells were re-suspended in complete medium and counted using a haemocytometer for required seeding density. CellTracker dyes allow for optimal cell monitoring for up to 72H. Beyond that time frame, dye becomes weaker, due to its transfer to daughter cells during proliferation.

2.3.11 BARRIER TESTING (TEER)

To determine if hREC formed a monolayer with functional barrier properties on the apical surface of the transwell inserts, trans-endothelial electrical resistance (TEER) measurements were performed using a Millicell® ERS-2 Voltohmmeter. This measures membrane potential and resistance of ECs in culture. TEER measurements of mono- and co-cultures were taken from 0-21 days. Briefly, electrodes were washed in 70% ethanol for 30 mins, to sterilise. Electrodes were removed from ethanol and left to dry within sterile hood, on sterile surface. To record readings, electrodes were attached to Millicell® ERS-2 Voltohmmeter and switch was set to measure Ohms. The silver/silver chloride (Ag/AgCl) pellet on each electrode tip sat below culture media level when introduced to the insert, but not touching. Duplicate readings were taken for: media only, empty transwell insert in media, and mono/co-cultures. This method is temperature sensitive, so measurements were taken quickly, or for large sample numbers, one set of readings was taken followed by an incubation period to equilibrate to 37°C before continuing with remaining readings. For reporting results, all readings were normalised against an empty insert, and divided by the surface area of the transwell insert to report Ohms/cm^2. This reduced the error associated with increasing surface area, as previously reported for this technique[136].

2.3.12 HUMAN ANGIOGENESIS MULTIPLEX ARRAY

To explore changes in secreted proteins in the healthy and diabetic models over time, cell culture medium was collected from both the mono- and co-culture model at multiple time points (Figure 2.6). The Q-Plex Human Angiogenesis Array *(Quansys, 150249HU)* uses multiplex technology to measure 9 angiogenic proteins of interest. 100µl of media was collected from the apical, and 100µl from the outer compartments of the mono and co-culture models at 7 time points (Figure 2.4). The 200µl total volume was stored immediately in -80°C to prevent degradation of proteins of interest within the media and also to allow samples to be analysed collectively. The 9 proteins included in the Q-Plex Human Angiogenesis array, and their concentration range are outlined in (Table 2.5).

Table 2.5. CALIBRATOR RANGE IN Q-PLEX HUMAN ANGIOGENESIS ARRAY

Analayte	Calibrator Range	LLD
Ang-2	10000 - 13.72 pg/ml	3.9
FGF basic	5000 - 6.86 pg/ml	12.7
HGF	14000 - 19.2 pg/ml	7.2
IL-8	2000 - 2.74 pg/ml	2.7
PDGF-BB	4000 - 5.49 pg/ml	2.2
TIMP-1	10000 - 13.72 pg/ml	10.2
TIMP-2	20000 - 27.43 pg/ml	15.9
TNFα	4000 - 5.49 pg/ml	5.2
VEGF	2000 - 2.74 pg/ml	2.74

All components to perform the assay were supplied in the kit. Oxford Biosystems kindly loaned a rotational rocker, for slow rotational washes, an automated plate washer *(TECAN-Columbus Washer)* to enable consistent and gentle washes, and the Q-Plex TM Imager LS with PC *(Quansys, 104250GR)*, to perform image analysis on the 96-w/p's. To optimise dilution of samples to fit within the calibrator range, one plate was used with sample added at varying concentrations. 1:3 was chosen as optimal sample concentration. A multichannel pipette was used for all measurements to reduce technical error and pipette tips were pre-wetted before use, to prevent any liquid retention. According to the manufacturer's instructions, an 8-point calibration curve was prepared using the calibrator *(Quansys, 102655HU)* and the human sample diluent *(Quansys, 110957HU)*, and added to each plate to enable direct quantification of each analyte (Figure 2.7). Samples were defrosted, spun for 5 mins at 400xg then diluted 1:3 with human sample diluent e.g. mix 30µl sample with 90µl

diluent. 50µl/well of the calibration curve and all samples were loaded on to the Q-Plex Array 96-w/p *(Quansys, 150252HU)*, in duplicate, within 10 mins of preparation. The plate was covered with the seal provided, and placed on the rotational shaker at 500RPM, at RT for 1H. 20X Wash Buffer *(Quansys, 101158GR)* was used at 1X working concentration with ddH_2O for all washes. Table 2.6 outlines the settings used to programme the coordinates into the automated plate washer. Plates were washed 3x using the automated plate washer. 50µl of Detection Mix *(Quansys, 150256HU)* was added to each well and the plate was covered with a new seal and returned to the rotational shaker at 500RPM, at RT for 1H. The plate was washed 3x as described above. 50µl of Streptavidin-HRP 1X *(Quansys, 101173GR)* was added to each well, the plate was covered with a new seal and returned to the rotational shaker at 500RPM, at RT for 15 mins. Plates were washed 6x to remove any unbound Streptavidin-HRP. RT Substrate was prepared 15 mins prior to use, by combining 3ml of Substrate A *(Quansys, 101159GR)* with 3ml of Substrate B+ *(Quansys, 101120GR)*, gently mixed and kept at RT in the dark. 50µl of previously prepared substrate was added to each well and imaging was commenced within 15 mins.

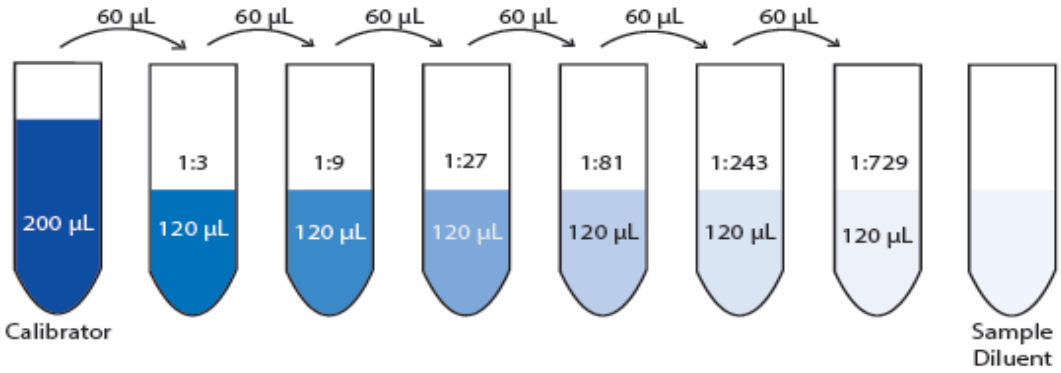

Figure 2.7. 8-point calibration curve for direct quantification

Instructions sourced from Quansys Q-Plex Human Angiogenesis instruction manual. Diagram showing how to create 8-point calibration curve, which must be plated in duplicate on each 96 w/p to enable direct quantification of analytes.

For imaging, the 96 w/p was placed into the Q-Plex TM Imager LS and Q-View Imager Pro Software was used. Exposure time was set to 270 seconds, with standard image processing. Ensuring correct well alignment on the software, images were captured and stored at multiple exposure times. For image analysis, by following software manual instructions to label samples with dilution factor, Q-View Imager Pro provided automated concentration calculations which were exported to GraphPad Prism 6 for statistical analysis.

Table 2.6. INSTRUCTIONS TO PROGRAMME AUTOMATED PLATE WASHER

INSTRUCTION	CO-ORDINATES
Plate	96 well, Greiner, clear flat bottom
Dispense Position	20
Dispense Rate	1
Aspiration Position	1:-36 2:-35
Aspiration Rate	2mm/sec for 2 seconds
Height	128
Wash Bottom	20
Wash Overflow	-6
Run 3x for 3x washes	

2.3.13 HUMAN ANGIOGENESIS ANTIBODY BLOT ARRAY

The Human Angiogenesis Antibody Blot Array *(Abcam, ab134000)* enabled detection of 20 cytokines in one blot, which is less labour intensive, uses fewer resources, and is more economically viable than the more traditional methods such as 2D SDS-PAGE or mass spectrometry. However unlike the multiplex data, these blot arrays do not provide concentrations, only amount relative to positive control. Therefore these data provide a more economical technique to further validate the results from the expensive Quansys multiplex array data. The 20 cytokines in this blot array and a summary of their biological function are listed in Table 2.7.

Table 2.7. ANALYTES IN Q-PLEX HUMAN ANGIOGENESIS ARRAY

ANALYTE	FUNCTION
Angiogenin	Interacts with the actin in ECs resulting in cell migration, proliferation, invasion, and formation of tubular structure via upregulation of proteases and plasmin that degrade the fibronectin and laminin layer of the BM.
Epidermal growth factor **EGF**	Binds to its receptor EGF-R, resulting in cell proliferation, differentiation and survival.
Epithelial Cell-derived Neutrophil-activating Peptide **ENA-78**	Is produced following stimulation of cells with the inflammatory cytokines IL-1 or TNF-α and has been implicated in connective tissue remodelling and regulation of neutrophil homeostasis.
Basic Fibroblast Growth Factor **bFGF**	Has broad mitogenic and cell survival properties and is involved in a variety of biological processes, including; cell growth, morphogenesis and tissue repair. During wound healing heparan sulfate degrading enzymes activate bFGF, resulting in the formation of new blood vessels.
Growth-Regulated Oncogene **GRO**	Involved in the processes of angiogenesis, wound healing, inflammation and tumorigenesis via signaling through the chemokine receptor CXCR2.
Interferon Gamma **IFN-γ**	Vital in innate and adaptive immunity against viral, some bacterial and protozoal infections. IFNγ has immunostimulatory and immunomodulatory effects and abnormal IFNγ expression is associated with a number of auto-inflammatory and autoimmune diseases.
Insulin-Like Growth Factor-1 **IGF-I**	Works downstream of growth hormone, has growth-promoting effects on most cell-types, showing insulin-like effects via the IGF-1R and insulin receptors. IGF-1 can also regulate DNA synthesis.
Interleukin-6 **IL-6**	Acts as both pro- and anti-inflammatory cytokine. IL-6 is produced by adipocytes, therefore obese individuals have higher endogenous levels. Its' anti-inflammatory action is mediated through inhibitory effects on TNF-α and IL-1 and activation of IL-1Ra and IL-10.
Interleukin-8 **IL-8**	A potent promoter of angiogenesis. In target cells IL-8 induces a series of physiological responses required for migration and phagocytosis.

Leptin	Outside its main function of promoting satiety in the brain, in the periphery, leptin modulates energy expenditure and activation of immune cells, β-islet cells, and growth factor.
Monocyte Chemoattractant Protein-1 **MCP-1**	Is anchored in the plasma membrane of ECs and recruits monocytes, memory T-cells, and dendritic cells to the sites of inflammation, produced by tissue injury or infection.
Platelet-Derived Growth Factor-BB **PDGF-BB**	A potent mitogen for mesenchymal cells; fibroblasts, smooth muscle and glial cells. Produced primarily by platelets but also other cells; activated macrophages, smooth muscle and ECs.
Placental Growth Factor **PlGF**	A member of the VEGF sub-family, with key roles in angiogenesis and vasculogenesis, mainly during embryogenesis. Increase in PlGF has been associated with increased inflammation and neovascularisation.
RANTES	A chemotactic cyto/chemokine for T-cells, eosinophils and basophils, and recruits leukocytes to sites of inflammation.
Transforming Growth Factor Beta-1 **TGF-β1**	A secreted protein involved in: control of cell growth, proliferation, differentiation and apoptosis. Dysregulation of TGF-β signalling can result in apoptosis. Has different effects on different cells, at different stages of maturity.
Tissue Inhibitor of Metalloproteinases-1 **TIMP-1**	A natural inhibitor of the matrix metalloproteinases (MMPs), can promote proliferation in numerous cell-types, and may have an anti-apoptotic function.
Tissue Inhibitor of Metalloproteinases-2 **TIMP-2**	A natural inhibitor of MMPs, and can directly suppress the proliferation of ECs, therefore has role in maintaining homeostasis by suppressing proliferation of quiescent cells in response to angiogenic factors, and by inhibiting protease activity during remodelling of ECM.
Thrombopoietin	Produced in the liver by parenchymal cells and sinusoidal ECs, as well as in the kidney by proximal convoluted tubule cells and involved in differentiation of bone marrow cells into megakaryocytes, and further maturation of these cells.
Vascular Endothelial Growth Factor **VEGF**	In adulthood, produced by cells to create new blood vessels after injury, muscle following exercise, and new vessels to bypass blocked or pathologically damaged vessels.
Vascular Endothelial Growth Factor-D **VEGF-D**	Is active in angiogenesis, lymphangiogenesis, and EC growth via activation of VEGFR-2 and VEGFR-3 receptors.

2.3.14 MICROSCOPY

The Nikon DIAPHOT microscope with Top View 3.7 software was used to capture phase contrast images of cells in culture. The Nikon E-TI microscope, with NIS Elements AR 4.51.01 software was used to perform cell counts, for live cell imaging and to image cells that were fixed and prepared for IF staining on 24 w/p's. The Zeiss Confocal M800 microscope with ZEN Blue 2.3 software was used for imaging cells grown on glass slides, and cells grown on PET membranes, mounted on glass slides. For co-culture PET membranes, after IF procedure described above, membranes were very delicately cut away from transwell frames using a scalpel. For mono-cultures, membranes were transferred directly on to glass slides, cells facing upwards, using mounting media underneath and on top, and covered with a glass coverslip. For co-cultures, membranes were transferred on to a thin glass coverslip using mounting media underneath and on top, and sandwiched with another glass coverslip on top. For imaging co-cultures, this sandwiching technique allowed the membrane to be flipped over on to glass slides, to provide best quality images of both sides during confocal microscopy.

2.3.15 STATISTICAL ANALYSIS

All statistics were analysed using GaphPad Prism 6 software. Significance level of $p<0.05$ was set for all experiments. Data were reported as mean, with standard deviation (SD). Two-Way AVONA with Sidak's multiple comparisons post-hoc test was used to report multiplexing data. Statistical analysis was not performed on human angiogenesis blot data (Figure 2.33) due to n=2.

2.4 RESULTS

2.4.1 hRP AND hREC RETAINED THEIR PHENOTYPE THROUGHOUT PASSAGING UP TO P10 *IN VITRO*

hRP and hREC were cultured *in vitro* and used in experiments from P3-10. No change in cell morphology of hRP and hREC from P3-10 suggests cells did not transition within experimental timeframe (Figure 2.8 A and B). hRP retained a large, irregular-shape, with finger-like projections (Figure 2.8 A). hREC retained a smaller, cuboidal and more uniform size and shape, and formed a monolayer sheet when confluent (Figure 2.8 B). hRP narrowed and elongated as the cells became more confluent.

2.4.2 IF ANALYSIS CONFIRMED hRP AND hREC EXPRESSED PHENOTYPE-SPECIFIC PROTEINS

IF analysis of hRP and hREC validated that both cell-types retained their phenotype *in vitro*, during normal cell culture conditions (Figure 2.9, Figure 2.10). IgG isotype controls were included to exclude non-specific staining. hRP in this study expressed NG2, Desmin and PDGFR-β, antibodies commonly used to confirm pericyte phenotype in culture[48] (Figure 2.9). hRP showed positive/negative expression for α-SMA and this a common phenomenon, described in the literature[50]. hRP also expressed CD90/Thy-1, which has been previously described by others[190]. Phalloidin was used to visualise the F-actin filaments to show organisation of components of the cytoskeleton. Some hRP expressed Ang-2.

hREC expressed CD31, vWF and Cx43 (Figure 2.10). vWF expression was localised to storage vesicles (Weibel-Palade bodies) in the cytoplasm of ECs and vWF is expressed constitutively by all ECs. CD31 is expressed by all mature ECs and is present at the border of cell membranes as an integral part of the cell junction. Typical pattern of CD31 expression on ECs can be observed in Figure 2.10. Positive expression of ZO-1 confirms TJs and VE-Cad confirms presence of adherens junctions, suggesting hRECs form cell-cell contacts with their neighbours, resulting in a monolayer with barrier function. Cx43 is a GJ protein and is present on hREC and is used in this study to monitor changes to the GJ complex during healthy or diabetic conditions.

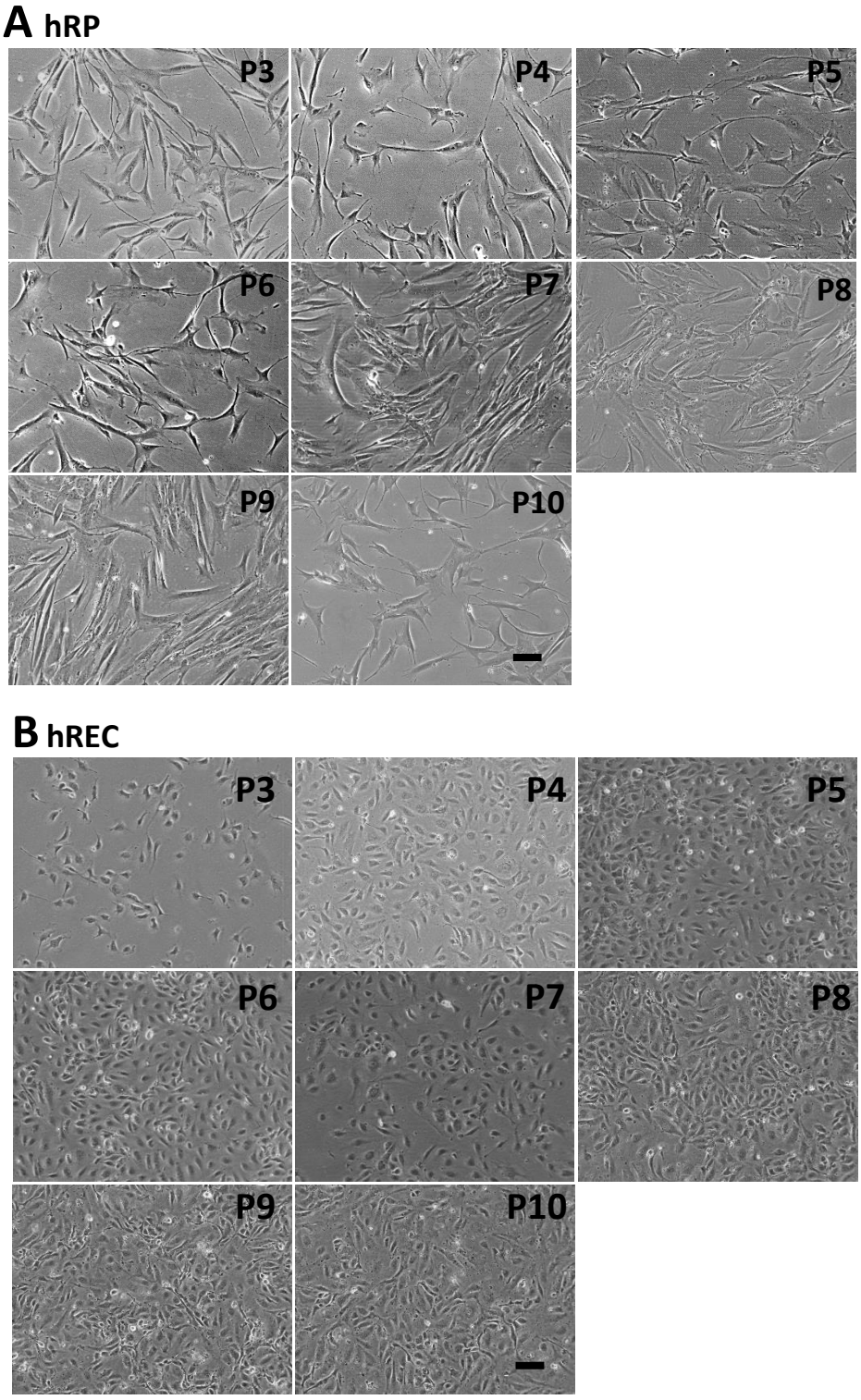

Figure 2.8. Light microscopy of hRP and hRP passage 3-10

Micrographs show both cell-types maintained their cell morphology from passage 3-10. **A**) hRP were large cells with non-uniform shape, with cytoplasmic finger-like projections. **B**) hREC were smaller, uniform, cuboidal-shaped cells which formed contact with neighbouring ECs. Phase contrast images were captured using Nikon DIAPHOT microscope, x10 objective. Scale bar =200µm.

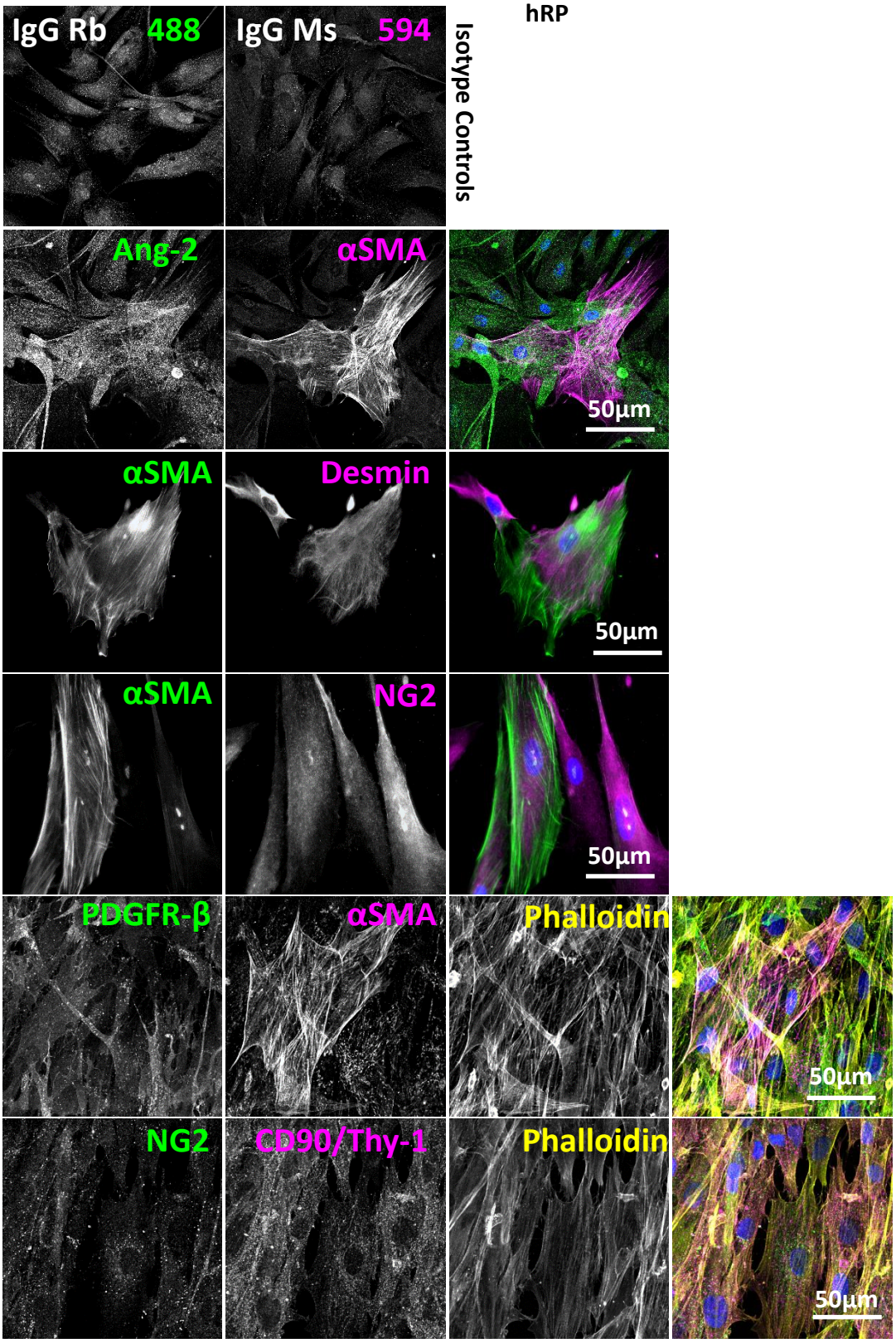

Figure 2.9. IF characterisation of hRP

Using double or triple labelling confocal microscopy, IF characterisation of hRP was performed using antibodies against common markers of hRP phenotype. hRP expressed NG-2, PDGFR-β, CD90/Thy-1 and desmin. hRP were +/- for αSMA. Phalloidin was used to explore the F-actin arrangement of the hRP cytoskeleton. IgG isotype controls were performed as negative controls for non-specific staining. Images were obtained using the Zeiss M800 confocal microscope, x40 oil objective. Scale= 50µm.

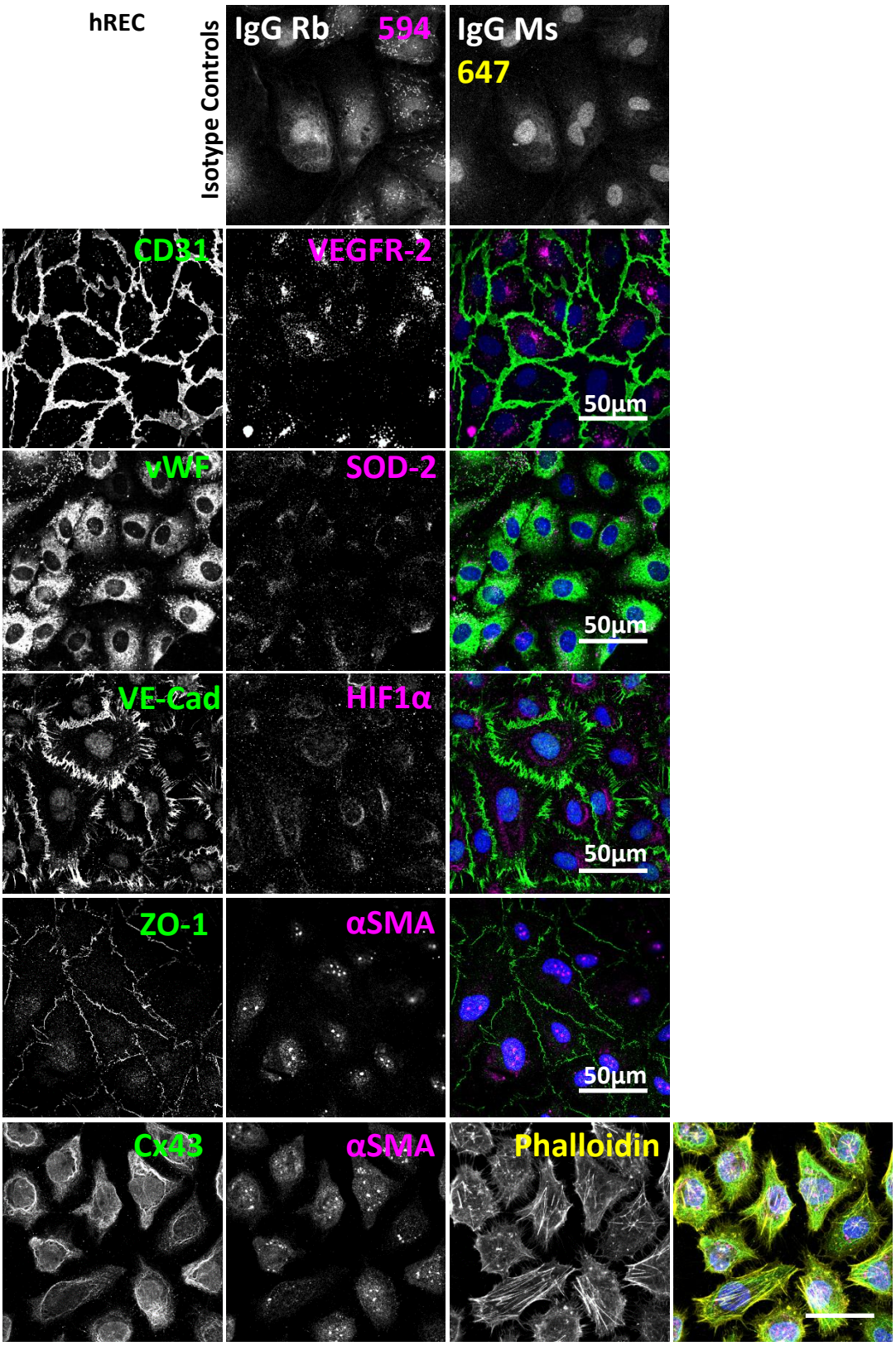

Figure 2.10. IF characterisation of hREC

Using double or triple labelling confocal microscopy, IF characterisation of hREC was performed using antibodies against common markers of hREC phenotype. hREC expressed CD31, vWF, VE-Cad, ZO-1 and Cx43. Phalloidin was used to explore the F-actin arrangement of the cytoskeleton. hREC were negative for αSMA. IgG isotype controls were performed as negative controls for non-specific staining. Images were obtained using the Zeiss M800 confocal microscope, x40 oil objective. Scale= 50µm.

2.4.3 FLOW CYTOMETRY ANALYSIS VALIDATED THE EXPRESSION OF CELL SURFACE MARKERS EXPECTED OF hRP AND hREC

CD31 and CD90 were used to confirm if hREC or hRP respectively were present in culture and also to determine the homogeneity of the *in vitro* cell populations. Cultures of hRP at P7 and hREC at P9 retained their expected morphology and reached 70-95% confluence before analysis. hRP were CD34 –ve, CD14 –ve, CD45 –ve, CD31 –ve, CD90 +ve (99.9%), CD105 +ve (98.9%) and CD146 +/-ve (26.3%) (Figure 2.11). 26.3% of hRP expressed CD146, which could in part be due to a heterogeneous population, considering the pluripotent nature of hRP. hRP were negative for both CD31 and CD34, validating they were not of EC-lineage. hREC were CD34 –ve, CD14 –ve, CD45 –ve, CD90 -ve, CD31 +ve (96%), CD105 +ve (100%) and CD146 +ve (99.9%) (Figure 2.12). CD31 is endothelial specific and 96% of hREC at P9 were CD31 positive, suggesting the primary hREC used in this model retained a strong EC phenotype throughout passaging. hREC were CD34 –ve, verifying they were a mature EC type, because more primitive or progenitor ECs, such as ECFCs, express the CD34 transmembrane protein. Both hREC and hRP were CD14 and CD45 negative, distinguishing them from hematopoietic cells. A summary of the flow cytometry results can be found in Table2.8.

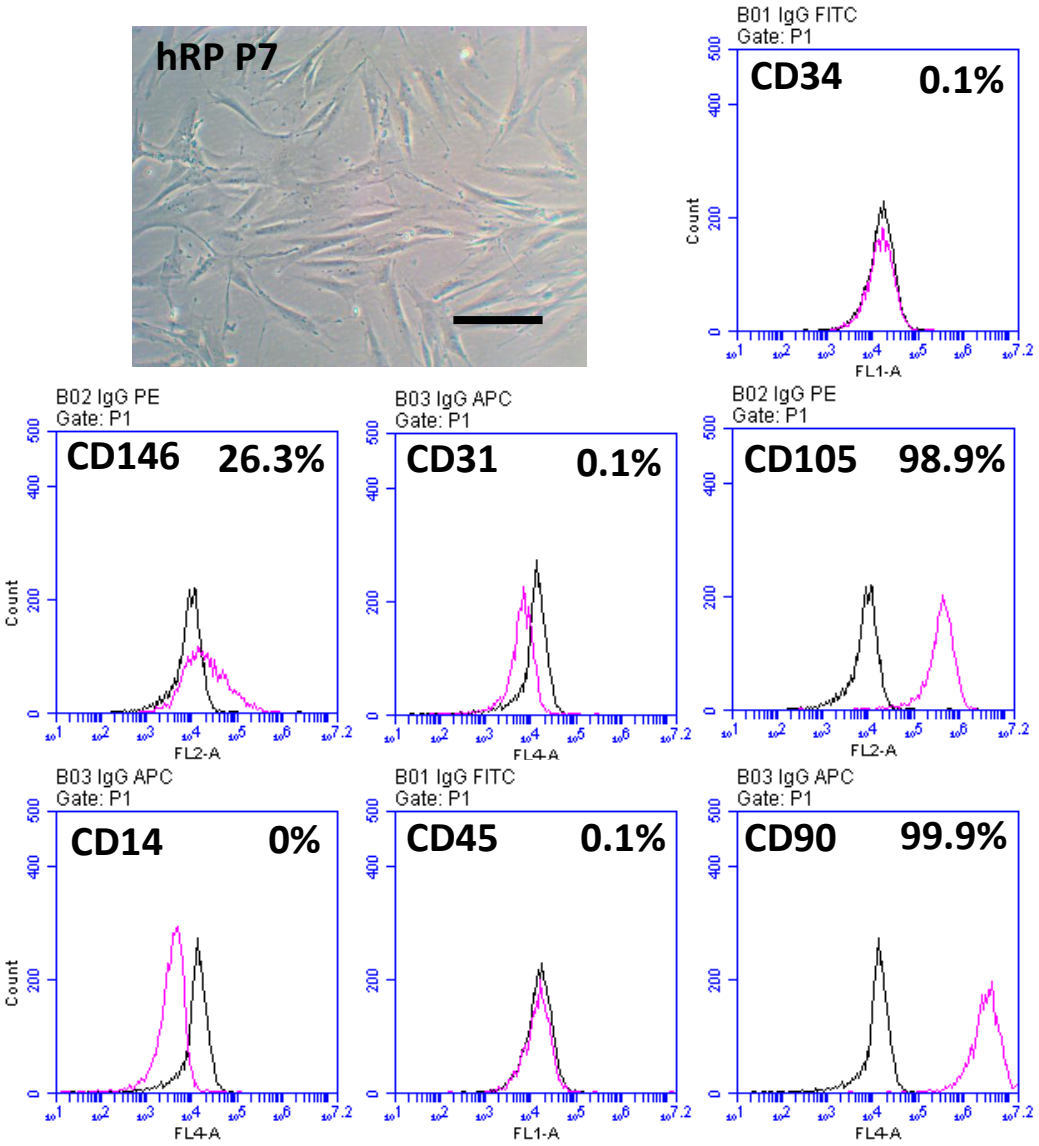

Figure 2.11. Flow cytometry analysis of hRP

Flow cytometry analysis of hRP at P7. Results were expressed as % positive expression of cell surface receptor (magenta) compared to IgG isotype control (black), for each corresponding fluorophore. hRP were CD34 –ve, CD14 –ve, CD45 –ve, CD31 –ve, CD90 +ve (99.9%), CD105 +ve (98.9%) and CD146 +/- ve (26.3%). Analysis was performed using BD Acuri C6. Phase image was captured using the Nikon Eclipse TS100 light microscope, x10 objective. Scale =200µm.

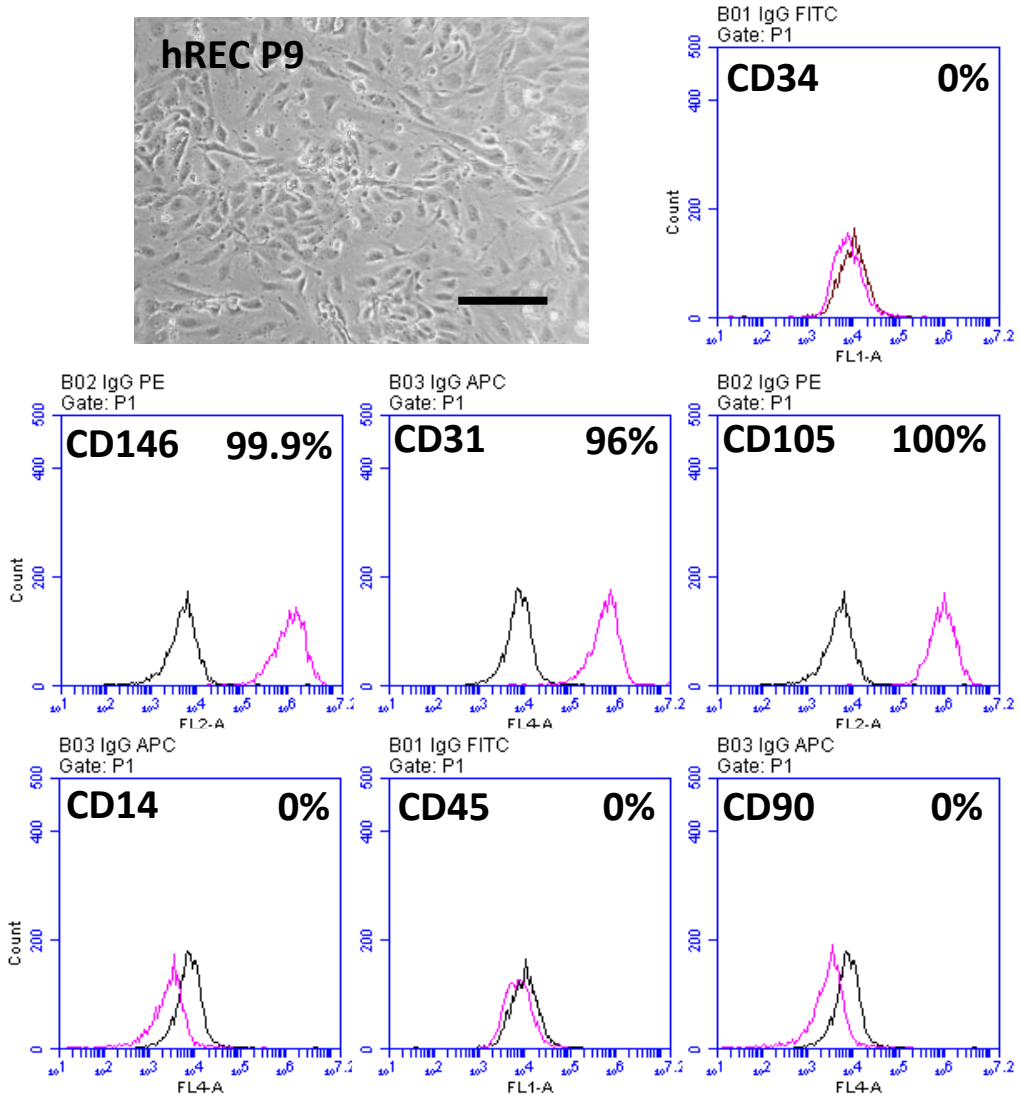

Figure 2.12. Flow cytometry analysis of hREC

Flow cytometry of hREC at P9. Results were expressed as % positive expression of cell surface receptor (magenta) compared to IgG control (black), for each corresponding fluorophore. hREC were CD34 –ve, CD14 –ve, CD45 –ve, CD90 -ve, CD31 +ve (96%), CD105 +ve (100%) and CD146 +ve (99.9%) Analysis was performed using BD Acuri C6. Phase image was captured using the Nikon Eclipse TS100 light microscope, x10 objective. Scale =200µm.

Table 2.8. OVERVIEW OF CELL SURFACE MARKER EXPRESSION ON hRP AND hREC

Cell Surface 'Marker'	hRP	hREC
CD34	X	X
CD146	X/✓	✓
CD31	X	✓
CD105	✓	✓
CD14	X	X
CD45	X	X
CD90	✓	X

2.4.4 SEEDING DENSITY AND LENGTH OF CULTURE IMPACTED GROWTH RATES OF THE TWO CELL-TYPES DIFFERENTLY

hREC and hRP grew at different rates, with hRP continuing to expand in number up to day 21, whereas hREC numbers increased until day 7, followed by a sharp decline from day 7-21 (Figure 2.13). Neither hREC nor hRP followed the typical sigmoid growth curve for cultured cells. When grown as monocultures, hRP continued to expand in number over the extended culture time period and depending on cell seeding density, did not reach a clear plateau even by day 21 (Figure 2.13A). This continued growth over an extended time may be in part due to their ability to become elongated and therefore take up less space on the culture dish, allowing continual expansion of cell numbers. The four seeding densities had very similar growth trends, suggesting seeding density between $5x10^3$-$4x10^4$ cells/well had little effect on the growth rates of hRP.

In contrast, the growth curves of hREC showed an initial small increase in cell number when seeded at ≤$2x10^4$ cells/well, followed by a sharp decline in cell number for all seeding densities after 7 days (Figure 2.13B). When seeded at $4x10^4$ cells/well, hREC exhibited cell loss at all time points. Overall this suggests there was less cell loss over time when cells were initially seeded at lower density (≤$2x10^4$ cells/well in a 24w/p). Seeding hREC at $5x10^3$, $1x10^4$ or $2x10^4$ cells/well resulted in gradual increase in cell number until day 7. Reporting the average, seeding density of $5x10^3$ cells/well surpassed cell number of those seeded at $1x10^4$/well, although there was no statistically significant differences between all seeding densities by day 7. These data suggest hREC seeded at a lower density grow at a faster rate in days 1-7 than those seeded at higher densities. During cell culture, hREC culture medium turned yellow indicating a drop in pH every 2-3 days. Therefore hREC metabolic activity may have caused toxic build-up of metabolites as well as lack of physical space for cell expansion. hREC reached the death phase by day 7 whereas pericytes did not appear to reach the death phase within the 21 day experimental timeframe.

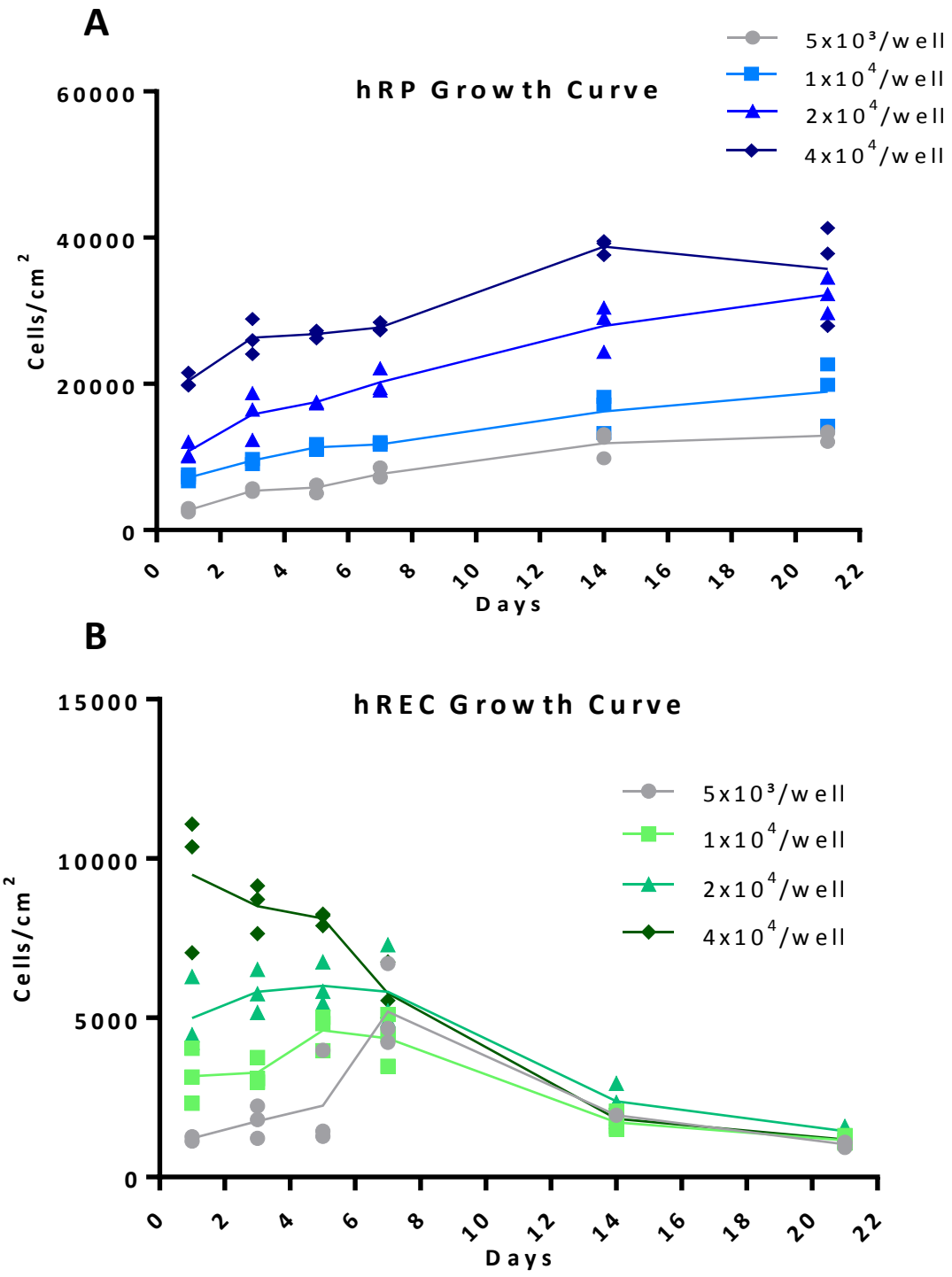

Figure 2.13. Growth curves of hRP and hREC at different seeding densities

hRP (**A**) and hREC (**B**) were seeded at $5x10^3$, $1x10^4$, $2x10^4$ and $4x10^4$cells/well on col. I coated 24 w/p's, to determine the effect of seeding density and time on cell growth rate. At time points day 1, 3, 5, 7, 14 and 21 cells were washed, fixed in 10% NBF, permeabilised using 0.5% Triton-X and DAPI stained, in preparation for cell counting using the Nikon E-Tie fluorescence microscope, x10 objective. ImageJ software was used to write a micro to perform automated cell counting. n=3 and lines represent average for each seeding density.

2.4.5 hRP METABOLIC ACTIVITY WAS NOT AFFECTED BY ADDITION OF FBS >5%

Images captured at days 2 and 12 show the effect of FBS on cell number (Figure 2.14A). At day 2 there were no significant differences in cell metabolic activity in hRP grown in 0-20% FBS (Figure 2.14B). From day 7-12 hRP grown in 0% FBS were significantly less metabolically active than those grown in 5-20% ($p<0.001$). Images captured at days 2 and 12 also show little/no increase in cell number in the hRP grown in 0% FBS (Figure 2.14A). hRP grown in 5-20% FBS all show increased in cell number, which all look comparable in the day 12 images. There was no statistically significant difference in the metabolic activity of hRP in 5, 10, 15 or 20% FBS at any time point (Figure 2.14B). Therefore, these data lead to the decision to use 5% FBS in culture medium for hRP for all future experiments. General observations from the resazurin sodium salt metabolic activity assay suggested that, overall, hRP had relatively low metabolic activity when compared to hREC.

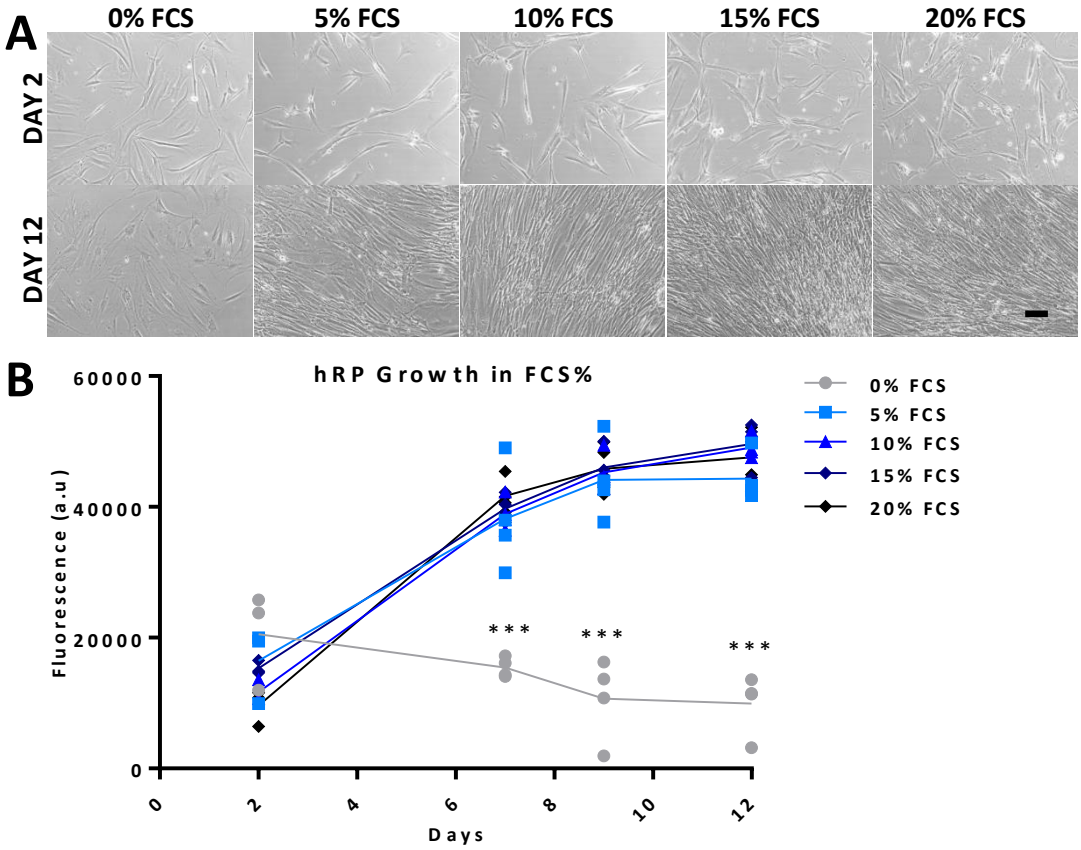

Figure 2.14. The effect of FBS concentration on hRP growth and metabolic activity

hRP P12, seeded at $2x10^4$ cells/well in 24 w/p's in 0-20% FBS, grown in physiologically healthy conditions (5.5mM Glucose with 20% oxygen) (**A**). Images were captured using the Nikon DIAPHOT microscope, x10 objective. Scale=200µm. Resazurin sodium salt was used to determine metabolic activity of hRP over 2Hs, in 0-20% FBS (**B**). 100µl resazurin of 0.01mg/ml media was analysed using a FLUOstar Optima plate reader at excitation 560nm and emission 590nm. Technical duplicates were read to account for error and n=4. Lines represent average fluorescence for each FBS concentration. For statistical analysis, one-way ANOVA with Tukey's post hoc test was performed. ***p<0.001.

2.4.6 GLUCOSE CONCENTRATION SIGNIFICANTLY AFFECTED hRP METABOLISM

hRP survived in all conditions up to day 14, and hRP in 5-35mM glucose appeared to increase in number over time(Figure 2.15A and B). Mannitol control and 0mM glucose had the lowest metabolic activity over 14 days, (Figure 2.15B), whilst the metabolic activity of hRP in 5-35mM glucose gradually increased from day 3 onwards. 5mM glucose was highlighted in red, as this is the average physiological glucose levels in humans, and 5.5mM glucose was used in healthy conditions for all following experiments. From day 5, the metabolic activity of hRP in the mannitol control and 0mM glucose were significantly different from all other conditions ($p<0.001$), and combined with images captured (Figure 2.15A), suggests the hRP survived but did not continue to expand in number when there was no glucose present.

Interestingly there were significant differences in the metabolic activity of 5mM glucose compared to 25mM ($p=0.0145$) and 30mM ($p=0.00330$) at day 5, but no difference compared with the highest glucose concentration 35mM (Figure 2.15C). By day 14 the metabolic activity of hRP in 15mM glucose was significant reduced compared to physiological 5mM ($p=0.0005$) and compared to the highest (35Mm) glucose concentrations ($p<0.0001$). 10mM ($p=0.0170$), 20mM ($p=0.0106$), 25mM ($p=0.0097$) and 30mM ($p=0.0041$) glucose all caused significant reduction in metabolic activity by hRP compared to 35mM glucose, but were not different from hRP grown in 5mM glucose. However, although not quantified, there appeared to be a similar number of hRP in 5mM-35mM glucose by day 14 (Figure 2.15A). Taken together these data support the hypothesis that at 35mM glucose levels there may be disruption to normal metabolic activity, which was not observed in the hRP grown in lower glucose concentrations. These data supported the decision to optimise future experiments to beyond 14 days and to use between 30-35mM glucose for diabetic conditions. Following reports from the literature, 33mM was chosen as diabetic glucose levels for *in vitro* experiments.

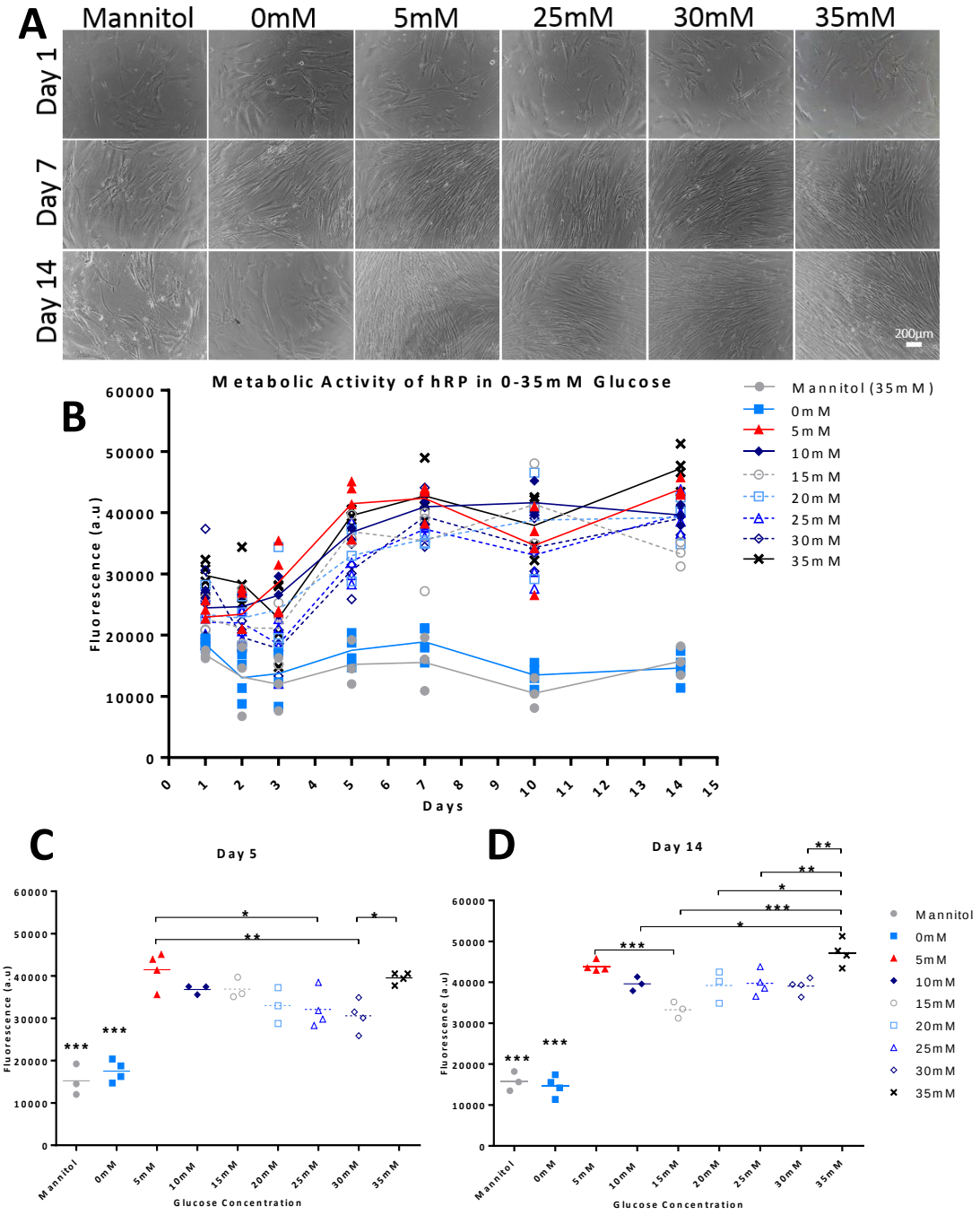

Figure 2.15. The effect of glucose concentration on hRP growth and metabolism

hRP P6, seeded at 2x10^4 cells/well in 24 w/p's, were grown in 20% oxygen, 10% FBS and 0-35mM glucose for 14 days. **A**) Images captured at D1, 7 and 14 using, the Nikon DIAPHOT microscope, x10 objective, scale=200µm. **B-D** Resazurin sodium salt was used to determine metabolic activity of hRP cultured in 0-35mM glucose. 100µl resazurin of 0.01mg/ml media was analysed using a FLUOstar Optima plate reader, at excitation 560nm and emission 590nm. Technical duplicates were read to account for error. **B**) Metabolic activity of hRP grown in 0-35mM glucose for 14 days. Lines represent average fluorescence for each glucose concentration. Red line highlights physiological glucose levels in humans. **C**) Day 5, where hRP grown in mannitol and 0mM glucose had significantly lower metabolic activity that those in 30 and 35mM, and there was no difference in hRP grown in 5mM and 35mM glucose. **D**) Day 14, where hRP grown in 35mM glucose had significantly higher metabolic activity than in all other concentrations. For statistical analysis, one-way ANOVA with Tukey's post hoc test was performed. n=3 or 4. *p<0.05, ** p<0.01, ***p<0.001.

2.4.7 hREC GROWN IN 5% OXYGEN AND 33mM GLUCOSE SHOWED ONLY MINOR DIFFERENCES IN PROTEIN EXPRESSION AT DAY 7

20% oxygen with 5.5mM glucose represented healthy conditions (Figure 2.16A) and 20% oxygen with 33mM glucose represented early stage diabetes, with hyperglycaemia present (Figure 2.16B). 5% oxygen with 5.5mM glucose represented disruption to blood supply, therefore reduced oxygen, but with normal physiological glucose levels (Figure 2.17A) and 5% oxygen with 33mM glucose represents the environment of damaged vessels with insufficient blood supply (reduced oxygen) and hyperglycaemia, i.e. a diabetic model (Figure 2.17B).

There was no noticeable difference in expression of SOD-1 and SOD-2 (Figure 2.16 and Figure 2.17). HIF1α becomes active once translocated to the nucleus, however it did not translocate to the nucleus in any of the experimental conditions. Therefore, oxygen levels were reduced to 2% for future experiments. VEGFR-2 binds soluble VEGF and is activated upon ligand-mediated dimerization. VEGFR-2 appeared to be upregulated in 5% oxygen with 33mM glucose, which represented the most diabetic-like conditions in this experiment (Figure 2.17B). ZO-1 was present across all conditions, which implied the hREC formed a functional barrier with their neighbouring cells, however in 5% oxygen (Figure 2.17) most of the ZO-1 was at the cell junctions, whereas in 20% oxygen (Figure 2.16) a higher proportion of ZO-1 was dispersed in the cell cytoplasm. In the right hand panel, vWF appeared unchanged across the four conditions and validated that hREC retain their endothelial phenotype *in vitro*. CD31 is expressed by all mature endothelium, and on the left panel CD31 was present in all conditions. In 20% oxygen with 33mM glucose, CD31 appeared to have more gaps in its expression on the hREC membrane. This suggests high glucose may have caused disruption to normal CD31 expression. Ang-2 becomes active when ECs undergo angiogenesis. The second panel shows Ang-2 expression was increased in 5% oxygen (Figure 2.17) compared to 20% oxygen conditions (Figure 2.16),. This suggests low oxgen appeared to drive an angiogenic response in hREC.

Overall, these data suggest the hREC cells were robust enough to withstand low oxgen and high glucose, and with the aim of inducing a more severe diabetic phenotype, oxygen levels for subsequesnt experiments were reduced to 2% and experiments were carried out for up to 21 days.

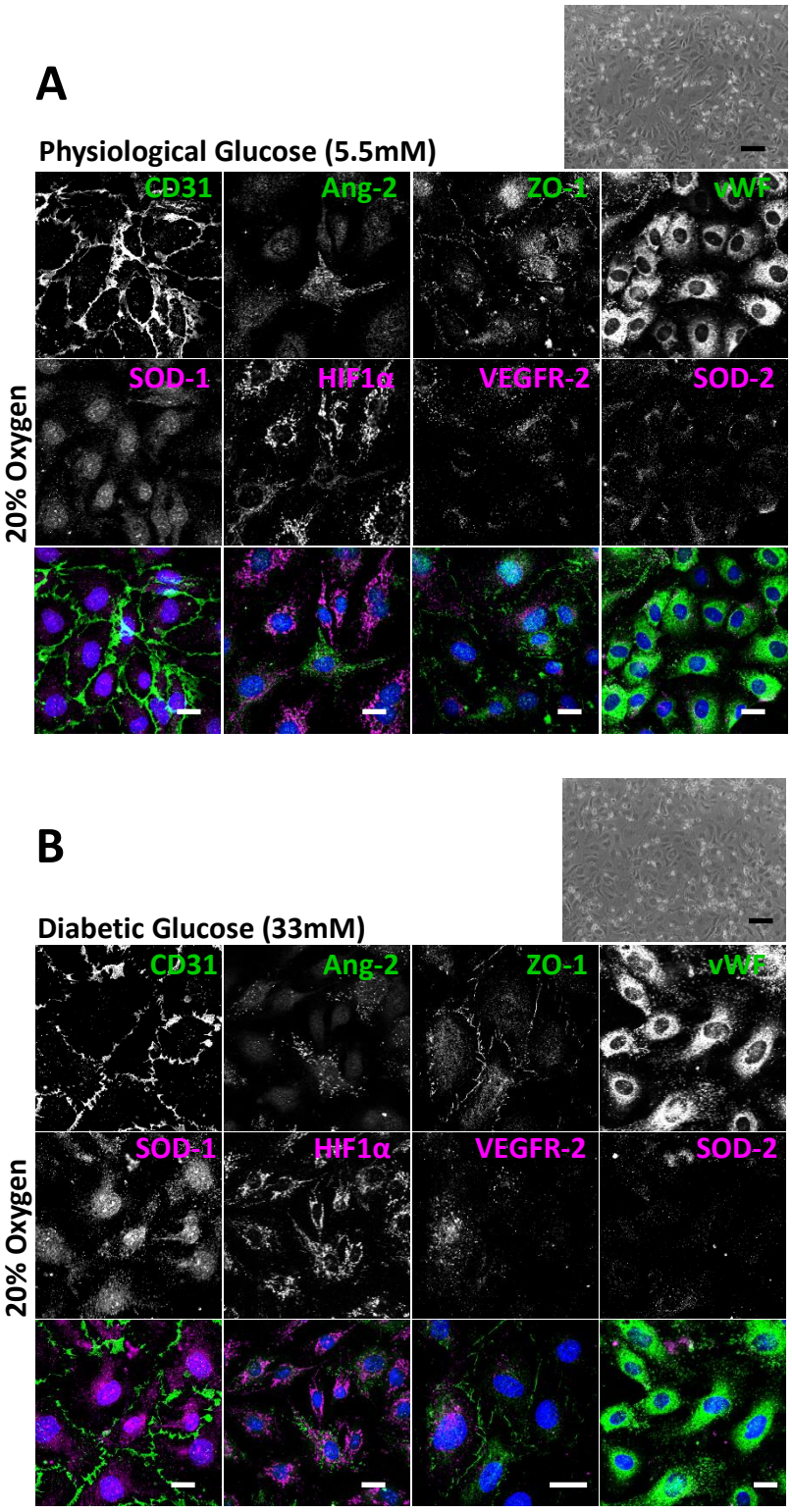

Figure 2.16. Assessing the effect of high glucose on hREC

hREC P8 were seeded on 8-well glass slides and left to adhere for 24H in healthy physiological conditions (20% oxygen and 5.5mM glucose). At 24H, hREC were either kept in healthy conditions (**A**) or moved to high glucose (33mM) conditions (**B**), and cultured for a further 7 days. CD31, ZO-1, vWF, SOD-1, SOD-2, Ang-2, VEGFR-2 and HIF1α expression were assessed to determine hREC phenotype, oxidative, angiogenic and hyperglycaemic stress response. Phase images were captured using Nikon DIAPHOT microscope, x10 objective, black scale bars =200µm. IF images were captured using the Zeiss M800 confocal microscope, x40 oil objective, white scale bars =20µm.

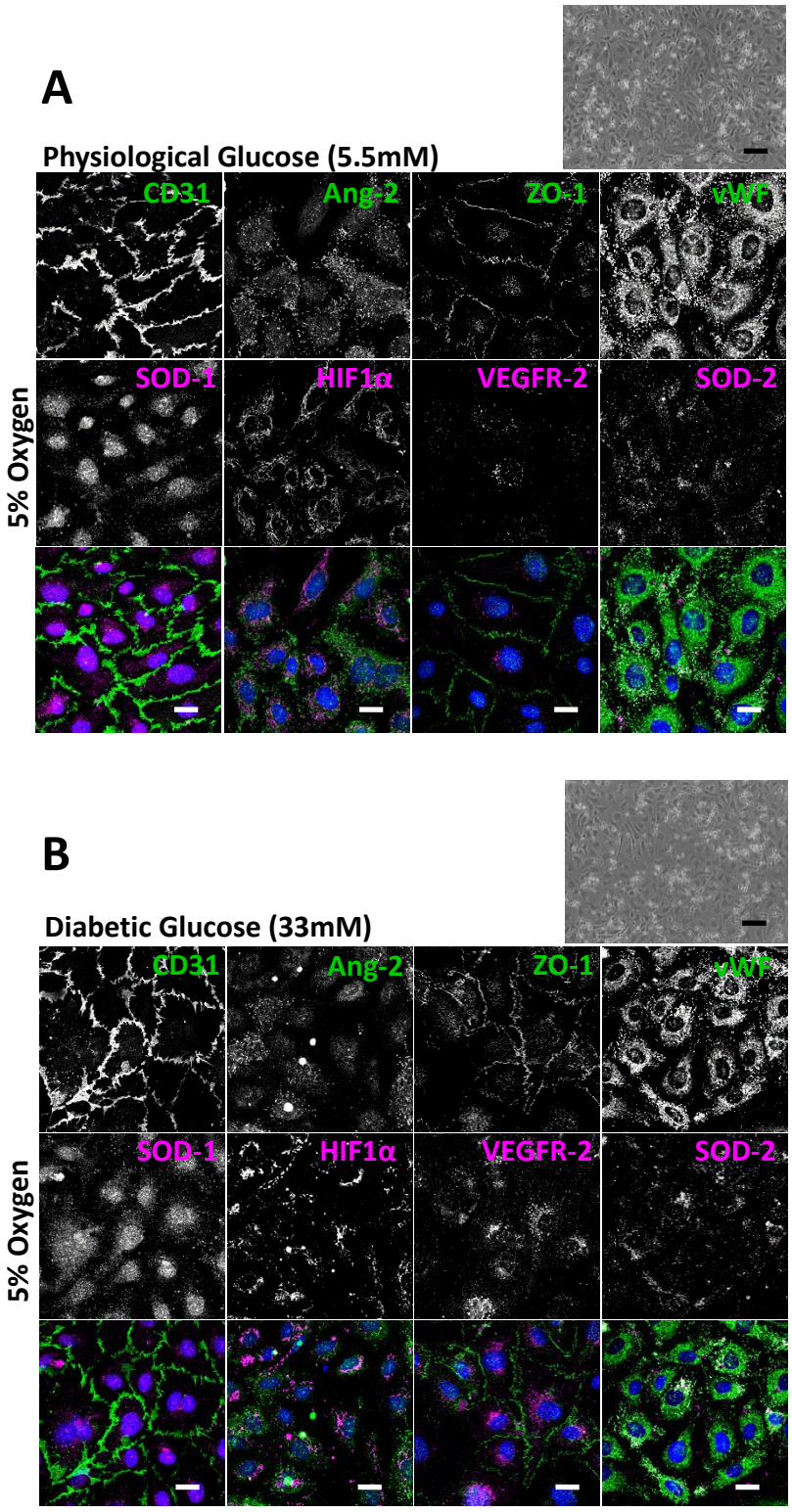

Figure 2.17. Assessing the effect of low oxygen and high glucose on hREC

hREC P8 were seeded on 8-well glass slides and left to adhere for 24H in healthy physiological conditions (20% oxygen and 5.5mM glucose). At 24H, hREC were transferred to low oxygen conditions (5%) (**A**), or low oxygen and high glucose (33mM) conditions (**B**), and cultured for a further 7 days. CD31, ZO-1, vWF, SOD-1, SOD-2, Ang-2, VEGFR-2 and HIF1α expression were assessed to determine hREC phenotype, oxidative, angiogenic and hyperglycaemic stress response. Phase images were captured using Nikon DIAPHOT microscope, x10 objective, black scale bars =200µm. IF images were captured using the Zeiss M800 confocal microscope, x40 oil objective, white scale bars =20µm.

2.4.8 hRP GROWN IN 5% OXYGEN AND 33mM GLUCOSE RETAINED THEIR PHEONTYPE AND SHOWED OXIDATIVE STRESS RESPONSE AT DAY 7

PDGFR-β, NG2, Desmin and αSMA remained unchanged in the four conditions studied, and were used to confirm hRP phenotype (Figure 2.18 and Figure 2.19). There was no clear difference in Ang-2 expression in any conditions, suggesting hRP did not undergo the angiogenic switch that was observed in the hREC in the same conditions. Also, HIF1α had cytoplasmic distribution, except for in 5% oxygen with 33mM glucose (Figure 2.19B), where it appeared HIF1α was clustered on the nuclear border. This translocation of HIF1α towards the nuclear compartment suggests the most diabetic-like conditions induced a major regulatory hypoxic response in the hRP by day 7. SOD-1 expression changed dramatically from a dispersed nuclear location in 20% oxygen (Figure 2.18) to distinctly perinuclear in both 5% oxygen conditions (Figure 2.19). This perinuclear pattern follows that of the ER, suggesting the low oxygen caused SOD-1 activity in the ER, as an oxidative stress response. There were no noticeable differences in SOD-2 expression across the different cell culture conditions. Due to artefacts, VEGFR-2 staining was inconclusive. Overall, these data confirm hRP can withstand low oxygen and high glucose insult over time, but undergo oxidative stress and hypoxic responses in the low oxygen conditions.

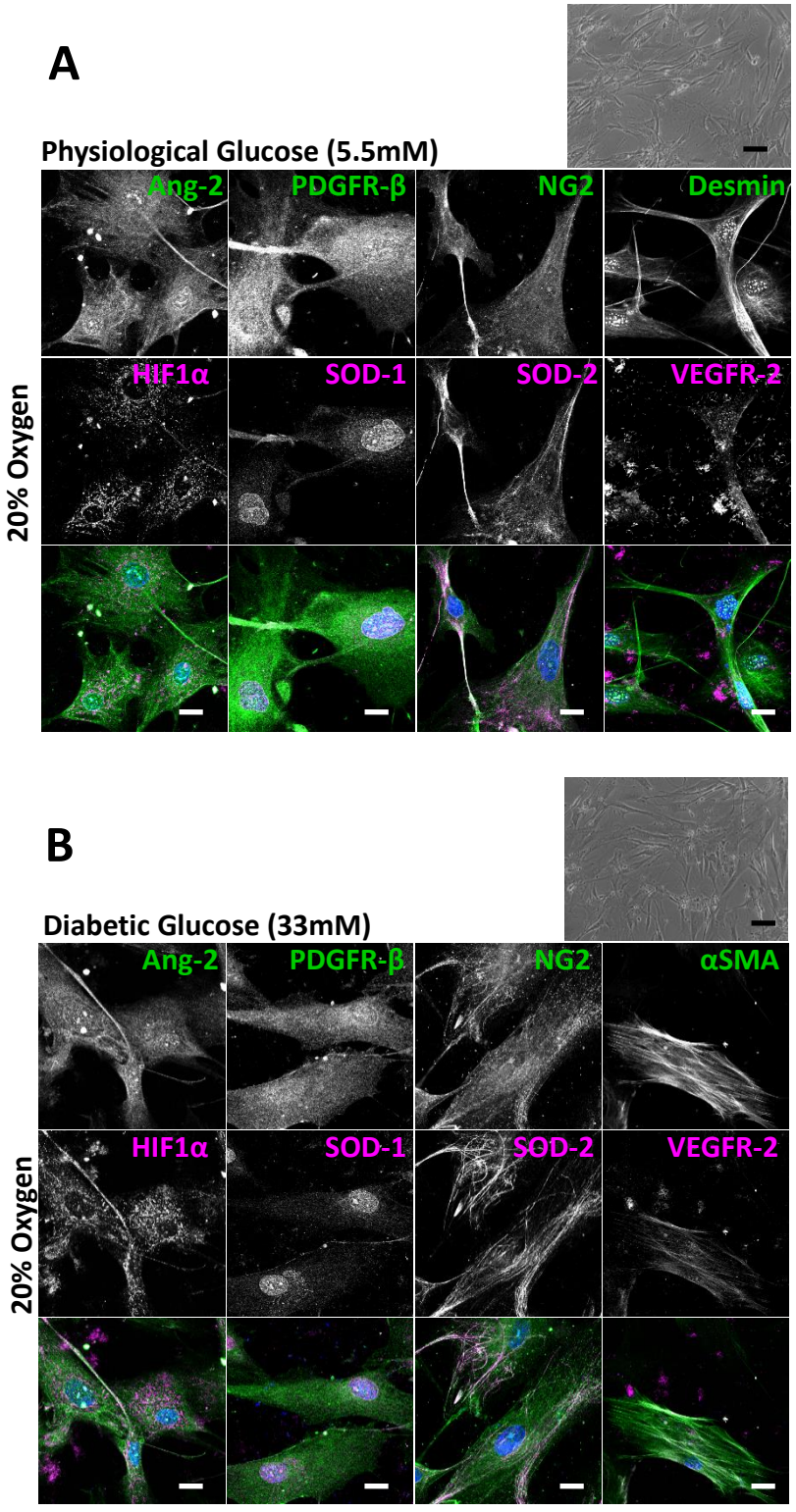

Figure 2.18. Assessing the effect of high glucose on hRP

hRP, P7, were seeded on 8-well glass slides and left to adhere for 24H in healthy physiological conditions (20% oxygen and 5.5mM glucose). At 24H, hRP were either left in healthy conditions (**A**) or moved to high glucose (33mM) conditions (**B**), and cultured for a further 7 days. PDGFR-β, NG2, αSMA, Desmin, SOD-1, SOD-2, Ang-2, VEGFR-2 and HIF1α expression were assessed to determine hRP phenotype, oxidative, angiogenic and hyperglycaemic stress response. Phase images were captured using Nikon DIAPHOT microscope, x10 objective, black scale bars =200µm. IF images were captured using the Zeiss M800 confocal microscope, x40 oil objective, white scale bars =20µm.

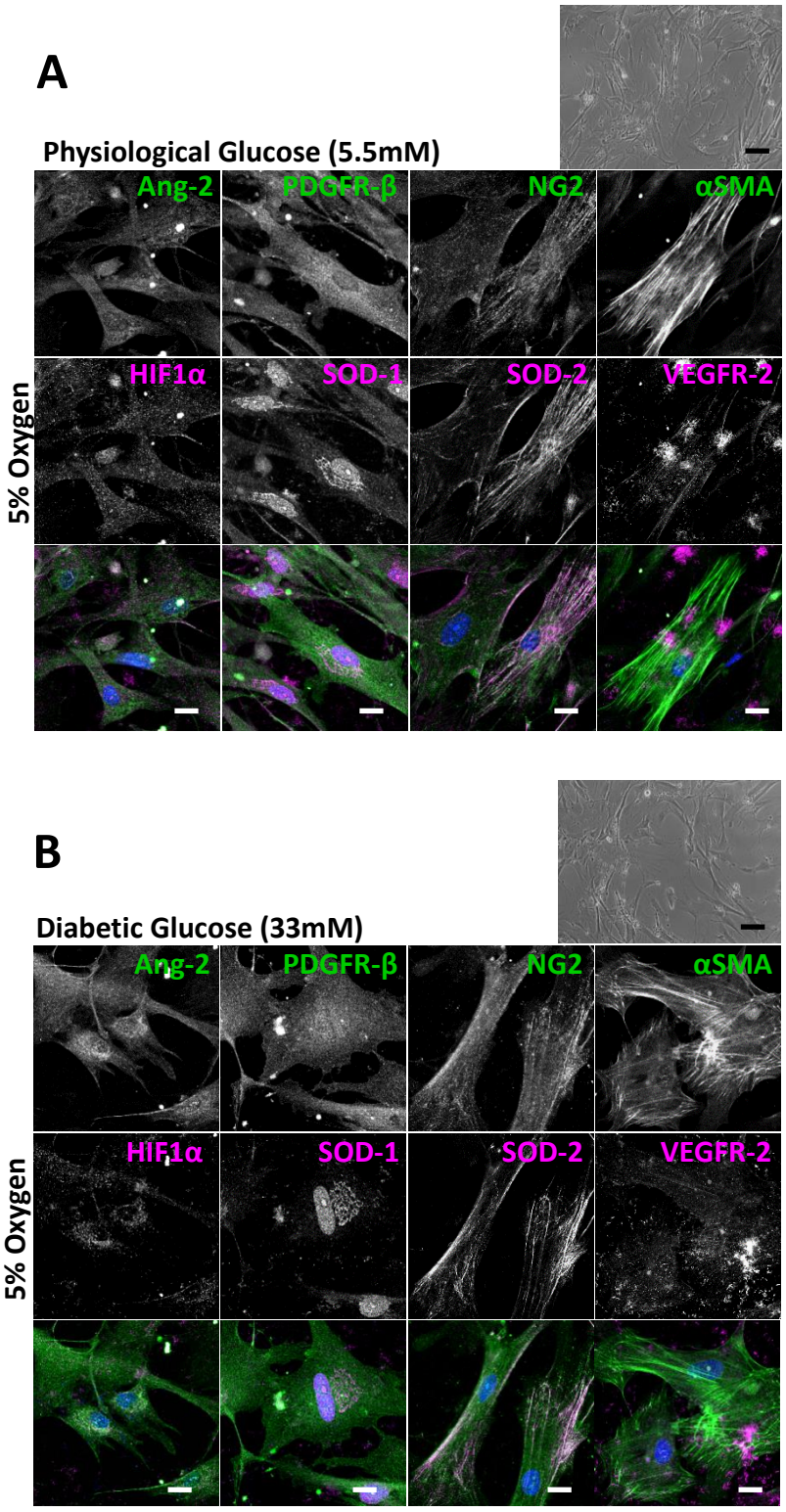

Figure 2.19. Assessing the effect of low oxygen and high glucose on hRP

hRP, P7, were seeded on 8-well glass slides and left to adhere for 24H in healthy physiological conditions (20% oxygen and 5.5mM glucose). At 24H, hRP were transferred to low oxygen conditions (5%) (**A**), or low oxygen and high glucose (33mM) conditions (**B**), and cultured for a further 7 days. PDGFR-β, NG2, αSMA, SOD-1, SOD-2, Ang-2, VEGFR-2 and HIF1α expression were assessed to determine hRP phenotype, oxidative, angiogenic and hyperglycaemic stress response. Phase images were captured using Nikon DIAPHOT microscope, x10 objective, black scale bars =200µm. IF images were captured using the Zeiss M800 confocal microscope, x40 oil objective, white scale bars =20µm.

2.4.9 SERUM WAS ESSENTIAL FOR ATTACHMENT AND GROWTH OF hRP ON THE UNDER SIDE OF PET MEMBRANES

There is limited data outlining the ability of human primary, retina-specific pericytes to adhere and expand on the underside of PET transwell membranes. When no serum was present, hRP did attach, but they had a rounded shape, and did not appear to increase in number from days 3-7 (Figure 2.20A). When 10% FBS was present in the growth medium, hRP attached and had characteristic elongated, non-uniform cell shape with finger-like projections from the cell cytoplasm. There was also an increase in cell number from day 3-7 in the cells seeded with 10% FBS in the growth medium (Figure 2.20B). However, even in the absence of FBS, hRP displayed significant increase in metabolic activity from Day 5-7 ($p < 0.0001$), increasing from 686 a.u. to 9301 a.u, a 13.5x increase, whereas on TC plastic, the data from the FBS % optimising (Figure 2.14) showed no significant increase in hRP metabolic activity across all time points in 0% FBS. Therefore, hRP in 0% FBS on PET membranes displayed increasing metabolic rate, but no increase in number of cells, whereas those in 0% FBS on TC plastic did not show any increase in metabolic activity (Figure 2.20 vs Figure 2.14). Directly comparing 0% FBS with 10% FBS conditions for hRP on PET membranes, metabolic activity was over 20 times higher in 10% FBS hRP cultures at day 5. But by day 7, the difference was only 3.6x higher in the 10% FBS cultures, even though cell number was much lower in 0% FBS. This means the hRP in 0% FBS were exhibiting a higher metabolic rate/cell than the 10% FBS cultured cells. This could be a sign of stress, via loss of metabolic control.

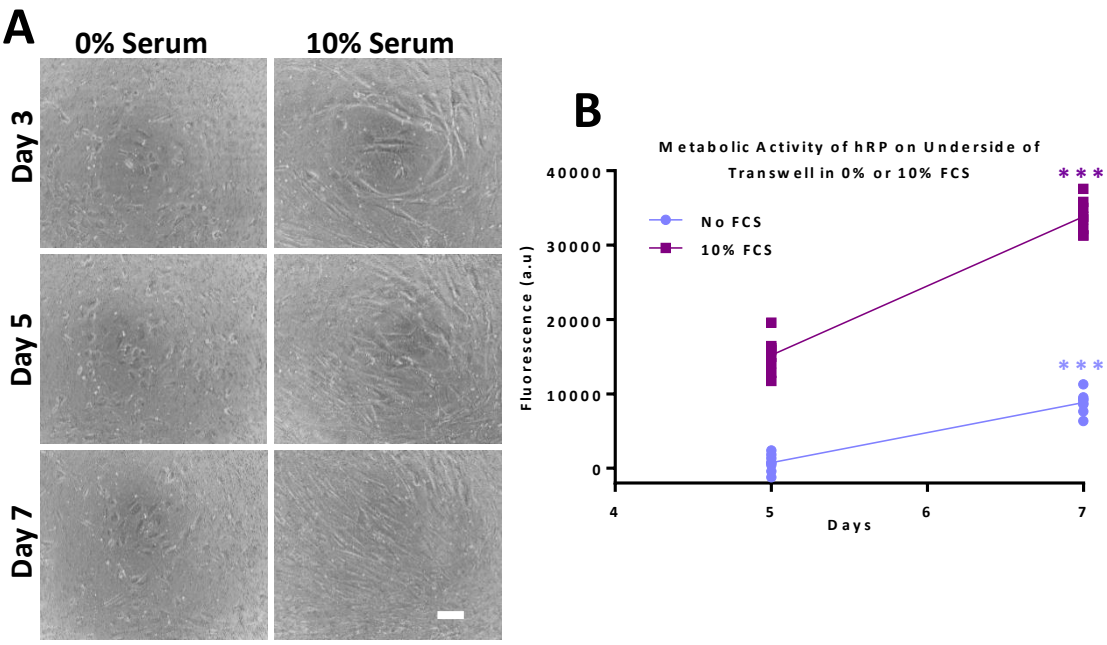

Figure 2.20. FBS is required for hRP to adhere to underside of PET membranes

hRP P10 were seeded on the underside of PET transwell membranes with 10% FBS, or no FBS, in DMEM for 1 hour to allow cells to adhere. hRP were then moved into DMEM with 10% FBS for up to 7 days. Images were captured at 3, 5 and 7 day after seeding cells (**A**), scale bar=200µm. Metabolic activity of cells seeded with or without FBS was assessed at day 5 and day 7 (**B**). Lines represent mean metabolic activity, which was higher at both time point in hRP seeded with 10% FBS. n=8. Data was analysed using un-paired T-test with Welch's correction. ***p<0.001.

2.4.10 hRP AND hREC GREW TOGETHER ON EITHER SIDE OF PET TRANSWELL MEMBRANES

During optimisation of the hREC-hRP co-culture model, MV medium only, DMEM only and 1:1 MV:DMEM media were tested. hRP were robust in all conditions, but hREC attachment and survival over long culture periods was only successful in MV medium in the co-culture. hREC:hRP seeding density was 1:1 ratio, as is described in the cerebral and retinal microvasculature *in vivo*[46]. hRP and hREC were monitored on the bottom and apical surface of PET membranes when grown as monocultures, using simple light microscopy (Figure 2.21A). When hRP and hREC were grown together on either side of the PET membranes, it was difficult to monitor the individual cell-types. Red arrows highlight hREC on the apical surface, with hRP underneath (Figure 2.21A). Therefore, to confirm successful attachment and monitor short term growth of the hRP and hREC in co-culture, CTR and CTG dyes were used, with IF microscopy. The cell trackers had no detrimental effect on proliferative of hRP or hREC monocultures, on TC plastic (Figure 2.21B).

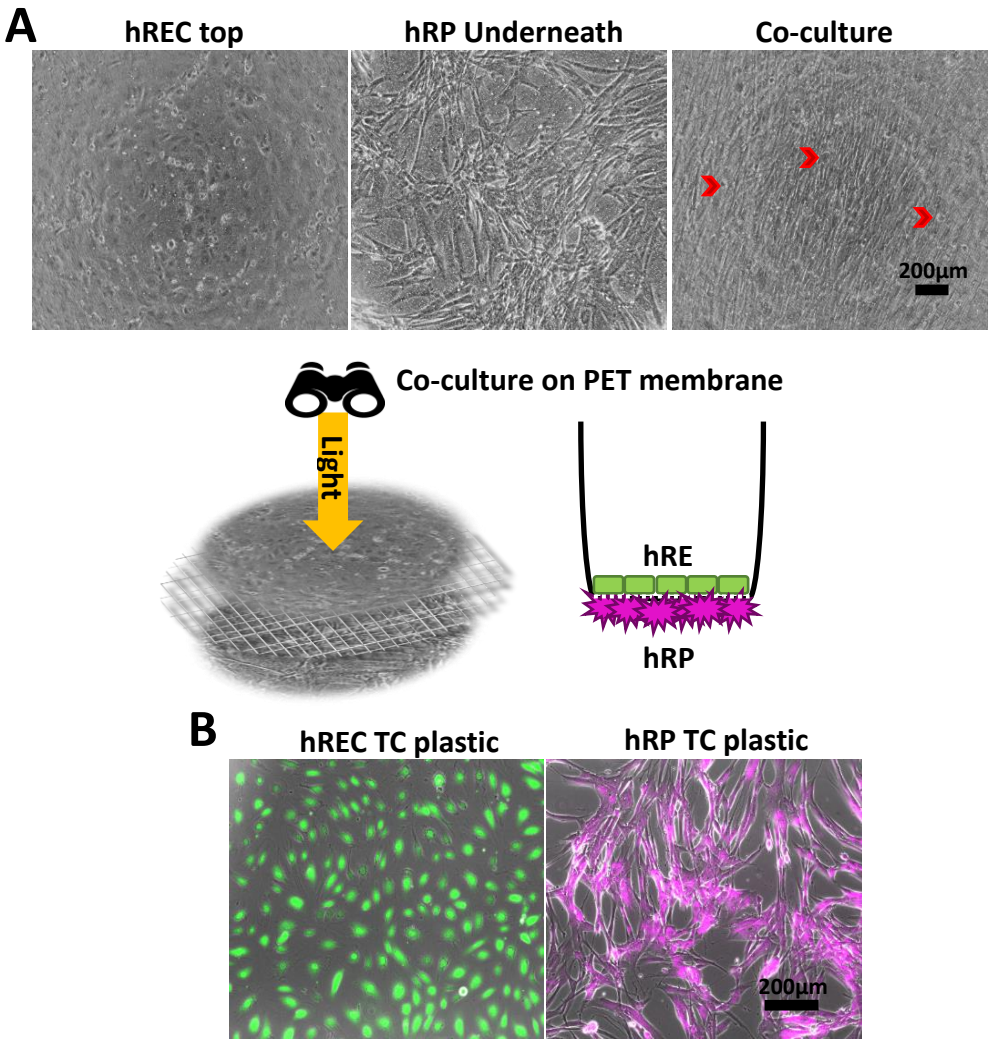

Figure 2.21. CellTracker red and green were used to distinguish hREC and hRP from one another in co-culture

A) Light microscope micrographs of hRP and hREC alone and together on PET transwell inserts. It was difficult to see hREC on co-culture images, but red arrow heads indicate possible hREC. **B**) CTR and CTG were used to enable cell tracking of hRP and hREC. Fluorescence images were captured using the Nikon E-Ti Live Cell Microscope, x10 objective. Scale bars=200µm.

2.4.11 CELL TRACKER DYE ENABLED LIVE CELL IMAGING OF BOTH CELL-TYPES IN CO-CULTURE

CellTacker dye was retained well for up to 48H (Figure 2.22) and cells could be distinguished in both mono-cultures (Figure 2.22A) and co-cultures (Figure 2.22B) on the PET inserts. Beyond 48H, the CellTracker dye decreased in intensity overall, and was also passed on to any daughter cells, therefore although very useful short term, CellTracker dye was not appropriate for long term monitoring of each cell-type.

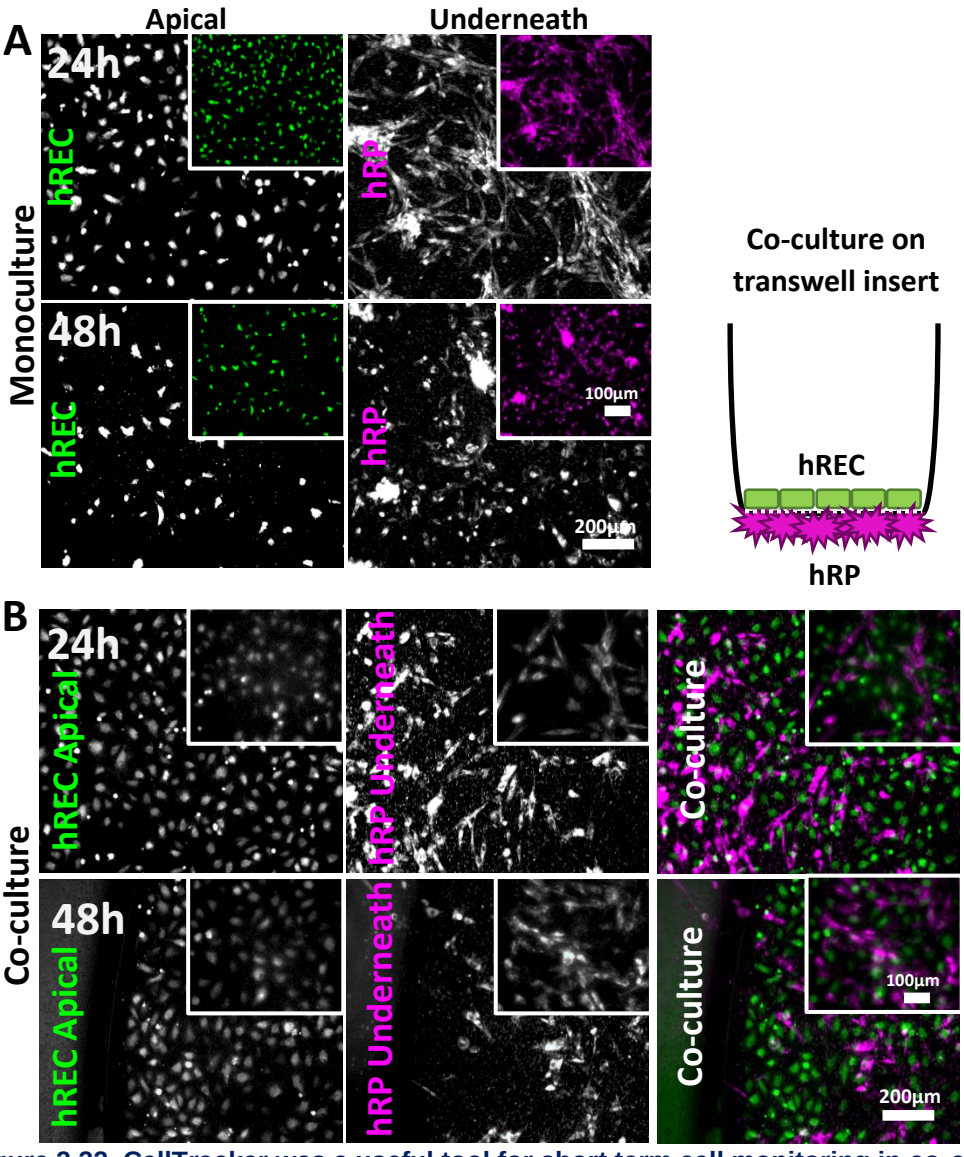

Figure 2.22. CellTracker was a useful tool for short term cell monitoring in co-cultures

CTG and CTR were added to hREC and hRP to enable cell tracking on the PET membranes. It was possible to see hRP on the underside and hREC on the top side, when each cell-type were grown as in monocultures (**A**). CTG-hREC could be distinguished from CTR-hRP when grow as a co-culture (**B**), for 24 and 48H. Fluorescence images were captured using the Nikon E-Ti Live Cell Microscope, x10 objective. Scale bars= 100 or 200µm.

2.4.12 TEER RESULTS WERE INCONCLUSIVE DUE TO LARGE VARIABILITY

TEER measurements are a quick, inexpensive and repeatable method used to test the barrier properties of the endothelial layer. However, the method is notorious for its error and high sensitivity to e.g. culture medium temperature and rod placement. Overall results were inconclusive, with generally very low TEER Ω/cm^2 compared to those reported in the literature (Figure 2.23A). This time point break down of the data highlights the inconsistent variation in the differences between different culture models. There were no significant differences between models on day 3 and day 21 (Figure 2.23B and C), however at all other time points, the TEER data showed significant differences between the groups, particularly differences compared to hREC only, which generally had lower TEER than the other groups. Overall there was no clear trend. TEER was performed on multiple occasions, however data was consistently variable, therefore, TEER was not useful for this application.

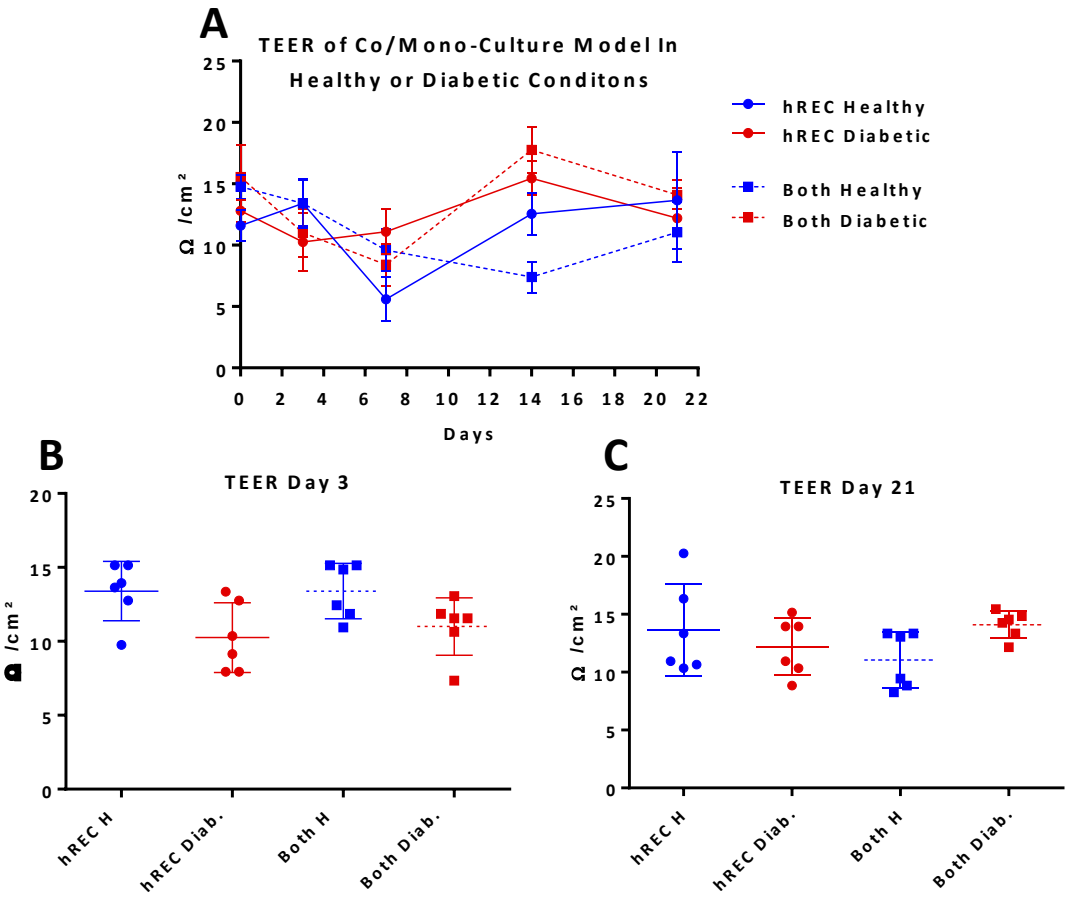

Figure 2.23. TEER provided inconclusive results

TEER was measured at 5 time points over 21 days (**A**). Reading were generally very low and error was large. Although barrier proteins were present (confirmed by IF imaging), TEER did not change over time or in any conditions. At day 3 there was no difference in TEER in healthy or diabetic, mono- or co-cultures (**B**), and the same results at day 21 (**C**). n=6, error bars show SD and all TEER measurements were performed in duplicate. One-Way ANOVA with Tukey's post hoc test was used to perform statistical analysis, although P-values are not reported.

2.4.13 hREC FORMED TJs UP TO DAY 14 WHEN GROWN ON PET AS MONOCULTURES

hREC attached and formed TJs (ZO-1) and adherens junctions (VE-Cad) which were present at days 7 (Figure 2.24) and 14 (Figure 2.25) in both healthy and diabetic conditions, when grown as monocultures. By day 21 hREC were still present, but there are fewer cells remaining in both healthy and diabetic conditions (Figure 2.26). This suggests after day 14 there is some cell loss, which is supported by the growth curve data (Figure 2.13B). By day 21 the adherent hREC were either remaining as patches, with neighbouring cell-cell contact, or more sparse, with large gaps between cells. This was variable from insert to insert when imaging hREC grown in healthy monoculture conditions. This may be due to the IF staining process, such as multiple washes and cutting out the PET membranes from their frames, resulting in cell detachment or peeling. Consequently, VE-Cad and ZO-1 were visible at the cell membrane border of hREC grown as monoculture by day 21, in both healthy and diabetic conditions, but the large gaps between the cells means there was no physical or functional barrier, unlike at earlier time points (Figure 2.26). Overall there was little difference between ZO-1 and VE-Cad expression in healthy compared to diabetic conditions at all three time points. The main differences were fewer cells in the diabetic conditions by day 21 (Figure 2.26) although this was variable from insert to insert, so would require further investigation.

2.4.14 CX43 WAS EXPRESSED AT CELL-CELL JUNCTIONS IN DIABETIC BUT NOT HEALTHY MONOCULTURE CONDITIONS

Cx43 is a component of the GJ complex and there are differences in its expression pattern in hREC grown as monoculture across days 14-21 and also differences when comparing healthy with diabetic. At day 7 in hREC monocultures, Cx43 looks distributed across the cytoplasm, with some concentrations at the cell membranes, i.e. where the gap junctions would be found, with little differences between healthy and diabetic conditions (Figure 2.24). By day 14, in diabetic conditions the Cx43 was prominently concentrated at the lateral border of the cell membranes, indicating the presence of GJs (Figure 2.25). However at day 14 healthy conditions, the Cx43 remains evenly distributed across the cytoplasm, similar to day 7.

By day 21 of hREC monoculture, there was noticeable reduction in cell number, and co-staining of Cx43 and F-actin highlights major differences in cytoskeletal organisation between healthy and diabetic conditions (Figure 2.26). hREC in healthy conditions have similar Cx43 distribution as day 7 and 14, but with more of a Cx43 concentration at the perinuclear area. F-actin filaments are clearly visible in the hREC grown in healthy conditions at day 21, whereas both Cx43 and F-actin distribution in the hREC in diabetic conditions for 21 days

show major changes. Overall the hREC in diabetic conditions for 21 days look very small in size, lacking normal cytoskeletal structure. This suggests hREC the attachment to the PET membrane may be compromised in the long term diabetic conditions. F-actin filaments were no longer visible, Cx43 was visible at the cell membrane although there were large gaps between the cells, so cell-cell contacts were not functional.

2.4.15 NO MAJOR DIFFERENCES IN HYPOXIC AND ANGOIGENIC RESPONSE FROM hREC MONOCULTURE ON PET

HIF1α and VEGFR-2 expression were assessed, to explore oxidative stress and angiogenic changes. There were no noticeable differences across time and in healthy or diabetic conditions (Figure 2.24, Figure 2.25, Figure 2.26).

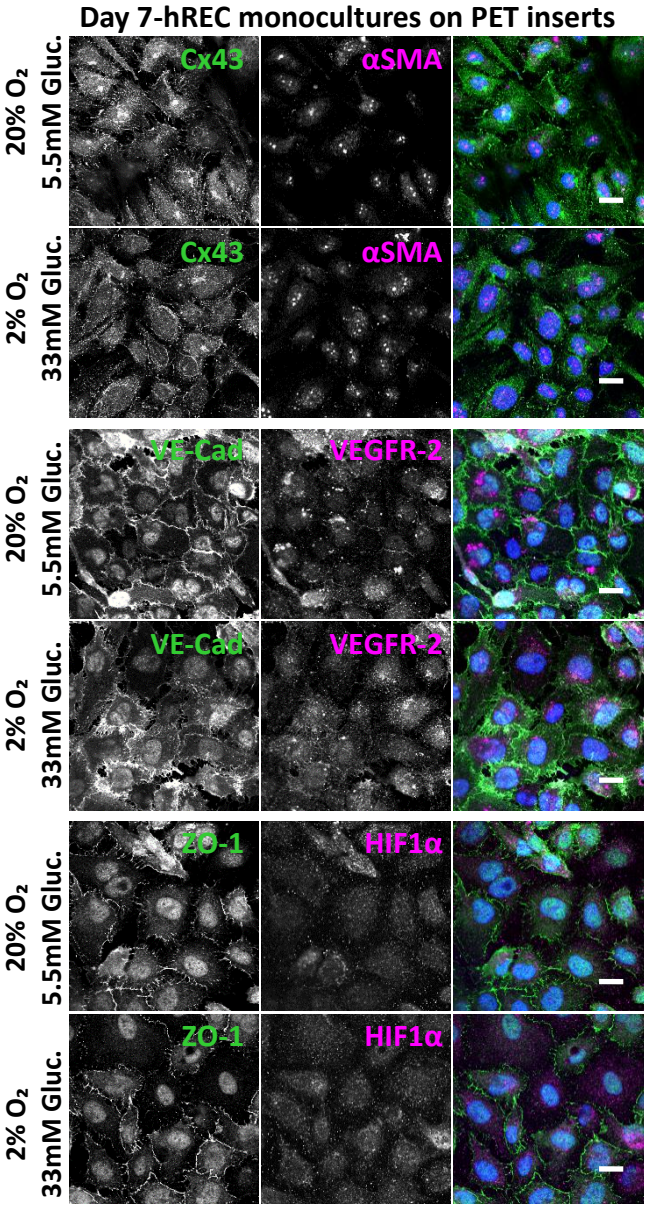

Figure 2.24. hREC form a monolayer with GJ protein expression in both healthy and diabetic conditions at day 7

hREC monocultures, P6, seeded at $2x10^4$ cells/well on the apical surface of PET transwell inserts with 1µm pores. Cells were grown in healthy conditions for 72H to allow hREC to become a monolayer. Cells were then kept in physiologically healthy conditions (20% O_2 and 5.5mM glucose) or moved to diabetic conditions (2% O_2 and 33mM glucose) for a further 7 days. Media was changed every 24-72H. Cells were fixed at day 7 and processed for IF analysis of ZO-1, VE-Cad and CX43 expression, to explore GJ and adherens junction formation, and for VEGFR-2 and HIF1α to analyses hREC response to hypoxia and angiogenesis. Images were captured using the Zeiss M800 confocal microscope, x40 oil magnification. Scale bars= 20µm.

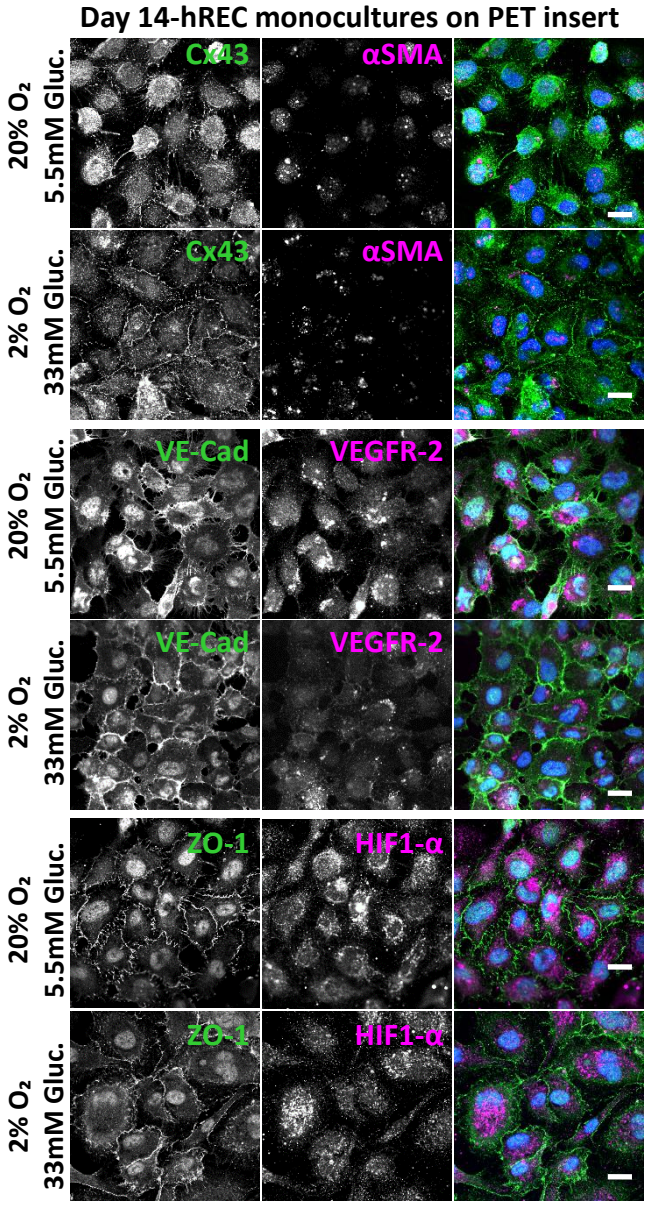

Figure 2.25. Cx43 was expressed at cell-cell borders only in diabetic conditions in hREC monocultures at day 14

hREC monocultures, P6, seeded at $2x10^4$ cells/well on the apical surface of PET transwell inserts with 1µm pores. Cells were grown in healthy conditions for 72H to allow hREC to become a monolayer. Cells were then kept in physiologically healthy conditions (20% O_2 and 5.5mM glucose) or moved to diabetic conditions (2% O_2 and 33mM glucose) for a further 14 days. Media was changed every 24-72H. Cells were fixed at day 14 and processed for IF analysis of ZO-1, VE-Cad and Cx43 expression, to explore GJ and adherens junction formation, and for VEGFR-2 and HIF1α to analyses hREC response to hypoxia and angiogenesis. Images were captured using the Zeiss M800 confocal microscope, x40 oil magnification. Scale bars= 20µm.

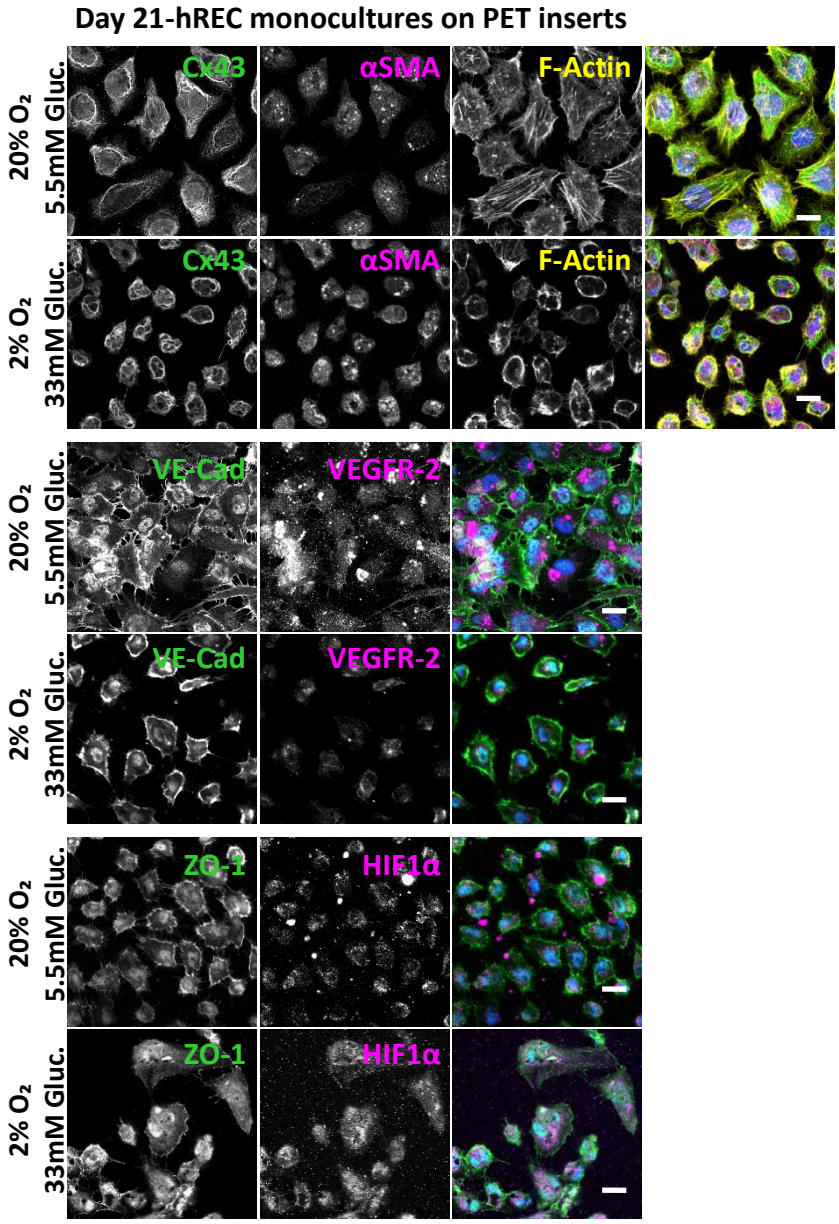

Figure 2.26. By day 21 there was cell loss in both healthy and diabetic conditions and cytoskeletal alterations in the diabetic hREC monocultures

hREC monocultures, P6, seeded at $2x10^4$ cells/well on the apical surface of PET transwell inserts with 1µm pores. Cells were grown in healthy conditions for 72H to allow hREC to become a monolayer. Cells were then kept in physiologically healthy conditions (20% O_2 and 5.5mM glucose) or moved to diabetic conditions (2% O_2 and 33mM glucose) for a further 21 days. Media was changed every 24-72H. Cells were fixed at day 21 and processed for IF analysis of ZO-1, VE-Cad and Cx43 expression, to explore GJ and adherens junction formation, and for VEGFR-2 and HIF1α to analyses hREC response to hypoxia and angiogenesis. Images were captured using the Zeiss M800 confocal microscope, x40 oil magnification. Scale bars= 20µm.

2.4.16 hRP RETAINED PHENOTYPE MARKERS WHEN GROWN ON THE UNDER SURFACE OF PET MEMBRANES

hRP were grown as monocultures during optimisation of the model to confirm hRP could attachment and growth on the underside of the PET material, whilst retaining their phenotype markers NG2, Desmin and +/- αSMA (Figure 2.27). αSMA was expressed in some hRP, which was a common feature of the hRP in all experiments, suggesting the hRP behaved in a similar way in both mono- and co-cultures and in healthy and diabetic conditions.

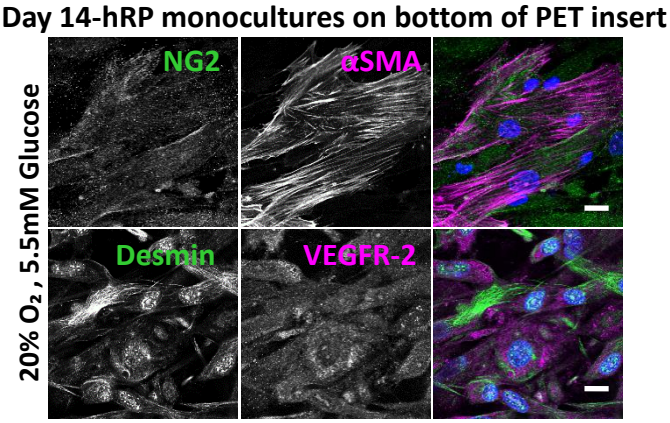

Figure 2.27. hRP retained their phenotype when cultured on the bottom of PET membranes at day 14

hRP monocultures, P6, seeded at $2x10^4$ cells/well on the under surface of PET transwell inserts with 1µm pores. Cells were grown in healthy conditions for 72H. Cells were then kept in physiologically healthy conditions) for a further 14 days. Media was changed every 24-72H. Cells were fixed at day 14 and processed for IF analysis of NG2, αSMA, Desmin and VEGFR-2 to analyse cell phenotype and response to culture conditions. Images were captured using the Zeiss M800 confocal microscope, x40 oil magnification. Scale bars= 20µm.

2.4.17 JUNCTIONAL PROTEIN EXPRESSION WAS NO DIFFERENT IN CO-CULTURED hREC COMPARED TO MONOCULTRED hREC

To provide *in vitro* data of vascular changes during diabetic conditions, hREC were grown on PET membranes, with hRP on the under surface; a model mimicking the human retinal capillary structure. Apical view, under surface view and z-stack projections were included to confirm the presence of both cell-types in the different models over time. VE-Cad and ZO-1 were present on the membrane at cell-cell junctions of hREC in both healthy and diabetic conditions at day 7, when cells were grown in co-culture with hRP (Figure 2.28). This shows hREC grown in co-culture form similar barrier properties to those grown as monocultures (Figure 2.24), by day 7 in both healthy and diabetic conditions. Cx43 distribution in hREC in the co-culture model is no different from Cx43 in monocultured hREC at day 7, with Cx43 present throughout the cytoplasm.

By day 21, there was a reduction in hREC number in both healthy and diabetic co-culture models. However, there is much more hREC cell loss in diabetic conditions, with only clusters of shrunken hREC remaining. hREC co-cultured in healthy conditions for 21 days retain similar cell size and VE-Cad and ZO-1 expression as day 7 time point, with physical cell-cell contacts and only a small (variable) reduction in cell number (Figure 2.28, Figure 2.29). These data suggest when hREC are grown in healthy co-culture with hRP, they remain attached to the PET (ECM mimic) with functioning cell-cell contacts by day 21, whereas when grown as mono-cultures, hREC appear to lose their cell-cell contacts when grown in the same conditions for the same period of time (Figure 2.26). In contrast, diabetic co-culture conditions have caused major hREC cell loss, shrinkage, clustering and possibly cells peeling off the PET membrane during the IF washing process (Figure 2.29). Similar to the monocultured hREC, the hREC co-cultured in diabetic conditions lose cell-cell contact and the cell size is noticeably reduced when compared to healthy co-cultured hREC. hRP remained attached to the under surface of the PET in all conditions, suggesting they can withstand diabetic conditions for long periods of time. Unfortunately Day 14 data are missing due to damage to the cells on the PET inserts during processing for IF.

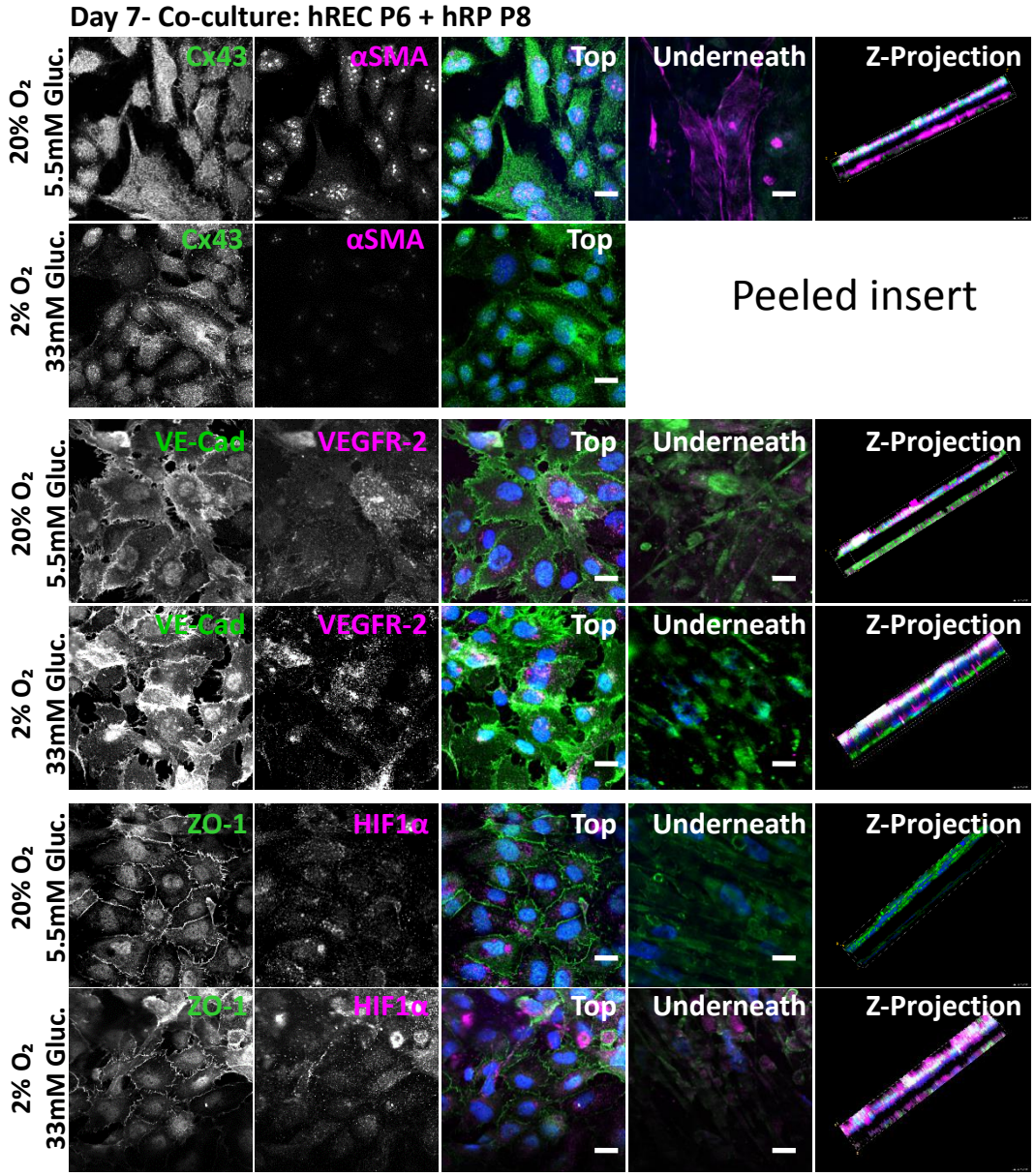

Figure 2.28. hREC co-cultured for 7 days expressed similar GJ proteins to monocultured hREC

hREC P6, and hRP P8 were seeded at a 1:1 ratio, with $2x10^4$ hREC/well on the apical surface and $2x10^4$ hRP/well on the under surface of PET transwell inserts with 1µm pores. Cells were grown in healthy conditions for 72H to allow hREC to become a monolayer. Cells were then kept in physiologically healthy conditions (20% O_2 and 5.5mM glucose) or moved to diabetic conditions (2% O_2 and 33mM glucose) for a further 7 days. Media was changed every 24-72H. Cells were fixed at day 7 and processed for IF analysis of ZO-1, VE-Cad and Cx43 expression, to explore GJ and adherens junction formation, and for VEGFR-2 and HIF1α to analyses hREC response to hypoxia and angiogenesis. Images were captured using the Zeiss M800 confocal microscope, x40 oil magnification. Z-stack projections were captured to view cells on either side of the transwells. Scale bars= 20µm.

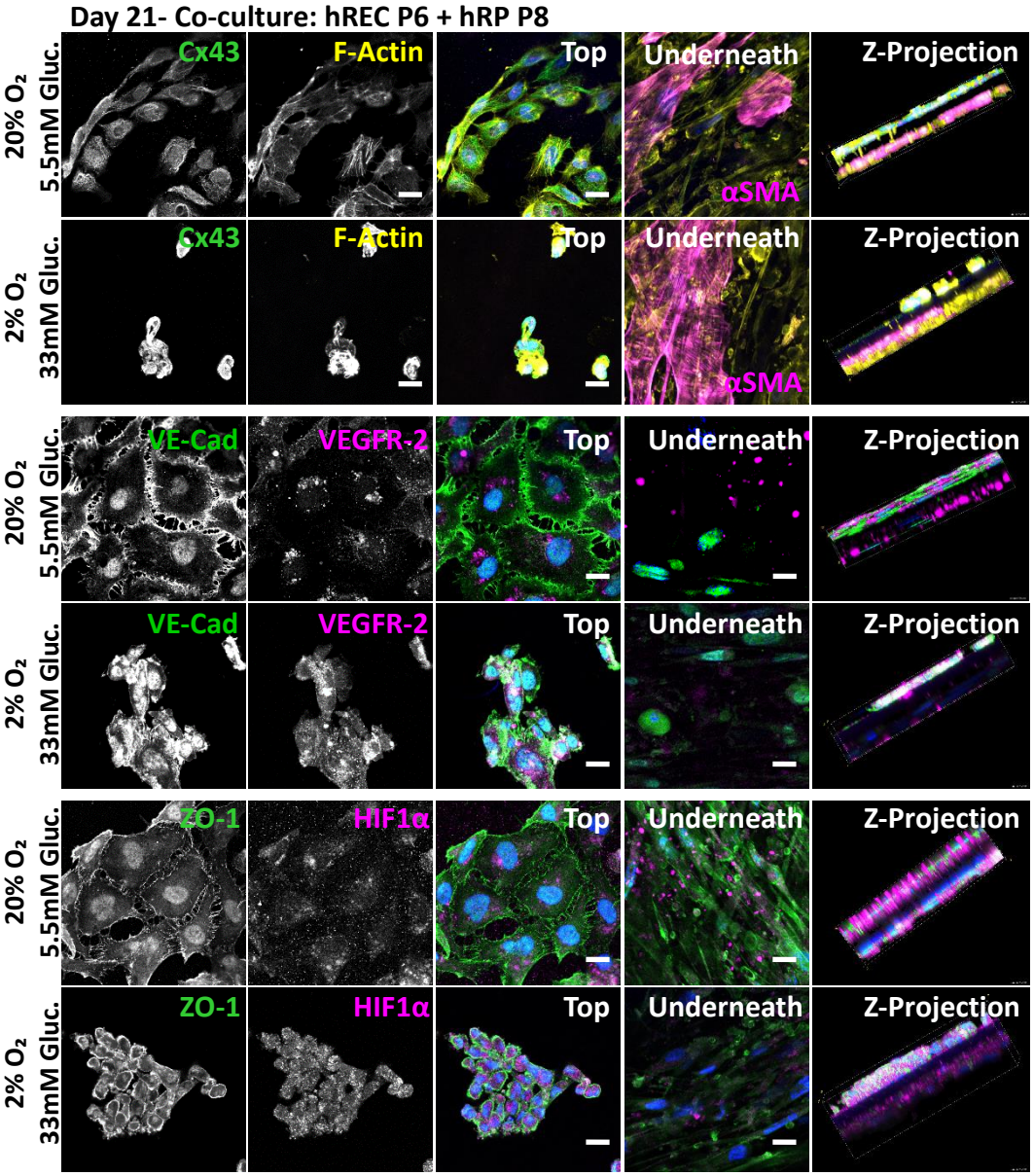

Figure 2.29. Co-cultured hREC retain healthy morphology and cell-cell contacts in healthy conditions at day 21

hREC P6, and hRP P8 seeded at a 1:1 ratio, with $2x10^4$ hREC/well on the apical surface and $2x10^4$ hRP/well on the under surface of PET transwell inserts with 1µm pores. Cells were grown in healthy conditions for 72H to allow hREC to become a monolayer. Cells were then kept in physiologically healthy conditions (20% O_2 and 5.5mM glucose) or moved to diabetic conditions (2% O_2 and 33mM glucose) for a further 7 days. Media was changed every 24-72H. Cells were fixed at day 7 and processed for IF analysis of ZO-1, VE-Cad and Cx43 expression, to explore GJ and adherens junction formation, and for VEGFR-2 and HIF1α to analyses hREC response to hypoxia and angiogenesis. Images were captured using the Zeiss M800 confocal microscope, x40 oil magnification. Z-stack projections were captured to view cells on either side of the transwells. Scale bars= 20µm.

2.4.18 HIF1α AND VEGFR-2 EXPRESSION WAS INCONCLUSIVE AT DAY 7 AND DAY 21 DUE TO CELL LOSS IN DIABETIC CONDTIONS

HIF1α is a major transcriptional regulator of a cells' response to hypoxia and should translocate to the nucleus when active. At day 7 in co-culture, there was no difference between HIF1α expression in healthy and diabetic conditions, displaying broad cytoplasmic distribution in both conditions (Figure 2.28). By day 21 of co-culture the HIF1α expression in hREC in healthy conditions remained unchanged from day 7. It was not possible to determine HIFα expression of hREC in co-culture diabetic conditions by day 21, due to the cytoplasmic shrinkage and clustering of the possibly partly detached hREC (Figure 2.29). Further imaging at earlier time points between day 7 and 21 may provide conclusive data on HIF1α activity.

VEGFR-2 is a receptor for VEGF and can be up/down regulated on the cell surface in different microenvironments, with a major role in angiogenesis. At day 7 of co-culture, VEGFR-2 appeared upregulated in hREC grown in diabetic conditions, compared with healthy conditions (Figure 2.28). Only one cell in the field of view appears to be expressing high levels of VEGFR-2 in day 7 healthy conditions, and that cell has 2 nuclei, suggesting it is undergoing mitosis. By day 21 of co-culture conditions, due to cell loss, clumping and shrinkage in diabetic conditions, similar to HIF1α, it was not possible to determine VEGFR-2 expression (Figure 2.29). Using the z-stack projection it is possible to see VEGFR-2 (magenta) was present in the healthy co-culture at day 21, in the perinuclear location, although it was not possible to compare these levels against the diabetic model.

2.4.19 hRP SHOWED DIFFERENTIAL EXPRESSION OF αSMA IN ALL CULTURE CONDITIONS AND THROUGHOUT PASSAGING

On TC plastic, TC treated glass and PET transwell membranes, hRP purchased from Cell Systems used throughout these experiments had positive/negative expression of αSMA. hRP grown on TC treated glass slides (Figure 2.30) highlights that some hRP were negative for αSMA and some were positive (green staining). There was no clear cause for this phenomenon, as hRP positive for αSMA had no obviously different morphology, and there was positive/negative αSMA expression in hRP in both healthy and diabetic conditions and in mono- and co-cultured hRP (Figure 2.27, Figure 2.29). hRP retained expression of PDGFR-β, NG2 and Desmin, which confirms they did not transition due to experimental conditions or passaging.

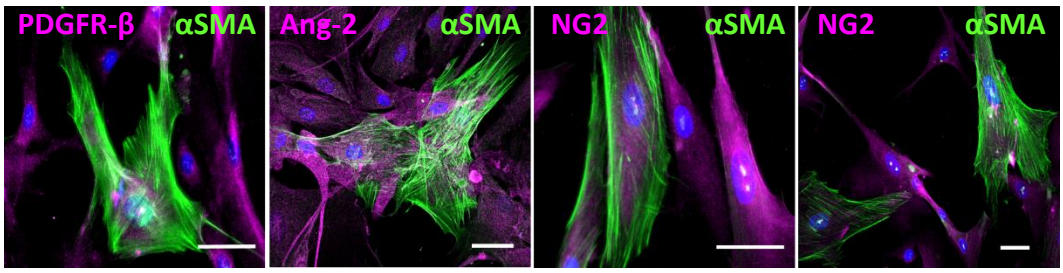

Figure 2.30. Some hRP expressed αSMA whilst others did not

hRP P6, grown on TC treated glass slides for 7 days in healthy conditions. Some hRP expressed αSMA and some didn't. This positive/negative αSMA expression did not appear to be influenced by the material the cells were grown on or the culture conditions. Images were captured using the Zeiss M800 confocal microscope, x40 oil magnification. Scale bars= 50µm.

2.4.20 hRP CYTOPLASMIC αSMA PROJECTIONS GREW THROUGH PET MEMBRANE PORES RESULTING IN AREAS OF DIRECT PHYSICAL CONTACT BETWEEN hRP AND hREC IN CO-CULTURE

Using IF confocal microscopy z-stacking applications, it was possible to build z-projections of the hREC and hRP on either side of the PET membrane, at high resolution. These data were used to confirm the presence of hREC on the apical surface and hRP on the underside of the PET membrane at multiple time points and in healthy or diabetic conditions, to aid in validating the use of a retina-specific, human primary co-culture model. By day 14 hRP grown on the underside of PET membranes sent finger-like projections from the cytoplasm through the 1µm pore up to the apical surface, if they were grown on their own (monoculture) (Figure 2.31 A) or grown in the presence of hREC on the apical surface (co-culture) (Figure 2.31B and C). The orange on the right panel highlights the projections which migrated to the apical surface of the membrane. This observation was important to take in to consideration as it confirmed areas physical contact between the hREC and hRP through the PET membrane.

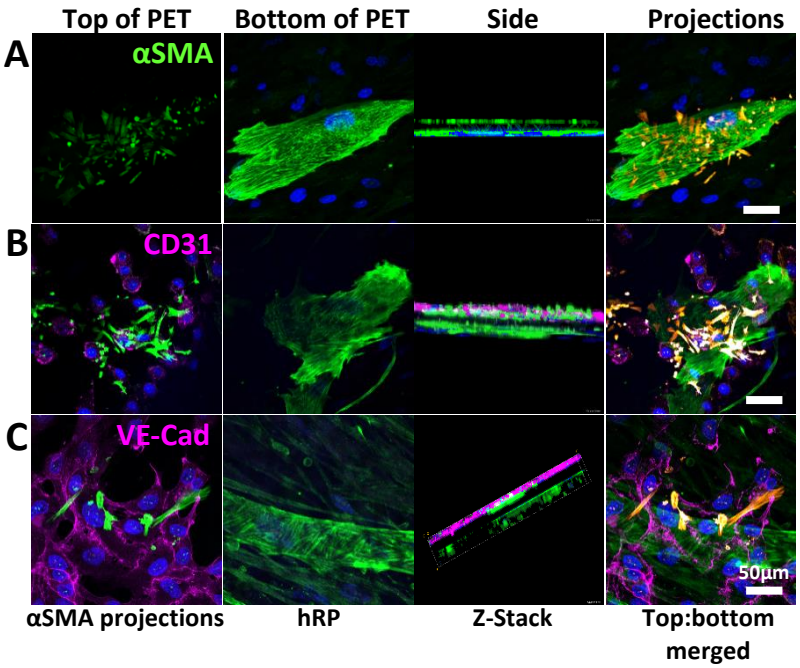

Figure 2.31. Cytoplasmic projection from hRP through PET membrane in both mono and co-cultures

hRP P8, cultured in healthy conditions for 14 (**A** and **B**) and 21 days (**C**) on the bottom of PET membranes. **A**) hRP monoculture at day 14, **B**) co-culture at day 14, and **C**) co-culture at day 21. CD31 and VE-cad confirmed the presence of hREC on apical surface of PET. Antibodies against αSMA were used to image cytoplasmic projections through PET membranes. Images were captured using the Zeiss M800 confocal microscope, x40 oil magnification. Z-stack imaging was sued to capture images of hRP projections passing through PET 1µm pores. Scale bars= 50µm.

2.4.21 ANG-2 WAS SIGNIFICANTLY INCREASED IN DIABETIC CONDITIONS BUT IN CO-CULTURES THE DIFFERENCE WAS SMALLER

Multiplex technology enabled quantification of 9 secreted proteins collected from cell supernatants at multiple time points, for mono and co-cultures, in healthy and diabetic conditions. Four out of nine proteins fell within range for quantification. Ang-2 is a soluble proangiogenic vascular growth factor, involved in adult angiogenesis. In monoculture, hRP did not secrete Ang-2. In monoculture, hREC secreted Ang-2 in low levels at all time points when in healthy conditions (Figure 2.32A). From day 7-21 hREC in monoculture in diabetic conditions secreted significantly more Ang-2 than those in healthy conditions ($P<0.01$). Ang-2 levels spiked at 12149.1pg/ml by day 7 in diabetic mono-cultured hREC conditions, compared to healthy 2998.86pg/ml ($p<0.001$). When hREC were co-cultured with hRP, Ang-2 levels remained higher in diabetic conditions, although this level only reached significant difference from healthy conditions at day 7 ($p<0.001$) and day 17 ($p<0.01$). Similar to

monocultured hREC, Ang-2 levels again peak at day 7 at 8813.86pg/ml in the diabetic co-culture model, compared to healthy 3490.6pg/ml, although the diabetic co-culture peak is over 3000pg/ml lower than in the hREC monocultured in diabetic conditions at day 7. When hREC and hRP were grown in co-culture in healthy conditions, Ang-2 levels reached a peak at day 14 at 5565.29pg/ml and levels were overall higher than those in healthy monocultured hREC, where Ang-2 levels peaked earlier and at day 7 and at lower concentration (2998.86pg/ml). By day 21 Ang-2 levels in the healthy co-culture model were almost three times (2.88) the levels of Ang-2 in hREC monocultures. By day 21 Ang-2 levels in the diabetic co-culture model were almost 1.5 times (1.48) the levels of Ang-2 in hREC monocultures.

Taken together, these three graphs show that Ang-2 secretion was increased in diabetic conditions and also secretion levels were altered when hREC and hRP are grown in co-culture, more closely mimicking the environment of the retinal microvasculature. The presence of hRP appears to reduce the difference between Ang-2 secretion in healthy and diabetic models, by increasing the Ang-2 levels secreted in healthy conditions

2.4.22 hRP CONTINUALLY SECRETED HGF OVERTIME ALTHOUGH DIABETIC CONDITONS AND PRESENCE OF hREC CAUSED A REDUCTION IN SECRETION LEVELS

Hepatocyte growth factor (HGF) or scatter factor, is a paracrine cellular growth, motility and morphogenic factor which acts primarily on ECs and is involved in adult wound healing and organ regeneration. HGF was not secreted by hREC grown on their own (Figure 2.32B). HGF was secreted by monocultured hRP, in both healthy and diabetic conditions, with an increasing amount secreted over time. By day 14 hRP monocultured in diabetic conditions secreted significantly less HGF than hRP grown in healthy conditions, 804.4pg/ml vs 1770.6pg/ml ($p<0.001$). HGF remained significantly reduced in hRP in diabetic conditions up to day 21, reaching peak in hRP monocultured in healthy conditions, at 3151.3pg/ml vs 1578.2pg/ml in diabetic conditions at day 21 ($p<0.001$). However, when hREC and hRP were grown in co-culture, HGF secretion was reduced overall, to levels below 700pg/ml, with no significant differences between healthy and diabetic co-culture conditions. Taken together, these three graphs suggest HGF is not secreted at all by hREC, HGF secretion was reduced in diabetic conditions and that in the presence of hREC, hRP secretion of HGF was reduced to very low, stable levels compared to a much higher, rising trend when hRP were grown in isolation.

2.4.23 BOTH hREC and hRP SECRETED IL-8 AND WHEN THE CELLS ARE CO-CULTURED, THE EFFECT ON IL-8 SECRETION APPEARED ADDITIVE

Interleukin-8 (IL-8) has two primary functions: induces chemotaxis in target cells, causing immune cells to migrate towards sites of injury/infection, and induced phagocytosis at sites of injury/infection. IL-8 is also a potent promoter of angiogenesis. When hREC were monocultured, IL-8 secretion was significantly increased at day 3 ($p<0.01$) at 2241.7pg/ml in diabetic conditions, compared to 1223.8pg/ml in healthy conditions (Figure 2.32C). However, at all other time points there were no significant differences in IL-8 secretion by monocultured hREC in healthy or diabetic conditions. There was a small dip in IL-8 secretion at day 10, but otherwise, levels remained relatively consistent over time. IL-8 secretion levels in hRP grown on their own, increase over time from day 10 onwards reaching 3217.6pg/ml by day 21, with no significant differences between healthy and diabetic conditions at any time point. When hREC and hRP were grown in co-culture, there appears to be an additive effect on IL-8 secretion. In co-cultures, IL-8 secretion remained relatively stable from day 0-10 (similar to hREC monocultures), with a sharp rise from day 10-21 in both healthy and diabetic co-cultures, peaking at 5927.2pg/ml in healthy and 5020pg/ml in diabetic co-culture conditions. IL-8 secretion was higher in the healthy co-culture model from day 10-21, but this difference only reached significance on day 17 ($p<0.05$) with 5408.5pg/ml in healthy conditions compared to 4025pg/ml in diabetic conditions. Overall, the differences between IL-8 secretion in healthy and diabetic conditions was small. Although, in the co-culture model by day 21, IL-8 secretion increased to double the level in hRP monocultures and triple the level of hREC monocultures. These data suggest both hREC and hRP can secrete IL-8, and when cultured together, IL-8 secretion is affected in additive manner.

2.4.24 DIABETIC CONDITIONS SIGNIFICANTLY REDUCED TIMP-2 SECRETION IN ALL MODELS

TIMP-2 is an inhibitor of MMPs. MMPs degrade numerous ECM proteins during cell proliferation, tissue rearrangement and wound healing, therefore TIMP-2's action inhibiting MMPs could be critical to the maintenance of tissue homeostasis and quiescence. When hREC were grown on their own, TIMP-2 secretion remained stable over time, although by day 7-10 TIMP-2 was significantly reduced in hREC grown in diabetic conditions ($p<0.01$) and from day 14-21 the difference between healthy and diabetic is more significant ($p<0.001$) (Figure 2.32D). Overall however, in monocultured hREC, levels of secreted TIMP-2 remained relatively low and did not surpass 6,264.1pg/ml in healthy conditions, or 4,765.2pg/ml in diabetic conditions. hRP secretion of TIMP-2 was much higher than hREC at all time points.

hRP displayed a rising trend of TIMP-2 secretion over time, with levels significantly lower in hRP grown in diabetic conditions compared to healthy, from day 7-21 ($p<0.001$). The highest levels of TIMP-2 were observed at day 14 in hRP monocultured in healthy conditions 24,878pg/ml, whereas in diabetic conditions, significantly lower TIMP-2 was secreted 15,345.1pg/ml. When hREC and hRP were co-cultured, a similar trend of increasing TIMP-2 secretion over time was observed. Likewise, TIMP-2 secretion was significantly reduced in diabetic co-culture conditions, from day 10 ($p<0.05$) to day 21 ($p<0.01$) compared to healthy conditions, although the difference between healthy and diabetic TIMP-2 levels was smaller than when hRP are grown on their own. Overall, when hREC and hRP were grown in co-culture, their interaction appears to have a small suppressive action on TIMP-2 secretion, because by day 21 both healthy and diabetic co-culture conditions show lower TIMP-2 levels than monocultured HRP.

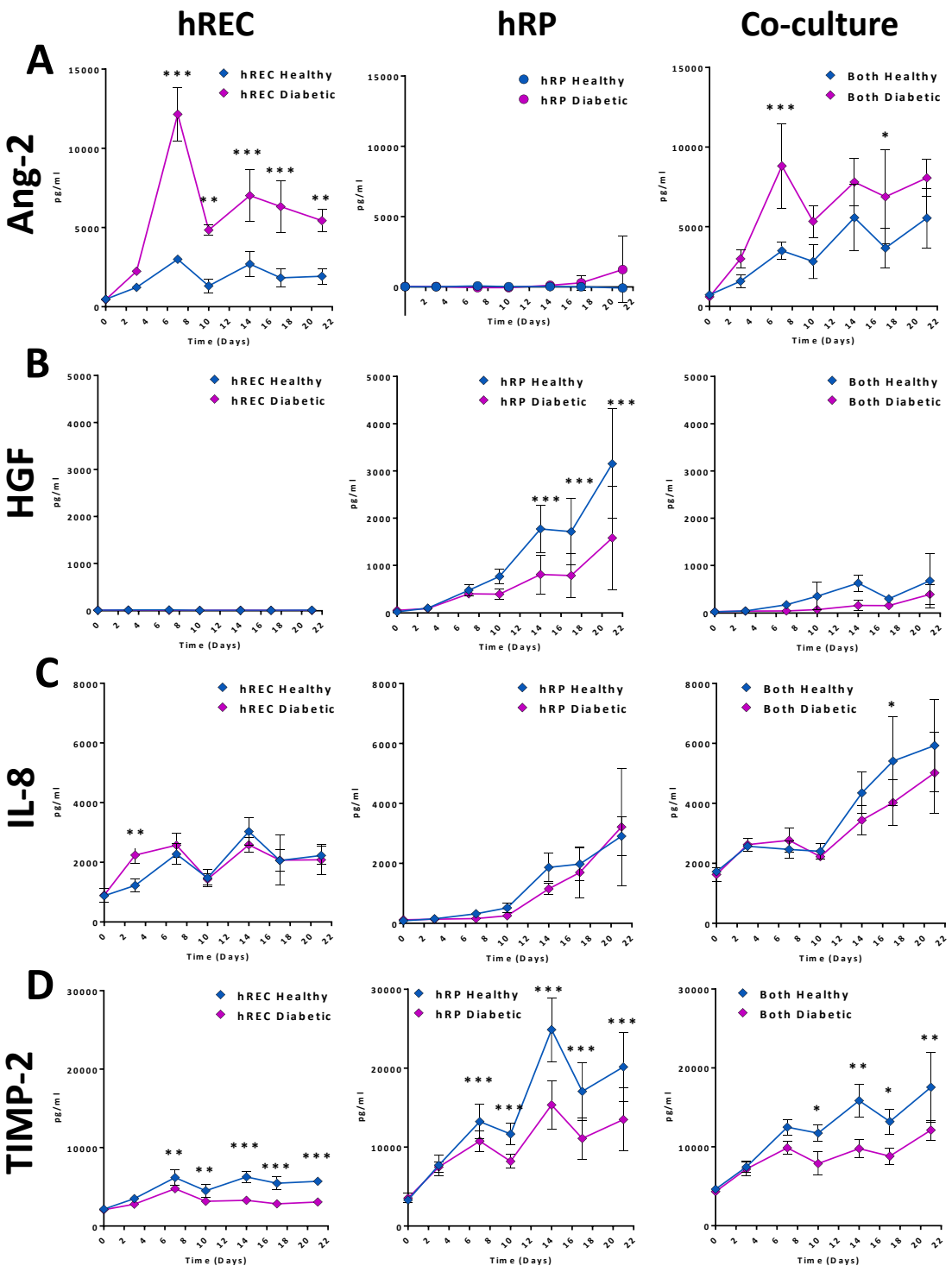

Figure 2.32. Different secretion profiles of hREC and hRP in mono- and co-cultures and the effect of diabetic culture conditions over time

hREC and hRP were cultured on PET membranes at 1:1 ratio, as mono- or co-cultures over 21 days. At seven time points media was collected and analysed for secreted Ang-2 (**A**), HGF (**B**), IL-8 (**C**) and TIMP-2 (**D**). All samples were tested in duplicate and corrected against a sample of media with no cells. Data presented is an average, n=3 and error bars represent SD. Two-way ANOVA with Sidak's multiple comparison test to account for errors from repeated measures was used to perform statistical analysis, using GraphPad Prism 6 software. *p<0.05, **p<0.01 and ***p<0.001.

2.4.25 VEGF RESULTS FROM ANGIOGENESIS BLOT CORROBORATE THAT MINIMAL VEGF WAS PRESENT

Results from the multiplexing data suggested VEGF levels at day 7 were overall very low (0-75pg/ml) (data not shown), with a large number of samples across all time points incalculably low, therefore it was not possible to analyse those results. In agreement with the multiplexing data, the VEGF and VEGF-D levels reported from the human angiogenesis antibody array at day 7 were also very low (0.06-0.28 relative to positive control) (Figure 2.32, Figure 2.33).

2.4.26 DIABETIC CO-CULTURE CONDITIONS CAUSED REDUCED LEVELS OF SECRETED ENA-78 AND IL-6 BY DAY 7

By day 7, Epithelial neutrophil-activating peptide 78 (ENA-78) levels were higher in the healthy co-culture model (1.5) compared to the diabetic co-culture model (0.84) (Figure 2.33). Both healthy and diabetic co-culture models displayed higher ENA-78 secretion than healthy and diabetic hREC monoculture models (0.06 and 0.1 respectively). Interleuikin-6 (IL-6) levels were highest in the healthy co-culture model (5.8), with one result reading as undetectably high (above the line), and at 2.15 in the diabetic co-culture model. Overall IL-6 levels were lower in the hREC monoculture model. Healthy hREC monoculture IL-6 secretion levels were 1.08 whilst diabetic IL-6 levels were almost half the levels at 0.59. Therefore, IL-6 levels were reduced in both mono- and co-culture diabetic models compared to healthy.

2.4.27 LEVELS OF SECRETED PDGF-BB AND TIMP-1 WERE REDUCED IN DIABETIC CO-CULTURE BUT NOT IN THE DIABETIC hREC MONOCULTURE CONDTIONS

Platelet derived growth factor-BB (PDGF-BB) levels were higher in the healthy co-culture model (1.01) than the diabetic co-culture model (0.34) at day 7 (Figure 2.33). PDGF-BB levels were the same in healthy hREC monoculture (1.51) as the healthy co-culture model (1.01). PDGF-BB levels in diabetic hREC monoculture (0.67) were double those of the diabetic co-culture model (0.34), although due to low n (2) this difference may not be significant. Overall, the diabetic co-culture model shows the lowest PDGF-BB expression. Both TIMP-1 and TIMP-2 density were relatively high, which corroborates multiplex day 7 data (Figure 2.32), where TIMP-1 levels were too high to quantify. For the angiogenesis antibody array, TIMP-2 levels were too high to quantify and therefore analyse, but TIMP-1 results fell within quantifiable range. TIMP-1 levels were lowest in diabetic co-culture (1.56) and highest in diabetic hREC monoculture (3.66), similar to but lower than the pattern of secreted PDGF-BB levels, suggesting the presence of hRP and diabetic conditions reduced the secretion of both proteins.

Overall, the angiogenesis blot data highlights differences in the secretome of angiogenic factors when ECs were grown on their own (circles) or as co-cultures (triangles) (Figure 2.33), which along with compelling evidence from the multiplex analysis data (Figure 2.32) supports the use of co-cultures to provide models closer to the *in vivo* environment when exploring changes to the retinal microvasculature.

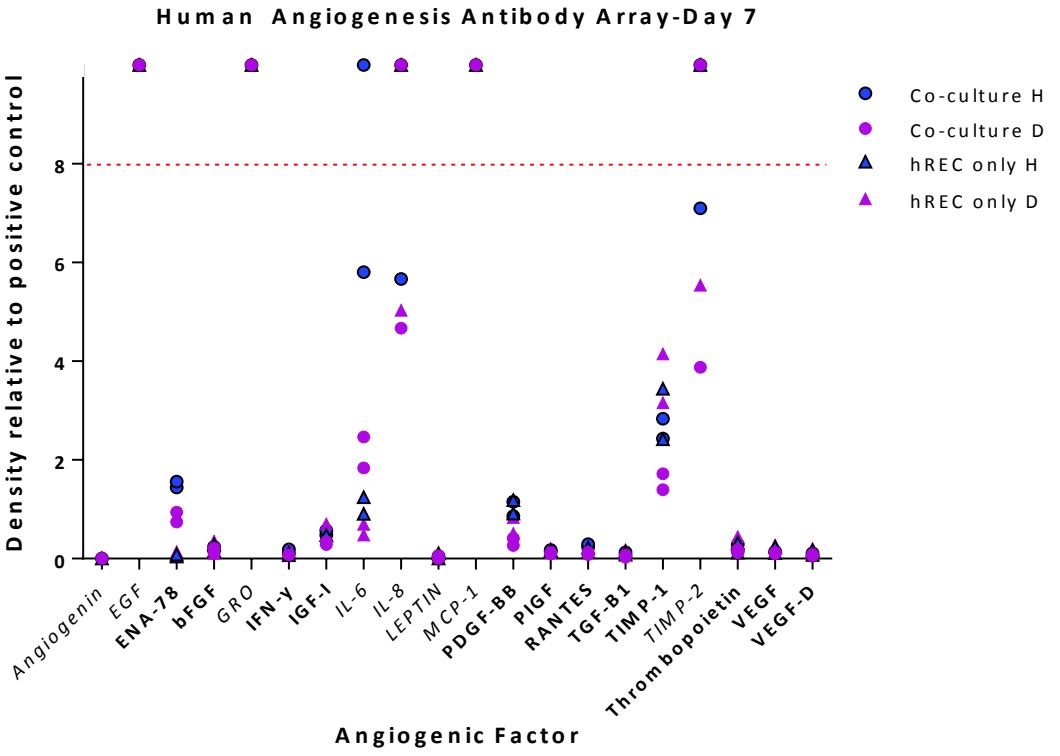

Figure 2.33. Different secretion profiles of hREC in mono- and co-cultures and the effect of diabetic culture conditions at day 7

Human Angiogenesis Antibody Array was used to analyse the same media used for the multiplex array (Figure 2.32). Data is from day 7 only, using multiple repeats pooled to make 1ml of supernatant, the volume required for the blot protocol. Models sampled were: hREC only healthy, hREC only diabetic, co-culture healthy and co-culture diabetic. 20 angiogenic proteins were analysed. Results above the red dotted line were too dense to be quantified. Results at 0 were not present in neat supernatant. Italics indicate when a result from one of the four models was too high or low to quantify. All blots were first normalised to positive control for each blot. Results are the mean of duplicates, with n=2.

2.5 DISCUSSION

2.5.1 OVERVIEW

The aim of this chapter was to develop and optimise a human primary, retina-specific, microvascular co-culture model to provide an *in vitro* environment to study; cellular changes, disease progression and future cellular or pharmacological intervention for conditions such as DR. Current treatment of DR only targets late stage disease, where dysfunction of the retinal capillary ECs and pericytes leads to microaneurisms, plasma exudates and edema and after an initial non-proliferative stage, new, leaky vessels form during PDR, further exacerbating the condition when large bleeds can lead to vision impairment or loss. This study aimed to explore the early changes in cell behaviour when cells comprising the retinal capillary (hREC and hRP) were subjected to either physiologically healthy or diabetic conditions. Traditional cell culture involves assessing the behaviour of cells grown on TC-treated plastic or glass, however, growing cells in isolation does not take in to consideration the effect of neighbouring cells, which would interact with each other *in vivo*. Therefore, growing hREC and hRP together with a shared BM mimic, in conditions optimised to maintain the phenotype/function of both cells would provide valuable data on the early cellular changes in T2DM.

This chapter provides data which confirm that hREC and hRP retained their phenotype *in vitro*, and can, therefore, provide human, tissue-specific data relating to changes between diabetic and healthy conditions, over time, unlike previous animal, immortalised or large vessel co-culture models reported in the literature. Differences in the cellular response to oxidative stress, angiogenesis and inflammation in healthy compared to diabetic conditions provided evidence that low oxygen (2%) and high glucose (33mM) insult induced a diabetic-like state in both hREC and hRP. The hREC and hRP response to oxidative stress, angiogenesis and inflammation were different when cells were grown as mono-culture compared to co-culture models, highlighting the importance of using co-culture models to elucidate modifications to the perivascular pericyte cells as well as the underlying EC layer during progression of DR.

2.5.2 hREC AND hRP ARE SUITABLE HUMAN PRIMARY CELLS TO STUDY THE CELLULAR RESPONSE DURING DIABETIC RETINOPATHY

In order to improve current treatment options for DR, investigation of early changes in the cells comprising the retinal microvasculature (hREC and hRP) would provide insight for potential new cellular or pharmaceutical therapies, to either slow or prevent progression to sight threatening stage of disease. Once taken from their *in vivo* tissue-specific environment, human primary cells grown for multiple passages *in vitro* can de-differentiate and become fibroblastic or senescent overtime, which is why many groups opt to genetically alter their primary cells to provide a stabilised cell line[191]. In particular, due to the pluripotent nature of the pericytes[192], it was important to ensure that there were no substantial changes in cell size and shape; which could indicate de-differentiation and provide irrelevant data. De-differentiation can be recognised using light microscopy by increased cell size and elongation when cells become fibroblastic, and also increase in size of the cell cytoplasm when cells become senescent[30,193]. In the present study, hREC and hRP maintained their characteristic morphology up to P10 without genetic modification, confirmed by regular light microscopy (Figure 2.8), IF staining (Figure 2.9, Figure 2.10) and flow cytometry analysis (Figure 2.11, Figure 2.12).

When investigating diseases of the vasculature, many groups exploring EC behaviour use macro-vascular sourced ECs such as HUVECs or aortic ECs *in vitro*, often from mouse or bovine tissue, simply due to ease of isolation from larger vessels and/or commercial availability[194], and validate their *in vitro* findings using an animal model. Human primary vascular ECs are commercially available sourced from pancreas or brain for example, however, there are differences reported between ECs isolated from different organs[14], and also between cells sourced from larger vessels compared to the microvasculature[42,195]. For example, long-term culture of capillary ECs requires specific protein coating of culture surfaces and specialised growth medium, compared to their large vessel counterparts[196]. These studies underline the importance of using human, primary, microvascular-sourced cells when investigating the retina, and also highlight some of the challenges faced when growing these cells *in vitro*.

To ensure the data reported were tissue-specific, hREC were regularly analysed to confirm endothelial functionality and ensure no endothelial to mesenchymal transition and hRP were assessed for cell-specific protein expression to ensure they had not de-differentiated to a fibroblastic phenotype, issues which have been reported by other groups when modelling

disease *in vitro*[48,197]. By day 21, hREC grown as monocultures retained expression of VE-Cad and ZO-1 (Figure 2.10, Figure 2.16, Figure 2.17, Figure 2.24, Figure 2.25), both of which are involved in the barrier function of ECs. At various time points hREC were tested for expression of CD31 and vWF, which are endothelial-specific, and hREC used in these experiments were always positive for both markers (Figure 2.10, Figure 2.12, Figure 2.16). Presence of αSMA in hREC would suggest trans-differentiation to smooth muscle cells or a fibroblast cell-type, due to the flexibility of primary cell fate *in vitro*[198], however hREC remained negative for αSMA expression throughout passaging (Figure 2.10, Figure 2.24, Figure 2.25, Figure 2.26).

In the present study, TEER was measured at multiple time points from experimental time 0 to day 21 and results were generally very low (6-18 Ω.cm^2) (Figure 2.23), when compared to similar contact co-culture experiments by other groups; Hayashi et al. reported up to 98 Ω.cm^2 and Wisniewska-Kruk et al. reported up to 380 Ω.cm^2 [62,199]. There was also no overall significant difference between mono- and co-cultured hREC TEER over the 21 days in our *in vitro* model, compared to the large differences reported in the study by Hayashi et al. *In vivo*, retinal ECs form a barrier between blood and the underlying tissue (BRB), with highly regulated permeability to allow nutrient exchange, and it is conjectured that this barrier regulation is disrupted in the early stages of DR[104]. TEER is often reported in EC studies as an indicator of the barrier function of an EC monolayer. Although it is a useful and relatively simple, high throughput method, several factors can influence TEER readings including but not confined to; temperature, surface area, passage number, culture period, cell culture medium components and shear stress[136]. In a tri-culture model of rat brain ECs, pericytes and astrocytes, TEER was reported as ~380 Ω.cm^2 by day 5, although the EC:Pericyte:Astrocyte seeding ratio was 10:1:1, quite different from my 1:1 ratio and cells were seeded on to 12 w/p transwell inserts with 0.4µm pores, all potential contributing factors in the discrepancies between our TEER results and other published groups[200]. Although every effort was made to ensure consistent temperature, appropriate transwell insert surface area and low cell passage number, it was not possible to draw any conclusions from the TEER data collected for this study.

Due to the pluripotency of the pericytes and dynamic expression of various markers, different groups use different antibodies to confirm phenotype. It is generally agreed that a panel consisting of antibodies against; PDGFR-β, NG2, desmin, αSMA and CD90 can be used to confirm hRP phenotype[47,201]. Throughout passaging, the hRP used in these experiments expressed these markers (Figure 2.9, Figure 2.18, Figure 2.19, Figure 2.30), albeit there was

a degree of heterogeneity within hRP cultures. Some hRP expressed αSMA, whilst some did not (Figure 2.30). This phenomenon has been reported in the literature[190,202], although the reason is not fully understood, and the positive/negative expression did not appear to be influenced by different culture conditions. CD146 was expressed by 26.3% of hRP (Figure 2.11) and this can be explained by the reported 'dynamic' expression of CD146 by pericytes, dependent upon specific *in vitro* environments[203,204]. hREC were CD31 positive and CD90 negative, in direct comparison with hRP which were CD31 negative, CD90 positive (Figure 2.12, Figure 2.11). CD90/THY-1 function is not yet fully understood but it is believed to be involved in adhesion and cell communication in numerous cell types, with highest expression in the neurovasculature in brain tissue of humans[190]. Interestingly, Park et al. found two distinct populations of human brain pericytes, one was CD90+ and 57% CD146+, one CD90- and 26.2% CD146+. However, the pericytes sourced from the human retina used in the present study appeared to be >99.9% CD90 positive (Figure 2.11), but also 26.3% CD146+, highlighting a broad similarity, whilst also emphasising differences in pericyte phenotype reported between different studies, and from brain as opposed to retinal tissue.

hRP function by wrapping around the perivascular surface of ECs, sharing physical contact through a shared BM and communicating via paracrine signalling (Figure 2.4)[205]. In the present study, hRP extended finger-like cytoplasmic projections through the 1µm pores when grown on the underside of the PET membrane, when cultured on their own or in co-culture, with hREC on the apical side (Figure 2.31). This happened in both healthy and diabetic conditions and was discovered using z-stack confocal imaging of anti-αSMA antibody staining, which labelled the actin cytoskeleton within the hRP cytoplasm. hRP morphology relates to function, enabling them to wrap around other cells, a function that has been observed *in vitro* when ECs and pericytes form structured tubules when cultured together in 3D gels[206–208]. Hence, the ability of hRP to send cytoplasmic projections through 1µm pores is not surprising, although this behaviour has not been reported in the literature before. The high resolution of the z-stack confocal images clearly showed the extension of the cytoplasmic αSMA projections through the pores and on to the top surface of the PET membrane. This altered the configuration of the co-culture in some areas, because the hREC and hRP were in direct physical contact rather than separated by the PET (ECM-substitute) membrane, and this finding should be taken into consideration when interpreting these data and designing future experiments.

As mentioned above, the phenomenon of some hRP expressing αSMA whilst others do not is not fully understood, but has been investigated by a number of groups to further elucidate the role of pericytes in vascular disease progression[190,202,209]. In the present study, there were no noticeable difference between percentage of αSMA positive/negative cells in healthy versus diabetic conditions (Figure 2.27, Figure 2.29). Because this αSMA positive/negative expression pattern has been reported by numerous groups, this corroborates our findings that the hRP in both mono- and co-culture experiments did not transition *in vitro* within our experimental timeframe, therefore validating our novel co-culture setup.

A combination of light microscopy, IF staining and flow cytometry has provided validation that hREC and hRP maintained their phenotype, confirming they could be grown together and were robust for long periods of time *in vitro.* Both hREC and hRP showed some degree of heterogeneity *in vitro*, however this is a common feature of human primary cells reported by other studies. hREC and hRP both grew in physiologically healthy conditions during growth optimisation and characterisation, and the next step was to assess their ability to withstand diabetic conditions mimicking DR.

2.5.3 DOUBLE INSULT OF LOW OXYGEN (2%) AND HIGH GLUCOSE (33mM) INDUCED CHANGES IN ANGIOGENEISIS, OXIDATIVE STRESS AND INFLAMMATION-REALTED PROTEIN EXPRESSION

Throughout onset and progression of T2DM, the ECs lining blood vessels and the perivascular pericytes progressively deteriorate due to the persistent, poorly controlled hyperglycaemic environment. Disruption to the EC capillary lining can lead to disrupted blood flow and ultimately vessel occlusion, which in turn causes ischemia, leading to hypoxia and subsequent non-perfusion of the underlying retina tissue. During T2DM, reduced insulin production or insulin resistance leads to an increase in blood glucose, and if poorly controlled or left untreated, causes a state of hyperglycaemia in the blood[66]. Therefore, in order to investigate cellular changes during T2DM, *in vitro* conditions were carefully optimised to mimic the *in vivo* glucose and oxygen concentrations reported in the healthy and diabetic retina.

In a healthy human, blood glucose levels should be between 4.0 to 5.4 mmol/L (72 to 99 mg/dL) when fasting and up to 7.8 mmol/L (140 mg/dL) 2 hours after eating[210]. For people with diabetes, the WHO defines hyperglycaemia as; blood glucose levels greater than 7.0 mmol/L (126 mg/dl) when fasting and greater than 11.0 mmol/L (200 mg/dl) 2 hours after meals (Table 1.3)[88]. Diabetes is a long onset, progressive disease (often 10-20 years before symptoms arise), so to mimic that condition *in vitro*, generally much higher glucose

concentrations are used. Several groups have used [D]+ glucose concentrations ranging from 20-35mM to represent high glucose conditions relevant to human T2DM *in vitro*[97,126,127,211–215]. Measurements of metabolic activity in hRP grown in 0-35mM glucose for over 14 days indicated a significant difference at 35mM, compared to 20-30mM (Figure 2.15), suggesting that this very high dose had an effect on cell function. 25mM or 30mM D-glucose is most commonly used to mimic diabetes *in vitro*, however following the trend of altered metabolic activity above 30mM glucose for hRP in the glucose concentration curve, I chose 33mM as this has previously been reported in the literature[126].

Modelling a disease *in vitro* is often a compromise between mimicking as closely as possible the *in vivo* disease, whilst working within the laboratory parameters. Choosing the appropriate oxygen tension presents a complicated issue for cell culture experiments. During optimisation, by day 7, hREC and hRP mono-cultures at high glucose and 5% oxygen were viable and showed only minor differences in angiogenic response compared with control, but no difference in junctional and oxidative stress protein expression (Figure 2.17, Figure 2.19), therefore, oxygen levels were reduced to 2% for subsequent co-culture experiments. This lack of difference between *in vitro* optimised 'healthy' and 'diabetic' conditions could in part be due to the use of sustained high glucose levels. Other groups report that intermittent high glucose has a more detrimental effect on both ECs and pericytes[97,127,216]. However, the multifactorial environment of diabetes progression makes it very difficult to account for every parameter, and sustained high glucose was used for my model. This prevented regular re-oxygenation of the cultures, which would have occurred if regular changes of medium were required to alter glucose levels. Intermittent glucose is, however, an important risk factor for disease progression and should, therefore, be considered for future work.

Oxygen levels *in vivo* vary between tissues, from 12% to 1%, depending on distance from the arterial blood vessel supply and the metabolic requirements of the tissue[12]. Oxygen levels in the human eye have been reported as ranging from 1 to 5%[217], and the tissue of the retina has the highest oxygen consumption in the body, due to the high metabolic activity and constant renewal of the photoreceptors in the neural retina[218]. Therefore, along with the brain, alterations in oxygen and nutrient supply caused by compromised blood flow, can have particularly profound effects on the cells of the retina, leading to vision loss[219]. It is widely accepted that human primary cells, and stem cells in particular, favour a low oxygen environment (<5%) similar to *in vivo* levels, to allow cell growth without de-differentiation[220]. This, therefore, is in opposition to the idea of growing human primary cells at ambient (20%)

oxygen, as hyperoxia as well as hypoxia can cause oxidative stress damage to the cell via ROS production[221,222]. This suggests during the process of primary cell isolation and culture, ambient 'physioxia' (20%) may induce some unavoidable, undesirable changes to the human primary cells that would not be seen *in vivo*[223]. However, with consideration of these cell culture limitations, data from this model remains very useful in beginning to elucidate cell changes in diabetic conditions.

In the present study, HIF1α expression in hRP subjected to 5% oxygen and 33mM glucose for 7 days (during initial optimisation of diabetic conditions), appears perinuclear, suggesting the hRP in the double insult conditions underwent a major transcriptional alteration to adapt to hyperglycaemic, hypoxic conditions (Figure 2.19). Early pericyte drop-out is characteristic of DR, alongside EC dysfunction and ultimately vascular leakage[108,157]. Disrupted blood supply and/or insufficient gas exchange at the capillary bed can create a hypoxic environment, leading to activation of HIF-1α within the cell, which is at the centre of complex pathways that enable cell survival, including initiating angiogenesis by activating VEGF gene transcription[224]. SOD-1 (CuZn-SOD) is the soluble cytosolic form of SOD, and along with SOD-2 (Mn-SOD, mitochondrial) and SOD-3 (EC-SOD, extracellular), are the primary anti-oxidant enzymes that protect cells from free radical damage[225]. SODs are highly conserved enzymes that catalyse the conversion of highly reactive superoxide anion into oxygen and hydrogen peroxide[124]. Decreased SOD-1 activity has been reported in obese humans[91], and SOD activity is reduced and its expression down regulated in the diabetic retina[226]. SOD-1 was expressed specifically at the ER compartment in hRP grown in 5% O_2 (Figure 2.19), suggesting the oxidative stress response was activated. However, unlike the hREC, hRP showed no difference in Ang-2 expression at 5% compared to 20% O_2, therefore, an antioxidant response, but not an angiogenic response had been initiated by the hRP (Figure 2.17, Figure 2.19).

In the present study, Cx43 was expressed throughout the cytoplasm at all time points, except for on day 14 in diabetic conditions, where Cx43 appeared to cluster at the cell-cell junction more than at any other time or condition, perhaps representing a tight monolayer (Figure 2.24, Figure 2.25, Figure 2.26, Figure 2.28, Figure 2.29). This suggests Cx43 expression is highly dynamic and is affected by oxidative and hyperglycaemic stress. Breakdown of the EC cell-cell junctions leads to leaky microvasculature, and during T2DM this EC barrier breakdown is insufficiently repaired for reasons not yet fully understood. Therefore, the expression of barrier proteins VE-Cad, ZO-1 and Cx43 was explored, due to their role in EC

cell-cell communication. Cx43 is a component of EC GJs, reported to be involved in numerous processes such as cell-cell communication, cell migration and survival signalling as well as proliferation and wound healing[227]. Of the three connexins expressed in the retinal vascular ECs (Cx37, Cx40 and Cx43), Cx43 is the most abundant type[228]. Various groups have suggested Cx43 expression is affected *in vitro* by diabetic cell culture conditions[229], which supports the change in Cx43 expression in the diabetic conditions observed in the present study.

ZO-1 is a TJ protein which regulates tension by acting on VE-Cad and is involved in barrier formation, cell migration and angiogenesis of primary ECs[60]. In a study using bovine retinal microvascular ECs, conditioned medium from cultured rat brain astrocytes was found to increase ZO-1 expression compared to controls, suggesting factors released by astrocytes (a perivascular cell-type) contribute to EC barrier function in, for example, the blood-brain barrier (BBB) and BRB[230]. This was more recently confirmed by Dohgu et al., who found increased BBB function with a significant decrease in the permeability to sodium fluorescein in a co-culture of immortalised mouse brain capillary ECs with primary rat brain pericytes, compared to mono-cultures, induced by Transforming growth factor-β (TGF-β) secretion from the pericytes[231] . Although Dohgu et al. did not investigate ZO-1 expression, TGF-β has been attributed to upregulation of ZO-1 and, therefore, improved barrier properties when added to quiescent, but not proliferating human primary corneal ECs *in vitro*[232]. TGF-β has not been explored in our study, however, these findings highlight the importance of release of growth factors from neighbouring cells, which directly influence EC behaviour, hence underlining the benefit of using *in vitro* co-culture models as opposed to traditional mono-cultures. These publications suggest co-culturing hRECs with a perivascular cell such as hRP may improve ZO-1 expression, however, ZO-1 was expressed equally in both mono- and co-cultures and in both healthy and diabetic conditions at day 7 (Figure 2.24, Figure 2.28). By day 21 in co-cultures, hREC maintained a healthy morphology with ZO-1 expression at cell-cell borders only in the healthy conditions, whereas in diabetic conditions there was cell rounding and shrinkage, creating large empty spaces on the PET membrane, suggesting dysfunctional hREC at this stage (Figure 2.29). In healthy mono-cultures, hREC number was reduced and there was loss of cell-cell contact, with large gaps between cells (Figure 2.26). This supports the hypothesis that co-culture with hRP in healthy conditions sustains hREC for extended culture periods (21 days) compared to mono-cultures and also that hREC do not survive as well in long term diabetic co-culture conditions compared to healthy. The effects of the diabetic insult were more noticeable in the co-culture compared to the mono-culture

at day 21 (Figure 2.26, Figure 2.29), highlighting the necessity to co-culture hREC with hRP to achieve more relevant results, considering they are so closely associated *in vivo*.

VE-Cad was expressed by hREC in both health and diabetic conditions and also in mono and co-cultures (Figure 2.10, Figure 2.24, Figure 2.25, Figure 2.28). By day 21, hREC in diabetic conditions in both mono- and co-cultures underwent cell rounding and shrinkage, creating large empty spaces on the PET membrane, suggesting dysfunctional hREC at this stage (Figure 2.26, Figure 2.29). As with the observations of ZO-1 expression, there was more cell shrinkage in the diabetic co-culture model, although the number of cells remaining was similar compared to diabetic mono-culture at day 21, suggesting the double insult of sustained low oxygen and high glucose for 21 days led to EC dysfunction, and barrier failure in both mono- and co-cultures over time (Figure 2.26, Figure 2.29). VE-Cad is a member of the cadherin family, the vascular endothelial-specific transmembrane component of the adherens junction complex. In a recent comprehensive study by Tornavaca et al., it has been found to be upstream of ZO-1, which indicates VE-Cad is essential to recruit ZO-1 through regulation of the actin cytoskeleton[60]. VE-Cad is also involved in multiple regulatory and signalling mechanisms such as modulating growth factor receptors, intracellular messengers and proteins for gene transcription regulation[59]. In a study using primary ECs, pericytes, and perivascular resident macrophage-type melanocytes isolated from cochleae of mice, Neng et al. found conditioned media from pericytes and perivascular macrophage-type melanocytes caused increased expression of ZO-1 and VE-Cad by ECs at the mRNA and protein level, and found increased barrier function[233]. Therefore, exploring the presence of both VE-Cad and ZO-1 would confirm the presence of mature and functional barrier junctions between ECs as well as normal EC regulation and signalling.

2.5.4 hREC AND hRP HAVE SIGNIFICANTLY DIFFERENT SECRETION PROFILES WHEN GROWN INDIVIDUALLY OR AS CO-CULTURES IN HEALTHY OR DIABETIC CONDITIONS

Cells cultured in co- or tri- culture models are continuously being investigated and re-developed, with the aim of developing highly reproducible, stable environments that can be used for applications such as disease modelling and drug testing[234]. To create environments as close as possible to *in vivo* human tissues, whilst reducing the complexity of multiple factors influencing results, simple but well characterised, species and tissue-specific co-culture models can provide invaluable data on, for example, toxicity reports, cell signalling pathways, cell growth etc., as a step before the use of animal models or clinical trials. To understand changes in the retinal microvasculature, where pericyte coverage is very high,

optimising a co-culture of hRP and hREC provides more relevant data that may not be present in mono-cultures of either cell-type. Several signalling systems have been implicated in pericyte:EC function, therefore, the breakdown or dysfunction of these interactions is likely to add to the diabetic milieu, and may provide a target for intervention at early stage DR[46].

In the present study, cell culture medium was collected at 7 time points, over 21 days, providing data on cell behaviour over time rather than a few early, or one single time point (Figure 2.32). Cell culture medium from day 7 was analysed for secreted proteins via both multiplex and antibody array techniques. Published co-culture models range in time scale from: unreported, to 2, 3 and 8 days, providing data on relatively short-term disease models[62,131,199]. In an *in vitro* study of the effect of hyperglycaemia on human retinal ECs, hRECs responded to cytokines rather than high glucose[235], suggesting diabetes–related EC injury in the retina may be caused by glucose-induced cytokine release by non-endothelial retinal cells, and hREC can in fact withstand high glucose insult alone. Therefore, we investigated the response of hREC grown alone and hREC co-cultured with hRP, and the results suggest the two cell-types do secrete different proteins when grown as mono- vs. co-cultures.

To improve understanding of the physiological changes occurring in a chronic disease such as T2DM, the secretion profile of 9 angiogenic proteins released from: hREC only, hRP only and co-cultures, in healthy and diabetic conditions was analysed at 7 time points, over 21 days and directly compared and quantified, using multiplex technology (Figure 2.32). Four proteins were too low to quantify using these experimental parameters: TNFα, VEGF, PDGF and FGF. TIMP-1 levels were too high to quantify in all conditions. Ang-2, IL-8, TIMP-2 and HGF were all secreted at levels within range for direct quantification and significant differences in cell secretion profile of these four angiogenic proteins were found when hRP and hREC were grown individually compared to when grown as co-cultures. Cells grown in diabetic conditions also had significant changes to all four proteins, compared to those grown in healthy conditions, in both mono- and co-culture models.

Table 2.9. SUMMARY OF SECRETED ANG-2 FROM EACH MODEL

ANG-2	Day 7		Day 14		Day 21	
Model	**Healthy**	**Diabetic**	**Healthy**	**Diabetic**	**Healthy**	**Diabetic**
hREC only	+	+++	+	++	+	++
hRP only	-	-	-	-	-	+
Co-culture	+	++	++	++	++	++

A summary of the results for Ang-2 expression is provided in Table 2.9. Under physiologically healthy conditions, Ang-1 binds to and activates the Tie-2 receptor, leading to increased; EC survival, vessel stability, TJ integrity and ultimately tissue homeostasis[236]. Under pathological conditions, such as T2DM, Ang-2 is upregulated and competes against Ang-1 for binging on the Tie-2 receptor, resulting in inactivation and ultimately destabilisation of the vasculature via an angiogenic shift in the target cells[34]. Current treatment for PDR involves a combination of laser therapy and anti-VEGF drugs, however new treatments based on targeting the effect of Ang-2 are currently at early clinical trial stage[99]. Data from the present study suggest hRP grown as monoculture do not secrete Ang-2, until day 21 when very low levels are secreted in diabetic conditions (Figure 2.32A). hREC grown as monocultures secreted Ang-2 at consistently low levels in healthy conditions over time, whereas in diabetic conditions hREC Ang-2 levels were significantly higher from day 3 onwards. Ang-2 levels in the co-culture model were also higher in the diabetic conditions at all time points. Ang-2 levels in healthy co-cultures were overall higher than EC grown in healthy monoculture, which implies the presence of hRP results in higher ambient Ang-2 secretion by either hREC alone, or both hREC and hRP in healthy co-culture conditions. In diabetic co-culture conditions, the peak in Ang-2 secretion at day 7 was 27.45% lower than the peak in the hREC only diabetic model. That being said, from days 10-21, Ang-2 levels remained higher in diabetic co-culture compared diabetic hREC monoculture conditions. By day 21 diabetic co-culture Ang-2 levels were 32.6% higher than levels in diabetic hREC monocultures. Taken together these data imply Ang-2 is highest in diabetic conditions. Ang-2 levels were generally higher in the co-culture model, except of a higher peak at day 7 in the diabetic hREC only model. This suggests the presence

of hRP increased Ang-2 secretion in both healthy and diabetic co-culture models compared to hREC grown on their own. Many studies using both animal and human retinae suggest Ang-2/Tie signalling is critical for pericytes survival and interaction with underlying EC, where increased Ang-2 activity leads to unstable pericyte:EC contact points[44,53]. In a mouse study, Park et al. found high glucose conditions resulted in Ang-2 induced pericyte apoptosis via α3β1 integrin[237]. Overall, in agreement with reports from the literature, we found a significant, very high peak in Ang-2 in diabetic conditions. My results highlight the difference between hREC and hRP grown in monoculture compared to co-cultures and also the importance of the 21 days duration of cell culture, considering changes were observed over a long period of time e.g. hRP do not secrete detectable levels of Ang-2 until very low levels in diabetic conditions at day 21.

Table 2.10. SUMMARY OF SECRETED HGF FROM EACH MODEL

HGF	Day 7		Day 14		Day 21	
Model	**Healthy**	**Diabetic**	**Healthy**	**Diabetic**	**Healthy**	**Diabetic**
hREC only	-	-	-	-	-	-
hRP only	+	+	++	+	+++	++
Co-culture	+	-	+	-	+	+

A summary of the results for Hepatocyte growth factor (HGF) expression is provided in Table 2.10. HGF, or scatter factor, has been described as both an adipocytokine and a hepatokine[238], which has a role in metabolic flux of glucose in various insulin-sensitive cells, with growing evidence suggesting HGF plays a role in metabolic disorders such as T2DM[239]. A study using bovine retinal ECs concluded retinal ECs secrete HGF and it is involved in EC proliferation and migration, although the concentrations of [D+]glucose used during cell culture were not specified[240]. In the present study, HGF was not secreted by hREC in monoculture. HGF was secreted by hRP, increasing over time, with significantly more HGF secreted in healthy conditions compared to diabetic (Figure 2.32B). When hREC and hRP were grown in co-culture, HGF levels remained very low across the 21 days, in both healthy and diabetic conditions. HGF levels peaked in healthy hRP monocultures, reaching 3151.3pg/ml by day 21, 4.7 fold higher than in healthy co-cultures. Taken together, these

data suggest the presence of ECs in the co-culture model reduced the level of HGF secreted by hRP, which over time cultured alone secreted over 4 times more in healthy conditions. In a study of 1,474 patients, significant increase in HGF levels was correlated with multiple components of the metabolic syndrome[241], however, this was a general disease-free population study, so these patients were not diagnosed with T2DM. A comprehensive study comparing human patients at various stages of eye disease, both diabetic and non-diabetic, found vitreous HGF levels significantly increase depending on severity of retinopathy[242]. This study suggests HGF levels vary depending on stage of retinopathy, and they focused on PDR. PDR has not been specifically pharmacologically induced in the present study, so although useful, Nishimura et al's. data is not directly comparable to the reduced HGF observed in the present study. These results further highlight the differences in hREC and hRP behaviour when grown as monocultures compared to co-cultures, and again the importance of monitoring protein secretion over an extended period of time, because some changes only became significant after 14 days.

Table 2.11. SUMMARY OF SECRETED IL-8 FROM EACH MODEL

IL-8	Day 7		Day 14		Day 21	
Model	**Healthy**	**Diabetic**	**Healthy**	**Diabetic**	**Healthy**	**Diabetic**
hREC only	+	+	+	+	+	+
hRP only	-	-	+	+	++	++
Co-culture	+	+	++	++	+++	+++

Interleukin-8 (IL-8) is a chemokine involved in systemic immunity, wound healing, macrophage infiltration, inducing chemotaxis in target cells, and also a potent promoter of angiogenesis[243]. A summary of the results for IL-8 expression is provided in Table 2.11. Both hREC and hRP secreted IL-8 when grown in monoculture, in both healthy and diabetic conditions (Figure 2.32C). Except for a rise in IL-8 in at day 3 in hREC grown as monocultures in diabetic conditions, there was no significant difference between healthy and diabetic conditions over time. hRP initially secreted very low levels of IL-8 until day 10, where in both healthy and diabetic conditions IL-8 levels increased until day 21, although there was no significant difference between healthy and diabetic conditions. In the co-culture model, IL-8

levels remained consistent from 0-10 days at roughly 2500pg/ml for both healthy and diabetic models, until day 10 where IL-8 levels increased over time, with higher levels in healthy conditions, although this only reached significance at day 17. Unfortunately no results could be extrapolated from the day 7 human antibody array IL-8 data, because IL-8 levels exceeded the maximum density for quantification (Figure 2.33), however, this does support the presence of IL-8 at day 7, in both the hREC and co-cultures, as detected from the multiplex data. Circulating IL-8 is elevated in patients with T2DM[244] and also elevated in Keratinocytes cultured in high glucose at both the mRNA and protein level[245]. Due to its role in the inflammatory pathway and because diabetes is a disease of chronic inflammation, IL-8 levels were expected to be significantly raised in the diabetic conditions, however this was not the case within the timeframe of this experiment. Nevertheless, the contrast between the mono- and co-culture results and the change in IL-8 secretion over a long period of time again highlights the importance of both co-culturing and longer experimental time scales, extending beyond 14 days.

Table 2.12. SUMMARY OF SECRETED TIMP-2 FROM EACH MODEL

TIMP-2	Day 7		Day 14		Day 21	
Model	**Healthy**	**Diabetic**	**Healthy**	**Diabetic**	**Healthy**	**Diabetic**
hREC only	+	+	++	+	++	+
hRP only	++	++	+++	++	+++	++
Co-culture	++	++	++	++	+++	++

TIMP-2 is constitutively expressed in most tissues and has highest affinity to inhibiting MMP-2 activity, important for maintaining ECM homeostasis in healthy and pathological conditions[246]. TIMP-2 inhibition of MMP-2 leads to reduced ECM remodelling. Capillary BM thickening is reported in DR[247]. Dysregulated remodelling of the ECM can lead to BM thickening, due to increased deposition of BM proteins, resulting in disruption to normal cell signalling in the over or underlying cells[248]. The ratio between MMPs and TIMPs can be predictors in wound healing, which is impaired in T2DM[249]. TIMP-2 was found to inhibit the proliferation of human microvascular ECs *in vitro*[250]. A summary of the results for TIMP-2 expression is provided in Table 2.12. In the present study, TIMP-2 was significantly reduced

in diabetic conditions for all models, compared to healthy conditions, from day 7-10 onwards (Figure 2.32D). TIMP-2 was secreted at higher levels overall by hRP than hREC. hRP TIMP-2 secretion increased over time, and was significantly higher in healthy than diabetic conditions. A similar trend but lower overall levels of TIMP-2 was secreted in the co-culture model. In my study, hREC cultured alone secreted relatively low, stable levels of TIMP-2. As observed with HGF and Ang-2, the presence of both cells in the co-culture appears to reduce the overall levels of TIMP-2 secretion. Unfortunately no results can be extrapolated from the day 7 human antibody array TIMP-2 data, because TIMP-2 levels exceeded the maximum density for quantification in all conditions (Figure 2.33).

In the diabetic environment, reduced TIMP-2 levels may result in increased activity of MMP-2, leading to ECM remodelling, and potentially interference with normal cell adhesion, function and cell:cell communication, mimicking an angiogenic switch, such as a progression towards PDR. MMP-2 levels in cultured HUVEC were reported as reduced over time, which conflicts somewhat with data from the present study, considering TIMP-2 secretion was stable over time in the healthy monoculture model[39]. MMP-2 and -9, along with their affiliated TIMPs; TIMP-1 and -2, were found to be elevated in the serum of diabetic patients compared to controls ($p<0.0001$)[251]. Our data does not agree with the report by Derosa et al., however they analysed human serum directly from patients whereas our TIMP-2 data were collected from conditioned cell culture medium. High levels of MMPs as well as their TIMPs may reflect abnormal ECM metabolism. In agreement with our discovery of reduced TIMP-2 in diabetic conditions, Lobmann et al. reported reduced TIMP-2 in tissue biopsies taken from chronic foot ulcers on diabetic patients, compared to healthy controls[252]. One suggestion for the discrepancy in reported TIMP-2 levels between Lobmann et al. and Derosa et al. is the duration of T2DM. Patients from the Lobmann study were on average 10 years older, with diagnosed T2DM for on average 15 years, whereas patients from the Derosa study had T2DM diagnosis for only roughly 5 years, with no pharmaceutical intervention. These two groups represent entirely different patient populations, where foot ulcers analysed in the Lobmann group come from a more progressed stage of disease. Therefore, it is possible TIMP-2 levels vary depending on disease stage, possibly increasing at early stage, followed by a decrease at later stage. Our data follows that of a putative later stage of T2DM, similar to the findings by Lobmann et al.

With regards to reporting human angiogenesis antibody array data, results were technical duplicates from two experiments (n=2), therefore statistical analysis was not performed,

although trends and general observations have been reported. It was also not possible to directly quantify protein levels, therefore all data is reported normalised to positive controls.

Human angiogenesis antibody blot data from day 7 shows diabetic co-culture conditions resulted in the lowest rates of TIMP-1 (Figure 2.33). However, TIMP-1 secretion was highest by hREC in diabetic monoculture conditions. These data further support the multiplex results, which suggest there are major differences between the secretion profiles of hREC in monoculture compared to co-culture. As described with TIMP-2, TIMP-1 has particular affinity to certain MMPs including MMPs 1, 3, 7 and 9, and binding leads to inactivation of ECM remodelling. In a study by Jayashree et al., where serum levels of TIMP-1 and MMP-9 were compared between patients with T2DM, with or without retinopathy, there were no statistical differences in TIMP-1 levels, although MMP-9 was significantly higher in patients with DR ($p=0.048$), with positive correlation with severity of disease[253]. Therefore, with greater activity of MMP-9 and unaltered TIMP-1 levels, this could lead to MMP-9-driven dysregulated ECM remodelling, which could contribute to the weakening of the BRB at this stage of DR.

Epithelial neutrophil activator (ENA-78)/CXCL5 is a proangiogenic chemokine which along with its family of CXCL proteins, promote vascular EC growth[93]. Levels of ENA-78 were very low in the hREC monocultures in both healthy and diabetic conditions. Interestingly ENA-78 levels were increased in co-culture conditions, with the highest levels observed from the healthy co-culture models (Figure 2.33). Yuen et al. showed silent information regulator protein-1 (SIRT-1) activation led to increased secretion of proangiogenic chemokines including ENA-78, restoring EPC function in *ex vivo* diabetic rat outgrowth ECs[254]. This suggests ENA-78 may be downregulated in diabetes, and our data does suggest reduced ENA-78 secretion from the diabetic co-culture model compared to the healthy co-culture at day 7. In an analysis of serum from 93 patients, Meleth et al. investigated a panel of cytokines and chemokines to assess their involvement in severity of DR. RANTES (regulated on activation, normal T cell expressed and presumably secreted) is a chemokine for recruiting T-cells, eosinophils, basophils, and leukocytes into inflammatory sites. They found significantly elevated levels of RANTES in severe NPDR and positive immunostaining for monocyte chemoattractant protein-1 (MCP-1) in the inner retina, but no significant differences between VEGF or ENA-78 levels when less severe DR samples were compared to severe DR samples[255]. The immunoblot data in the present study for MCP-1 secretion was too high to quantify in all conditions, whilst negligible levels of RANTES were detected in all conditions.

However, the data from Meleth et al. was healthy controls, therefore is not directly comparable to our healthy mono- or co-culture data.

IL-6 is a cytokine involved in the infection and inflammation immune response and also in regulation of metabolic, regenerative and neural processes[256]. IL-6 levels are raised in most inflammatory diseases and both obesity and T2DM are considered long term inflammatory diseases, where cytokines and chemokines such as IL-1β, IL-6 and C-reactive protein (CRP) are elevated[257]. Contrary to reports of elevated IL-6 in obesity and T2DM, data from the present *in vitro* models suggests IL-6 levels were highest in the healthy co-culture model, where levels unfortunately exceeded the maximum quantifiable density, so therefore could not be measured (Figure 2.33). This discrepancy could possibly be due to very long onset of DR *in vivo* compared to relatively short *in vitro* disease modelling, which will always be a limiting factor. IL-6 levels were much lower in the hREC monocultures compared to co-cultures and lowest overall in diabetic monocultures, although this would need to be repeated to determine if the difference was significant. These results suggest that growing hRP and hREC together increases IL-6 secretion overall.

PDGF-BB is an important growth factor for all phases of wound healing as well as a potent mitogen for mesenchymal cells[258]. In a study focused on diabetic nephropathy, urinary excretion rates of PDGF-BB from 65 cases of diabetes and 27 controls were analysed using ELISA and urinary PDGF-BB rates significantly increased congruent to urine albumin excretion[259]. This implies PDGF-BB may play a role in the onset of diabetes, linked with early microvascular changes. In a study comparing vitreous and serum levels of PDGF isoforms (-AA, -AB and –BB) with VEGF levels in 31 patients with PDR and 15 non-diabetic controls, all isoforms of PDGF along with VEGF were significantly increased in the vitreous samples from PDR group compared to controls, although this was not evident from serum samples[260], which may suggest a tissue-specific (posterior compartment of the eye) response. In contrast to the two aforementioned studies, in the present study, PDGF-BB levels were lowest in the diabetic co-culture model and highest in the healthy co-culture model (Figure 2.33). It is possible this data contrasts with data from human clinical samples due to different stage of disease, or because although co-culturing aims to improve the *in vitro* similarity to the *in vivo* environment, the retinal vasculature is a multifaceted environment, and it remains difficult to replicate all elements in a laboratory model .

Surprisingly, data from the multiplex and blot arrays indicated that levels of secreted VEGF and VEGF-D were negligible (Figure 2.32, Figure 2.33). VEGF levels increase in the ocular fluid

of patients with varying stages of DR, with a large increase particularly during PDR[261]. In a study of 65 patients, Baharivand et al. found serum (515.21 vs 343.58 pg/ml) and vitreous (383.1 vs 24.81 pg/ml) concentration of VEGF were significantly raised in patients with PDR compared to NPDR, and that vitreous and serum VEGF levels were correlated, although serum levels were always much higher[102]. However various groups have reported a wide range of VEGF levels in vitreous and serum, from both healthy and diabetic patients, suggesting VEGF levels may be quite variable on an individual basis and also highly dependent on stage of DR. That being said, all the concentrations reported in the literature fall within range for detection using the multiplex system used in the present study, therefore it is unclear why VEGF could not be detected. Individual variation and precise disease stage is very difficult to model *in vitro*, using primary human cells in a highly simplified environment. Kumar et al. detected secreted VEGF from their mono- and co-culture *in vitro* models made using human retinal progenitor cells and HUVEC, over a 48H period, where levels peaked at ~90pg/ml/mg at 24H in the contacting co-culture model in 1% oxygen conditions[130]. For the multiplex analysis, VEGF detection range was 2.7-2000pg/ml, which would enable detection if VEGF levels were similar to those found by Kumar et al.. It is not fully understood why VEGF appears absent from all conditions, however some factors may include; cell type (HUVEC vs hREC), cell number (6-well inserts vs 24-well inserts), transwell insert material (polyester vs PET), smaller transwell pore size (0.4µm vs 1µm), 1% lower oxygen, duration of experiments (24H vs 7 days).

2.6 LIMITATIONS & FUTURE WORK

There are already multiple variables to the different mono-/co-culture, healthy/diabetic, 0-21 day models discussed in this chapter, however further optimisation could include adding flow, fluctuating glucose levels and reducing oxygen tension to 1%, and should all be considered when taking this model forward. Taking into account multiple factors, these variables were adapted from previous successful co-culture models[62], according to primary cell availability, time and financial constraints. Seeding density and ratio was optimised for initial 1:1 hREC:hRP coverage, however growth curve data suggests lower seeding density of hRP may be required to maintain that ~1:1 ratio at later time points. Blot data was analysed from only one time point; day 7. It would be interesting to see the change in secretion of angiogenic factors at multiple time points, as was performed in the multiplex array data, however this was beyond the scope of this study. Angiogenesis blot data reported was n=2 and multiplex data was n=3, therefore to give greater power and confidence, repeats should

be carried out. Fluctuating glucose has been reported to have more detrimental effect on both the ECs and pericytes[97,216], therefore, in future experiments fluctuating glucose from low-mid range to high range may result in a more diabetic-like phenotype. Adding flow to the mono- and co-culture models may result in changes to the barrier function of the hREC[63], and create a model closer to the BRB. That being said, overall this work has produced a human, primary co-culture model of the retinal vasculature, which can withstand long term diabetic insult. This model can be further adapted or modified to suit purpose by adding any of the variables mentioned above, and is a useful tool for modelling diabetes *in vitro.*

2.7 CONCLUSIONS

The major hurdles in optimising this human primary model of the retinal microvasculature involved first optimising growth conditions to maintain two different cell-types for multiple passages and extended periods of time, on both TC plastic and PET membranes, and second growing these cells together on either side of the same PET membrane for up to 21 days in culture. Data presented in this chapter confirms successful growth of human primary hREC and hRP and these cells have been stringently characterised. Introducing carefully optimised healthy and diabetic conditions to the mono- and co-culture models enabled data collection up to 21 days and the differences in the secretion profile of the healthy compared to diabetic models suggest the cells have undergone changes in the low oxygen, high glucose environment. Significant differences were discovered in the secretion profile of hREC grown as mono-culture compared to co-culture with hRP, highlighting the importance of studying the behaviour of these two closely interacting cells together rather than in isolation.

3 CHAPTER 3

Isolation and expansion of human ECFCs for incorporation into an *in vitro* model of DR

3.1 OVERVIEW

Since their discovery in 1997, ECFCs have been identified as a prospective autologous cell therapy for blood vessel repair. With developments in cell culture technology, identification and expansion of this small population of cells from human blood have improved and there has been a focus on standardising protocols. Animal studies using the OIR model have provided evidence that ECFCs can physically incorporate and contribute to repairing vessels damaged by ischemia *in vivo.* During T2DM, the microvasculature is damaged due to persistent hyperglycaemia, disrupted blood supply and, therefore, reduced oxygen delivery and due to the high metabolic activity of the photoreceptor cells, the retina is particularly sensitive to this damage. ECFCs were isolated from UCB and APB and characterised, before adding to the optimised co-culture model of DR described in chapter 2, to test their ability to integrate into a mature EC layer.

3.2 AIMS & OBJECTIVES

To isolate, characterise and expand ECFCs from human UCB and APB and test their capability to incorporate into healthy and diabetic human primary co-culture models of the retinal microvasculature

1. Collect samples of APB and UCB and isolate and expand populations of ECFCs
2. Characterise ECFC populations using cell-surface markers and proliferative potential
3. Lentivirally transduce ECFCs to express green fluorescent protein (GFP) for monitoring of cells on various biomaterials over time
4. Test incorporation potential of ECFCs into *in vitro* healthy and diabetic co-culture models or retinal microvasculature

3.3 METHODS

3.3.1 PERIPHERAL BLOOD ISOLATION

Ethical approval for the collection of human adult peripheral blood and umbilical cord blood was obtained from North of Scotland Research Ethics Committee (17/NS/0071). Umbilical cord blood collection was carried out at Liverpool Women's Hospital and peripheral blood collection at the University of Liverpool. Healthy adults were recruited to donate 50ml of peripheral blood. Donors were not taking vitamin or antioxidant supplements and were without diabetes. A trained blood extractor carried out the blood collection procedure. Briefly, adult peripheral blood was collected from the median cubital vein using a tourniquet *(Greiner, 840050)*, a SAFETY Blood Collection Set + Holder, size 23G or 21G *(Greiner, 450086, 450085)* and 9 ml K3EDTA VACUETTE® Tubes *(Greiner, 455036)*. Extracted blood was processed immediately at RT.

3.3.2 UMBILICAL CORD BLOOD ISOLATION

Pregnant women undergoing planned caesarean section surgery were recruited at pre-operative clinic by NHS staff at Liverpool Women's Hospital. Consent was obtained to collect the umbilical cord with attached placenta immediately after surgery. Cords were clamped at either end by the surgery team to improve retention of blood within the umbilical cord. The umbilical cord blood (UCB) collection procedure was carried out as soon as possible after delivery of placenta, to prevent blood clotting and cell death. UCB collection was performed in a class II hood using aseptic technique. Placenta with attached cord was elevated using a clamp stand with modified platform, to enable gravitational flow (See Figure 3.1). Cord was cleaned using antiseptic wipes *(Brosch, DW4220)* and blood was extracted from the cut (distal) end of the cord, just above the clamp, using a 19G needle *(NHS Supply Chain, AN1950R1)* attached to a 10ml syringe *(BD, 305959)*. Once blood from one region was extracted, the needle was re-inserted further towards the proximal end and the procedure was repeated until the umbilical vein and artery were empty of blood. Blood was also extracted in the same way from the large vessels of the placenta. The volume of blood extracted was variable from each donor depending on size of placenta, length of cord, delayed cord clamping at birth and time since placenta delivery (due to blood clotting), see Figure 3.1. According to the protocol described by Medina et al., fresh UCB was mixed with equal parts Alsever's solution *(Sigma, A3351)* in sterile 50ml tubes, to prevent coagulation[153].

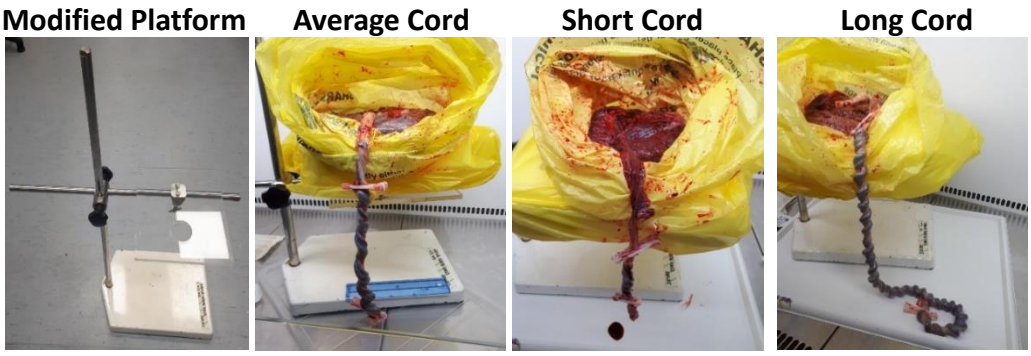

Donor No.	Date	Volume Collected
17-002	23.11.17	17.5ml
17-003	27.11.17	30ml
17-004	04.12.17	10ml
17-005	05.12.17	11ml
17-006	11.12.17	35ml
17-007	12.12.17	35ml
17-008	13.12.17	62.5ml
17-009	13.12.17	20ml
18-001	09.01.18	5ml
18-002	11.12.18	30ml
18-003	15.01.18	5ml
18-004	15.01.18	12ml
18-005	15.01.18	18ml
18-006	16.01.18	18.5ml
18-007	16.01.18	10ml
18-008	16.01.18	23.5ml
18-009	17.01.18	43.5ml

Figure 3.1. Elevated extraction method for collecting umbilical cord blood

Images showing modified clamp stand used to elevate placenta with clamped umbilical cords, and variation in cord lengths and placenta size. Table shows variation in total blood volume collected from a total of 17 umbilical cords and placenta. Volumes ranged from 5-62.5ml.

3.3.3 ECFC CULTURE

From this point on, both adult peripheral (APB) and UCB were processed in the same way, at RT, following the protocol described by Medina et al., outlined below[153]. Using non-skirted sterile 50ml tubes *(Greiner, 227261)*, 30ml dPBS was added for every 20ml blood with anticoagulant and gently mixed, i.e. 3 parts dPBS to 2 parts blood solution. In fresh non-skirted sterile 50ml tubes, 20ml blood-dPBS solution was very gently layered on top of 20ml Histopaque *(Sigma, 10771)*, avoiding any mixing. The tubes of blood layered on Histopaque were centrifuged at 400rcf for 30 minutes, with slow break applied to separate blood via centrifugation fractionation. Using a sterile Pasteur pipette, the buffy coat layer of mononuclear cells was removed from each tube (red arrow, Figure 3.2) and transferred to a new non-skirted 50ml tube and topped up with 30ml dPBS. Buffy coat-dPBS mixture was centrifuged for 8 minutes at 330rcf using normal break, resulting in a large, loose, pink-

coloured pellet of cells in the bottom of the tube. dPBS was removed, leaving a small volume covering the cell pellet. 3ml of 1X red blood cell (RBC) lysis buffer *(Invitrogen, 00-4300-54)* was added to the cell pellet and after gentle mixing, was left for 10 minutes to lyse any contaminating RBCs. The solution changed to a glossy/ less opaque colour. This solution was centrifuged at 330rcf for 10 minutes, to form a cell pellet. Using a sterile 1000µl tip, supernatant was removed, avoiding the large cell pellet. 1ml Endothelial Growth Medium-2 (EGM-2) *(PromoCell, C22011)* with 20% FBS was added and gently but thoroughly mixed with cell pellet. The solution was very thick, due to high cell number and small media volume ($1x10^7$cells/ml).

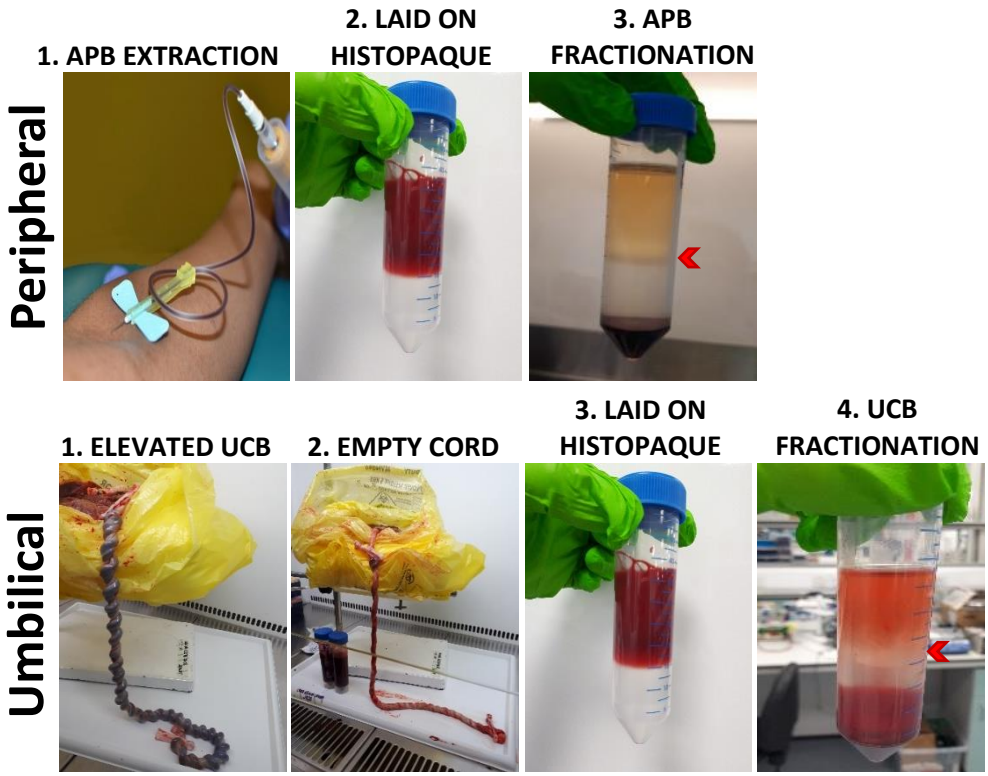

Figure 3.2. Steps in the procedures of collecting ECFC from umbilical cords and adult peripheral blood

Images of UCB and APB extraction and processing by density gradient centrifugation. Red arrows highlight the mononuclear layer of cells which was collected then seeded on to col I. coated TC plastic 24 w/p. Peripheral no.3 and Umbilical no.4 Images demonstrate the difference in the quality of the separated blood from the two different sources.

Before adding mononuclear cells to 24 well plates(w/p), wells were coated with collagen I (col I.) solution *(Corning, 354236)* at 50µg/ml. Col I. solution was mixed with sterile ddH_2O and sterile filtered using 0.2µm filter *(Appleton Woods, 16532)* and 10ml syringe. 200µl of col.I solution was added to each well in 24w/p and left in sterile hood at RT for 1H. Col I. solution was then removed and wells were washed once with sterile dPBS and once with EGM-2 media. One extra row of wells was col.I coated for cells to be re-seeded at 24H, and left covered with dPBS. Mononuclear cell pellet was thoroughly mixed with EGM-2 with 20% FBS then added to each well at 500µl/well at a density of ~$5x10^6$cells/well. Therefore, 1x 50ml tube of cells collected from UCB/APB was transferred to 2x wells in a 24w/p. EGM-2 was supplemented with 20% FBS until cells reached P2. Thereafter, EGM-2 was supplemented with 10% FBS for ECFC culture.

At 24H after seeding, unattached cells in media from two wells were collected in to a 15ml centrifuge tube *(Greiner, 188261)* and spun for 5 minutes at 400rcf. Supernatant was removed and cell pellet was re-suspended in 500µl EGM-2 with 20% FBS and re-seeded in spare col I. coated well on 24w/p. Due to very high seeding density, this allowed a second chance for putative ECFCs to attach to TC plastic. All other wells had a complete media change, performed gently so as not to disrupt any loosely attached cells. Media was gently changed every day for the first 7 days, as there was a large number of cells and debris floating in the media. Cells were monitored and imaged daily, until over time cell debris decreased and cells could be seen attached to TC plastic from ~day 7 onwards. From day 7, media was changed every 48H. From day 10 (UCB) or 21 (APB) populations of cuboidal, colonies of ECFCs appeared in the culture (Figure 3.3). Once these cells filled each well, they were trypsinised (as described in 2.3.3) and transferred to col I. coated 6w/p's, where they were cultured in 2ml EGM-2 with 20% FBS/well and media was changed every 2-3 days. After 4-10 days (UCB) or 5-14 days (APB), passage 1 (P1) ECFCs filled the wells of a 6w/p. Cells were trypsinised and each well of ECFCs was transferred to a col I. coated T25 flask. At this stage (P2) EGM-2 serum content was reduced to 10% FBS.

After 2-7 days, at 80% confluence ECFCs were either frozen for use at later date or used immediately in experiments. For freezing, after tryspinisation ECFCs were re-suspended in 900µl +100µl DMSO at a density of ≥$1x10^6$ cells/ml, in a cryovial and transferred to -80°C in a Mr Frosty container containing isopropanol for freezing at a rate of -1°C/minute. For long term storage, cells were transferred to liquid nitrogen. To recover cells from liquid nitrogen, vials were defrosted quickly at 37°C in a water bath over 2-4 minutes. The defrosted cell

suspension was dispersed into a col I. coated T75 flask of warmed EGM-2 with 10% FBS medium and left to adhere overnight. The next morning medium was completely changed to remove remnants of DMSO from culture flask.

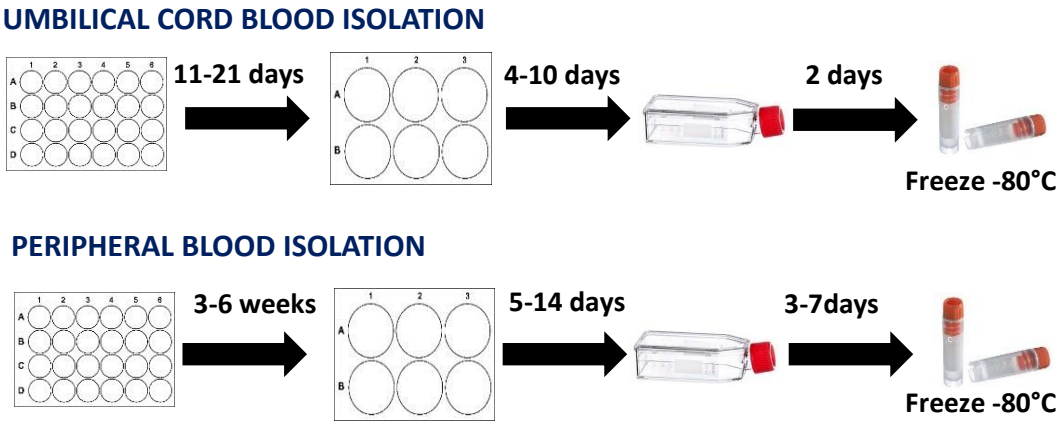

Figure 3.3. Timescale of isolation and expansion of ECFCs from UCB and APB

Timeline depicting the stages involved in ECFC isolation and *in vitro* expansion from UCB and APB. Mononuclear cells were first seeded on col I. coated 24 w/p's, and non-adherent cells were re-plated at 24H into new wells. From 11-21 days, ECFCs appeared in culture. UCB-ECFCs appeared earlier than APB-ECFCs. Once confluent, ECFCs were transferred to 6w/p's, followed by T25 flasks. ECFCs were frozen at ≥1x10^6 cells/ml. Overall more ECFCs were successfully isolated from UCB and they grew at a faster rate than APB-ECFC.

3.3.4 IMMUNOFLUORESCENCE

ECFC clones from healthy UCB-ECFCs, APB-ECFCs and one GD-UCB-ECFC donor were characterised using IF confocal imaging of antibodies against specific markers for endothelial cell-types. ECFCs were seeded at 2x10^4 cells/well on col I. coated 8-well EZ-glass slides. At days 2-5 ECFCs were washed for 3x 5 mins in warm dPBS to remove remnants of cell culture medium. Cells were fixed, permeabilised and blocked according to the protocol described in section 2.3.4. After 1H blocking, primary antibodies diluted to optimal working concentration in dPBS (see Table 3.1), were added to cells and left on a slow rocking platform overnight at 4°C. 3x 5 mins 0.1% Tween-20 in dPBS washes at RT on a rocker removed any unbound primary antibody. Secondary antibodies (see Table 2.2), were added at 5µg/ml in dPBS for 45 mins at RT on a slow rocking platform, in the dark. Cells were washed, DAPI stained and mounted with a glass coverslip as described in section 2.3.4.

Table 3.1. PRIMARY ANTIBODIES FOR IF CHARACTERISATION OF ECFCs

Primary Antibody	Species	Supplier/Code	Concentration
Platelet Endothelial Cell Adhesion Molecule-1 (**CD31/PECAM-1**)	Rabbit	Abcam ab28364	1:20
Vascular Endothelial Cadherin (**VE-Cad**)	Rabbit	Abcam ab33168	1:200
Zonula Occludens-1 (**ZO-1**)	Rabbit	ThermoFisher Scientific 61-7300	2.5µg/ml
Von Willebrand Factor (**vWF**)	Rabbit	Abcam ab6994	21.5µg/ml
CD34	Mouse	Abcam ab8536	5µg/ml
CD34	Rabbit	Abcam ab81289	2.64µg/ml
Connexin 43 (**Cx43/GJA1**)	Rabbit	Abcam ab11370	3.5µg/ml
Angiopoietin-2 (**Ang-2**)	Rabbit	Abcam ab153934	5µg/ml
Desmin	Rabbit	Abcam ab15200	1:200
Alpha-smooth Muscle Actin (**αSMA**)	Mouse	Abcam ab7817	5µg/ml
Vascular Endothelial Growth Factor Receptor-2 (**VEGFR-2**)	Mouse	Abcam ab9530	10µg/ml
Hypoxia Inducible Factor 1-α (**HIF1-α**)	Mouse	Abcam ab199004	1µg/ml
Superoxide Dismutase-1 (**SOD-1**)	Mouse	Merck MABC684	1:200
Superoxide Dismutase-2 (**SOD-2**)	Mouse	Invitrogen A21990	5µg/ml
Thymocyte Antigen (**CD90/Thy-1**)	Mouse	Abcam ab23894	2µg/ml
Conjugated Phallotoxin			
Phalloidin-647- **F-actin**		ThermoFisher Scientific A22287	0.22µM

3.3.5 FLOW CYTOMETRY

Flow cytometry was performed to determine the cell surface receptors expressed by ECFCs isolated from either APB or UCB and from different donors. A panel of proteins was selected to distinguish ECFCs from mature ECs. Cells were prepared for flow as described in section 2.3.5. Each clone was photographed before flow cytometry to compare morphology and to record confluence (target~80-90% confluent).

3.3.6 GROWTH CURVES

To determine the growth rate of ECFCs, cells were grown for 21 days in EGM-2 with 10% FBS medium. Cells were seeded at $5x10^3$, $1x10^4$, $2x10^4$ and $4x10^4$ cells/well in col I. coated TC plastic 24 w/p, to determine the effects of seeding density and time on cell growth rate. For fixing and quantification procedure see section 2.3.6.

3.3.7 OPTIMISING CELL-SPECIFIC MEDIUM

To determine if ECFCs were viable in the optimised healthy and diabetic conditions of the co-culture model, ECFCs were grown in healthy (5.5mM glucose + 20% O_2), hypoxic (5.5mM glucose + 2% O_2) and diabetic (33mM glucose + 2% O_2) conditions for 4 days and their metabolic activity was tested. ECFCs were seeded at $2.5x10^4$ cells/well on col I. coated TC plastic 24 w/p in EGM-2 with 10% FBS and left to form a monolayer for 48H. 48H after seeding (experimental time point 0) a resazurin assay was performed (see section 2.3.8), to determine metabolic activity of ECFCs at baseline. Culture medium was changed and ECFCs were moved to low or normal oxygen conditions and healthy or diabetic glucose levels. Subsequent resazurin assays were performed at 24H and 4 days of experimental conditions, with media changed at 48H. Data presented was normalised to healthy controls (5.5mM glucose and 20% O_2), and data was adjusted across plates using standard curve to account for gain (Figure 2.2). Images of the cells were captured from experimental day 0-21, to monitor cell morphology and cell number.

To determine if ECFC were viable in the optimised healthy and diabetic conditions of the co-culture model, switching from EGM-2 with 10% FBS to MV with 5% FBS medium, ECFCs were grown in healthy (20% O_2 and 5.5mM glucose) and diabetic (2% O_2 and 33mM glucose) conditions and compared to ECFC metabolic activity in the same conditions, but in their original EGM-2 with 10% FBS growth medium. UCB-ECFCs were seeded at $2x10^4$ cells/well on col I. coated TC plastic 24w/p's, straight in to healthy or diabetic conditions with either MV with 5% FBS or EGM-2 with 10% FBS medium. As a control, hREC were seeded at $2x10^4$ cells/well on TC plastic 24w/p straight in to healthy or diabetic conditions in MV with 5% FBS medium. Media was changed every 48H. Resazurin assays were performed (see section 2.3.8) to determine ECFC and hREC metabolic activity in different media, oxygen and glucose conditions at 48H and 7 days after seeding. Results were adjusted for gain across plates. Results were reported as relative fluorescence units. Images were captured of cells in each condition at 48H and day 7, to assess cell morphology and cell number.

3.3.8 INCORPORATION OF CELLTRACKER LABELLED ECFCs

To enable monitoring of attachment and growth of ECFC with hREC on TC plastic and PET membranes, CellTracker Green (CTG) and CellTracker Red (CTR) dyes were used. hREC were labelled with CTR and UCB-ECFCs were labelled with CTG, according to the protocol described in section 2.3.10. Culture medium was MV with 10% FBS for ECFC incorporation with hREC experiments. ECFC and hREC were seeded 1:1 at the same time, at $1x10^4$ or $6.67x10^4$ cells/well in a 24-well TC plate, or $1.5x10^3$ or $1x10^4$ cells/well in PET transwell inserts. Densities represent low or high seeding density and are scaled up from optimised transwell cell density to TC plastic, taking in to account surface area. Cells were imaged at 24H and 72H to explore incorporation and retention of ECFC in 1:1 culture with hREC.

To test APB-ECFC incorporation into an established hREC monolayer in diabetic or healthy conditions, hREC were seeded first at $2x10^4$ or $1.334x10^5$cells/well on col I. coated TC plastic, and grown for 48H, in MV with 10% FBS medium. APB-ECFCs from two donors were labelled with CTG (CTG-ECFC) (section 2.3.10), and added to hREC at 48H. Due to slow growth of APB-ECFC, the cell number added was as close to $2x10^4$ as possible (17,188 ECFC/well from donor #1042 ad 11,975 ECFC/well from donor #332). Cells in healthy and diabetic and at lower and high seeding density were imaged at 24 and 48H using fluorescent Nikon E-Tie microscope. 48H after seeding CTG-ECFC on to hREC monolayer, cells were fixed using 10% NBF and processed for IF imaging (see section 2.3.4), to explore expression of the GJ protein ZO-1 and the hypoxic response (HIF1α).

3.3.9 VIRAL TRANSDUCTION OF GFP INTO ECFCs

To enable long term monitoring of ECFC on PET transwell inserts and on pεK hydrogel microparticles, stable GFP expression was achieved by lentiviral mediated transduction of pGIPz. This plasmid uses CMV to drive expression of tGFP, puromycin and a validated non-silencing shRNA sequence from the same promoter. Lentiviral particles were generated as previously described[262] (DNA/RNA Delivery Core, Northwestern University, Chicago, IL) using 293T packaging cells (Gene Hunter Corporation, Nashville, TN). The vector map is shown below (Figure 3.4).

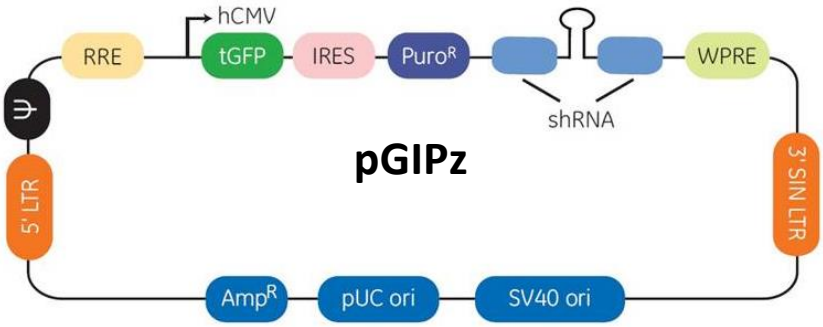

Figure 3.4. GFP lentiviral particle composition

Vector map. hCMV (human cytomegalovirus)=promoter. tGFP= green fluorescent protein. IRES= internal ribosomal entry site; allows for two transcripts to be driven from the same promoter. Puro= puromycin resistance cassette. shRNA is where the non-silencing shRNA is inserted. WPRE=woodchuck hepatitis virus posttranscriptional regulatory element: increases expression of genes. 3' SIN LTR and 5'LTR are long tandem repeats used for integration into the viral genome. Psi= is a lentiviral protein. RRE= rev response elements, a binding site for retrovirus specific enzymes. Amp, pUC and SV40 are for growing in bacteria. Virus was added to confluent ECFCs in 6w/p and incorporated into cells over a 48H period.

To generate stable clones, ECFCs were seeded at 100-200,000/well in a 6 w/p and grown for 24-48H, until 80-90% confluent. The flow diagram (Figure 3.5) outlines the procedure of viral transduction. In brief, virus was added at 20µl/well into fresh EGM-2 with 10% FBS media containing 6ug/ml of sterile filtered polybrene (*Sigma, TR-1003-G)* at a total volume of 500µl media/well. After 24H, media volume was replenished to total volume of 1.5ml/well. 48H after adding virus, cells were imaged using Nikon E-Tie fluoresecent microscope to determine percentage of green cells in ECFC cultures. Once cells were confluent, to remove any non-transduced ECFCs, cells were treated with sterile filtered puromycin *(Gibco, A1113803)* at 2ug/ml in fresh growth media. Virally-transduced cells had puromycin resistance, therefore only transduced ECFCs survived after puromycin treatment.

Transduced ECFCs were monitored for 7 days (or until confluent), with fresh puromycin added at 2ug/ml in EGM-2 with 10% FBS media every 48H. From days 4-7 post-puromycin treatment, wells became confluent with ECFCs virally transduced with GFP (GFP-ECFC) (excitation 488 nm, emission510 nm). Confluent cells were sub-cultured (as described in section 2.3.3) and each well from a 6 w/p was transferred to a T25 flask, in EGM-2 with 10% FBS containing 2ug/ml puromycin, to prevent expansion of any remaining non-transduced ECFCs. Once GFP-ECFC were 90% confluent in T25 flasks, cells were used in experiments or sub-cultured in T75 flasks for further expansion.

3.3.10 INTEGRATION OF GFP-ECFCs INTO HEALTHY hREC MONOLAYERS

To determine if GFP-ECFCs integrated in the same way as CTG-ECFCs, integration experiments similar to section 3.3.8 were performed. $2x10^4$ or $6.67x10^4$ GFP-ECFCs/well were seeded at the same time, 1:1, with hREC on col I. coated TC plastic 24 w/p's in MV with 10% FBS medium. $1.5x10^3$ or $1x10^4$ GFP-ECFCs/insert were seeded at the same time, 1:1 with hREC on to the apical surface of PET transwell inserts. Cells were imaged at 24H and day 7 to determine the presence of GFP-positive cells.

To assess the ability of GFP-ECFCs to incorporate into an already established hREC monolayer, hREC were seeded first at low ($2x10^4$/well) or high density ($1.334x10^5$ cells/well) on col I. coated TC plastic 24 w/p's, or low ($3x10^3$) or high density ($2x10^4$ cells/well) on transwell inserts and grown for 48H. At 48H, $2x10^4$/well GFP-ECFCs were added to hREC in TC plastic or transwell inserts, and fresh MV with 10% FBS medium was added. Cells were imaged at 24H and day 7. On day 7, cultures were fixed using 10% NBF and processed for confocal IF imaging (see section 2.3.4), to explore expression of pro-angiogenic protein Ang-2, and junctional proteins ZO-1 and VE-Cad.

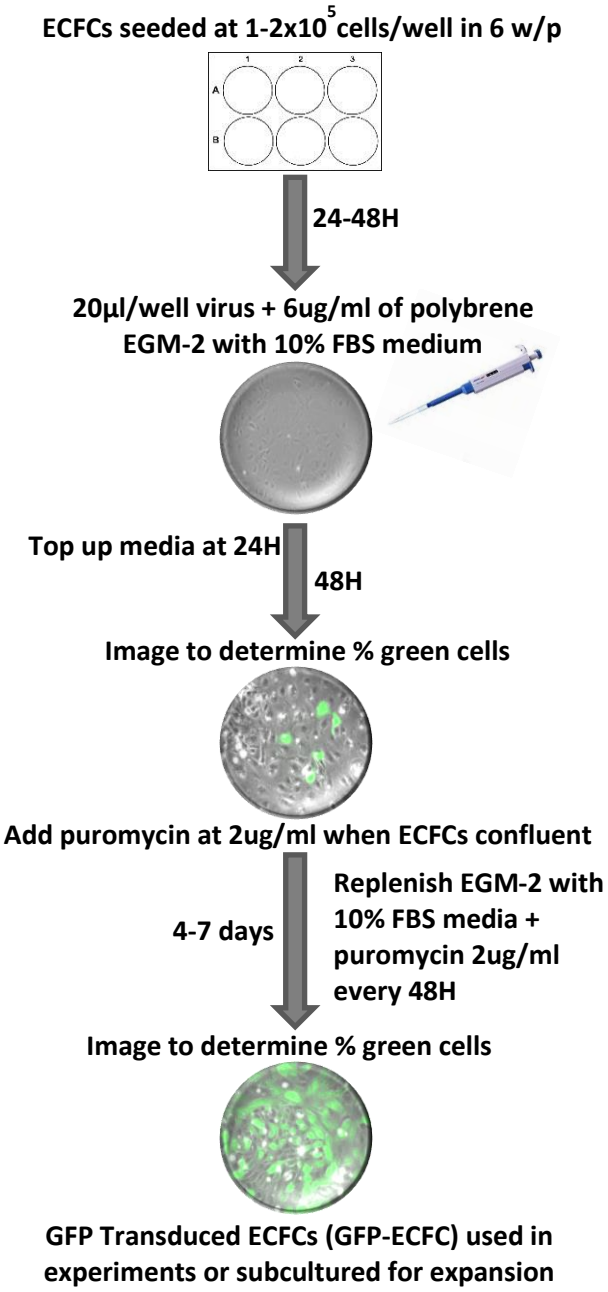

Figure 3.5. Steps to virally transduce GFP expression in ECFCs

Flow diagram of lentiviral mediated transduction of pGIPz, to enable stable GFP expression in UCB-ECFC. Polybrene enabled virus to enter ECFCs during vrial transduction. Successful transduction resulted in GFP expression and antibiotic resistance. Puromycin treatment killed non-transduced ECFCs. GFP-expressing ECFCs continued to expand in culture at the same rate as non-transduced cells.

3.3.11 ASSESSING INCORPORATION OF GFP-ECFCs INTO MONO AND CO-CULTURES IN DIABETIC CONDITIONS

GFP-ECFCs from healthy and GD-UCB were added to mono- and co-cultures grown under healthy and diabetic conditions, to test their ability to incorporate into the hREC layer. Co-cultures of hREC and hRP seeded at 1:1 ratio on transwell inserts, were grown for 72H, then moved to either healthy or diabetic conditions for a further 7 days (see Figure 2.6). On experimental day 7 of co-culture, $2x10^4$ GFP-ECFCs from either healthy or GD-UCB were added to the hREC layer (apical side of insert) in 200µl MV with 5% FBS medium with either 5.5mM or 33mM glucose. Co-cultures were placed back into healthy or diabetic conditions for 24H. 24H after seeding UCB-GFP-ECFCs, inserts were imaged using Nikon E-Tie live cell fluorescence microscope to assess GFP-positive cell incorporation. Cells were then fixed using 10 % NBF and processed for confocal IF imaging (see section 2.3.4). In both mono- and co-cultures, GFP-positive cells were assessed for expression of junctional proteins (VE-Cad and ZO-1), and hREC and ECFC morphology and cell number were analysed. For co-cultures, Z-stack images were produced to confirm the presence of hRP on the underside of the PET membrane, using the Volume Viewer plug-in 2.01.1, on ImageJ software.

3.3.12 MICROSCOPY

The Zeiss Axiovert25 with TopupView 86 software was sued to capture phase contrast images of the ECFCs during isolation and expansion of the cells. The Nikon Eclipse TS100 fluorescence microscope with Nikon Digital Sight software was used to monitor GFP viral transduction in ECFCs.

3.4 RESULTS

3.4.1 APB AND UCB-ECFCs WERE SUCCESSFULLY ISOLATED AND EXPANDED *IN VITRO*

ECFCs were isolated the protocol described by Medina et al.[153]. UCB-ECFCs were present in culture from 11-21 days, recognisable by their cobblestone morphology (Figure 3.6A). APB-ECFCs were also successfully expanded in culture, but took longer to become established (3-6 weeks), although ultimately presenting the same cobblestone morphology as those isolated from UCB (Figure 3.6B). Once 24 w/p's were confluent, when cultured with medium supplemented with 20% FBS, both APB and UCB-ECFCs were transferred first to 6 w/p's, followed by T25 flasks for continued expansion in medium containing 10% FBS. APB-ECFCs were successfully expanded from 5 out of 10 (50%) donors. UCB-ECFCs were successfully isolated from 16 out of 17 (94.1%) donors.

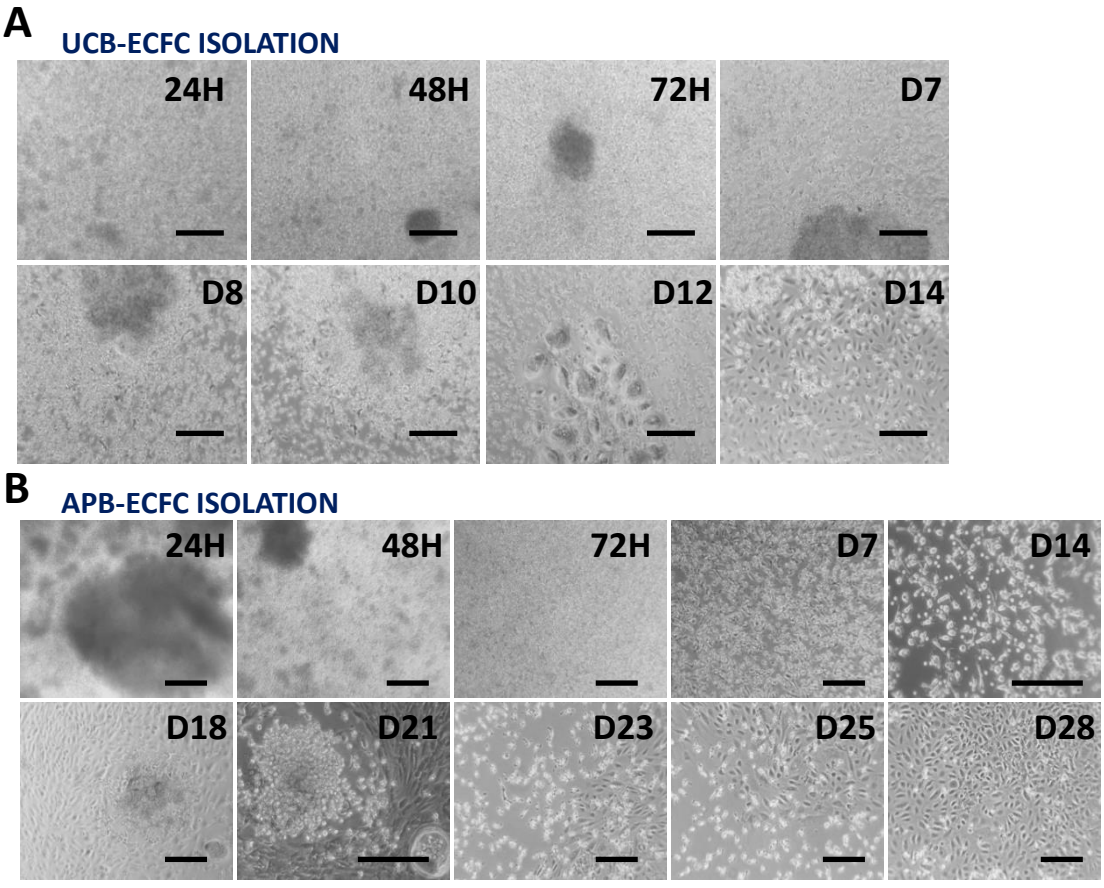

Figure 3.6. Timescale of UCB and APB-ECFC *in vitro* expansion from the mononuclear cell fraction

Isolation of ECFCs using col I. coated TC plastic and EGM-2 with 20% FBS medium, for EC-specific attachment and expansion. (**A**) Expansion of ECFCs from umbilical cord blood, where ECFC grew out as colonies and filled the well from D14-21. (**B**) Expansion of ECFCs from adult peripheral blood, where ECFC grew out as colonies and filled the well from D21-35. Images were captured using the Zeiss Axiovert 25 microscope, x10 magnification. Scale bars= 200µm.

3.4.2 ECFCs EXPRESSED EC-SPECIFIC MARKERS CONFIRMING THEIR ENDOTHELIAL LINEAGE

IF imaging of ECFCs isolated from APB, healthy UCB and cord blood from mothers with gestational diabetes (GD-ECFCs), showed some variation in expression of a panel of endothelial-specific antibodies, although overall cell morphology remained uniformly cobblestoned. APB-ECFCs showed positive expression for CD31, VE-Cadherin and vWF and did not express CD90 or αSMA (Figure 3.7A). Healthy UCB-ECFCs expressed ZO-1 and vWF (Figure 3.7B) and were negative for CD90 and αSMA (Figure 3.7C). CD31 and VE-Cad were present, but not at their expected location at the lateral border of the cytoplasm (Figure 3.7B and C). GD-ECFC had positive expression of ZO-1 (Figure 3.8A), vWF (C) and CD31 (E), and 50% of cells positively expressed Ang-2 (H). As with the ECFCs sourced from healthy umbilical cords, VE-Cad was present, but not specifically at the cell-cell borders where it would be involved in cell-cell adhesion. VEGFR-2 was expressed across the membrane of APB and UCB-ECFCs (Figure 3.7A, B and C), and expressed less in the GD-ECFCs (Figure 3.8). CD90 and αSMA were not present on GD-ECFCs. Phalloidin staining shows the cytoskeletal arrangement of F-actin, and there is one very large cell (white arrow, Figure 3.8), with different F-actin arrangements to the other cells, which may be a contaminating mononuclear cell-type which adhered during the ECFC selective isolation method (Figure 3.8F). Results for CD34 expression across ECFCs from all sources was inconclusive.

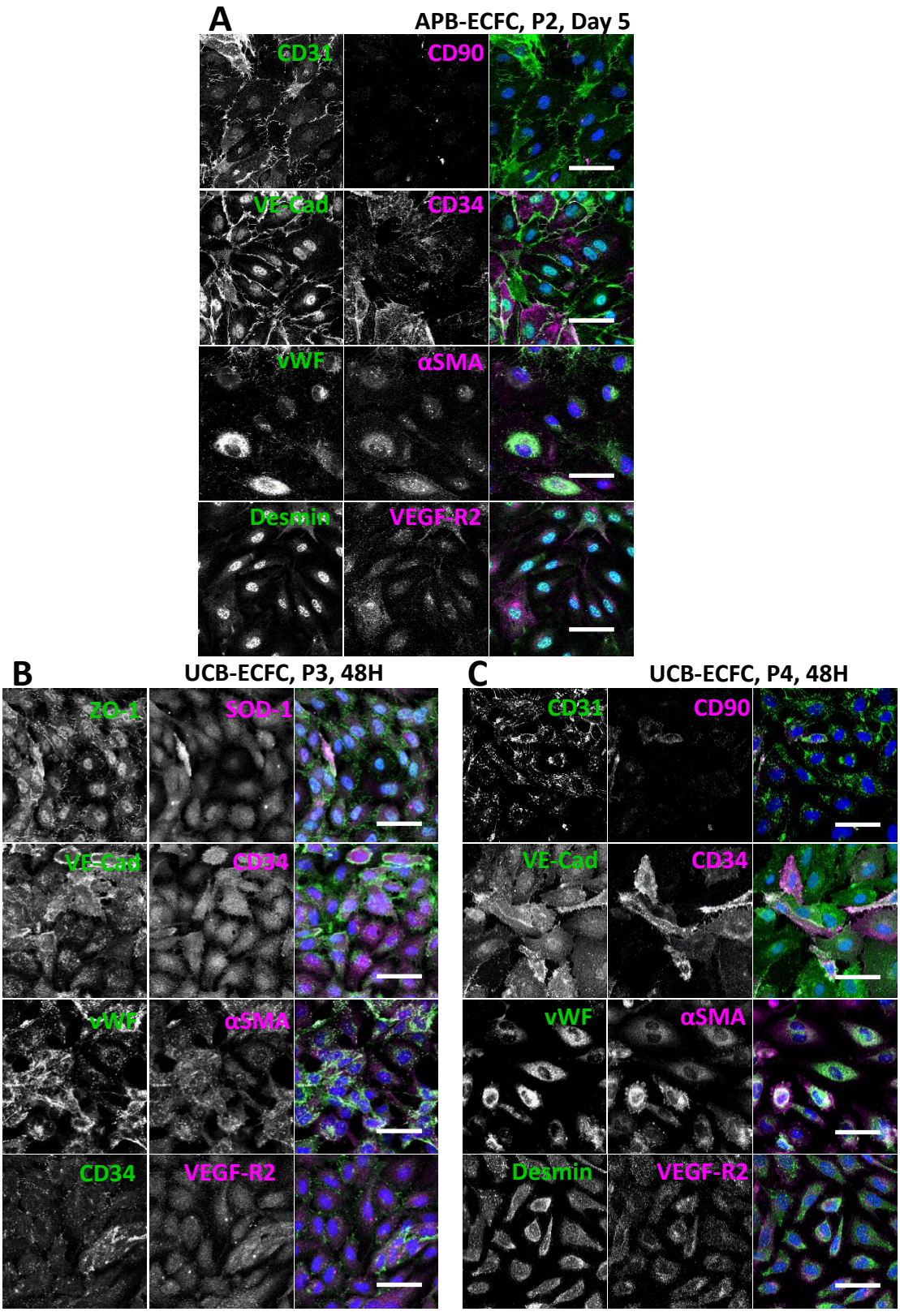

Figure 3.7. APB and UCB-ECFC express markers confirming their EC-lineage

IF antibody analysis of APB-ECFCs fixed at day 5 (**A**) and UCB- ECFCs fixed at 48H (**B** and **C**), where all expressed vWF. APB-ECFC expressed CD31 and VE-cad. All ECFCs were CD90 and αSMA negative. Images were captured using the Zeiss M800 confocal microscope, x40 oil magnification. Scale bars= 50μm.

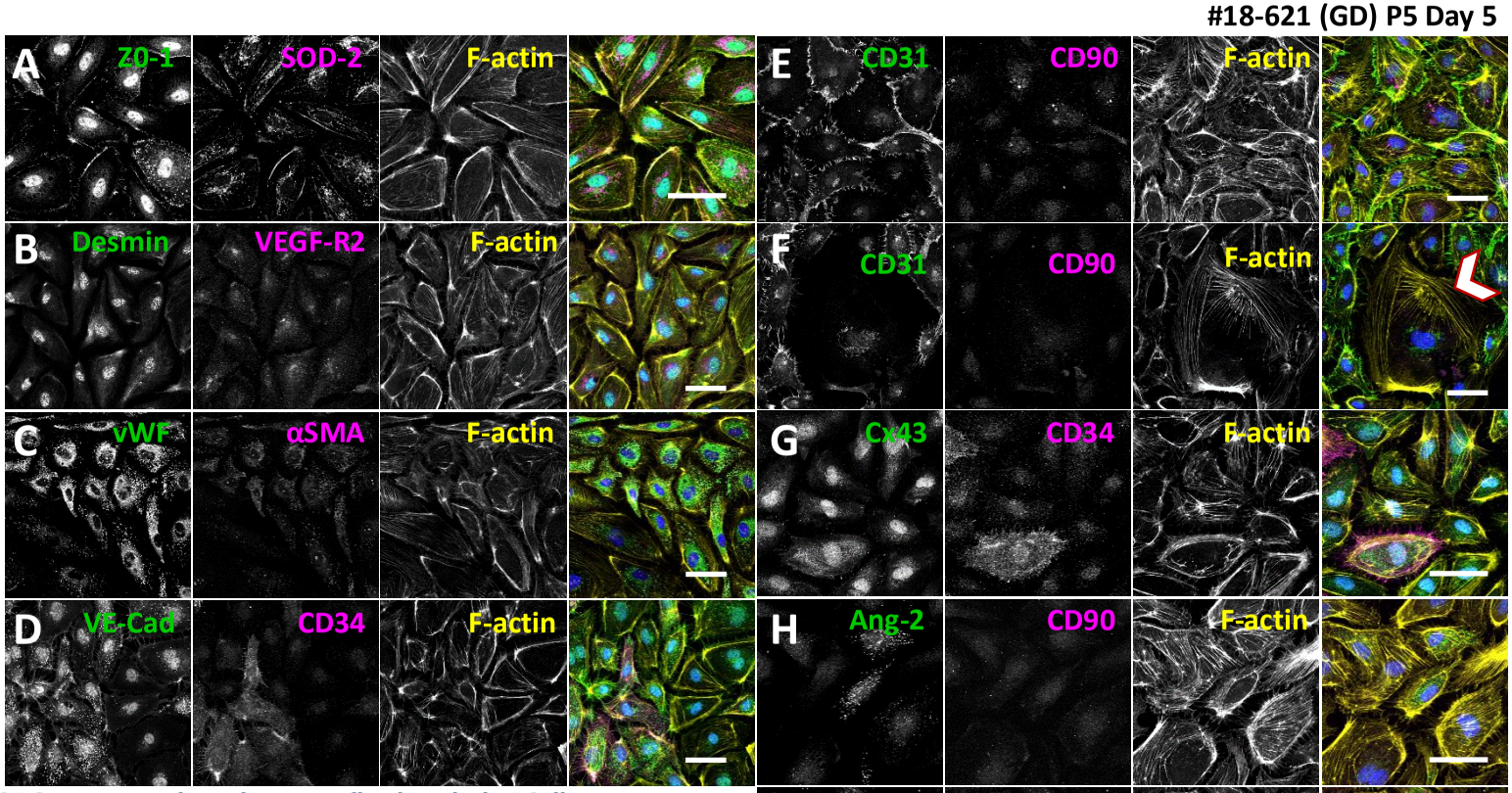

Figure 3.8. GD-UCB-ECFC expressed markers confirming their EC-lineage

IF antibody analysis of GD-UCB-ECFCs fixed at day 5. GD-UCB-ECFCs all expressed vWF (**C**), ZO-1 (**A**) and CD31 (**E** and **F**). VE-Cad was dispersed across the cell cytoplasm (**D**). Phalloidin staining of F-Actin filaments highlights possible contamination with a very large, different mononuclear cell-type (**white arrow**) (**F**). CD34 expression results were inconclusive (**G** and **I**). All GD-UCB-ECFCs were CD90 and αSMA negative (**C**, **E**, **F** and **H**). Images were captured using the Zeiss M800 confocal microscope, x40 oil magnification. Scale bars= 50µm.

3.4.3 UCB AND APB-ECFCs WERE POSITIVE FOR EC-SPECIFIC CELL SURFACE MARKERS AND NEGATIVE FOR HAEMATOPOIETIC LINEAGE MARKERS

8 healthy UCB clones from 7 donors, 2 GD-UCB clones from 1 donors, 3 healthy APB clones from 3 donors were analysed for expression of cell surface markers (Figure 3.9). Cells were used at early passage (3-5) and similar confluence wherever possible (Figure 3.9A). There was variation in CD34 expression analysed using flow cytometry, ranging from 0.1-63.1% positivity. The majority of clones had low CD34 expression but APB clones P#322 and P#942B had much higher CD34 expression than APB clone P#1042 and all of the UCB clones, at 63.1% and 24% respectively (Figure 3.9B). Putative ECFCs from all donors showed CD31 expression 89.5-100%, CD105 expression 98.5-100% and CD146 expression 98.5-100%. Putative ECFC from all donors were negative for CD45 0-3%, negative for CD14 0-0.1% and negative for CD90 0-3.6% expression. Collectively, these cells were positive for endothelial markers, negative for fibroblast marker (CD90) and negative for haematopoietic/immune cell markers (CD14 and CD45).

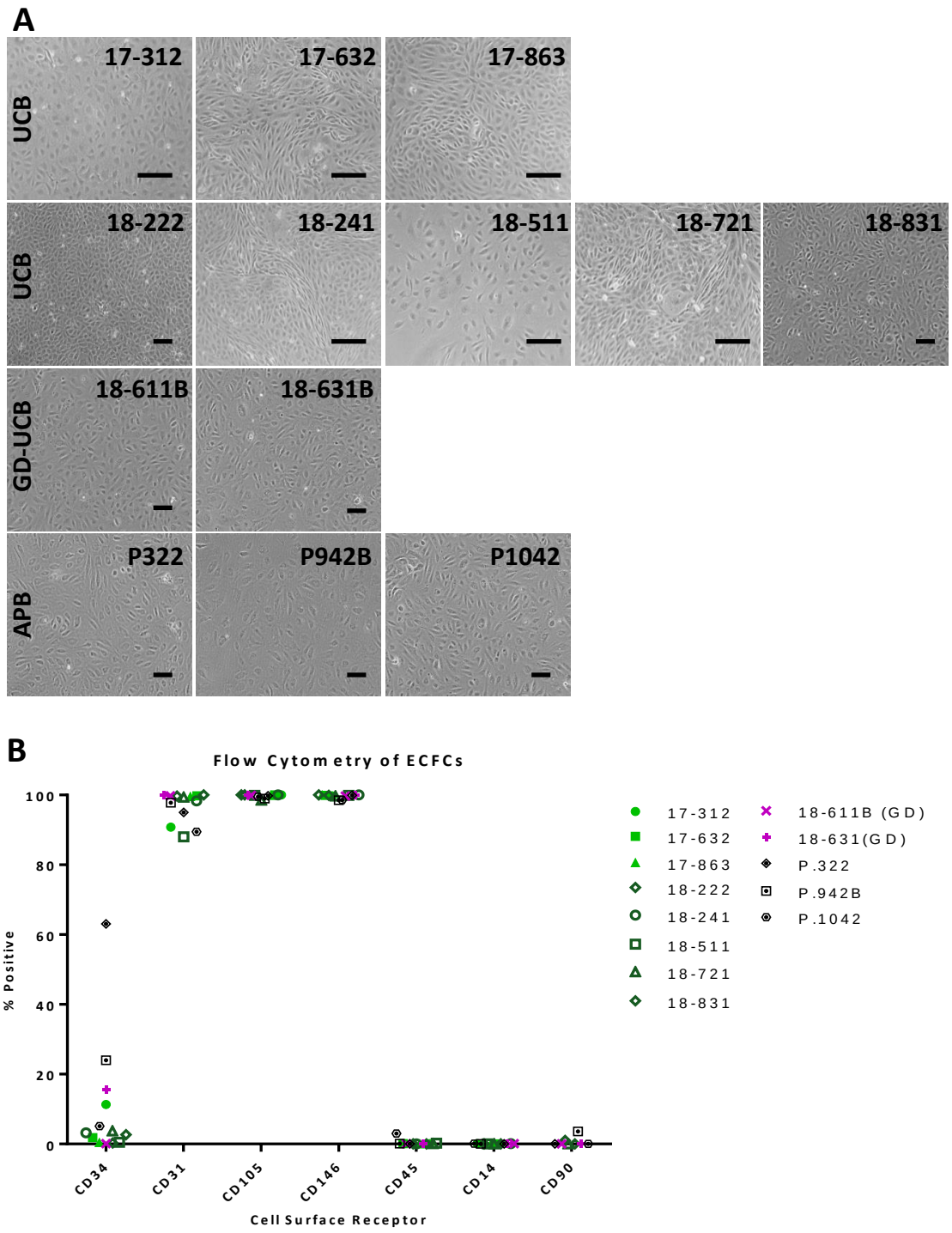

Figure 3.9. Flow cytometry analysis confirmed APB and UCB-ECFCs were of EC-lineage and not haematopoietic or fibroblastic cells

(**A**) Phase contrast images were captured before flow cytometry analysis of ECFCs, with the aim of analysis at similar confluence and passage number. (**B**) Flow cytometry analysis of cell surface markers used to determine EC/progenitor-lineage (CD34, CD31, CD105, and CD146), haematopoietic lineage (CD14, CD45) or a common fibroblast marker (CD90). UCB-ECFCs= green, GD-UCB-ECFCs= magenta and APB-ECFCs= black. Phase contrast images were captured using the Nikon DIAPHOT or Zeiss Axiovert 25 microscopes, x10 magnification. Scale bars =200µm.

3.4.4 ECFCs DISPLAYED SIMILAR GROWTH PATTERNS TO MATURE hREC ALTHOUGH OVERALL CELL NUMBERS WERE HIGHER BY DAY 21

UCB-ECFCs seeded at $5x10^3$-$4x10^4$ cells/well on 24 w/p's showed an increase in cell number up to 7 days (Figure 3.10). This increase was at a similar rate for all seeding densities except $4x10^4$ cells/well, which plateaued earlier. From day 7 to 21 there was a decline in ECFC number, at the same rate for all seeding densities. By day 21 ECFCs seeded at $4x10^4$ cells/well had the lowest remaining cells at 10210 ±1844.3cells/cm^2, which was significantly lower than those seeded at $5x10^3$ cells/well (p=0.0047) and those seeded at $1x10^4$ cells/well (p=0.0043). ECFCs seeded at $1x10^4$ cells/well had the highest number of cells remaining at 16118 ±2388.9 cells/cm^2. Overall, there was a reduction in ECFC number after 7 days for all seeding densities, and the cell loss is greatest at the highest seeding density. However ECFCs were used in subsequent experiments with the co-culture for a maximum of 7 days, where the growth curve suggests ECFCs expanded in number in culture.

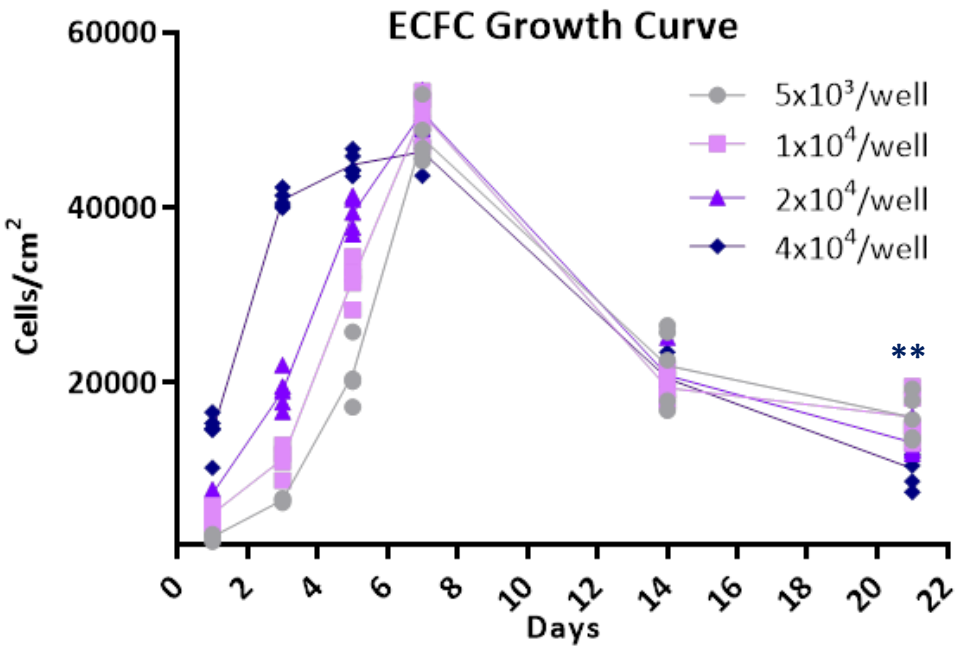

Figure 3.10. Growth curves of ECFCs at different seeding densities

UCB-ECFCs, P5, were seeded at $5x10^3$, $1x10^4$, $2x10^4$ and $4x10^4$cells/well on col I. coated 24 w/p's in healthy conditions (20% O_2 and 5.5mM glucose), with EGM-2 containing 10% FBS medium, to determine the effect of seeding density and time on cell growth rate. At time points day 1, 3, 5, 7, 14 and 21 cells were washed, fixed in 10% NBF, permeabilised using 0.5% Triton-X and DAPI stained, in preparation for cell counting using the Nikon E-Tie fluorescence microscope, x10 objective. ImageJ software was used to write a micro to perform automated cell counting. n=4 or 5 and lines represent average for each seeding density. One-way ANOVA with Tukey's correction was used to perform statistical analysis. n=5. **p<0.01 comparing $4x10^4$ cells/well vs. $5x10^3$ cells/well and $1x10^4$ cells/well.

3.4.5 UCB-ECFCs SURVIVED LOW OXYGEN HIGH GLUCOSE *IN VITRO* CULTURE CONDTIONS

There was no significant difference in the metabolic activity of UCB-ECFCs grown in 2% oxygen and physiological glucose (5.5mM) or UCB-ECFCs grown in 2% oxygen and high glucose (33mM) when compared to healthy controls (20% oxygen and 5.5mM glucose) for 4 days (Figure 3.11A). Micrographs of ECFCs gown on col I. coated glass slides show cells retained their cobblestone morphology for up to 21 days, forming a confluent layer, in both healthy and diabetic conditions (Figure 3.11B). These data support the hypothesis of UCB-ECFC capability and robustness for survival and expansion in *in vitro* conditions.

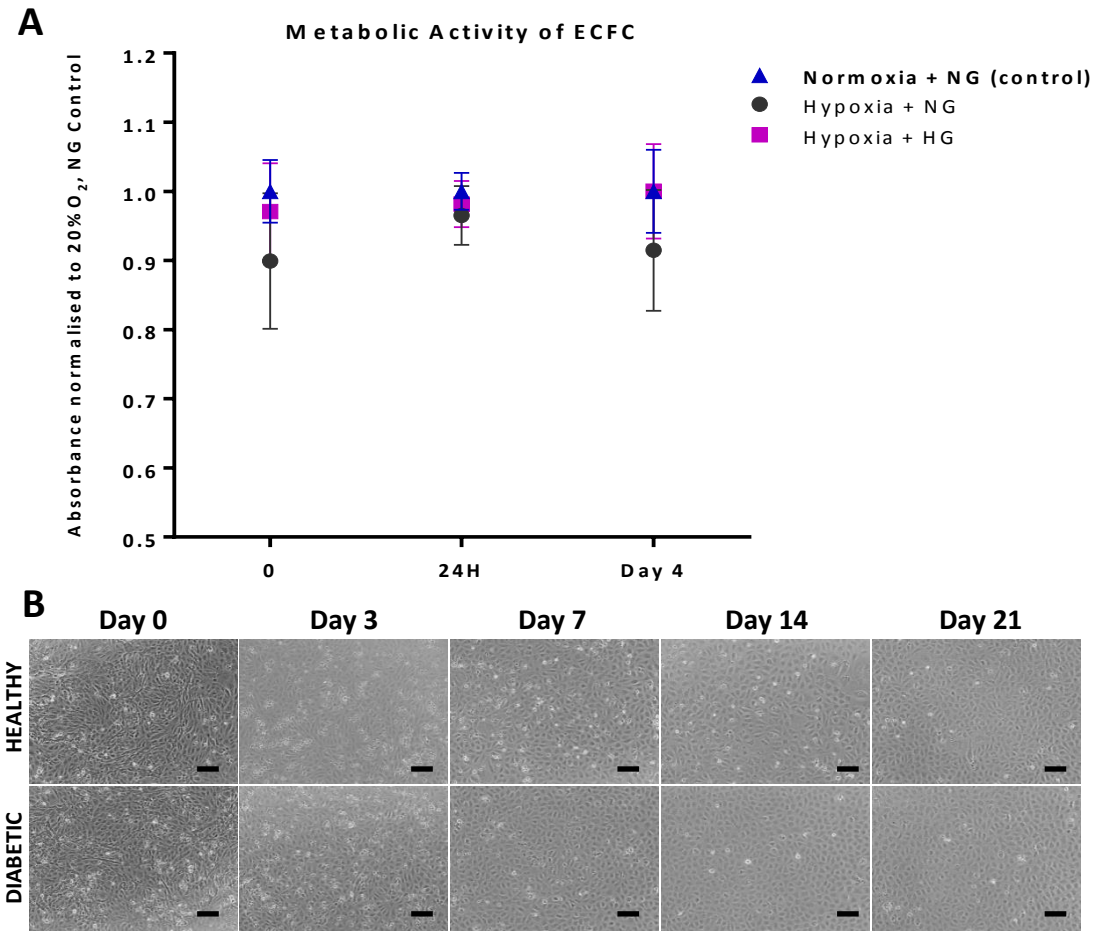

Figure 3.11. UCB-ECFCs withstood diabetic *in vitro* culture conditions

UCB-ECFCS, P6, were seeded at 2.5x10^3 cells/well in col I. coated TC plastic 24w/p's and left to form a monolayer for 48H. At experimental time point 0 (48H after seeding), ECFC metabolic activity was assessed using resazurin sodium salt colorimetric assay, then cells were transferred into 20% or 2% oxygen and 5.5mM or 33mM glucose. Results were adjusted for gain across plates. Results were normalised to Normoxia + NG control (**A**). There were no statistical differences in ECFC metabolic activity in the different conditions. n= 6 or 8, assayed in duplicate. Phase images were captured of the ECFCs grown in healthy and diabetic conditions over 21 days, using the Nikon DIAPHOT microscope, x10 magnification (**B**). Scale bars= 200µm.

3.4.6 ECFC METABOLIC ACTIVITY WAS NOT ALTERED DUE TO THE SWITCH TO OPTIMISED CO-CULTURE MEDIUM

ECFC metabolic activity was within normal range when grown in healthy or diabetic conditions, in EGM-2 with 10% FBS medium or MV with 5% FBS medium for 7 days. From day 2-7, metabolic activity remained within healthy range for both hREC and ECFCs when switched from healthy conditions to diabetic conditions and also when ECFCs were changed from their preferred growth medium (EGM-2 with 10% FBS) to the optimised co-culture medium (MV 5% with FBS) (Figure 3.12). Micrographs of hREC and ECFCs at days 2 and 7 showed cells have expanded in number in all conditions and the reduction in serum from 10% to 5% did not appear to prevent ECFC viability and expansion, confirming the MV with 5% FBS was for hREC, hRP and ECFCs in the co-culture model.

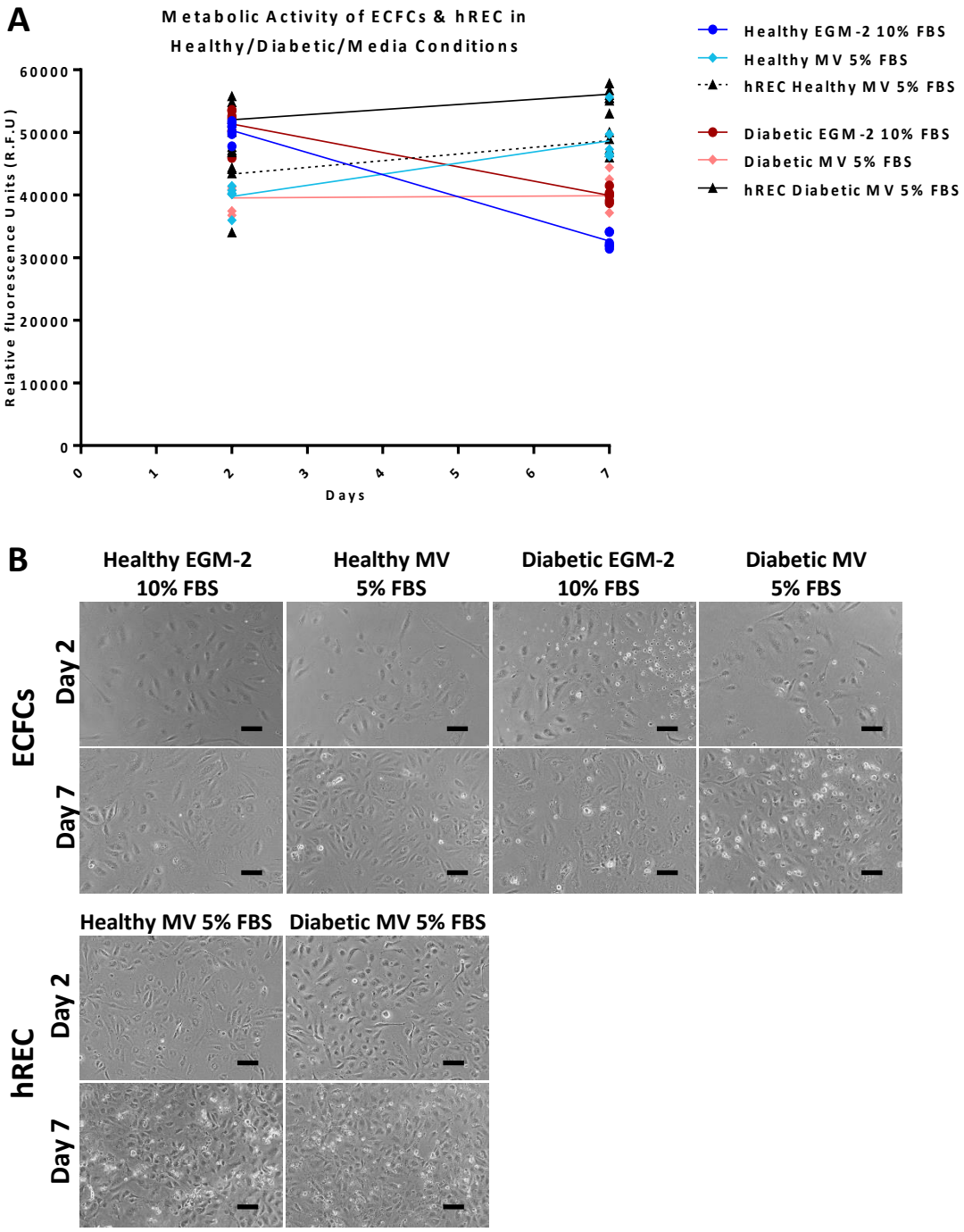

Figure 3.12. ECFC metabolic activity was not affected when cells were cultured in optimised co-culture medium

(**A**) UCB-ECFCs, P6 were seeded at 2x10^4 cells/well in col I. coated TC plastic 24 w/p's, straight in to healthy or diabetic conditions, in either MV with 5% FBS or EGM-2 with 10% FBS media. hREC, P8 were seeded at 2x10^4 cells/well on TC plastic 24 w/p's, straight in to healthy or diabetic conditions in MV with 5% FBS medium. At day 2 and day 7 cells were tested for metabolic activity using resazurin sodium salt colorimetric assay. Results were adjusted for gain across plates. n=6, assayed in duplicate. (**B**) Phase contrast images were captured of the cells at days 2 and 7 using the Nikon DIAPHOT microscope, x10 magnification. Scale bars= 200µm.

3.4.7 ECFCS RETAINED THEIR ENDOTHELIAL PHENOTYPE AFTER 21 DAYS IN HEALTHY OR DIABETIC CONDITIONS

ECFCs from healthy UCB were successfully grown on col I. coated 8-well EZ glass slides for up to 21 days in both healthy and diabetic conditions (Figure 3.13). At day 21 junctional proteins VE-Cad and CD31 were expressed on the lateral borders of ECFCs grown in both healthy and diabetic conditions, with no noticeable differences. ECFC in both healthy and diabetic conditions expressed vWF, confirming their endothelial phenotype. CD34, VEGFR-2 and SOD-1 did differ in expression between ECFCs in healthy or diabetic conditions for 21 days. CD34 was expressed at the lateral border of the cell cytoplasm in ECFCs grown in diabetic conditions, but was expressed in the perinuclear area of ECFCs grown in healthy conditions for 21 days. VEGFR-2 expression was minimal in ECFCs in diabetic conditions, but was expressed across the cytoplasm of ECFCs grown in healthy conditions. SOD-1 appeared upregulated in the cytoplasm of ECFCs grown in healthy conditions compared to those grown in diabetic conditions. Comparing cell number, size and the shape of ECFCs grown in healthy or diabetic conditions, there was no major differences. IgG isotype, no primary and no secondary controls showed background/non-specific staining, used to validate the antibodies used for IF characterising of ECFC.

3.4.8 HEALTHY UCB-ECFCs ADHERED AND GREW SUCCESSFULLY WITH MATURE hREC

hREC and ECFCs both integrate on to TC plastic and PET transwell inserts when seeded at a 1:1 ratio at the same time, in healthy conditions (Figure 3.14). ECFCs tagged with CTG (CTG-ECFC) and hREC tagged with CTR (CTR-hREC) (Figure 3.14A) both integrated at 1:1 seeding density of $2x10^4$ cells/well and $6.67x10^4$ cells/well on TC plastic. Both cell-types with CellTracker were visualised for up to 72H after seeding. However, some cells took up both dyes, making it difficult to determine between hREC and ECFCs (white circles Figure 3.14B). CTG-ECFCs and CTR-hREC both also integrated successfully on to the transwell inserts (Figure 3.14C), at both low and high seeding density and could be monitored for up to 72H after seeding. Beyond 72H, the CellTracker faded and therefore cannot be used for long term tracking of cells.

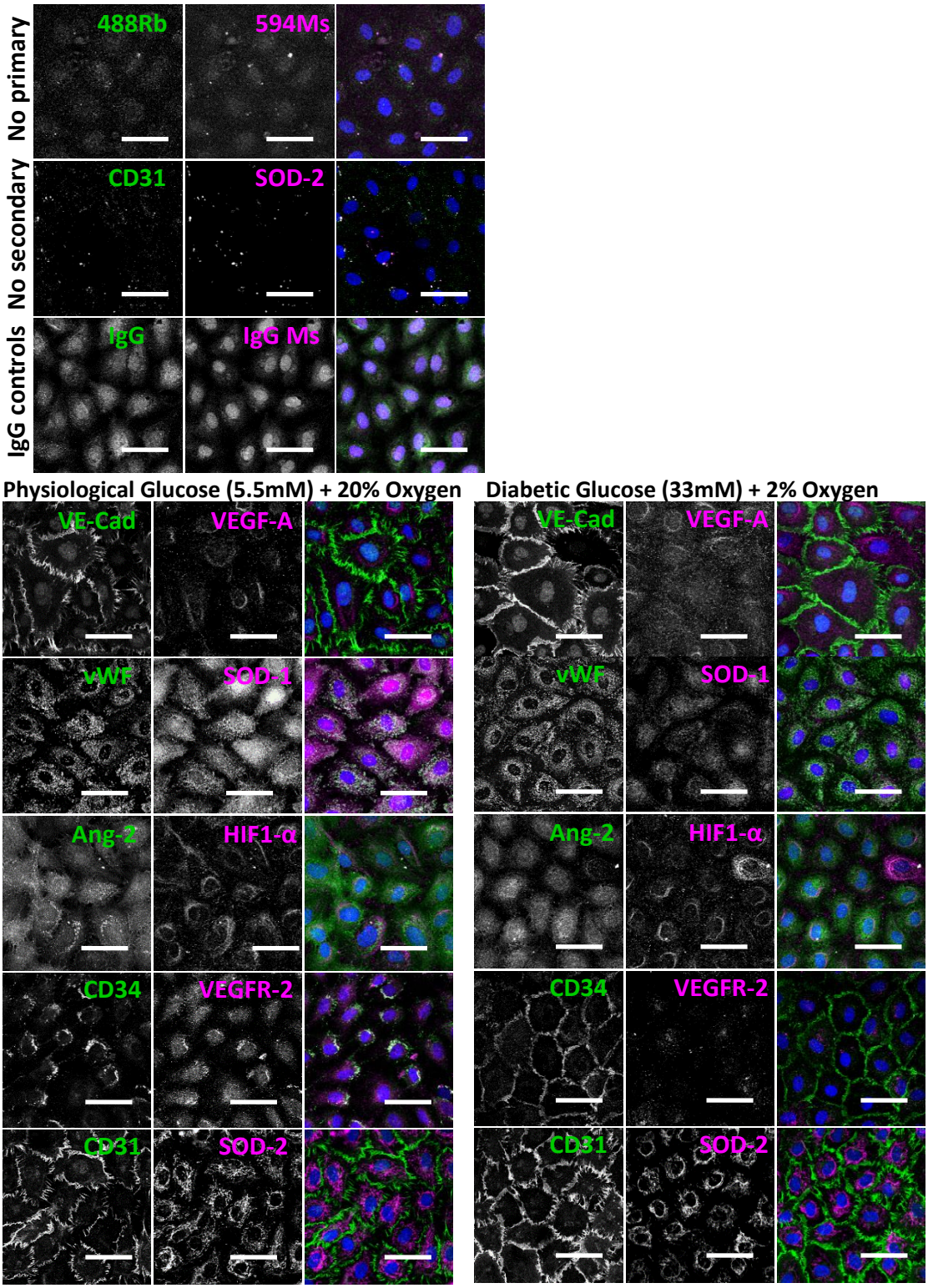

Figure 3.13. ECFCs maintained their phenotype for 21 days in healthy or diabetic conditions

UCB-ECFCs, P5 were seeded at $2x10^4$ cells/well on col I. coated glass 8-well EZ glass slides. Cells were grown in either healthy (20% O_2 and 5.5mM glucose) or diabetic conditions (2% O_2 and 33mM glucose) for 21 days, in EGM-2 with 10% FBS, changed every 24-48H. On day 21, cells were fixed and processed for IF antibody labelling. No primary, no secondary and IgG isotype controls were included to exclude non-specific staining. Images were captured using the Zeiss M800 confocal microscope, x40 oil magnification. Scale bars= 50µm.

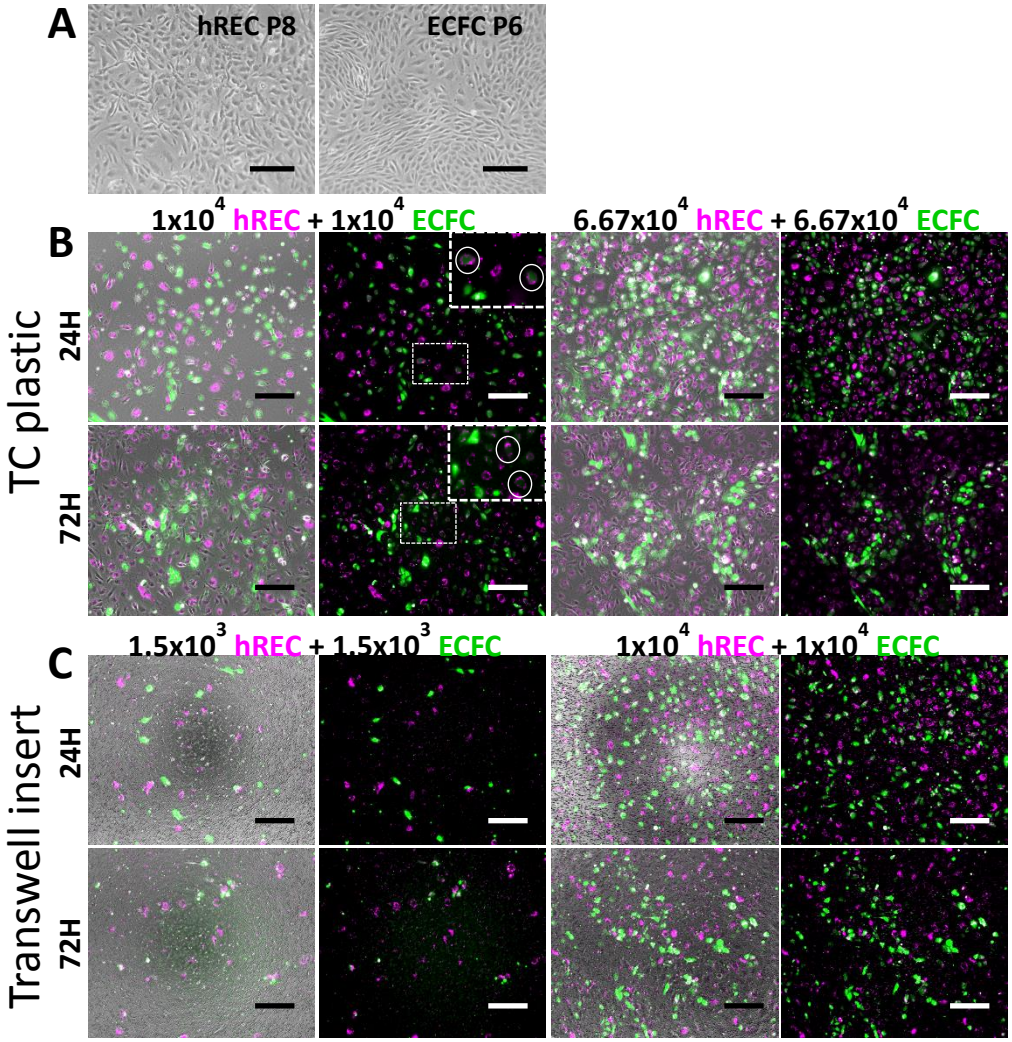

Figure 3.14. UCB-ECFCs adhered and grew when seeded 1:1 with hREC

hREC, P8 tagged with CTR were added at same time as CTG-tagged UCB-ECFCs, P6 at a 1:1ratio in 24 w/p's or transwell inserts. (**A**) hREC and ECFCs used for the experiment. (**B**) 1:1 seeding at low ($1x10^4$/cell-type) or high ($6.67x10^4$/cell-type) density, on TC plastic. (**C**) 1:1 seeding at low ($1.5x10^3$/cell-type) or high ($1x10^4$/cell-type) density, on 24 w/p PET transwell inserts. Magnified boxes (white dotted lines) highlight cells (white circles) which have taken up both CTR and CTG. Phase images were captured using the Nikon DIAPHOT microscope and IF images were captured using the Nikon E-Ti live cell microscope. Scale bars= 200µm.

3.4.9 APB-ECFCs INTEGRATED INTO AN ESTABLISHED hREC MONOLAYER

APB-ECFCs integrated into an already established hREC monolayer on TC plastic, in both healthy and diabetic conditions. Two different APB donor ECFC clones were analysed concurrently, tagged with CTG, and ECFCs from both donors integrated into a low and high seeding density hREC monolayer and successfully integrated in both healthy and diabetic conditions (Figure 3.15 A and B). CTG-ECFCs were still present at 48H. Beyond 72H, green cells could no longer be distinguished due to fading of the CellTracker dye.

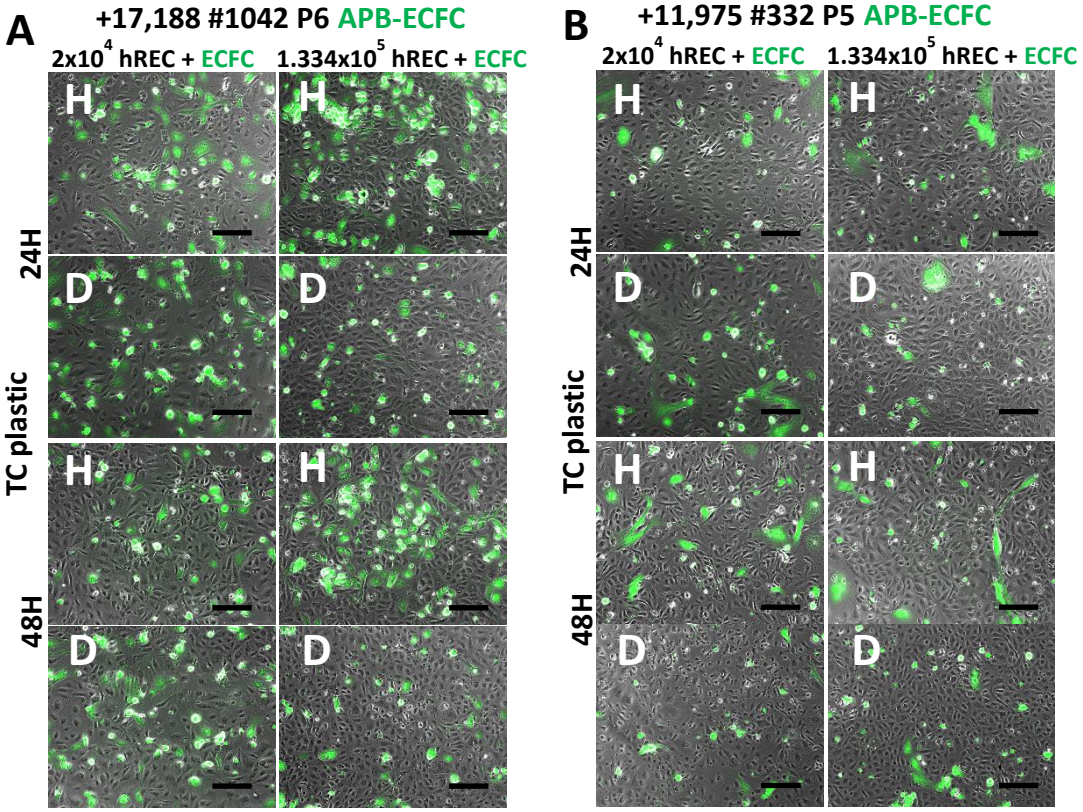

Figure 3.15. APB-ECFCs integrated into an established hREC monolayer

hREC, P8 were seeded at $2x10^4$ (left panel) or $1.334x10^5$ cells/well (right panel) on a 24 w/p's, directly in to healthy (**H**) or diabetic (**D**) conditions. At 48H, CTG-APB-ECFCs #1042 P6 were seeded at 17,188 cells/well (**A**) and CTG-APB-ECFCs #322 P5 were seeded at 11,875 cells/well (**B**). Images were captured at 24H and 48H after seeding the CGT-APB-ECFCs, using the Nikon E-Ti live cell microscope, x10 magnification. Scale bars= 200µm.

3.4.10 SOME APB-ECFCs TRANSITIONED INTO SENESCENT OR DEDIFFERENTIATED CELLS WHEN INTEGRATED INTO A hREC MONOLAYER

The incorporated ECFC were fixed and stained to determine if ECFCs physically incorporated into a hREC monolayer or remained on top. CTG-APB-ECFCs #1042 and the surrounding hREC were positive for ZO-1 staining, in both healthy and diabetic conditions, and ZO-1 was still present, even with some gaps between neighbouring cells in the healthy conditions (Figure 3.16A). Cell-cell contact and monolayer integrity appeared tighter at high hREC seeding density in diabetic conditions. CTG-APB-ECFCs #322 and the surrounding hREC expressed ZO-1 in both healthy and diabetic conditions, but similar to the #1042 APB-ECFCs, ZO-1 positivity, cell-cell contacts and monolayer integrity looked more cell-cell border/GJ-specific in the diabetic conditions compared to healthy conditions (Figure 3.16B). Some of the CTG-APB-ECFC #1042 appeared to be undergoing cell senescence (red circle, Figure 3.16A), APB-ECFCs #322 tagged with CTG had a different morphology to UCB-ECFCs, due to their larger size and finger-like projections (white circles, Figure 3.16B). There was also contamination of multinucleated, very large cells in the 1:1 hREC-APB-ECFC #322 healthy cultures (red arrow heads, Figure 3.16A), suggesting APB-ECFCs #322 have de-differentiated, or are contaminated with immune cells as remnants from the isolation process. HIF1-α remains unchanged in all conditions.

3.4.11 HEALTHY AND GD-UCB-ECFCS WERE SUCCESSFULLY TRANSDUCED TO EXPRESS GFP USING LENTIVIRUS

UCB-ECFCs were successfully transduced with GFP using GIPz-lentivirus, to remove the time limiting factor of using CellTracker dye. UCB-ECFCs from multiple donors were grown on 6 w/p's in healthy conditions and by day 9-12 (donor variability) after initial seeding, UCB-ECFCs were successfully transduced with GFP (Figure 3.17). GFP transduction via lentivirus was successful in all healthy and GD UCB-ECFCs, although the rate of transduction was variable, with the example of clone #18-241 showing better transduction rate than clone #17-321. However, with continued puromycin treatment over time, the result was close to ≥95% GFP expression as non-transduced cells were killed and transduced cells grew into the new spaces. If no virus was added, cells were killed when puromycin was added (right panel). Lentivirus transduction of GFP was not possible for APB-ECFCs, which failed to expand after puromycin treatment, on multiple attempts (data not show).

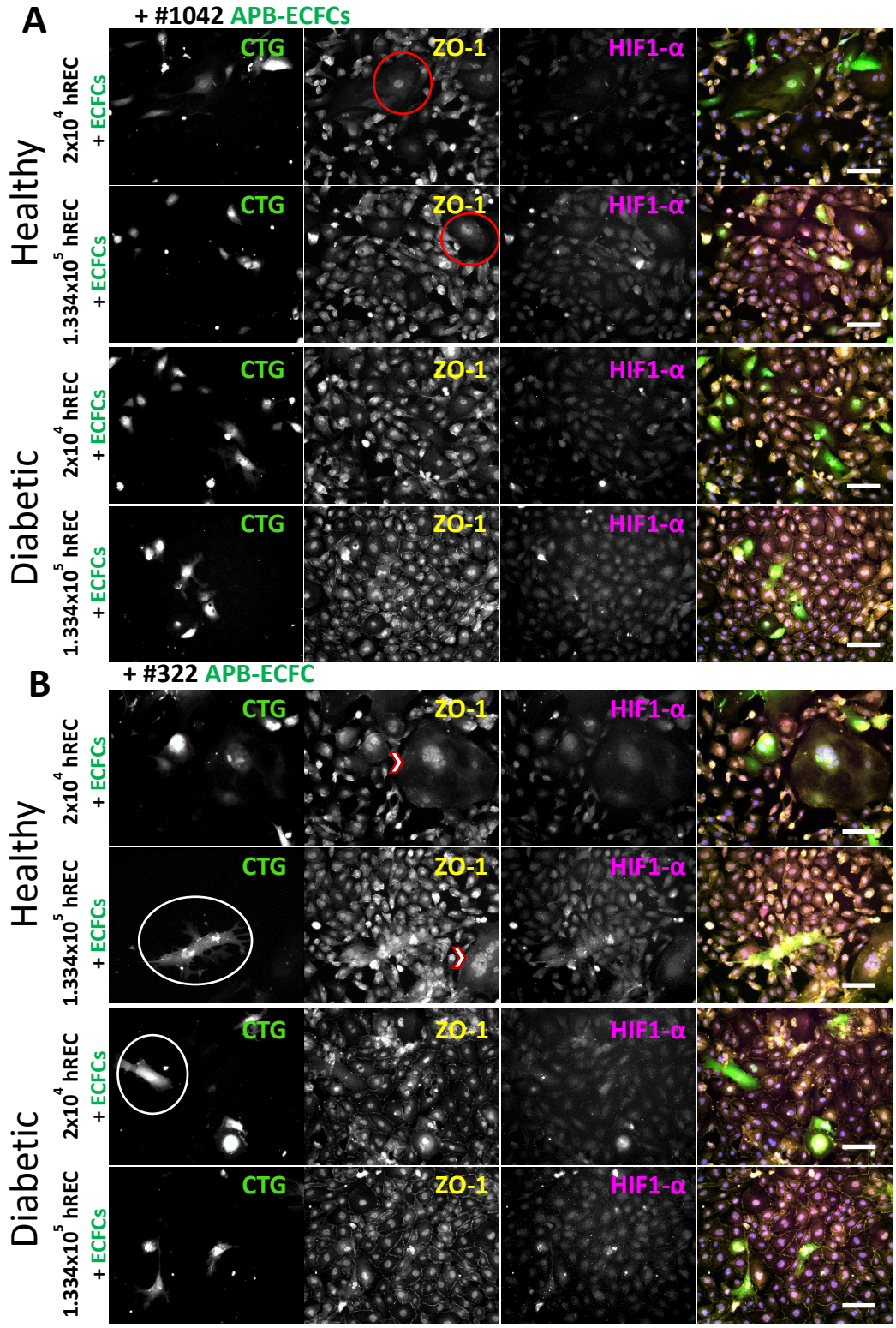

Figure 3.16. APB-ECFCs integrated with hREC but some APB-ECFCs transitioned *in vitro*

hREC, P8 were seeded at $2x10^4$ or $1.334x10^5$ cells/well on 24 w/p's, directly in to healthy or diabetic conditions. At 48H, CTG-APB- ECFCs #1042, P6 were seeded at $1.7188x10^4$ cells/well (**A**) and CTG-APB-ECFCs #322, P5 were seeded at $1.1875x10^4$ cells/well (**B**). Red circles highlights senescent cells, white circles highlight de-differentiated ECFCs and arrowheads highlight large multinuclear cell contamination. Cells were fixed 48H after adding APB-ECFCs. Images were captured using the Nikon E-Ti microscope, x20 objective. Scale bars= 100µm.

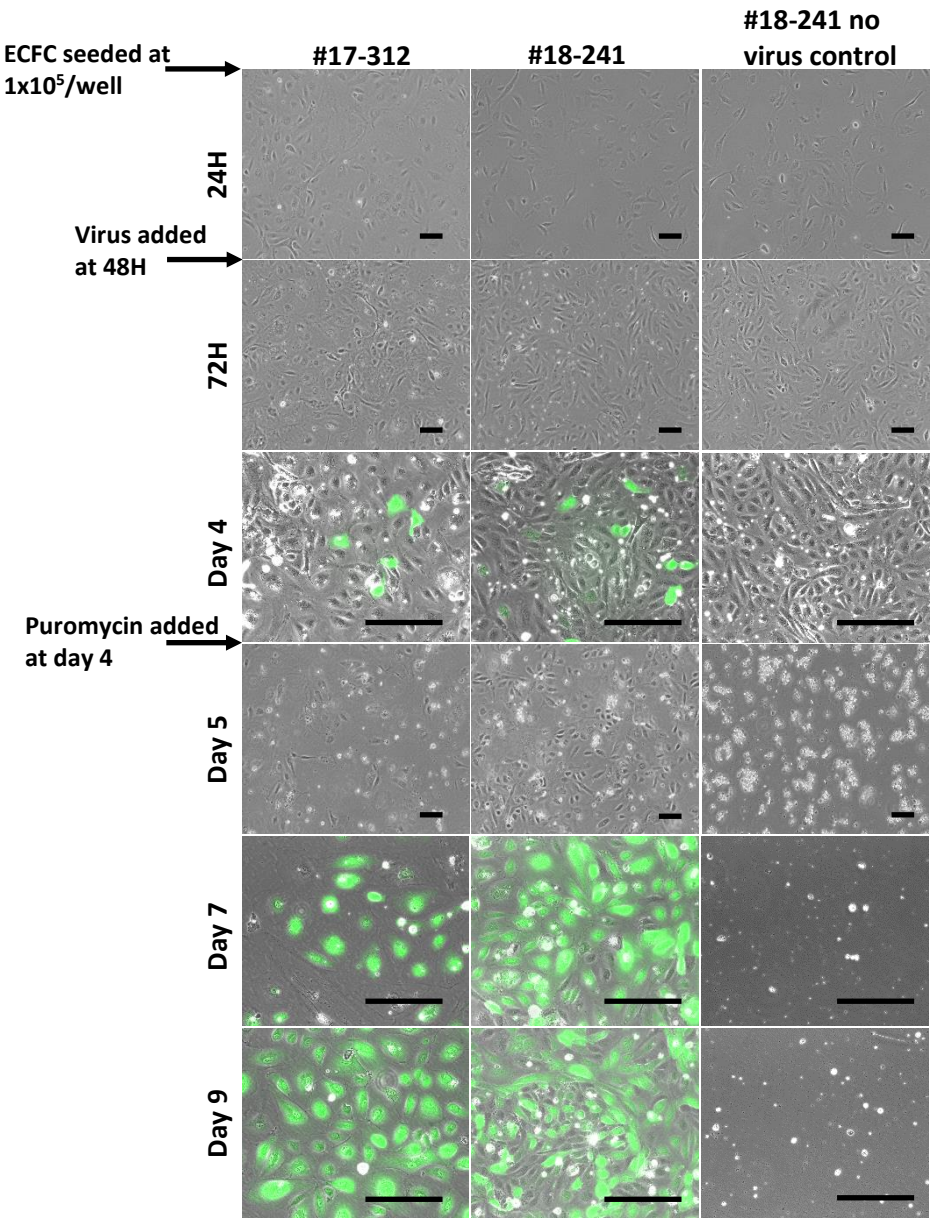

Figure 3.17. UCB-ECFCs were transduced to express GFP using lentivirus

UCB-ECFCs #17-321 and #18-241, both P5, were seeded at 1.5x10^5 cells/well in 6 w/p's for 48H. 20µl of virus was added to each well, with 500µl EGM-2with 10% FBS and 6ug/ml of sterile filtered polybrene. Puromycin was added 48H after virus (day 4). All non-transduced cells were killed by puromycin treatment (right panel). From ~day 7 GFP expressing UCB-ECFCs expanded in the wells. GFP-UCB-ECFCs could be expanded for multiple passages. The Nikon DIPHOT microscope was used to capture phase images at x10 magnification and the Nikon E-Ti microscope was used for fluorescence imaging, x20 magnification. Scale bars= 200µm.

3.4.12 GFP-UCB-ECFCs SUCCESSFULLY INTEGRATED WITH MATURE hREC

Transducing healthy UCB-ECFC with GFP did not appear to affect their ability to adhere and integrate with hREC when seeded at the same time, at a ratio of 1:1, on TC plastic or PET transwell inserts. GFP-UCB-ECFCs, (shown in green) incorporated at high and low seeding density on both TC plastic and PET transwell membranes, and remained for up to 7 days in healthy conditions (Figure 3.18A and B).

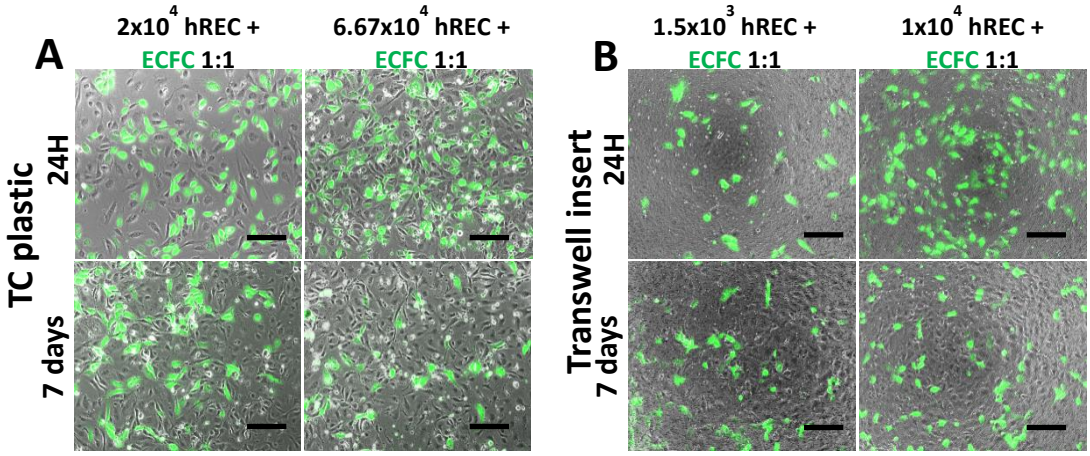

Figure 3.18. GFP-UCB-ECFCs integrated with hREC when seeded at 1:1 ratio on TC plastic or PET membranes

hREC, P7 and GFP-UCB-ECFC, P8 were seeded at same time at a 1:1 ratio, at low ($1x10^4$/cell-type) or high ($6.67x10^4$/cell-type) density, on TC plastic 24 w/p's. (**A**). Or, 1:1 seeding at low ($1.5x10^3$/cell-type) or high ($1x10^4$/cell-type) density, on 24 w/p PET transwell inserts (**B**). Images were captured using the Nikon E-Ti live cell microscope, x10 magnification. Scale bars= 200µm.

3.4.13 GFP-UCB-ECFCs SUCCESSFULLY INTEGRATED INTO AN ESTABLISHED hREC MONOLAYER

To mimic the scenario of *in vivo* migration of ECFCs to sites of vascular injury, hREC were allowed to form a monolayer for 48H, with $2x10^4$ GFP-UCB-ECFCs added afterwards. GFP-UCB-ECFCs incorporated in to both low and high hREC seeding density cultures, on both TC plastic and PET transwell membranes. GFP-UCB-ECFCs were still present at day 7 (Figure 3.19).

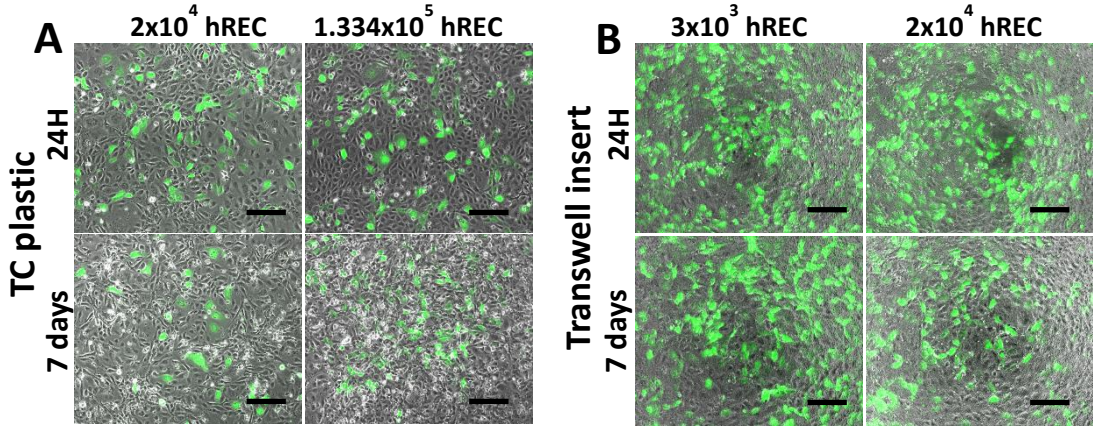

Figure 3.19. GFP-UCB-ECFCs integrated into both high and low density hREC

hREC, P8 were seeded at $2x10^4$ or $1.334x10^5$ cells/well on 24 w/p's (**A**), and $3x10^3$ or $2x10^4$ cells/well on PET transwell inserts (**B**). 48H later, $2x10^4$ GFP-UCB-ECFCs, P8 were added to each well/insert. Images were captured at 24H and 7 days after seeding GFP-UCB-ECFCs, using the Nikon E-Ti Live cell microscope, x10 magnification. Scale bars= 200µm.

3.4.14 GFP-UCB-ECFCs FORMED GJS AND ADHERENS JUNCTIONS WITH NEIGBOURING hREC

7 days after seeding $2x10^4$ GFP-UCB-ECFCs on to the hREC monolayers on PET transwell inserts in healthy conditions, both ECFCs and mature hREC expressed ZO-1 and VE-Cad, at both high and low hREC seeding density (Figure 3.20). These data confirm that the GFP-UCB-ECFCs physically incorporated into the mature hREC monolayer. VEGFR-2 expression appeared upregulated in hREC seeded at lower density. Ang-2 expression was upregulated at high hREC seeding density. The cells expressing Ang-2 were GFP-negative, suggesting they are hREC, although one GFP-positive ECFC is expressing both Ang-2 and CD34 at high levels. CD34 expression overall was inconclusive.

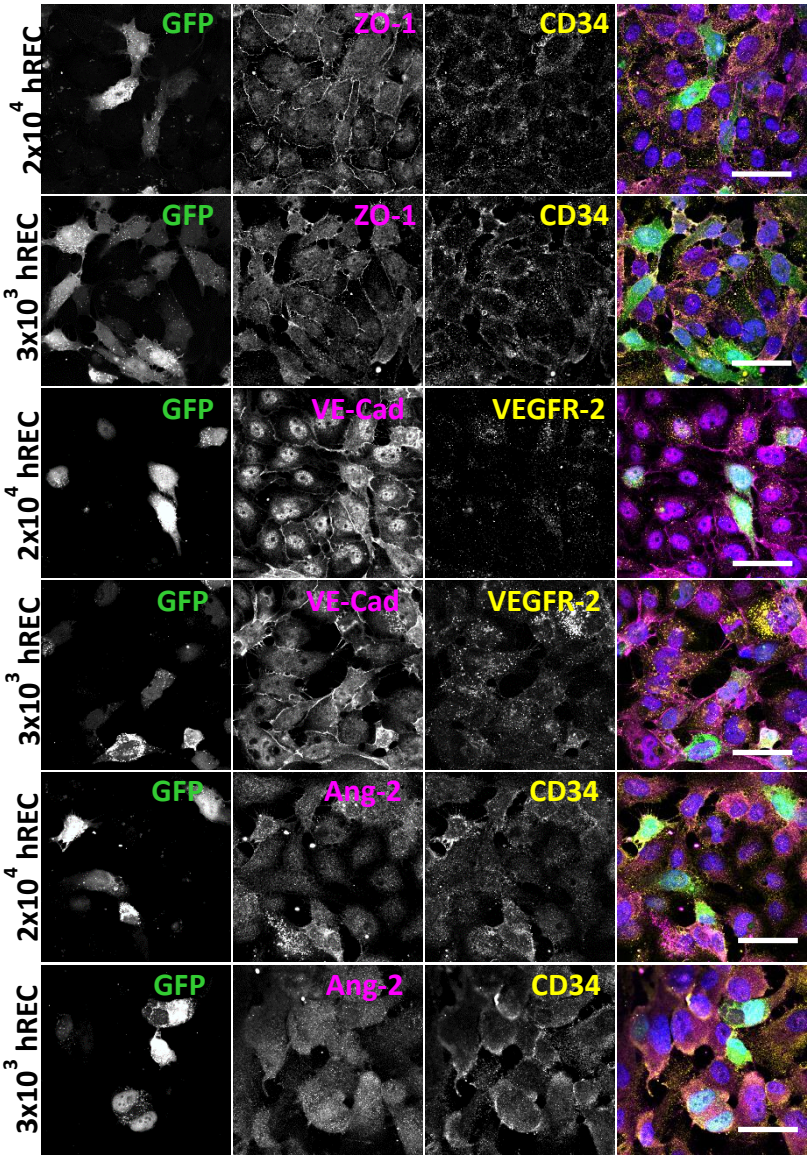

Figure 3.20. GFP-UCB-ECFCs formed GJs and adherens junctions with neighbouring hREC

hREC were seeded at $3x10^3$ or $2x10^4$ cells/well on PET transwell inserts. 48H later, $2x10^4$ GFP-UCB-ECFCs, P8 were added to each well/insert. All cells were grown in healthy conditions (20% O_2 and 5.5mM glucose). Cells were fixed at 7 days after seeding GFP-UCB-ECFCs. Cells were processed for IF imaging to assess integration of ECFCs into a mature hREC layer. Antibodies against ZO-1 and VE-Cad were used to assess the formation of GJs and adherens junctions and VEGFR-2 and Ang-2 were used to assess the angiogenic response of the two cell-types. Images were captured using the Zeiss M800 confocal microscope, x40 oil magnification. Scale bars= 50µm.

3.4.15 HEALTHY GFP-UCB-ECFCs INCORPORATED INTO THE hREC LAYER OF HEALTHY AND DIABETIC CO-CULTURE MODELS

Healthy GFP-UCB-ECFCs incorporated into a monolayer of hREC grown on PET transwell inserts and a layer of hREC grown with hRP in co-culture, on the underside of the PET membrane (see Figure 2.4), which were subjected to healthy conditions for 7 days. 24H after UCB-ECFCs were added to the hREC layer in mono- or co-cultures in healthy conditions, VE-Cad was present on the cell membranes of GFP-UCB-ECFCs and mature hREC (Figure 3.21). ZO-1was present on mature hREC membranes, but not on GFP-UCB-ECFC membranes. Z-stack projections confirmed the presence of hRP on the underside of the PET membrane in the co-culture models.

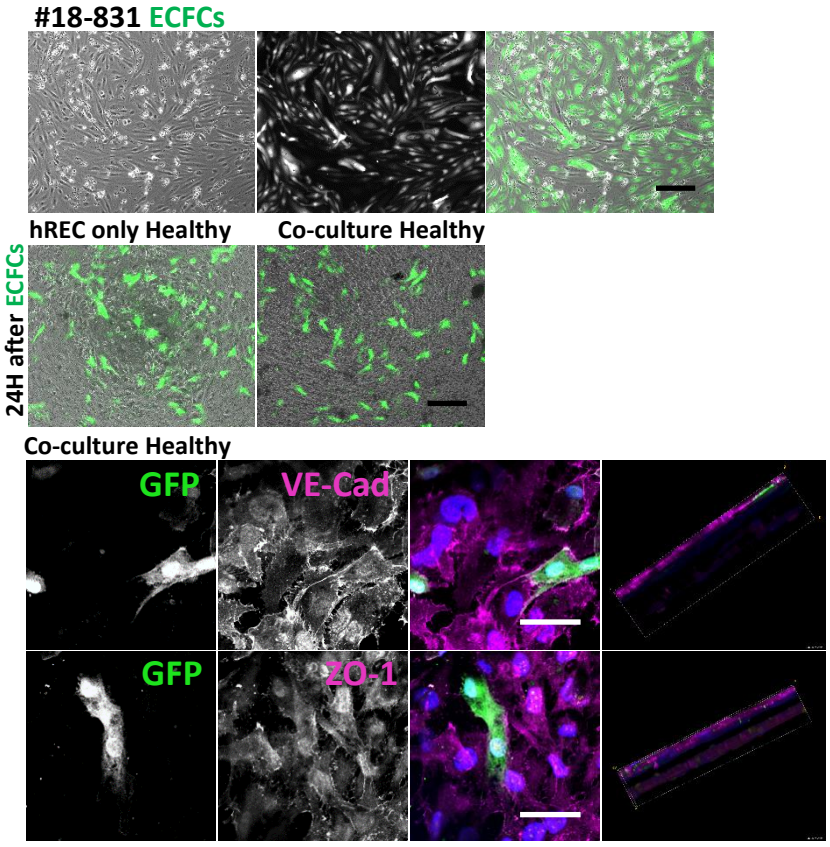

Figure 3.21. GFP-UCB-ECFCs formed VE-Cad adherens junctions with hREC when added to the healthy co-culture model at day 7

hREC P8 and hRP P8 were seeded at $2x10^4$ cells/insert on either side of the PET membrane, or hREC were seeded alone, and grown for 3 days to enable hREC to form a monolayer. Cells were then cultured in healthy conditions for 7 days. Healthy GFP-UCB-ECFCs, P6 were seeded at $2x10^4$ cells/insert on the apical hREC monolayer, on day 7. 24H later, cells were fixed and processed for IF analysis of ZO-1 and VE-Cad expression to analyse ECFC integration. Images were captured using the Zeiss M800 confocal microscope, x40 oil magnification, and z-stacking to images cells on both sides of the PET membrane. White scale bars= 50µm, black Scale bars= 200µm.

Healthy GFP-UCB-ECFCs incorporated into the same conditions described above, but the mono- and co-cultures had been subjected to diabetic conditions for 7 days. 24H after UCB-ECFCs were added to the hREC layer in mono or co-culture in diabetic conditions, both ZO-1 and VE-Cad were present on the cell membranes of GFP-UCB-ECFCs and mature hREC (Figure 3.22). The staining specificity of ZO-1 at the cell-cell junction, confirms GJ formation, with tighter contact with cell neighbours compared to the healthy co-culture hREC and ECFCs (Figure 3.21). Z-stack projections confirmed the presence of hRP on the underside of the PET membrane.

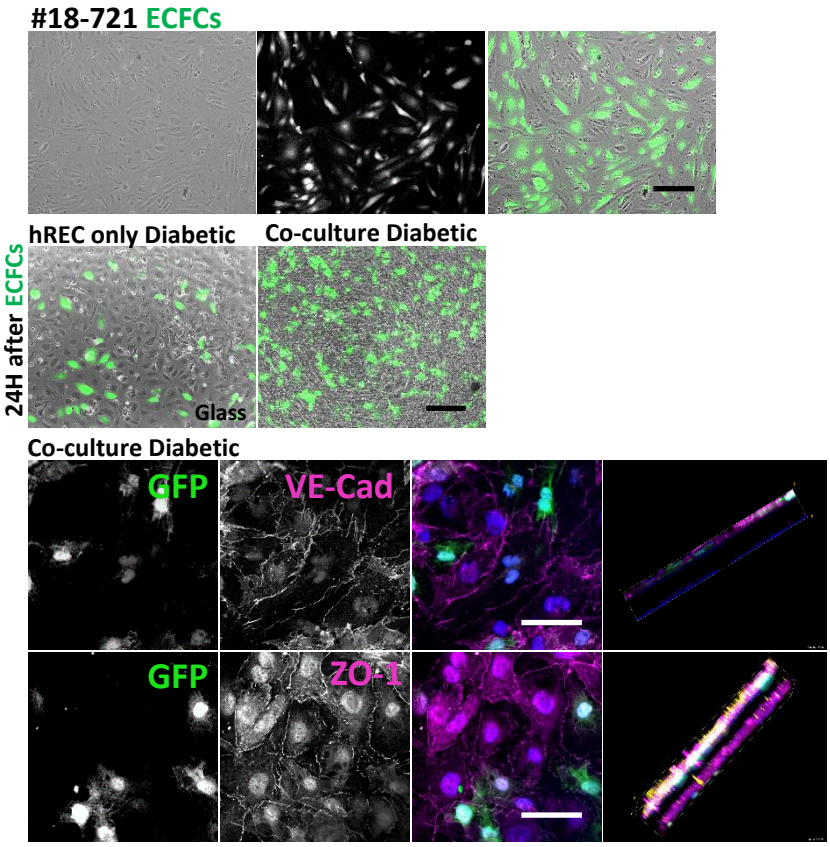

Figure 3.22. GFP-UCB-ECFCs formed ZO-1 GJs and VE-Cad adherens junctions with hREC when added to the diabetic co-culture model at day 7

hREC P8 and hRP P8 were seeded at $2x10^4$ cells/insert on either side of the PET membrane, or hREC were seeded alone, and grown for 3 days in healthy conditions to enable hREC to form a monolayer. Cells were then cultured in diabetic conditions for 7 days. Healthy GFP-UCB-ECFCs, P6 were seeded at $2x10^4$ cells/insert on the apical hREC monolayer, on day 7. 24H later, cells were fixed and processed for IF analysis of ZO-1 and VE-Cad expression to analyse ECFC integration. Images were captured using the Zeiss M800 confocal microscope, x40 oil magnification, and z-stacking to images cells on both sides of the PET membrane. White scale bars= 50µm, black Scale bars= 200µm.

3.4.16 GD-GFP-UCB-ECFCs INCORPORATED INTO THE hREC LAYER OF HEALTHY AND DIABETIC MONO-AND CO-CULTURE MODELS

GD-GFP-UCB-ECFCs were lentivirally transduced with GFP the same way as healthy UCB-ECFCs were. GD-GFP-UCB-ECFCs incorporated into established hREC layers grown in both healthy and diabetic conditions for 7 days, and grown either as mono-culture or co-culture with hRP, all on PET transwell inserts. Green GD-UCB-ECFCs were present at 24H and 5 days after seeding at $2x10^4$ cells/insert (Figure 3.23).

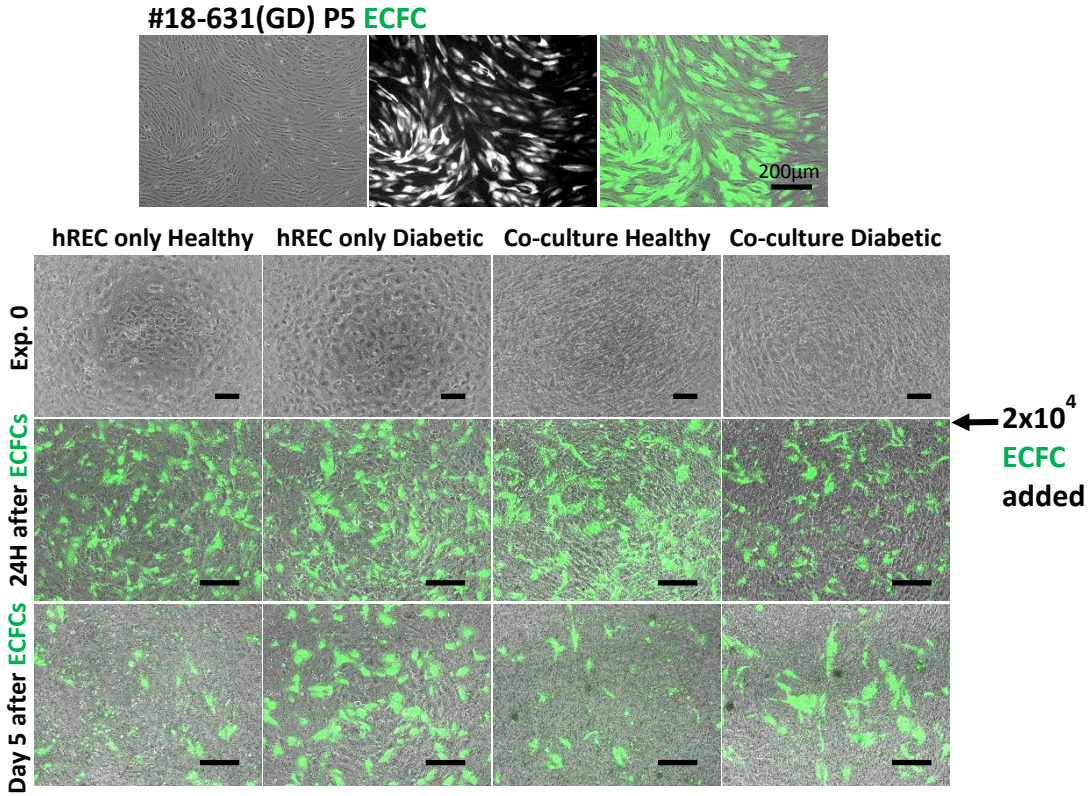

Figure 3.23. GD-GFP-UCB-ECFCs integrated into mono- and co-cultures models in both healthy and diabetic conditions

hREC P8 and hRP P8 were seeded at $2x10^4$ cells/insert on either side of the PET membrane, or hREC were seeded alone, and grown for 3 days in healthy conditions to enable hREC to form a monolayer. Cells were then cultured in either healthy or diabetic conditions for 7 days. At day 7 of healthy or diabetic conditions, $2x10^4$ cells/well GD-GFP-UCB-ECFCs, P5 were added to the hREC layer of each insert. Images were captured at 24H and day 5 after ECFCs were added. Images were captured using the Nikon Eclipse TS100, the Nikon DIAPHOT and the Nikon E-Ti live cell microscopes, all at x10 magnification. Scale bars=200µm.

24H after adding GD-GFP-UCB-ECFCs to mono-cultured hREC subjected to 7 days of healthy or diabetic conditions, both mature hREC and GD-GFP-UCB-ECFCs showed positive staining for ZO-1, specifically at the cell-cell borders, confirming GJ formation (Figure 3.24). 24H after

adding GD-GFP-UCB-ECFCs to a diabetic co-culture model, subjected to 7 days of diabetic conditions, both mature hREC and ECFC expressed ZO-1, specifically at the cell-cell borders, confirming GJ formation. The Z-stack projection confirmed the presence of hRP on the underside of the PET membrane in the diabetic co-culture model.

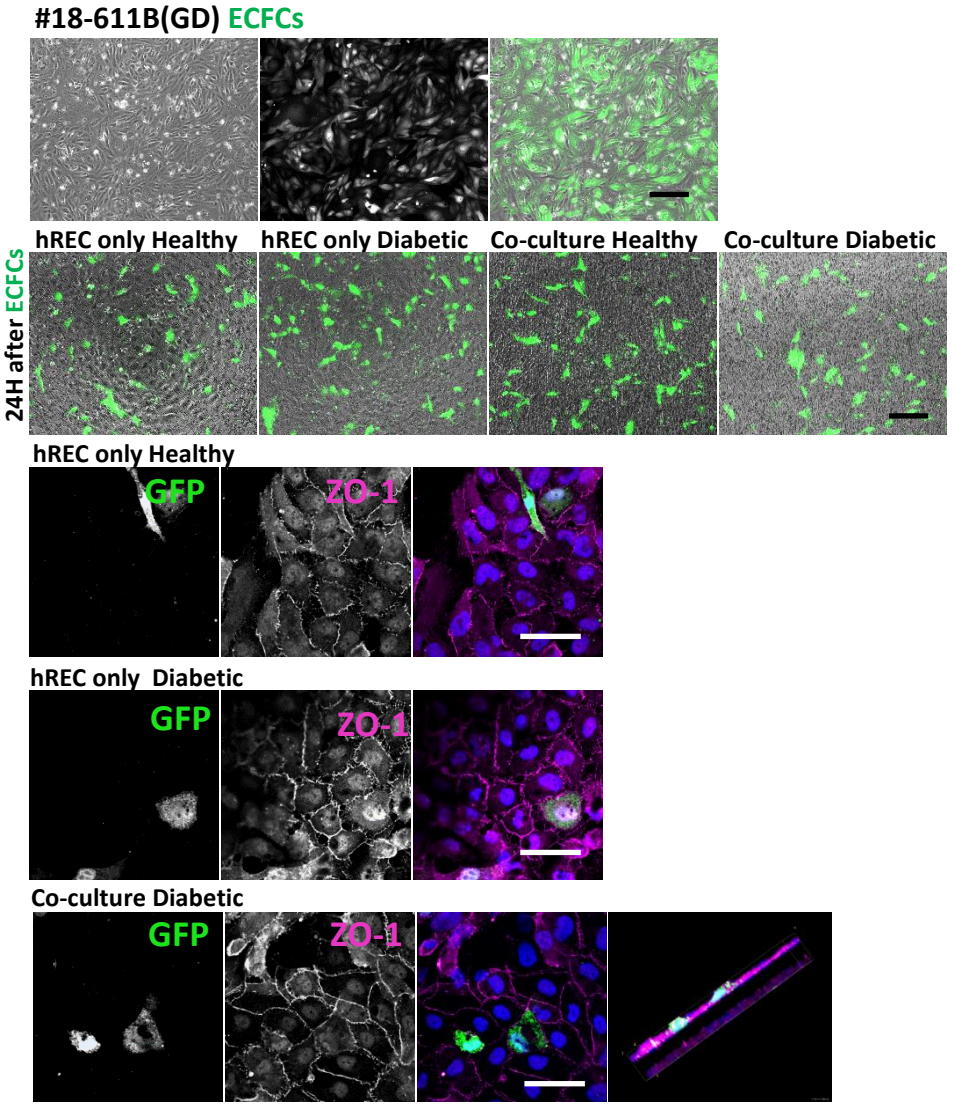

Figure 3.24. GD-GFP-UCB-ECFCs formed ZO-1 GJs and VE-Cad adherens junctions with hREC when added to healthy and diabetic hREC and the diabetic co-culture model at day 7

hREC P8 and hRP P8 were seeded at $2x10^4$ cells/insert on either side of the PET membrane, or hREC were seeded alone, and grown for 3 days in healthy conditions to enable hREC to form a monolayer. Cells were then cultured in either healthy or diabetic conditions for 7 days. GD-GFP-UCB-ECFCs, P9 were seeded at $2x10^4$ cells/insert on the apical hREC monolayer, on day 7. 24H later, cells were fixed and processed for IF analysis of ZO-1 and VE-Cad expression to analyse ECFC integration. Images were captured using the Zeiss M800 confocal microscope, x40 oil magnification, and z-stacking to images cells on both sides of the PET membrane. White scale bars= 50µm, black Scale bars= 200µm.

3.5 DISCUSSION

3.5.1 OVERVIEW

The aim of this chapter was to determine if ECFCs isolated from umbilical cord (UCB) or adult peripheral blood (APB) were capable of re-populating a mature retinal microvascular EC layer subjected to diabetic conditions *in vitro*, and therefore a potential candidate for allogeneic or autologous cell therapy to repair the damaged retinal microvasculature in early-stage DR. In healthy adults, ECFCs repair damage to the vasculature during normal tissue homeostasis, however wound healing and vascular maintenance is impaired in people with T2DM, leading to gradual decline in microvascular function. Ultimately this can lead to DR and sight loss, neuropathy, chronic wounds and limb amputation. It is not yet fully understood if ECFCs decline in number due to constant renewal of the EC damaged by hyperglycaemia, or due to a dysfunction in either migration or integration at sites of damage. This question has been studied by hundreds of researchers in the past 20 years, since the discovery of ECFCs. In order to test ECFC capability of repopulating the damaged retinal microvasculature, this study used the optimised co-culture model from Chapter 2 for *in vitro* testing of survival and integration of GFP-labelled ECFCs (GFP-ECFCs) into established hREC layers in healthy or diabetic co-culture conditions.

UCB-ECFCs and APB-ECFCs could be expanded *in vitro* for multiple passages, although APB-ECFCs took longer to initiate at P0, were slower to grow and began to transition *in vitro* when tested for their incorporation capability with hREC. UCB-ECFCs grew at a fast rate, retained their phenotype throughout passaging and successfully incorporated in to hREC monolayers. GFP-UCB-ECFCs could withstand diabetic insult and incorporated into the optimised co-culture model in both healthy and diabetic conditions, suggesting UCB-ECFCs may be a suitable allogeneic cell population to aid in retinal microvascular repair in people with T2DM and early-stage DR.

3.5.2 ECFCs WERE SUCCESSFULLY ISOLATED AND EXPANDED *IN VITRO* FROM HUMAN UCB AND APB

Historically, correct nomenclature and identification of true ECFCs from a heterogeneous EPC population has been highly debated, but according to a recent review summarising two major EPC populations: MACs and ECFCs, the present study defines ECFCs according to the definition agreed by Medina et al.[155]. To date, the minimal requirement to distinguish true ECFCs from MACs *in vitro* assesses: cell proliferative capacity, morphology, expression of specific cell-surface antigens and IF antibody labelling of endothelial-specific antigens. In the

present study, analysis of putative ECFCs from each donor was carried out before using the cells in experiments. ECFCs were isolated from the mononuclear layer of blood, seeded on col I. coated plates (rather than fibronectin), in EGM-2 with 20% FBS, and clones appeared in culture from day 14-40 (Figure 3.6), similar to reports from the literature[153,173,263]. Colonies appeared earlier in the cells isolated from UCB compared to APB. UCB-ECFCs and APB-UCBs were positive for CD31, CD105 and CD146 expression, and negative for CD45, CD14 and CD90 expression (Figure 3.9B) and had general cobblestone morphology (Figure 3.9A). CD34 expression was generally low 0.1-15.6%, although clones from two adult peripheral blood donors expressed much higher CD34; 24% and 63.1%. This variation in CD34 expression by ECFCs has been reported in the literature, where CD34+ ECFCs had higher proliferative potential[264]. A generally held opinion is that CD34 expression reduces over time during culture of ECFCs[155], therefore CD34 alone no longer confirms ECFCs *in vitro*. Importantly, in the present study, ECFCs were negative for CD45 (common leukocyte antigen), CD90 (mesenchymal stem-cell marker) and CD14 (haematopoietic-specific), clearly indicating the isolated cells were not from a haematopoietic lineage[149].

Some endothelial-specific markers are not expressed on the cell surface so cannot be assessed using flow cytometry, therefore, to confirm the cells isolated were true ECFCs, IF antibody labelling and confocal microscopy was performed on early passage cells from multiple donors. All UCB and APB donors were healthy, except for one GD-UCB donor. Healthy UCB-ECFCs and APB-ECFCs had positive expression for CD31 and vWF, confirming their endothelial-specificity (Figure 3.7, Figure 3.8). As with mature ECs, ECFCs make connections with neighbouring cells, therefore, VE-Cad should be present[40]. VE-Cad was present on APB-ECFCs (Figure 3.7A), although there was variability in VE-Cad expression on UCB-ECFCs, most likely due to time of fixation, considering the UCB-ECFC were fixed at 48H (Figure 3.7 B and C) and APB-ECFC were fixed later, at Day 5. ECFCs isolated from the one GD-UCB donor expressed vWF, CD31 and ZO-1, confirming endothelial-lineage, and similar to the healthy UCB donors, VE-Cad was not expressed at the cell borders, even though these cells had been fixed at day 5 (Figure 3.8). All UCB- and APB-ECFCs were negative for CD90 and αSMA, evidence they had not transitioned to a fibroblastic phenotype *in vitro*.

VEGFR-2 (KDR) was one of the earlier cell surface receptors reported as highly expressed by EPCs[138,143,156]. IF data from the present study suggests VEGFR-2 was dispersed across the cell membrane of UCB- and APB-ECFCs (Figure 3.7A, B and C), although lower expression levels were observed in GD-UCB- ECFCs (Figure 3.8). VEGFR-2 expression in healthy and diabetic

retinae was analysed using immunohistochemistry, and was moderate/intense in intra- and pre-retinal vessels in retinae with pre-retinal neovascularisation, compared to healthy controls[265]. Successful laser therapy diminished this VEGFR-2 overexpression in intra-retinal vessels, highlighting the dynamic expression of VEGFR-2 throughout disease progression and treatment, which may explain why VEGFR-2 expression was variable between healthy UCB- and GD-UCB-ECFCs.

A characteristic of ECFCs is their high proliferation rate *in vitro*[147], and the UCB-ECFCs isolated in the current study, seeded at four increasing densities, shared this highly proliferative characteristic, demonstrated by the steep increase in cell number over 7 days at all seeding densities, all peaking at a similar number of ~50,000 cells/well by day 7 (Figure 3.10). Comparable to the growth behaviour exhibited by the mature hREC (Figure 2.13), ECFC numbers decline from day 7-21, although numbers remaining at day 21 were over 10 times higher than the average number of hREC remaining (1,203 hREC vs. 13,357 UCB-ECFC). This decline in ECFC number after day 7 may in part be due to contact inhibition caused by overcrowding in the well, which is a limiting factor for expanding cell numbers *in vitro*. Overall, the UCB-ECFCs isolated for this study displayed a rapid growth stage (0-7 days) followed by a gradual decline phase (7-14 days) and a final plateau stage (14-21 days) *in vitro*. A general observation with the UCB-ECFCs, was retention of morphology throughout continuous growth (Figure 3.6, Figure 3.9, Figure 3.11B, Figure 3.12B, Figure 3.13), and expression of endothelial-specific antigens throughout passaging, as others have found[141,144]. ECFCs were successfully isolated from fewer APB donors (5/10) compared to UCB donors (16/17), and the number of wells producing ECFC colonies from each donor was much higher from the UCB, which also grew at a faster rate than the APB-ECFCs. This outcome has been reported by other groups, where the number of endothelial colonies/ml of blood was 15-fold higher in UCB compared to APB[141]. Taken together with the comprehensive cell phenotyping data from IF and flow analysis using a comprehensive and up-to-date panel of widely used ECFC markers, the ECFC growth potential data further validate that ECFCs were successfully isolated and expanded from UCB and APB.

Throughout ECFC passaging and from numerous donors, there was evidence of minor contamination with multinuclear (Figure 3.16) or very large cells (Figure 3.8F). This is a common issue when isolating blood from a mononuclear layer where multiple cell-types are present. Selective culture techniques such as; col I. coating plates, endothelial specific medium (EGM-2) and selective trypsinisation improves EC expansion[173], but some non-ECs

can persist. The enlarged cells with peripheral expression of phalloidin (Figure 3.8F) could represent senescent cells, although this would need to be further investigated. Overall, the level of contaminating cells was very low, so should have had minimal effect on results.

ECFCs have been successfully transfected with GFP by several groups[8,264,266], and for the present study stable GFP expression was achieved by lentiviral mediated transduction of pGIPz into healthy and GD-UCB-ECFC, for the purposes of long term fluorescence monitoring *in vitro* (Figure 3.17). With continuous puromycin treatment during expansion, UCB-ECFC cultures became ~80% GFP expressing. These GFP-UCB-ECFC were expanded and passaged further *in vitro*, over at least 3 passages and used in experiments, where due to their GFP expression they could be easily distinguished from hREC when grown in co-culture.

3.5.3 EXPANDED ALLOGENEIC UCB-ECFCs OFFER A POTENTIAL CELLULAR THERAPY FOR REPAIRING DAMAGED VESSELS IN EARLY STAGE DR

In order to be considered as a cellular therapy option, ECFCs need to show the capacity to incorporate into damaged EC layers in challenging environments, such as the high glucose, low oxygen environment of the retinal tissue during DR. It has been reported that ECFCs show a robust response to oxidative stress, and may in fact expand more successfully *in vitro* in low (5%) oxygen conditions[267,268], suggesting they may be a good candidate for repairing the damaged vasculature in the diabetic retina. Therefore, UCB-ECFCs in the present study were tested for their ability to withstand the *in vitro* diabetic insults optimised for the co-culture model (see section 2.3.7) (2% O_2 and 33mM glucose). UCB-ECFCs successfully grew on col I. coated glass slides in both healthy and diabetic conditions for 21 days (Figure 3.11B, Figure 3.13), retaining high cell number, confluent cobble-stone monolayer morphology and metabolic activity within a healthy range (assessed up to day 4) (Figure 3.11A), displaying no noticeable differences between healthy and diabetic conditions.

To further explore any changes in antigen expression caused by the *in vitro* diabetic conditions, UCB-ECFCs were stained with endothelial-specific, junction-specific and oxidative stress-associated antibodies after 21 days of culture (Figure 3.13). Overall, UCB-ECFCs retained their EC-specific cobblestoned morphology and expressed EC-specific markers (vWF and CD31) in both healthy and diabetic conditions, with no noticeable difference. As with mature endothelium, ECFCs expressed VE-Cad at cell junctions in both healthy and diabetic conditions, suggesting they formed a functional monolayer with the ability to control permeability[40]. There was a reduction in VEGFR-2 expression in the diabetic compared to healthy conditions by day 21 (Figure 3.13). Fadini et al. defined EPCs as CD34/CD133/VEGFR-

2 positive, and found a reduction in EPC number in patients with T2DM by 40%, and for patients with the added burden of peripheral vascular disease, EPC number were reduced 47% compared to healthy controls[156]. In a more recent review, Fadini et al. summarised 10 clinical studies that report reduced VEGFR-2+ EPC/ECFCs from patients with some form of cardiovascular risk factor[151]. These data suggest either overall ECFC number, or ECFCs expression of VEGFR-2 is reduced in diabetic and cardiovascular disease. The ECFC used in the present study were isolated from healthy donors, then subsequently subjected to a diabetic environment *in vitro*, and the IF data corroborates with the literature in that VEGFR-2 is reduced in diabetic conditions compared to healthy (Figure 3.13). This adds to the compiled evidence that these *in vitro* diabetic optimised conditions were sufficient to induce a switch to diabetic phenotype in ECFCs as well as hREC.

CD34 has long been associated with haematopoietic stem/progenitor cells but is now more widely accepted as a common marker for diverse progenitors, including vascular endothelial progenitors such as ECFCs[269]. Its function is not fully understood although it had been suggested that CD34 expression is associated with migration and adhesion, and is often found at the luminal membranes when analysed in capillary tissue, where more ECs of the small vessels were CD34 positive compared to ECs from large vessels[270]. In the present study, CD34 expression in early passage ECFCs, fixed at 2-5 days, was variable, with different expression patterns observed between the two different monoclonal antibodies used (Figure 3.7, Figure 3.8). This brought in to question the validity of the CD34 antibodies, which can be a common pitfall for researchers investigating CD34, due to the sensitivity of some CD34 antibodies to cleavage by neuraminidase and glycoprotease[271]. However, the rabbit monoclonal antibody (EP373Y- Synthetic peptide within Human CD34 a.a. 350 to the C-terminus) used in this study has been validated by Abcam and published in over 160 papers. Interestingly, passage 5 UCB-ECFCs grown on col I. coated glass expressed CD34 in the perinuclear area in healthy conditions, compared to specifically at the cell borders in diabetic conditions, by day 21 (Figure 3.13). In a recent study, CD34 expression in ECFCs was found to be an interchangeable phenotype *in vitro*, whilst VE-Cad, CD31 and VEGFR-2 remained unchanged. CD34-negative cells could re-acquire CD34 antigens, with no influence from cell culture medium except for presence of TNFα, and no influence from whether FBS was present or not[272]. Tasev et al. also report that high seeding density resulted in increased CD34 expression in ECFCs and postulate CD34 may be upregulated with increased neighbouring cell-cell contact, although they suggest this actually leads to reduced endothelial barrier function, due to the role of CD34 in destabilizing cell-cell contact in order to form a vessel

lumen. Taking this into consideration, in the present study where ECFCs were cultured for 21 days in diabetic conditions, distinct CD34 expression at the lateral borders of 100% of cells in field of view (Figure 3.13) may represent a weakened EC barrier, possibly mimicking a PDR stage where ECFCs receive signals to proliferate, due to a combination of oxidative stress and angiogenic signalling. The perinuclear expression of CD34 in healthy conditions may be due to blocked trafficking of the phosphoglycoprotein, which would normally be expressed as transmembrane.

ECFCs express higher ambient SOD-2 than mature ECs[267], similar to the results in the present study, when comparing UCB-ECFCs with retina-specific hRECs (Figure 2.10, Figure 2.16, Figure 2.17, Figure 3.13), where ECFC SOD-2 expression was higher than hREC SOD-2 expression in both healthy and diabetic conditions. In an *in vitro* study using bovine aortic ECs, hyperglycaemia increased ROS inside the cells and treatment with SOD-2 haemagglutinating virus of Japan (HVJ)-liposomes significantly reduced activation of mitochondrial pathways associated with hyperglycaemia-induced pathogenesis[273]. Therefore, if the optimised diabetic conditions were causing ROS production, SOD-2 activation should be observed when the cells activate a protective response to this insult. High basal expression of SOD-2 may explain why ECFCs are more resilient to damage from oxidative stress, making them an ideal candidate for cell therapy to repopulate areas where oxidative stress may continue to contribute to tissue damage during T2DM.

3.5.4 APB-ECFCs MAY REQUIRE FURTHER MANIPULATION *IN VITRO* TO BE USEFUL CLINICALLY

Unfortunately, after multiple attempts, using ECFCs from different donors, it was not possible to transduce GFP expression in APB- ECFCs, which would initially express GFP but then fail to proliferative after puromycin treatment. Therefore, ABP-ECFCs could not be tested for incorporation into the co-culture model because it would not have been possible to distinguish them from the hREC without the GFP expression. APB-ECFCs have been reported to possess differences in 20% of a panel of genes regulating a variety of EC function: including permeability and vessel tone, cell activation, injury response, angiogenesis, cell survival and apoptosis, when compared to UCB-ECFCs[274]. Overall, APB-ECFCs upregulate immune and thrombotic response compared to UCB-ECFCs. These genotypic differences combined with the reduced proliferative potential of APB-ECFCs *in vitro* could explain why GFP-APB-ECFCs were unable to continue expanding for multiple population doublings after lenti-viral GFP transduction and puromycin treatment.

A simple technique to test if APB-ECFCs were capable of integrating into a monolayer of mature endothelium was to label ECFCs with a fluorescent tracker (CTG) and add CTG-APB-ECFCs 48H after hREC were seeded at high or low density on TC plastic. CTG-APB-ECFCs incorporated successfully in both healthy and diabetic conditions (Figure 3.15). Ideally, for direct comparison with CTG-UCB-ECFC incorporation experiments, $2x10^4$ APB-ECFCs would have been seeded, but APB-ECFCs were much slower to expand *in vitro,* with some ECFCs expanding in size and not proliferating, which may have represented cell senescence (Figure 3.16). Therefore, numbers as close as possible to $2x10^4$ were seeded. APB-ECFCs that incorporated in to high and low density hREC in healthy and diabetic conditions were analysed 48H later for HIF1α (to assess response to diabetic (hypoxic) environment), and ZO-1 expression (to assess physical incorporation and barrier formation) (Figure 3.16). HIF1α can mediate the cellular response to low oxygen by regulating glucose uptake and shifting to anaerobic respiration, activated when HIF1α translocates from the cytoplasm to the nucleus[275]. In the present study, HIF1α remained inactive (cytoplasmic) in all conditions, however 48H at 2% oxygen may not be sufficient time to cause this activation of major cellular transcriptional adaptions, in light of the low HIF1α activity reported at 3% oxygen compared to 1% oxygen at 8H in HEK293 cells[276]. Another hypothesis is; normal HIF1α regulation of cell proliferation and migration may have been altered due to the paradox of *in vitro* 'standard cell culture normoxia (20% O_2)' compared to 'physiological normoxic conditions (~2-8%)[277]. HIF1α activity is difficult to determine using IF, due to its fast translocation from the nucleus when re-oxygenation occurs during stages of washing and fixing to prepare samples for imaging. Therefore, although HIF1α expression at the protein levels remained cytoplasmic, exploration at the transcriptional levels may reveal otherwise.

CTG-APB-ECFCs and hREC both expressed ZO-1, 4 days after hREC were seeded and 48H after APB-ECFCs were added to the monolayer, in both healthy and diabetic conditions (Figure 3.16). ZO-1 expression at cell-cell junctions was junction-specific in diabetic conditions with high density hREC, where both hREC and incorporated CTG-APB-ECFC expressed ZO-1 at the cell-cell borders, indicating the two cell-types physically incorporated to form a monolayer with TJ barrier properties. These data suggest at the early stage (day 4) both hREC and APB-ECFCs could withstand diabetic insults and in fact displayed enhanced barrier properties and proliferation compared to those grown in healthy conditions. A small number of CTG-APB-ECFCs from donor #1042 appeared to become senescent in culture (Figure 3.16red circles), corroborating reports from the literature that adult ECFCs become senescent much earlier than UCB-ECFCs[149]. Integrated CTG-APB-ECFCs from donor #322 were larger in size and some

displayed finger-like cytoplasmic projections, which may represent differentiation *in vitro* possibly to a fibroblast-like cell; considering ECFCs are human primary cells, with progenitor plasticity (Figure 3.16B). A small number of very large, multinuclear, CTG-positive cells were present amongst APB-ECFCs from donor #322, representing cells which may have dedifferentiated to an unknown multinuclear cell-type, only present in the healthy conditions, or represent a small number of contaminating cells from the selective cell culture procedure (Figure 3.16 arrow heads).

Overall, this study provided evidence that APB-ECFCs from healthy donors can physically incorporate into hREC monolayers in both healthy and diabetic conditions. However, proliferative potential and growth rate of APB-ECFCs was much lower than UCB-ECFCs. Increase in cell size and change in morphology, particularly from donor #322, cultured in healthy conditions, suggests some of the APB-ECFCs transitioned *in vitro*. These data indicated donor variability relating to expansion capability of APB-ECFCs and that current cell culture expansion protocols, which are sufficient for UCB-ECFC expansion, may require modification to prevent senescence or de-differentiation of APB-ECFCs *in vitro*, if they are to be developed as an autologous cell therapy in the future.

3.5.5 THE OPTIMISED CO-CULTURE MODEL OF THE RETINAL VASCULATURE PROVIDES A USEFUL TOOL TO ASSESS ECFC INTEGRATION INTO A MODEL OF DR

ECFCs may fail to integrate and repair the retinal microvasculature due to either impaired migration, or reduced ECFC number[156], both caused by chronic hypertension, dyslipidaemia and hyperglycaemic environment, along with persistent EC turnover as a result of long onset of T2DM[278]. In order to improve our understanding of this gradual ECFC failure, incorporation of ECFCs into animal models of diabetes and/or ischemia can be used to validate ECFC function, but with the absence of an available animal model, *in vitro* ECFC incorporation into mature EC monolayers provides proof of principle that the cell population isolated has the ability to physically incorporate, or 'repair' a simplified model of a diseased blood vessel[153,279–281]. CTG- and GFP-UCB-ECFCs successfully incorporated into high and low density hREC cultures when seeded at the same time, on both TC plastic and PET, and remained incorporated for up to 7 days (Figure 3.18). Having confirmed incorporation with hREC when the two cell-types were seeded at the same time, moving forward to better reflect the disease environment of the microvasculature during DR; where ECs become damaged and slough off[282], hREC were seeded first at high or low density on TC plastic or PET, followed by

addition of GFP-UCB-ECFCs after 48H, to analyse the ability of the ECFCs to 'fill' the gaps. At 24H and day 7, GFP-UCB-ECFCs incorporated in all conditions (Figure 3.19).

In order to confirm that the GFP-UCB-ECFCs physically incorporated with the pre-existing hREC (rather than settling on top), ZO-1, VE-Cad, VEGFR-2 and Ang-2 were analysed to explore junctional protein/barrier formation (VE-Cad and ZO-1) and angiogenic response (VEGFR-2 and Ang-2). In healthy conditions, GFP-UCB-ECFCs were present in all fields of view, proving UCB-ECFCs remained embedded within the hREC monolayer at day 7, at both low and high hREC seeding densities (Figure 3.19, Figure 3.20). GFP-UCB-ECFCs and GFP-negative hREC both expressed VE-Cad and ZO-1, confirming that the two cell-types formed functional cell-cell junctions with one another, mimicking how ECFCs may contribute to repair *in vivo*.

Both Ang-2 and VEGFR-2 are upregulated *in vivo* during diabetes, linked with the proliferative stage of DR when new vessels are formed on the retina in response to hypoxia, induced by chronic ischemia, as a result of degradation of the retinal capillaries over time[58,236,283]. In the diabetic retina, VEGFR-2 and its downstream mediators are important therapeutic targets for anti-VEFG drugs[284], to prevent uncontrolled proliferation of improperly formed, leaky blood vessels. In the present study, the cells expressing Ang-2 were GFP-negative, suggesting they were hREC rather than ECFCs, with the exception of one GFP-positive ECFC which expressed both Ang-2 and CD34 (Figure 3.20). This implies that hREC express Ang-2 more so than UCB-ECFCs, and points toward the hREC 'recruiting' ECFCs to gaps within the EC layer via secretion of pro-angiogenic Ang-2, although paradoxically, VEGFR-2 is downregulated at high hREC seeding density. GPF-UCB-ECFCs seeded on low density hREC did not express any Ang-2, although VEGFR-2 expression was upregulated (Figure 3.20). It should be noted that Ang-2 is a secreted protein, therefore, concentrations may be high within the media even if at the time of fixation this may not be reflected by levels within the cell (Figure 2.32). VEGFR-2 expression did not co-locate with GFP-UCB-ECFCs, suggesting, similar to Ang-2, it was the hREC expressing VEGFR-2 rather than the ECFCs.

Testing the ability of GFP-UCB-ECFC to incorporate into the optimised co-culture model (Chapter 2), provided an *in vitro*, simplified, and high throughput option to assess ECFC functionality rather than using an *in vivo* animal model of DR. The co-culture model aims to better mimic the *in vivo* architecture of a damaged capillary compared to traditional monoculture experiments, and therefore, provide more relevant data on whether ECFCs are a suitable candidate for allogeneic cell therapy. GFP-UCB-ECFCs integrated at day 7 in both healthy and diabetic co-culture conditions (Figure 3.21, Figure 3.22, Figure 3.24). DAPI, VE-

Cad and ZO-1 labelling and z-stack confocal microscopy confirmed that GFP-UCB-ECFCs physically incorporated with their hREC neighbours in the presence of both hREC and hRP layers. ZO-1 and VE-Cad were expressed by ECs in both healthy and diabetic co-culture conditions, however the pattern of expression was much more junction-specific in the diabetic conditions, compared to a more cytoplasmic dispersed expression in the healthy co-culture conditions. This implies the cell-cell junctions and therefore the barrier properties were improved in the diabetic rather than the healthy co-culture model at day 8, 24H after adding healthy UCB-ECFCs.

3.5.6 ECFCs FROM GD-UCB MAY OFFER A POPULATION OF CELLS RESILIENT AGAINST HYPERGLYCAEMIC INSULT

Gestational diabetes is defined as any degree of glucose intolerance with onset or first recognition during pregnancy, and the prevalence may range from 1-14% of all pregnancies[69]. Due to the sudden onset and short duration of GD compared to the prolonged onset and progression of T2DM and DR, GD likely has different effects on progenitor cell populations. Also, the different nature of the diseases means results from studies investigating pre-existing T2DM in mothers (DIP) is therefore, not directly comparable to GD. Three reviews focusing on the function of ECFCs in T2DM or DR, summarise multiple studies which report both increased and decreased ECFC number, and both increased and decreased ECFC functionality with risk factor or disease progression, highlighting the controversy surrounding the role of ECFCs in vessels repair during T2DM[151,157,285]. Regarding specifically GD, in a small study on 45 mothers with GD compared to 42 controls, ECFC numbers isolated from GD-UCB was significantly higher ($p<0.05$) than controls, which suggests altered foetal stem cell mobilisation in GD pregnancy[286]. Another group report GD-UCB-ECFCs were more proliferative than control UCB-ECFCs, but that GD-UCB-ECFCs had decreased tube-forming capacity and reached senescence earlier *in vitro*, however most interestingly the GD-UCB-ECFCs were resistant to hyperglycaemia induced senescence via no change to p38MAPK[71]. Linking pre-existing T2DM to pregnancy (DIP), in a study assessing diabetic intrauterine environment caused by mothers' diagnosis of Type I or T2DM pre-pregnancy, UCB-ECFCs displayed reduced colony formation, self-renewal capacity and tube formation *in vitro*[72]. These studies indicate GD and DIP have different effects on ECFC number, and that GD-UCB-sourced ECFCs may in fact represent an enriched ECFC source, able to withstand hyperglycaemic insult compared to healthy UCB.

In the present study, GD-UCB-ECFCs were collected from only one donor, and their ability to integrate with hREC was assessed using the same experiments as healthy UCB-ECFCs. GFP-GD-UCB-ECFCs were added to monolayers of hREC, or hREC co-cultured 1:1 with pericytes underneath to determine: 1) if GFP-GD-UCB-ECFCs could incorporate with mature hREC just as healthy UCB-ECFCs did, 2) if the presence of hRP changes the incorporation behaviour and 3) if healthy or diabetic conditions impairs GD-UCB-ECFC incorporation. When added to either mono- or co-cultures, GFP-GD-ECFCs successfully incorporated with hREC in all conditions, remaining for up to 7 days (Figure 3.23, Figure 3.24). Similar to healthy GFP-UCB-ECFCs, GFP-GD-UCB-ECFCs expressed cell junction-specific ZO-1 with their neighbouring hREC (Figure 3.24). Unfortunately the healthy co-cultures were damaged during processing so it was not possible to analyse this. Multiple passage expansion, GFP transduction, phenotype retention and successful incorporation of GD-UCB-ECFCs *in vitro* are promising results, considering general agreement in the field that ECFCs become dysfunctional or reduced in number during diabetes. In this n=1 study, GD did not appear to have the same reported detrimental effects as T2DM, although ECFCs from more GD donors need to be tested to fully validate this result.

3.6 LIMITATIONS & FUTURE WORK

To improve the power of my study, more donors, and more experimental repeats are required, however due to time constraints and the long process of ECFC isolation from human blood, data reported have provided important information regarding the ability to expand ECFCs *in vitro* and test their integration into a novel *in vitro* model of DR. In order to asses barrier function, permeability assays as well as IF staining of VE-Cad and ZO-1 would provide quantification of functionality across different experimental conditions. As observed with the hREC (Chapter 2), ECFC proliferation, junctional protein expression and metabolic activity was resilient during *in vitro* diabetic conditions and this result is a recurring output from my data (Figure 3.11, Figure 3.13, Figure 3.22). All ECFCs were expanded in physiologically healthy conditions (20% O_2 and 5.5mM glucose). However, in future studies it would be interesting to attempt to expand ECFCs in <5% O_2 from the offset, following reports that *'in vitro* hyperoxia' (20% O_2) may in fact be detrimental and also reports that stem/progenitor cells grow better in low oxygen. Similarly, it would be interesting to grow a population of ECFCs in high glucose (33mM) from the offset, to ascertain if initial expansion in healthy conditions is involved in recovery or alteration of ECFCs collected from GD or T2DM

patients, and if continual hyperglycaemic insult throughout *in vitro* expansion may provide a truer illustration of ECFC behaviour during diabetes.

3.7 CONCLUSIONS

Overall, work from this chapter covers successful isolation, stringent characterisation and expansion of healthy UCB-ECFCs, GD-UCB-ECFCs and APB-ECFCs *in vitro*, observing the highest proliferative potential and integration by the UCB-ECFCs. Therefore, UCB-ECFCs (either healthy or GD) currently show the most promise as an allogeneic cell therapy to repopulate depleted ECFCs in the retina in early stage or pre-diabetic patients. APB-ECFCs may indeed have the ability to expand and function *in vitro*, however genetic modification or manipulation of the culture environment may be necessary to prevent senescence or trans-differentiation after passaging. UCB-ECFCs grew well in the hREC-specific growing conditions and were robust in withstanding diabetic insult and long term *in vitro* culture (21 days). ECFCs from both UCB and ACB consistently expressed endothelial cell-specific markers (vWF and CD31) and successfully incorporated into mature hREC monolayers, confirming their endothelial cell-type. The paradox of consistent ECFC proliferation, incorporation and improved cell-cell junction formation in diabetic conditions (2% O_2 and 33mM glucose) may in fact represent an early stage compensation reaction, comparable to *in vivo* early stage or pre-diabetes. An alternative theory is that possibly after very long progressive onset of T2DM, ECs eventually become dysfunctional due to the hyperglycaemic environment, but rally to survive before finally succumbing to cell death. To confirm these theories, more in depth analysis of the oxidative stress, angiogenic and apoptotic molecular pathways would be required.

4 CHAPTER 4

Assessing pεK hydrogels for *in vitro* expansion of ECFCs and controlled delivery of cells into an *in vitro* model of the retinal microvasculature

4.1 OVERVIEW

ECFCs are currently expanded *in vitro* on rat tail col I. coated TC plastic. To enable ECFCs to be used in human cell therapy in the future, xeno-free or GMP-compliant conditions must be met. Due to their progenitor nature and because they are primary cells, ECFCs require specific ECM protein coatings to adhere and expand *in vitro*, without differentiation or senescence. pεK is a naturally occurring biomaterial that is non-toxic to humans and the environment. Peptide hydrogels, such as those made from pεK, can provide the chemical functionality of the col I. which is currently used, while being non-animal derived and consistently reproduced. Due to free-amine groups on the surface of pεK hydrogels or microparticles, surfaces can be further modified according to cell-specific requirements. One example is covalent binding of RGD peptide, to enhance cell attachment to the pεK surface. This chapter focuses on using pεK hydrogels to expand ECFCs and maintain their early passage phenotype. pεK microparticles either unmodified or with RGD covalently bound to the surface were assessed as a controlled delivery tool of ECFCs to the co-culture model of DR.

4.2 AIMS & OBJECTIVES

To assess the capacity of pεK for ECFC attachment, viability and expansion without differentiation, and targeted delivery of ECFCs to an *in vitro* model of diabetic retinopathy.

1. Determine if ECFCs can attach, expand and survive on pεK cross-linked with decanedioic acid gels in experimental healthy and diabetic conditions
2. Determine if pεK microparticles can be used to delivery ECFCs to the endothelial layer of an *in vitro* co-culture model of DR

4.3 METHODS

4.3.1 PRODUCTION OF pεK GELS

Hydrogels were made using poly-ε-lysine, cross-linked 60% with decanedioic (sebasic) acid. Compounds used to make hydrogels were as follows: poly-ε-lysine (pεK) *(Bainafo- Zhengzhou Bainafo Bioengineering Co. Ltd. (supplied by Spheritech))*, sebacic acid 98+% *(A14158, Alfa Aesar)*, 1-(3-Dimethylaminopropyl)-3-ethylcarbodiimide HCl (EDCI) (*FD05800, Carbosynth)*, 4-Methylmorpholine Reagentplus 99% (NMM) *(Sigma, M56557-500ML)* and N-hydroxysuccinimide (NHS) *(Sigma, 130672-100G)*. Gels of 1g/ml pεK and 1.33g/ml pεK were cast on 100mm dishes, at RT, using the compounds and amounts outlined in Table 4.1. pεK gel components were measured and prepared in 2 separate tubes.

Table 4.1. REAGENTS AND AMOUNTS REQUIRED TO CAST PεK GELS

60% Cross-linked with Decanedioic acid Gels

	5ml total volume for 1x 100mm dish					
	PεK (g)	**di-acid (g)**	**NMM (ul)**	**Tween (ul)**	**NHS (g)**	**EDC (g)**
Se 60% 0.1g/ml	0.49	0.174	315	50	0.165	0.826
Se 60% 0.13g/ml	0.66	0.232	420	50	0.22	1.101
	tube 1- in total 2.5ml ddH_2O				**tube 2 – in total 2.5ml ddH_2O**	

pεK and decanedioic acid with added NMM were fully dissolved in two separate containers in 1ml ddH_2O each, on a rolling platform. These solutions were then mixed, and Tween added, to make the solution in container 1. NHS and EDC were solubilised at the very last moment; 1ml ddH_2O was added to NHS in 7ml bijou tube, and 1.5ml dH_2O was added to EDC in a separate bijou tube, and both vortexed for ~30 seconds until fully dissolved, then NHS and EDC were combined in container 2, then quickly mixed with container 1. Total volume of components was topped up to 5ml. Solution was inverted 10 times to ensure mixing, then solution was poured into 100mm dish on level surface and left with lid off at RT, for gel to set overnight.

Once set, gels were washed 5x with ddH_2O, to remove debris and to fully rehydrate gels. Gels were then UV sterilised for 5 mins at 1,500v on each side. Gels were further sterilised in 70% ethanol for 1H. Gels were washed 3x 5 mins in sterile PBS to remove ethanol. Gels were punched using 0.9m diameter tool to produce gel discs to fit into the bottom of the wells of

24 w/p (Figure 4.1). Gel discs were washed in sterile dPBS to remove any remaining debris, then carefully transferred to 24 w/p using sterile, blunt ended tweezers, in a class II hood. Sterile dPBS was added to each well with each pεK gel disc, to keep gels hydrated until ECFCs were added (ideally same day).

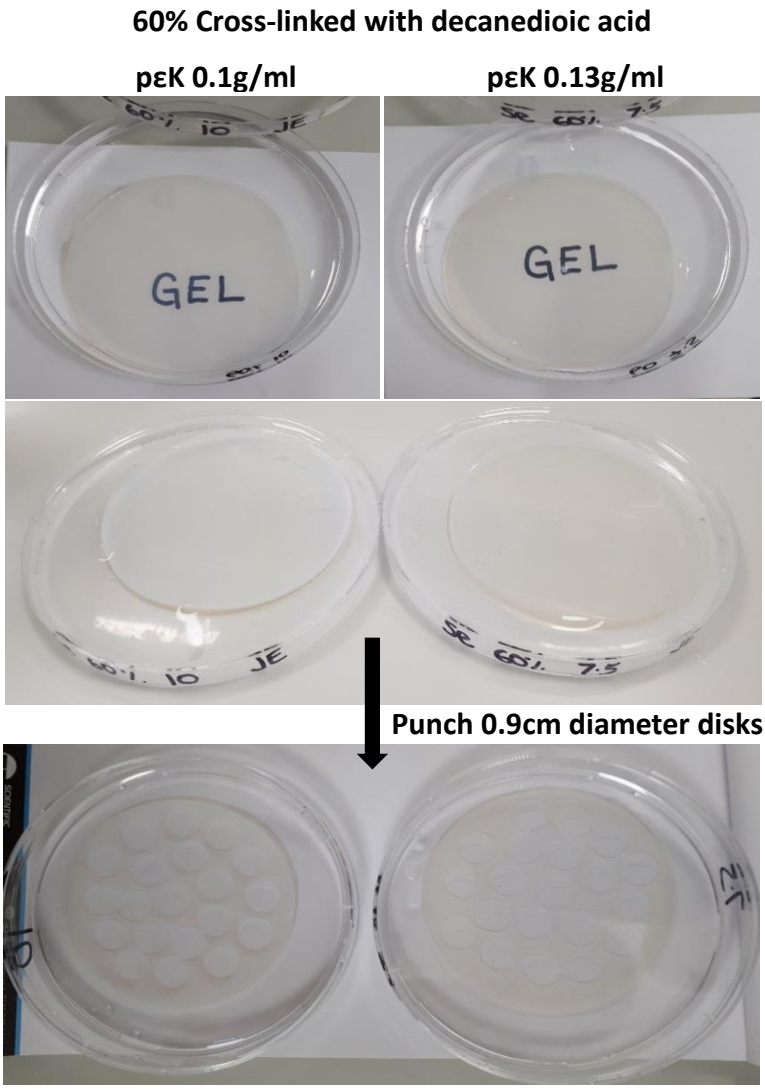

Figure 4.1. Casting and punching of pεK gels into 0.9cm diameter disks

5ml of pεK gel ingredients were poured into 100mm diameter dishes, and set as flat gels overnight. A 0.9cm diameter punch was used to make pεK gel disks that would fit into the bottom of the wells of a 24 w/p. 'GEL' text written on paper underneath the gels made from different concentrations of pεK highlight the transparency of the material.

4.3.2 SEEDING ECFCs ON TO pεK GELS

ECFCs were subcultured (as described in section 3.3.3) and prepared to seed on gel discs in 24 w/p's at $5x10^4$ cells/well, in 500µl/well EGM-2 with 10% FBS, 5.5mM glucose and normal incubator conditions. To prevent gels floating when ECFCs in media were added, cell-media solution was gently added drop by drop, directly on top of the gel discs, with the aim of directing ECFCs to seed on the top of the gel, as opposed to the underside, or the TC plastic if gels floated upon agitation. Cells were left to grow in normal conditions for 48H, before being moved to either healthy or diabetic conditions.

4.3.3 IMAGING CELLS ON pεK GELS

pεK gels of 1g/ml and 1.33g/ml both had sufficient transparency for light microscopy imaging, enabling monitoring of cells growing on the surface over time. For IF imaging, all solutions were very gently added to ECFCs on the pεK gel disks, and gel disks were handled very gently with rounded tweezers, to prevent ECFCs from peeling off the gel during processing. Cell culture medium was removed and cells on pεK gels were gently washed using warm sterile dPBS 3x for 5 mins. 10% NBF was added for 9 minutes, at RT, to fix ECFCs. NBF was removed and cells were washed 3x 5 mins in dPBS. 0.5% Triton-X in PBS was added for 4 mins at RT to permeabilise cells. Cells were then washed 3x 5 mins with dPBS. 5% normal goat serum (NGS) in dPBS was added to cells for 1H at RT to block non-specific binding sites. NGS was removed and primary antibodies, diluted to optimised working concentration in dPBS (Table 2.4Table 3.1), were added to cells and left to bind overnight at 4°C in the dark. The next day, 3x 5 mins 0.1% Tween-20 in dPBS washes at RT removed any unbound primary antibody. Secondary antibodies (Table 2.2), were added at 5µg/ml in dPBS for 45 mins at RT in the dark. Cells were washed 3x 5 mins in 0.1% Tween-20 in dPBS at RT, in the dark, to remove any unbound secondary antibody. 300 nM of DAPI in dPBS was added for 20 mins at RT. 2x 5 mins washes with 0.1% Tween-20 in dPBS, and final 10 min wash were performed to remove any unbound DAPI, due to strong retention of DAPI in the pεK gels. 1x 5 min dPBS wash removed any remnants of Tween-20. 1x 2 min ddH_2O wash removed any salt crystals from the surface of the cells and gels. Gel disks were then gently lifted out of 24 well plates using curved tweezers, and placed on to glass slides. Mounting media was dropped on top of the gel disk and a cover slip was placed on top, with gentle pressure. Due to the thickness of the gel disks, cover slips did not seal tight against glass slide, so confocal imaging was performed with particular care, to prevent movement which may cause cells to peel off, or gel tearing. ECFCs stained with IF antibodies were imaged using the Zeiss M800 confocal microscope.

4.3.4 PRODUCTION OF pεK MICROPARTICLES

PεK microparticles were manufactured and provided by Andrew Gallagher from SpheriTech. Briefly, 0.286g/ml pεK was cross-linked 50% with decanedioic acid, using the protocol described above for preparing gels, (4.3.1), and formed into microparticles via emulsification polymerisation. Beads were provided at 4 size ranges (Figure 4.2): 1mm-500µm (18-30-2), 500-250µm (18-30-3), 250-150µm (18-30-4) and <150µm (18-30-5). The beads had amine functionality, with a loading capacity of 3mmol/g. For use unmodified, 0.04g of beads were weighed dry into a 7ml bijou for washes. Microparticles were left overnight in 5ml of 70% ethanol, on a rolling platform, to sterilise. The next morning, tubes were stood upright to allow microparticles to sink to the bottom, then ethanol was gently removed. 3x 10 min sterile dPBS washes were performed in a class II hood to remove remnants of ethanol. A final wash was performed in serum-free, phenol red-free EGM-2 medium, at 37°C. Microparticles could be left in medium for several hours if there was any delay in adding cells. Otherwise, beads were immediately transferred to 24-well suspension plates (*Merck, M9312-100EA*). Use of suspension plates prevented preferential attachment of ECFCs to TC treated plastic, rather than the surface of the microparticles. To optimise ECFC viability on pεK microparticles, ECFC attachment and survival was tested on both unmodified microparticles and with ~10% RGD peptide covalently attached to surface amine groups.

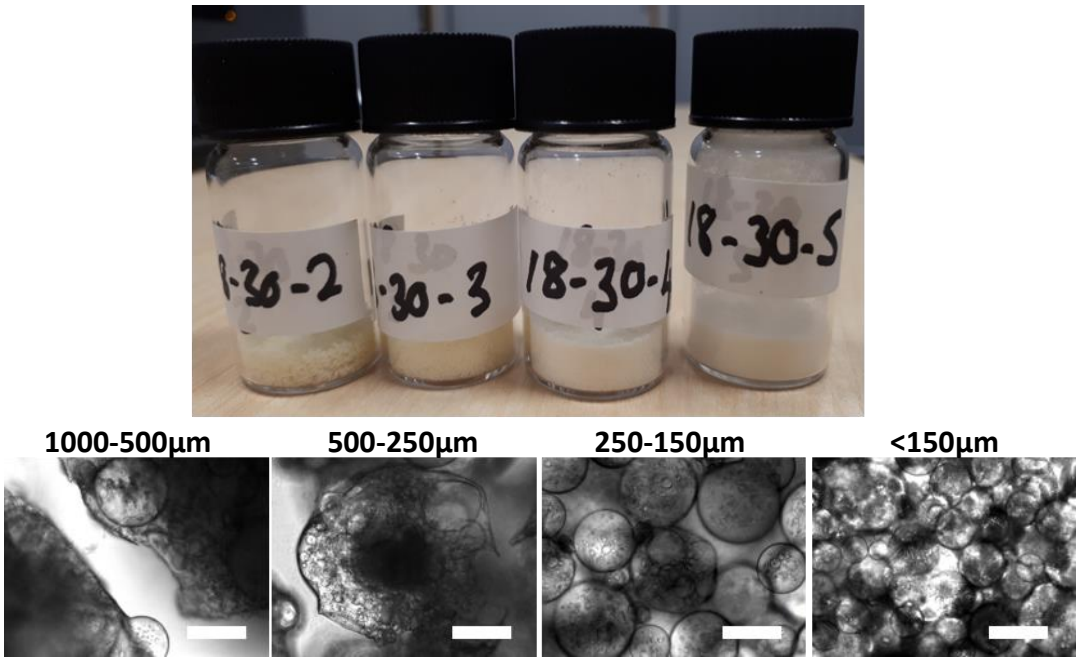

Figure 4.2. pεK gel microparticles of four size ranges supplied by SpheriTech

pεK gel microparticles were formed by emulsification polymerisation and supplied in four size ranges Images were captured using the Nikon E-Ti microscope, x20 magnification. Scale bars= 100µm.

4.3.5 RGD PEPTIDE BINDING TO pεK MICROPARTICLES

Arg-Gly-Asp (RGD) peptide was synthesised by SpheriTech and provided in powder form. For RGD binding, microparticle sizes 500-250µm (18-20-3) and 250-150µm (18-20-4) were used. 0.04g dry microparticles were added to a 7ml bijou. This weight was optimised for microparticles to fully cover the bottom of a 24 w/p, in a single layer. The calculation of how much RGD to add to 3x full wells of 18-20-3 microparticles and 3x wells of 18-20-4 microparticles is found in Figure 4.3. Before binding RGD peptide, microparticles were washed in bijou tubes with 10% NMM in ddH_2O 3x 10 mins, on a roller. Microparticles were then washed 3x10 mins in ddH_2O on a roller, with final wash having bijou tubes standing upright. To covalently bind RGD to ~10% of the surface of the pεK microparticles, RGD peptide was added to microparticles at 250µl/well volume in a 0.25M solution of NHS (0.0287g/ml) and EDCI (0.048g/ml) in water. Microparticles were left on a rocking platform at RT with RGD binding solution, for 1H. Microparticles were then washed 3x5 mins in sterile PBS, in a Class II hood, then left on a roller at RT in sterile PBS for an overnight wash.

4.3.6 ADDING ECFCs TO pεK MICROPARTICLES

Before adding ECFCs, microparticles were transferred to a 24-well suspension plate (1 bijou tube to 1 well) using a sterile scooper, and washed briefly in serum-free phenol red-free EGM-2. When adding ECFCs to microparticles, phenol red-free EGM-2 with 10% FBS medium was used. If phenol was present, red colour was taken up by microparticles, making light microscopy difficult. In a Class II hood, microparticles with or without covalently bound RGD peptide were scooped out of the bijou tube using a sterile scoop tool, into 24-well suspension plates, enough to fully cover the bottom of the well, avoiding layering of microparticles. Once hydrated, microparticles became aggregated to each other when trying to use various sized gauge needles to move the microparticles (Figure 4.4). Microparticles of the two smaller sizes (18-30-4 and 18-30-5) could fit though a 21G needle, but size 18-30-3 and 18-30-2 were too large when hydrated to fit through an 18G needle. Therefore, sterile metal scoops were used for transferring beads from container to well.

RGD Calculation

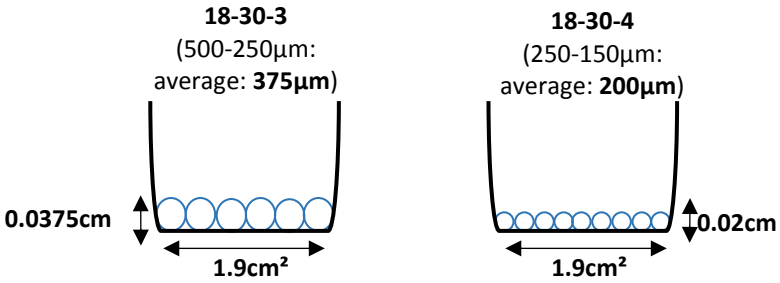

$\pi r^2 h$

1. **18-30-3:** (3.14 x 0.95^2 x 0.0375) x3 (for 3 wells) =**318.9µl volume**
   18-30-4: (3.14 x 0.95^2 x 0.02) x3 (for 3 wells) = **170.1µl volume**

pεK in beads = 0.286g/ml

2. **18-30-3:** 0.286g x 0.3189ml = **0.091g pεK**
   18-30-4: 0.286g x 0.1701ml = **0.049g pεK**

Capacity = 3mmol/g

3. **18-30-3:** 1/0.091g = dilution factor of **11** ∴ 3/11 = **0.273mM** for 100% RGD binding
   18-30-4: 1/0.049g = dilution factor of **20.4** ∴ 3/20.4 = **0.147mM** for 100% RGD binding

Want 10% RGD binding

4. **18-30-3:** 0.273mM/10 **= 0.027mM** for 10% RGD binding
   18-30-4: 0.147mM/10 **= 0.014mM** for 10% RGD binding

RGD: Mw=784g/mol
g= moles x Mw

5. **18-30-3: $2.7x10^{-5}$** moles x 784 **= $2.12x10^{-2}$g** = **21.17mg** RGD
   18-30-4: $1.47x10^{-5}$ moles x 784 **= $1.15x10^{-2}$g** = **11.52mg** RGD

RGD 0.1mg/µl stock in PBS

6. **18-30-3: 211.7µl** of 0.1mg/µl stock
   18-30-4: 115.5µl of 0.1mg/µl stock

Figure 4.3. How to calculate how much RGD to add to pεK microparticles

This flow diagram demonstrates how the calculation steps required to achieve 10% RGD peptide covalent binding to amine functional groups on the surface of the pεK microparticles. Previous work by SpheriTech found 10% RGD surface binding improved call attachment (unpublished data), so 10% RGD binding was the target in the present study.

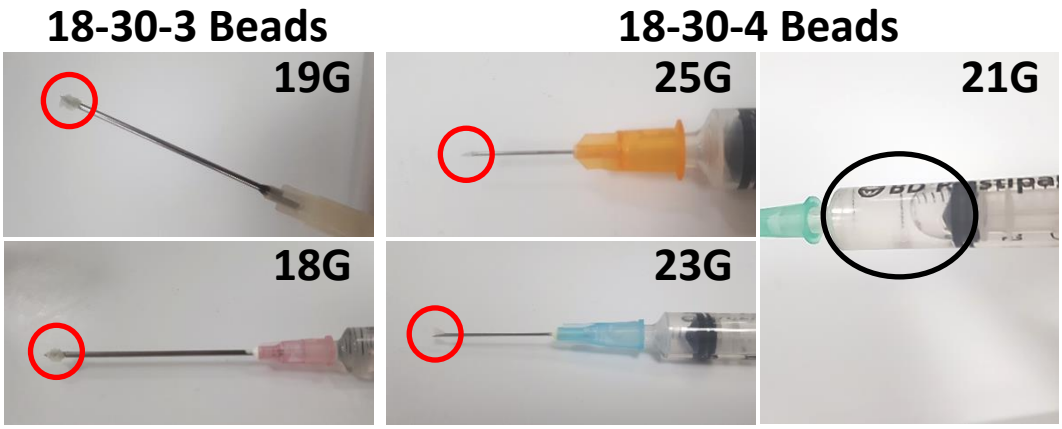

Figure 4.4. Needles of various sizes were assessed for transferring microparticles

Testing ability to transfer hydrated pεK microparticles using various gauge needles and syringe sizes. 21G enabled some 18-30-4 beads to enter syringe. Red circles highlight where hydrated microparticles have aggregated at the tip of 25-19G needles and did not pass through, and the black circle highlights where 250-150µm microparticles passed through a 21G needle into the syringe.

4.3.7 ADDITION OF ECFC LADEN pεK MICROPARTICLES TO MONO/CO-CULTURE MODELS

Once GFP-ECFCs were added to microparticles and left to attach overnight in a 24 well-suspension plate, ECFC-laden microparticles were scooped out of the 24 w/p and added 1:3 into the apical side of the transwell membranes, with the aim of achieving roughly a single layer of cell-laden microparticles across the top of the hREC. When ECFCs were added, hREC had been grown in either healthy or diabetic conditions for 7 days, with or without hRP on the underside of the PET membrane, seeded at a 1:1 ratio. The apical side of the transwell was topped up with MV with 5% FBS medium to 200µl total volume. 24H after addition of ECFC-laden microparticles, microparticles were gently washed away by inverting the transwell, and adding dPBS drop by drop until the microparticles spilled out into a separate dish. Microparticles were then washed, fixed and processed for IF imaging. For analysis of transfer of GFP-ECFCs from microparticles onto the hREC layer, PET membranes were fixed and processed for IF imaging, to confirm the presence of GFP positive cells integrated into the hREC layer.

4.3.8 IMAGING ECFCs ON pεK MICROPARTICLES

To test the capability of imaging CTG-ECFCs and GFP-ECFCs on the microparticles, z-stack imaging was performed using the Zeiss Apotome microscope for live cell analysis. For end point analysis, cells on microparticles were fixed and permeabilised using 10 % NBF and Triton-X, and labelled using phalloidin and DAPI staining (see section 2.3.4). Minor changes

to the protocol included gentle washes and removing cell supernatant very carefully to avoid aspirating the smaller sized microparticles. For confocal analysis of fixed ECFCs on microparticles, once stained, microparticles were gently aspirated with a 1000µl siliconized tip (*DAIGGER, EF19615*) with the end modified to make it wider, and slowly dropped onto a glass slide. PBS supernatant quickly evaporated and another volume of microparticles were gently dropped onto the glass slide. Once sufficient amount of cell-laden beads were on the glass slide, beads were covered in mounting medium and a cover slip was placed on top, with very gentle pressure. Cove slips did not make contact with the glass slide underneath due to microparticles diameter, so imaging was performed very gently, to avoid crushing of the microparticles between the glass.

4.4 RESULTS

4.4.1 UCB-ECFCs MAINTAINED THEIR PHENOTYPE IN LONG TERM CULTURE ON pεK HYDROGELS IN HEALTHY AND DIABETIC CONDITIONS

UCB-ECFCs seeded onto TC plastic coated with col I. or unmodified pεK gels, adhered to all surfaces and expanded for up to 21 days. At experimental day 0 (48H after seeding), ECFCs on TC plastic or pεK gels were moved to healthy or diabetic conditions. At experimental time point 0, the ECFCs seeded on col I. coated TC plastic formed a confluent layer, whereas very few ECFCs were observed on the 0.1g/ml or 0.13g/ml pεK gels (Figure 4.5, D0). At experimental day 7, in healthy conditions, some ECFCs had expanded in size on the col I. coated TC plastic (Figure 4.5, black arrow), whereas ECFCs grown at 2% oxygen on the col I. coated TC plastic (Figure 4.6) retained the same cobblestone morphology up to experimental time point 21. By day 7 in healthy (20% O_2, 5.5mM glucose), hypoxic (2% O_2, 5.5mM glucose) or diabetic (2% O_2, 33mM glucose) conditions, ECFCs on the 0.1g/ml or 0.13g/ml pεK gels had expanded in number and formed a monolayer, comparable to ECFCs grown on col I. coated TC plastic at the same time point (Figure 4.5, Figure 4.6). Therefore, although initially fewer ECFCs appeared to adhere to the pεK gels, by day 7, ECFCs formed a confluent monolayer on all surfaces tested, in healthy, low oxygen and diabetic culture conditions. By day 21, ECFCs on pεK gels appeared to retain a more homogenous cell size and shape (cobblestone)(Figure 4.5 D21), particularly in low oxygen (Figure 4.6 D21) compared to those grown of col I. coated TC plastic, which suggests pεK gels may have desirable properties to enable ECFC expansion whilst retaining their progenitor phenotype.

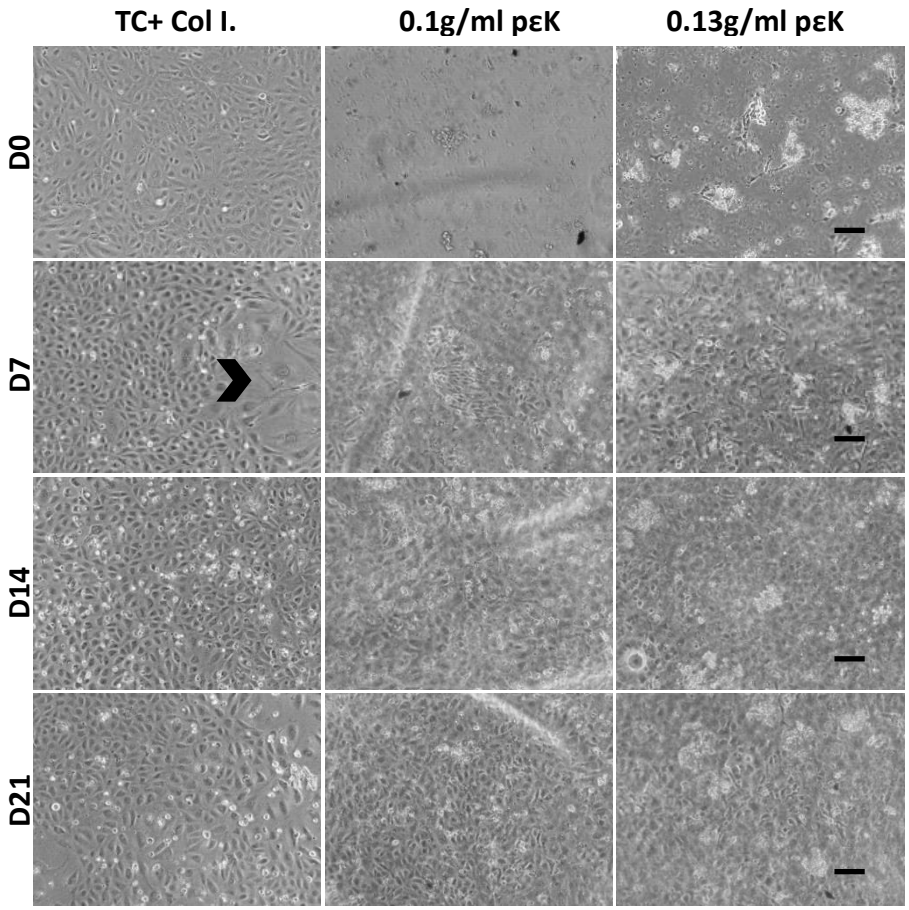

Figure 4.5. UCB-ECFCs adhered and expanded on col I. coated TC plastic and both pεK hydrogels in healthy conditions for up to 21 days

UCB-ECFCs, P5 were grown on: TC plastic coated with collagen I (left panel), 0.1g/ml pεK gel (middle) or 0.133g/ml pεK gel (right) and pictures were captured at experimental days 0, 7, 14 and 21, all in healthy conditions (20% oxygen and 5.5mM glucose). Arrowheads indicate enlarged cells, possibly a mature or senescent EC phenotype. Phase contrast images were captured on The Nikon DIAPHOT microscope, using x10 objective. Scale bars= 200µm.

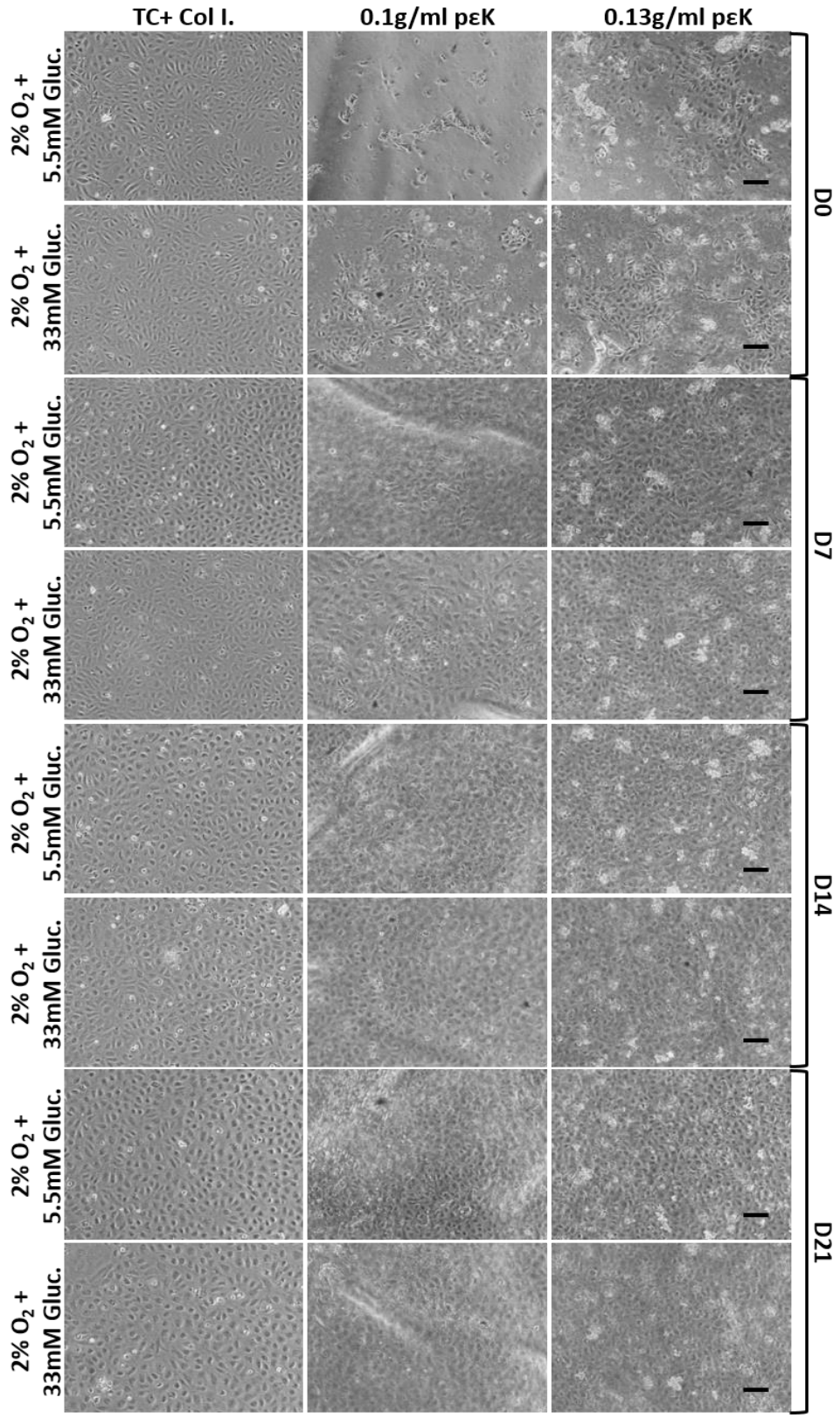

Figure 4.6. UCB-ECFCs adhered and expanded on col I. coated TC plastic and both pεK hydrogels in hypoxic and diabetic conditions for up to 21 days

UCB-ECFCs, P5 were grown on: col I. coated TC plastic (left panel), 0.1g/ml pεK gel (middle) or 0.133g/ml pεK gel (right) and pictures were captured at experimental days 0, 7, 14 and 21, all in 2% oxygen and either 5.5mM or 33mM glucose. Phase contrast images were captured on The Nikon DIAPHOT microscope, using x10 objective. Scale bars= 200µm.

4.4.2 ECFCS GROWN ON COL I. COATED TC PLASTIC SHOWED SIGNS OF DIFFERENTIATION OR SENESCENCE AT DAY 14

IF imaging was performed at day 14, on UCB-ECFCs grown on col I. coated TC plastic and 0.1g/ml or 0.13g/ml pεK gels, to investigate differences in expression of junctional proteins, angiogenic response and oxidative stress response. At day 14, ECFCs grown on col I. coated TC plastic in healthy conditions all expressed CD31 and CD34 at cell-cell junctions suggesting the cells have formed a tightly packed monolayer (Figure 4.7). Ang-2 expression was confined to a small number of cells. Overall, across the wells, ECFCs appeared similar in size and shape although arrow heads indicate where two ECFCs have enlarged nuclei, suggesting the possibility of de-differentiation or cell senescence.

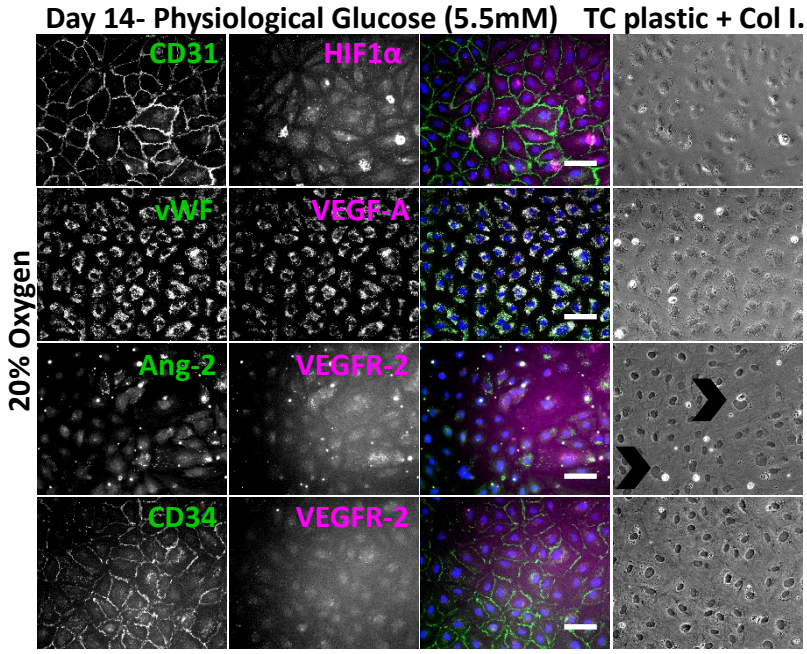

Figure 4.7. UCB-ECFCs adhered and expanded on col I. coated TC plastic with a small number of cells becoming senescent or differentiating by day 14

UCB-ECFCs, P5 were seeded at $5x10^4$ ECFCs/well in a 24 w/p on col I. coated TC plastic. ECFCs were culture in EGM with 10% FBS, in healthy conditions (20% oxygen, 5.5mM glucose) with the media changed every 48-72H. On day 14 cells were fixed and stained for IF analysis of proteins involved in junctional protein formation and angiogenic response. Black arrowheads show some enlarged ECFCs, which may have differentiated or become senescent on the col I. coated TC plastic. Images were captured using the Nikon E-Ti fluorescence microscope, x20 magnification. Scale bars= 100µm.

4.4.3 UCB-ECFCS CULTURED ON pεK GELS HYDROGELS RETAINED THEIR PHENOTYPE AT DAY 14

IF imaging was performed at day 14, on UCB-ECFCs grown on 0.1g/ml and 0.133g/ml pεK gels (Figure 4.8, Figure 4.9) and expression of a panel of proteins was compared to ECFCs grown in the same conditions on col I. coated TC plastic (Figure 4.7). x10 magnification images provided gross morphology information on ECFCs on 0.1g/ml pεK gels. The x10 panels highlight some of the issues associated with the washing and handling procedure for IF analysis of the ECFC monolayers on pεK gels, such as; auto-fluorescence of the pεK gel (CD31 panel and no secondary control), lifting of the ECFC layer (ZO-1 panel), the gel not flat mounting which creates a shadow or wrinkle (CD34 panel), cell layer tearing off (VE-Cad panel) or cell loss (vWF and Ang-2 panel) (Figure 4.8). Images on the right at x40 magnification showed that ECFCs grown on 0.1g/ml and 0.133g/ml pεK gels expressed CD31 and VE-Cad at cell-cell junctions, suggesting a monolayer with barrier function. ECFCs expressed vWF on both pεK hydrogels, confirming endothelial phenotype. ECFCs expressed SOD-2 in healthy conditions on 0.1g/ml and 0.133g/ml pεK gels after 14 days. ECFCs on both gels expressed CD34 at the lateral cell border. Surprisingly, ECFC did not express ZO-1 on either of the pεK gels after 14 days (data not shown). Overall, there was no difference in expression of the panel of proteins of interest between ECFCs grown on 0.1g/ml or 0.133g/ml pεK gels. ECFCs appeared to retain their phenotype when grown in healthy conditions on pεK gels for 14 days.

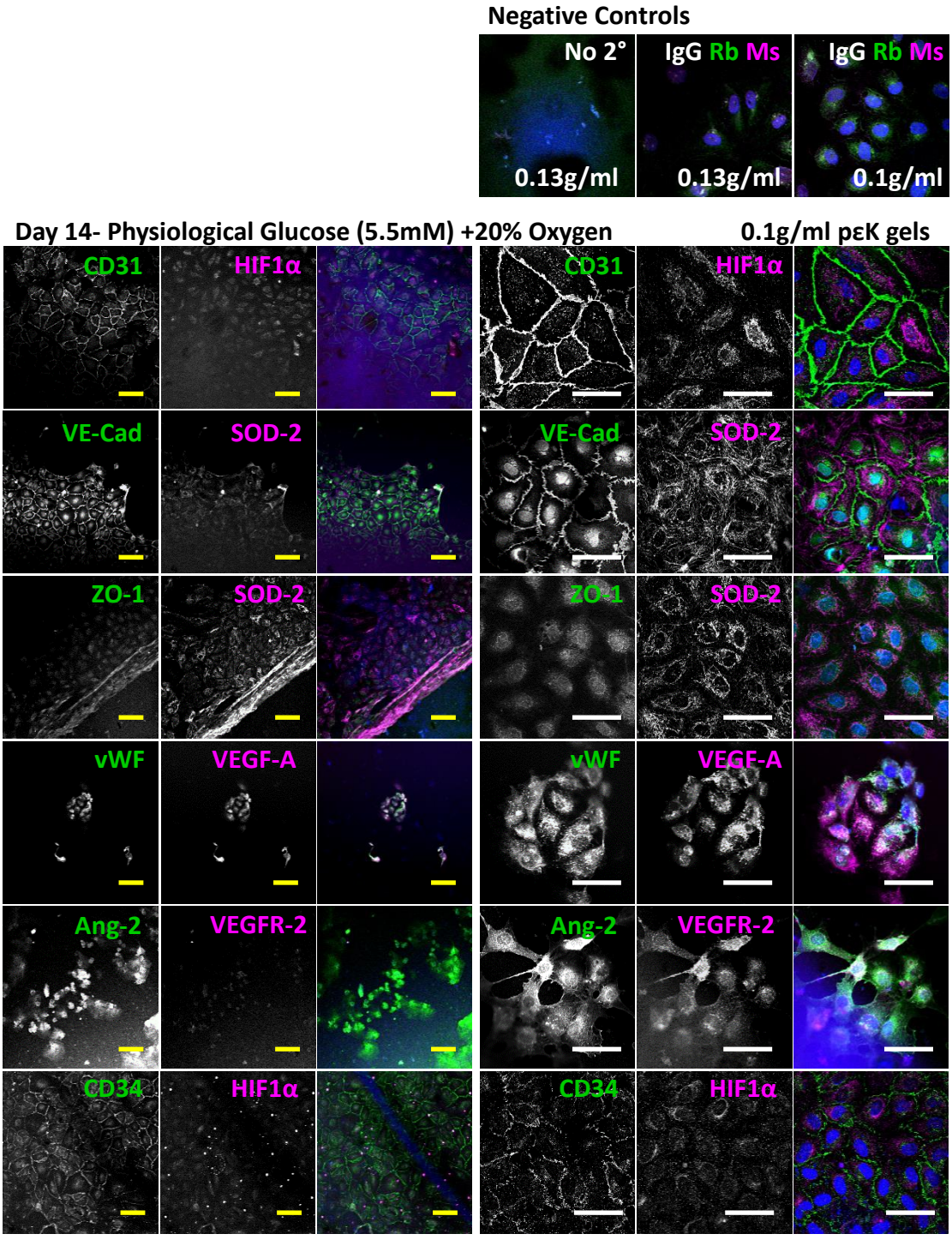

Figure 4.8. UCB-ECFCs retained their phenotype when cultured on 0.1g/ml pεK hydrogels in healthy conditions for 14 days

UCB-ECFCs, P5 were gently seeded at $5x10^4$ ECFCs/well in a 24 w/p with the pεK gel disk on the bottom. ECFCs were culture in phenol red-free EGM-2 with 10% FBS, in healthy conditions (20% oxygen, 5.5mM glucose) with the media changed every 48-72H. On day 14 cells were fixed and stained for IF analysis of proteins involved in junctional protein formation and angiogenic response. The no secondary negative control highlights the issue of auto-fluorescence, particularly in the blue channel, and IgG Isotype controls are used to show non-specific staining. Images were captured using the Zeiss M800 confocal microscope, x10 or x40 oil magnification. Yellow scale bars= 100µm, white scale bars= 50µm.

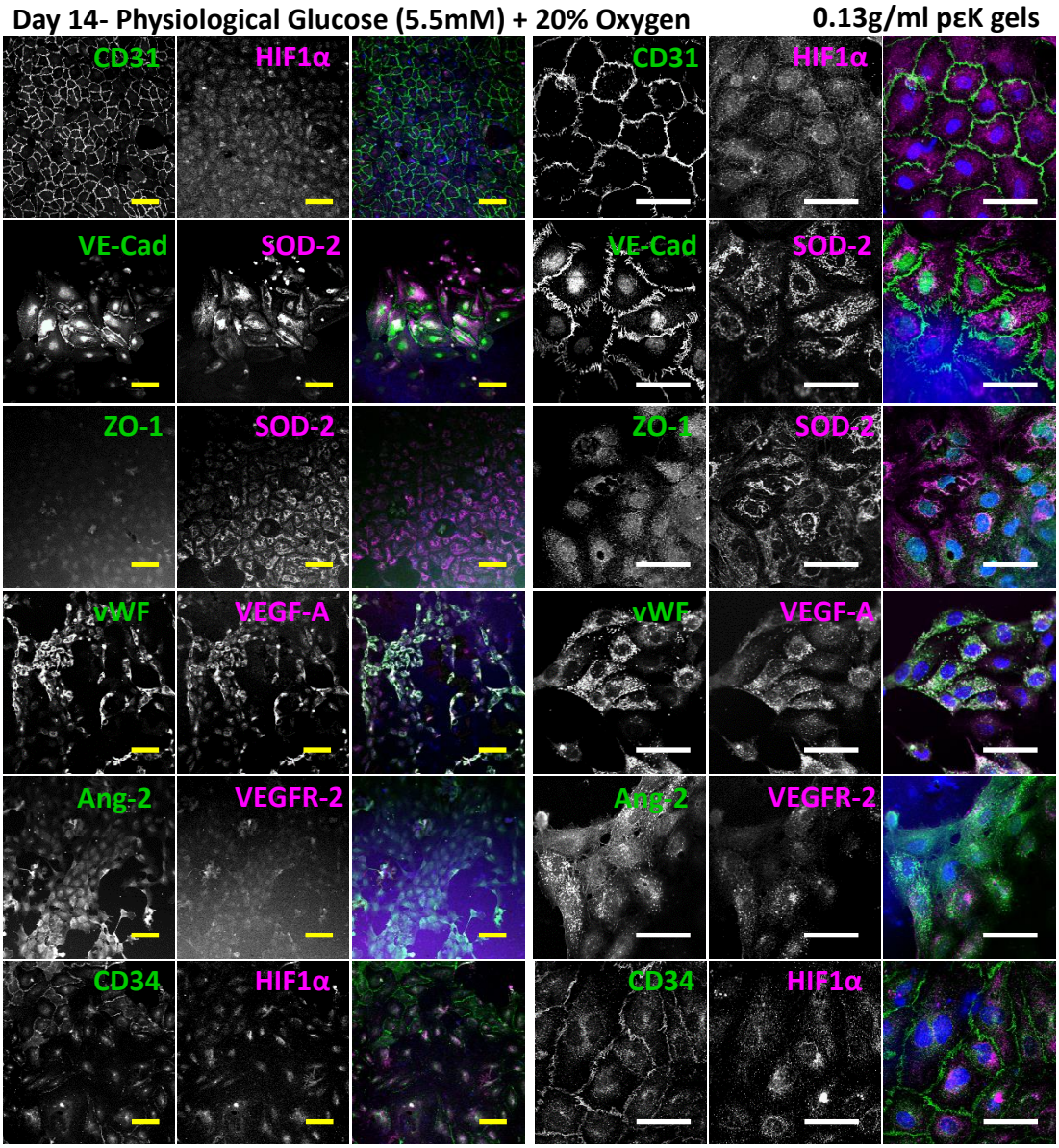

Figure 4.9. UCB-ECFCs retained their phenotype when cultured on 0.13g/ml pεK hydrogels in healthy conditions for 14 days

UCB-ECFCs, P5 were gently seeded at $5x10^4$ ECFCs/well in a 24 w/p with the pεK gel disk on the bottom. ECFCs were culture in phenol red-free EGM-2 with 10% FBS, in healthy conditions (20% oxygen, 5.5mM glucose) with the media changed every 48-72H. On day 14 cells were fixed and stained for IF analysis of proteins involved in junctional protein formation and angiogenic response. Images were captured using the Zeiss M800 confocal microscope, x10 or x40 oil magnification. Yellow scale bars= 100µm, white scale bars= 50µm.

4.4.4 UCB-ECFCs NO LONGER EXPRESSED CD34 AND CD31 EXPRESSION BECAME HETEROGENEOUS WHEN CULTURED ON COL I. COATED TC PLASTIC FOR 21 DAYS

IF imaging was performed at day 21, on UCB-ECFC grown on col I. coated TC plastic and 0.1g/ml or 0.13g/ml pεK gels, with the same proteins of interest as day 14 (Figure 4.7, Figure 4.8, Figure 4.9). ECFCs formed a confluent monolayer when grown on col I. coated TC plastic in either heathy conditions, hypoxia (2% oxygen), or diabetic conditions for 21 days (Figure 4.10). ECFCs retained the morphology and cell number comparable to day 14 (Figure 4.7), showing robustness during long term culture. In healthy conditions, approximately half of the ECFC grown on col I. coated TC plastic did not express CD31, whereas ECFCs grown in low oxygen conditions all expressed CD31 at day 21. SOD-2 expression followed the same pattern as the 50% expression of CD31 in ECFCs grown on col I. coated TC plastic in healthy conditions, suggesting a heterogeneous cell population by day 21. In healthy conditions, ECFCs on col I. coated TC plastic did not express CD34, when compared to day 14 (Figure 4.7), and Ang-2 expression could only be detected on a small number of ECFCs (Figure 4.10, green arrow heads). Ang-2 expression was increased when ECFCs were grown in low oxygen conditions with both physiological and diabetic glucose levels. When comparing ECFCs grown in 2% oxygen in either physiological or diabetic glucose levels for 21 days on col I. coated TC plastic, HIF1α expression appeared different, with HIF1α having translocated to the perinuclear compartment in high glucose, whereas HIF1α remained dispersed across the cytoplasm of ECFCs in 2% oxygen with 5.5mM glucose.

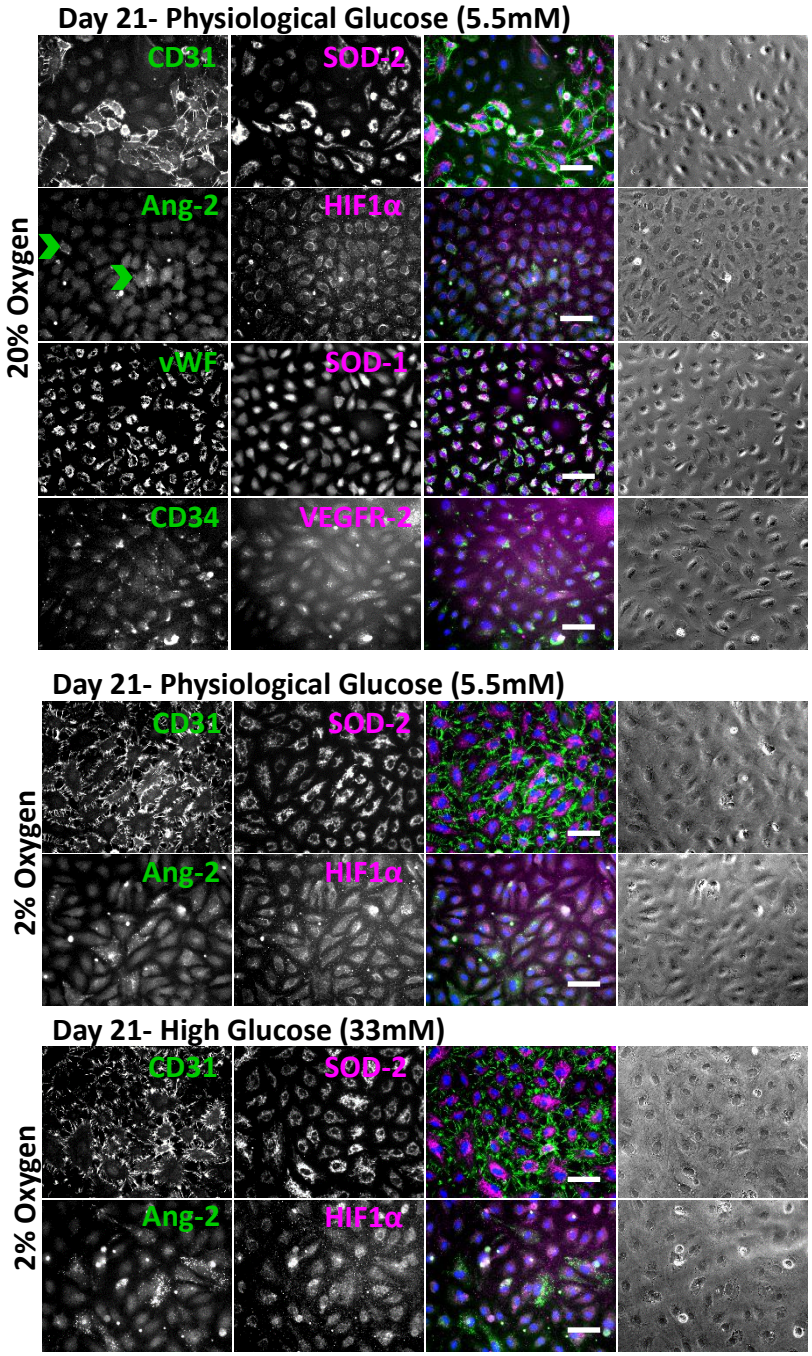

Figure 4.10. By day 21 on col I. coated TC plastic UCB-ECFCs became a heterogeneous population in healthy conditions

UCB-ECFCs, P5 were seeded at $5x10^4$ ECFCs/well in a 24 w/p on col I. coated TC plastic. ECFCs were culture in EGM with 10% FBS, in healthy conditions (20% oxygen, 5.5mM glucose), low hypoxic conditions (2% oxygen) or diabetic conditions (2% oxygen and 33mM glucose), with the media changed every 48-72H. On day 21 cells were fixed and stained for IF analysis of proteins involved in junctional protein formation, oxidative stress angiogenic response. Green arrowheads show some Ang-2 positive ECFCs within the healthy conditions. Images were captured using the Nikon E-Ti fluorescence microscope, x20 magnification. Scale bars= 100µm.

4.4.5 UCB-ECFCs RETAINED A HOMOGENEOUS EC-SPECIFIC PHENOTYPE WITH TJS AND ADHERENS JUNCTIONS ON pεK HYDROGELS IN HEALTHY CONDITIONS FOR 21 DAYS

UCB-ECFCs survived for up to 21 days when grown on 0.1g/ml or 0.13g/ml pεK gels in healthy, hypoxic and diabetic conditions. In all conditions, ECFCs remained on the pεK gels as monolayers, retaining their original cell morphology (Figure 4.11, Figure 4.12, Figure 4.13). ECFCs grown on 0.1g/ml or 0.13g/ml pεK gels in healthy conditions for 21 days, all expressed CD31, VE-Cad and ZO-1, confirming TJs, adherens junctions, EC-phenotype, and a homogenous cell population, which differed to the heterogeneous ECFC population when grown on col I. coated TC plastic for 21 days (Figure 4.11, Figure 4.12, Figure 4.13). ECFCs expressed ZO-1 at day 21, but not at day 14 when grown on 0.1g/ml or 0.13g/ml pεK gels in healthy conditions (Figure 4.8, Figure 4.9, Figure 4.11, Figure 4.12). ECFCs grown on 0.1g/ml or 0.13g/ml pεK gels expressed vWF, confirming EC-phenotype. All ECFCs on pεK gels expressed SOD-2, with no noticeable difference between those grown in healthy or 2% oxygen conditions for 21 days (Figure 4.11, Figure 4.12, Figure 4.13). Ang-2 expression was difficult to determine when imaging ECFCs on pεK gels, therefore no conclusions could be drawn.

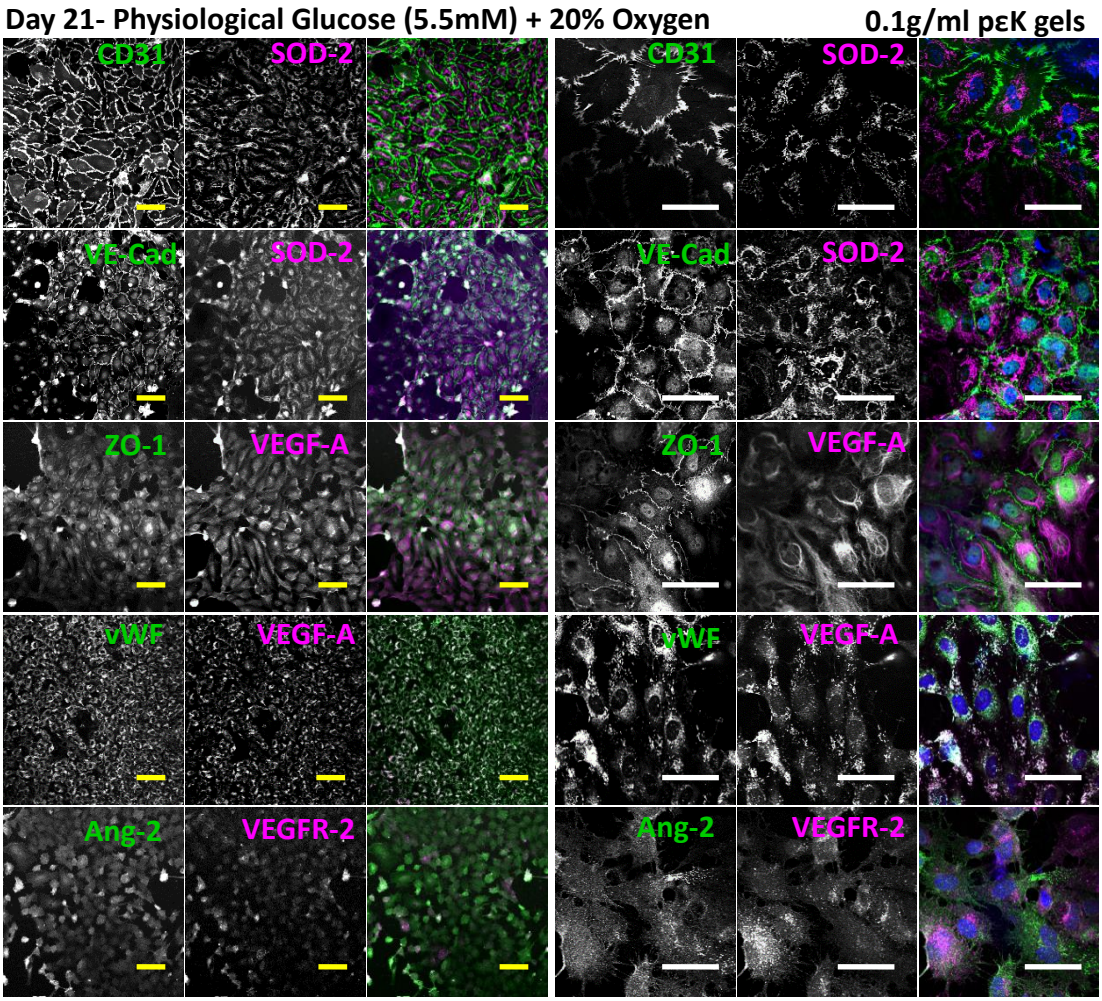

Figure 4.11. UCB-ECFCs retained their phenotype when cultured on 0.1g/ml pεK hydrogels in healthy conditions for 21 days

UCB-ECFCs, P5 were gently seeded at $5x10^4$ ECFCs/well in a 24 w/p with the pεK gel disk on the bottom. ECFCs were culture in phenol red-free EGM-2 with 10% FBS, in healthy conditions (20% oxygen, 5.5mM glucose) with the media changed every 48-72H. On day 21 cells were fixed and stained for IF analysis of proteins involved in junctional protein formation and angiogenic response. Images were captured using the Zeiss M800 confocal microscope, x10 or x40 oil magnification. Yellow scale bars= 100µm, white scale bars= 50µm.

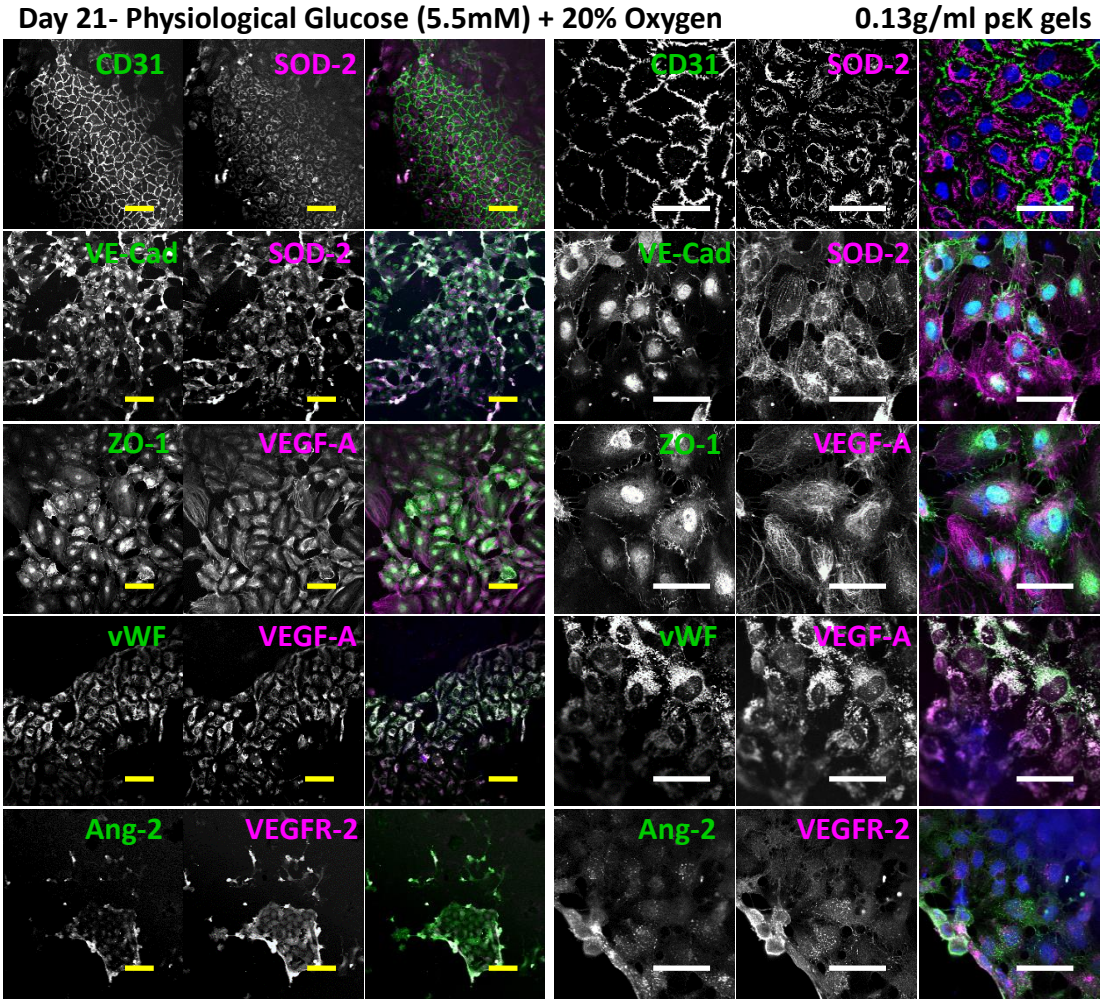

Figure 4.12. UCB-ECFCs retained their phenotype when cultured on 0.13g/ml pεK hydrogels in healthy conditions for 21 days

UCB-ECFCs, P5 were gently seeded at $5x10^4$ ECFCs/well in a 24 w/p with the pεK gel disk on the bottom. ECFCs were culture in phenol red-free EGM-2 with 10% FBS, in healthy conditions (20% oxygen, 5.5mM glucose) with the media changed every 48-72H. On day 14 cells were fixed and stained for IF analysis of proteins involved in junctional protein formation and angiogenic response. Images were captured using the Zeiss M800 confocal microscope, x10 or x40 oil magnification. Yellow scale bars= 100µm, white scale bars= 50µm.

4.4.6 UCB-ECFCs RETAINED A HOMOGENEOUS EC-SPECIFIC PHENOTYPE WITH TJS AND ADHERENS JUNCTIONS ON pεK HYDROGELS IN LOW OXYGEN AND DIABETIC CONDIONS FOR 21 DAYS

UCB-ECFCs grown on 0.1g/ml or 0.13g/ml pεK gels in 2% oxygen combined with either 5.5mM glucose (hypoxia) or 33mM glucose (diabetic) expressed CD31 (Figure 4.13). SOD-2 was expressed by all ECFCs, with no difference in expression pattern in different conditions, grown pεK gels for 21 days. HIF1α expression did not appear to differ in low oxygen with different glucose concentrations. Ang-2 expression was difficult to determine when imaging ECFC on pεK gels, therefore no conclusions could be drawn. Cell size and shape did not appear to differ across the different culture conditions, suggesting ECFCs retained their cell phenotype after 21 days on pεK gels. Overall ECFCs showed minimal differences when expanded on 0.1g/ml or 0.13g/ml pεK gels in healthy, low oxygen or diabetic conditions for 21 days, and did not show the possible de-differentiation observed when ECFCs were expanded on col I. coated TC plastic in the same conditions (Figure 4.10, Figure 4.11, Figure 4.12, Figure 4.13).

4.4.7 UCB-ECFCs ATTACHED TO UNMODIFIED pεK MICROPARTICLES OF FOUR DIFFERENT SIZES RANGES

Microparticles of 4 different sizes were made by emulsification polymerisation, 50% cross-linked with decanedioic acid, and with 0.286g/ml pεK. UCB-ECFCs tagged with cell tracker green (CTG-ECFC) attached to these microparticles and were monitored for up to 72H using live cell IF microscopy (Figure 4.14). Without any modification, the pεK microparticles supported adhesion of CTG-ECFCs, although adhered cells remained rounded in shape, suggesting ECFC adhesion may have been weak. Beyond 72H, CTG dye began to fade and it was not possible to monitor ECFCs on the microparticles. The microparticles also auto-fluoresced, combined with CTG dye increasing background noise, as seen in the 18.30.3, 48H image (Figure 4.14), therefore, structured illumination using an ApoTome microscope was essential to enable live cell 3D imaging of ECFCs on pεK microparticles.

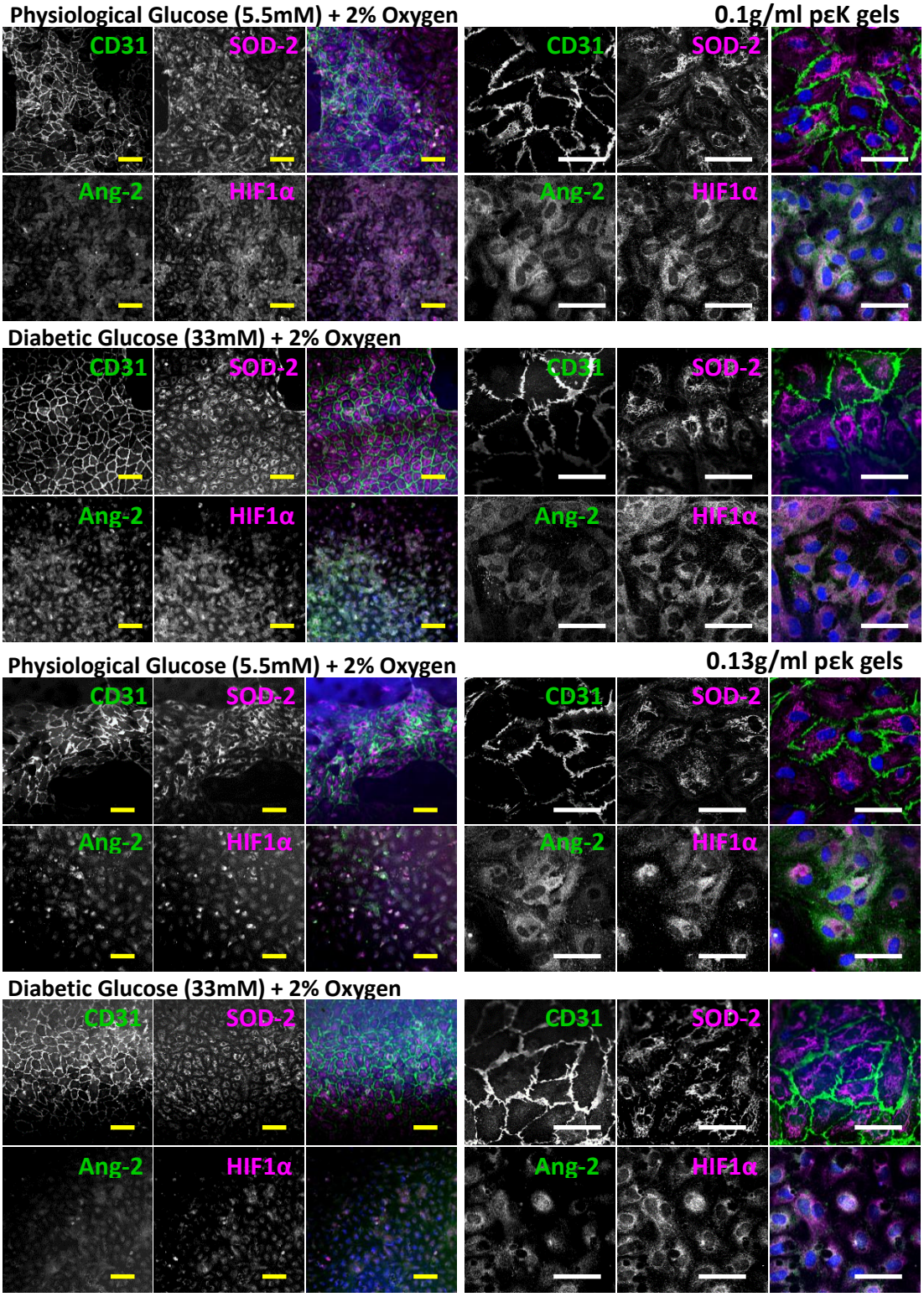

Figure 4.13. UCB-ECFCs retained their phenotype in low oxygen and high glucose for 21 days when frown on pεK hydrogels

UCB-ECFCs, P5 were seeded at $5x10^4$ ECFCs/well in a 24 w/p with the pεK gel disk on the bottom. ECFCs were culture in EGM with 10% FBS, in healthy conditions (20% oxygen, 5.5mM glucose), low hypoxic conditions (2% oxygen) or diabetic conditions (2% oxygen and 33mM glucose), with the media changed every 48-72H. On day 21 cells were fixed for IF analysis of proteins involved in junctional protein formation, oxidative stress angiogenic response. Images were captured using the Zeiss M800 confocal microscope, x10 and x40 oil magnifications. Yellow scale bars= 100µm, white scale bars= 50µm.

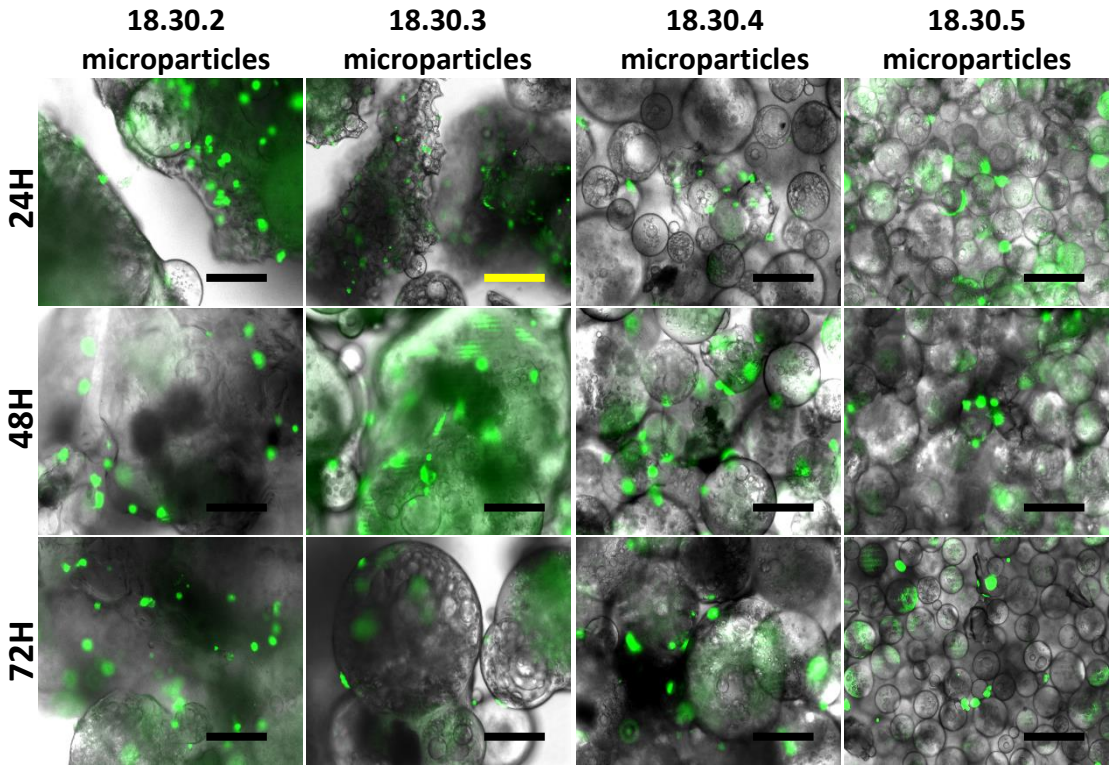

Figure 4.14. UCB-ECFCs adhered to unmodified pεK microparticles of four sizes for up to 72H

CTG-UCB-ECFCs, P4 were gently seeded at $5x10^4$ ECFCs/well in a 24 w/p with unmodified pεK microparticles on the bottom. ECFCs were culture in phenol red-free EGM-2 with 10% FBS. Images were captured at 24H, 48H and 72H using the Zeiss ApoTome microscope, x10 and x20 magnifications. Yellow scale bars= 200µm, black scale bars= 100µm. Z-stack images were produced using ZEN blue software.

4.4.8 ECFCs SHOWED IMPROVED ATTACHMENT TO pεK MICROPARTICLES WITH RGD BOUND ON THE SURFACE

CTG-ECFCs attached to microparticles with diameters in the range 500-250µm and 250-150µm, made by emulsification polymerisation, 50% cross-linked with decanedioic acid, with 0.286g/ml pεK, and ~10% covalently bound RGD peptide on the surface. The CTG-ECFCs could be monitored for up to 72H using live cell IF microscopy (Figure 4.15). When microparticles were covalently bound with RGD peptide on ~10% of the surface, ECFCs adhered and the cell cytoplasm appeared to cover a larger surface area compared to ECFCs adhered to non-modified pεK microparticles (Figure 4.15, Figure 4.14). Using z-stack imaging, 3D images were constructed and CTG-ECFCs could be observed wrapping around the surface of the pεK microparticles of both sizes. By 72H, the CTG dye began to fade and it became difficult to differentiate between auto-fluorescence of the pεK microparticles, compared to the CTG-ECFCs.

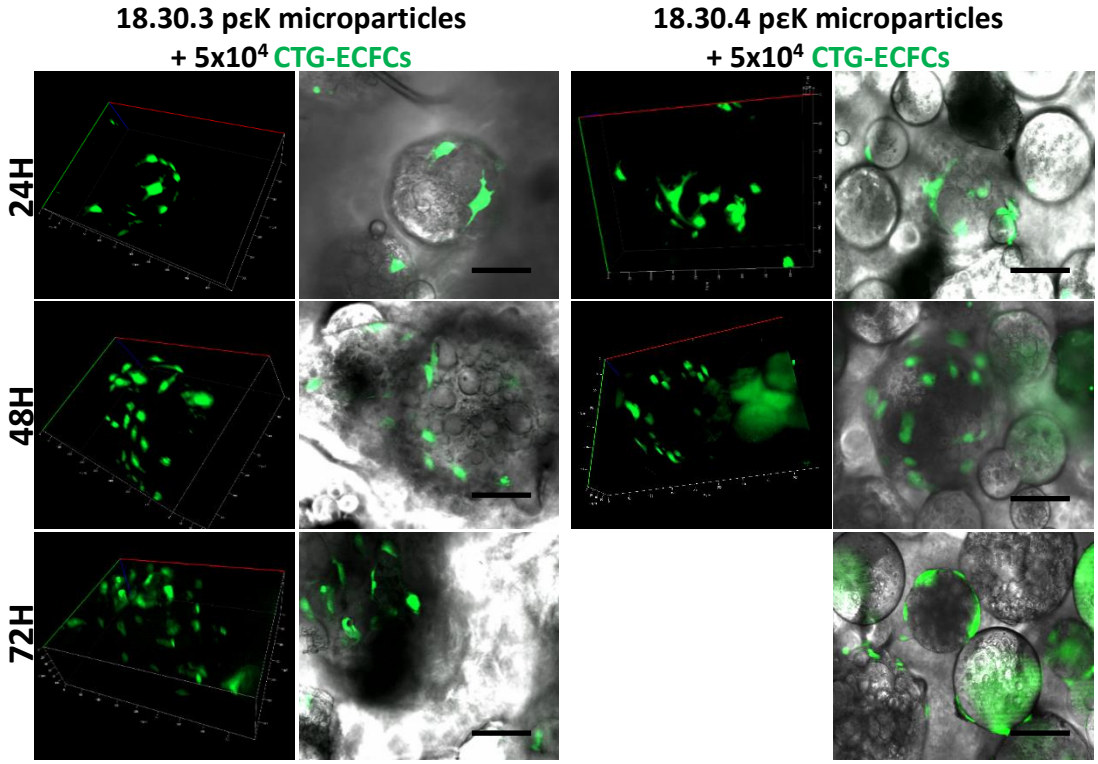

Figure 4.15. UCB-ECFCs adhered and spread on RGD modified pεK microparticles of two size ranges for up to 72H

CTG-UCB-ECFCs, P5 were gently seeded at $5x10^4$ ECFCs/well in a 24 w/p with RGD covalently bound to the surface of pεK microparticles, on the bottom. ECFCs were culture in phenol red-free EGM-2 with 10% FBS. Images were captured at 24H, 48H and 72H using the Zeiss ApoTome microscope, x20 magnification. Black scale bars= 100µm. Z-stack images were produced using ZEN blue software.

4.4.9 GFP-ECFCs ADHERED TO UNMODIFIED pεK MICROPARTICLES

In order to enable longer term monitoring of ECFCs on pεK microparticles, ECFCs transduced with GFP, using lentivirus, were seeded onto unmodified pεK microparticles, sized 250-150µm and <150µm. GFP-ECFCs attached to the two smaller sized beads, and at 24H after seeding, could be imaged using 3D z-stacks, with reduced interference from background caused by CTG (Figure 4.16). Viral transduction of GFP into ECFCs did not appear to have any effect on ECFC ability to attach and survive on the pεK microparticles. Passaging GFP-ECFCs did not affect GFP expression. 3D projections showed good coverage of cells all around the pεK microparticles of the two smaller sizes.

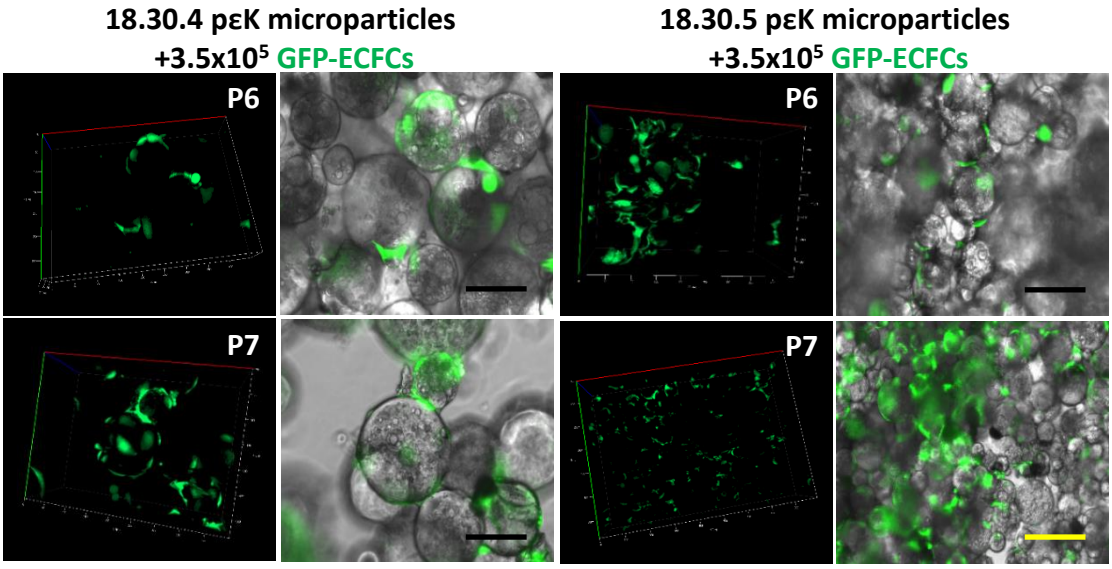

Figure 4.16. GFP-UCB-ECFCs adhered and spread on unmodified pεK microparticles of two size ranges for up to 24H

CTG-UCB-ECFCs, P6 were gently seeded at 3.5x10^5 ECFCs/well in a 24 w/p with unmodified pεK microparticles on the bottom. ECFCs were culture in phenol red-free EGM-2 with 10% FBS. Images were captured at 24H, using the Zeiss ApoTome microscope, x10 and x20 magnification. Yellow scale bars= 200µm, black scale bars= 100µm. Z-stack images were produced using ZEN blue software.

4.4.10 GFP-ECFCs DID NOT DETACH FROM pεK MICROPARTICLES WHEN ADDED TO HEALTHY OR DIABETIC MONO- OR CO-CULTURE MODELS

UCB-GFP-ECFCs attached to unmodified 18.30.5 (<150µm) pεK microparticles were added into the apical surface of mono/co-culture models in either healthy or diabetic conditions 24H or h8H, to determine if GFP-ECFCS would detach from pεK microparticles and incorporate into the hREC monolayer on the PET membrane. GFP-ECFCs appeared to attached to pεK microparticles, and did not incorporate into the hREC monolayer underneath (

Figure 4.17). During live cell imaging, no GFP-ECFCs were observed incorporated in to the hREC layer. After processing for IF imaging, GFP-ECFCs remained attached to pεK microparticles, 24-48H after adding to either mono- or co-culture models suggesting the GFP-ECFCs preferentially remained attached to unaltered pεK microparticles, in healthy and diabetic *in vitro* model of the retinal microvasculature.

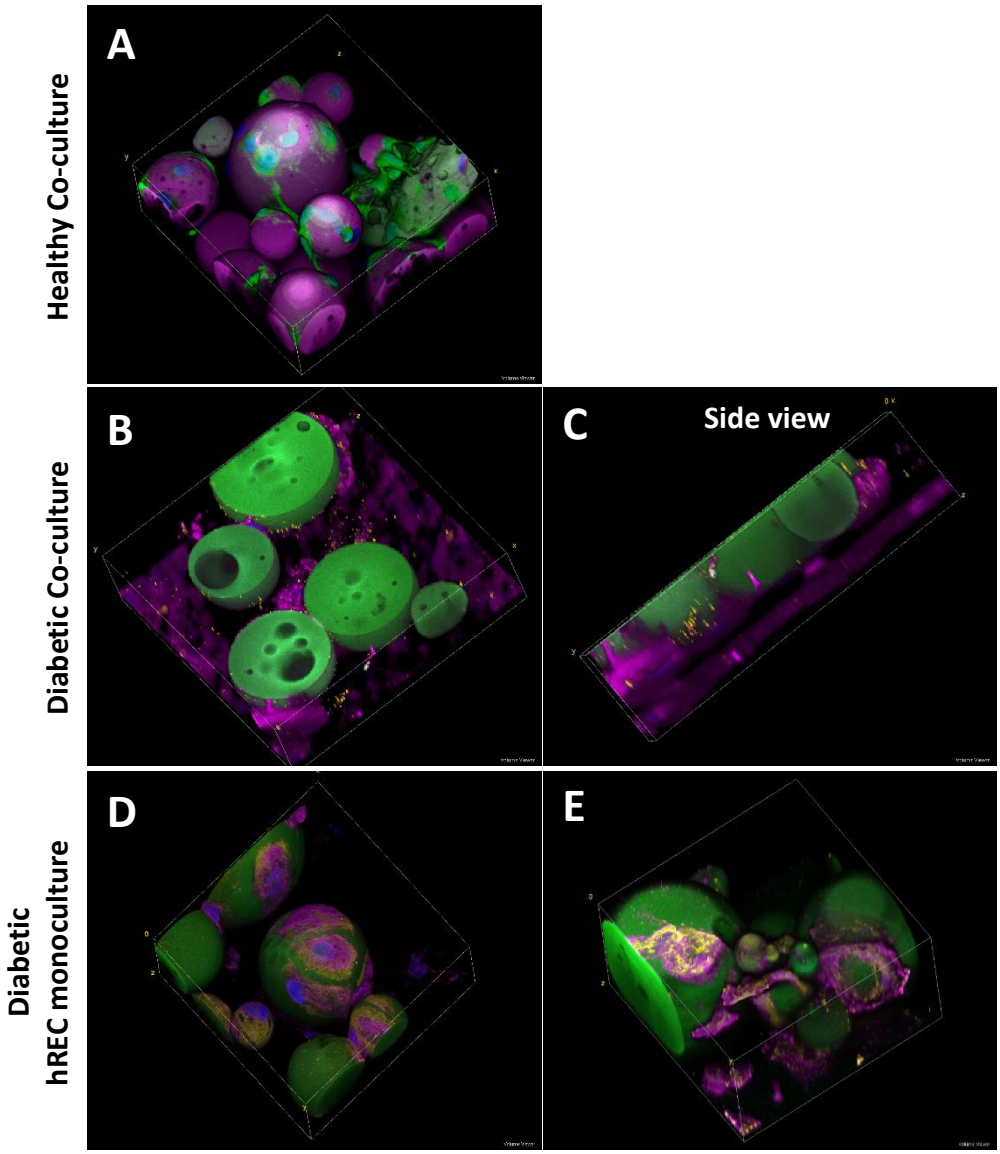

Figure 4.17. GFP-UCB-ECFCs do not detach from pεK microparticles when added to healthy or diabetic mono/co-cultures for 24-48H

(**A**) GFP-ECFC, P6 remaining on <150µM sized microparticles 48H after being added at culture day 7 of a healthy co-culture model. Microparticles were scooped out of the transwell insert and imaged on a glass slide. Magenta= phalloidin. (**B and C**) GFP-ECFC, P6 remaining on <150µM sized microparticles 24H after being added at culture day 7 of a diabetic co-culture model. Cell-laden microparticles were processed for IF whilst on the surface of the PET membrane. Magenta= Ang-2, Green =GFP. (**D**) GFP-ECFC, P6 remaining on <150µM sized microparticles 24H after being added at culture day 7 of a diabetic hREC monoculture model Magenta= Cx43, yellow= VEGFR2 and green= GFP. (**E**) GFP-ECFC, P6 remaining on <150µM sized microparticles 24H after being added at culture day 7 of a diabetic hREC monoculture model. Magenta= ZO-1, yellow= SOD-2 and green= GFP. Images were captured using the Zeiss M800 confocal microscope, x40 oil magnification.

4.5 DISCUSSION

4.5.1 OVERVIEW

The aims of this chapter were to: assess pεK hydrogels as a suitable biomaterial for expanding ECFCs whilst retaining early passage phenotype, and consider pεK microparticles as a tool for controlled delivery of ECFCs to the back of the eye. The peptide nature of pεK provides a cell adhesive surface which may be useful for ECFC expansion whilst maintaining a stem-like phenotype in order to expand numbers to levels which would be useful in the clinic (>1x10^7). ECFCs are currently expanded on rat tail collagen I coated TC plastic, which is not manufactured under GMP conditions. To use *in vitro* expanded ECFCs for a cell therapy in humans, xeno-free or GMP culture conditions are a requirement. Following the hypothesis that optimised pεK cast gels could support ECFC growth *in vitro,* UCB-ECFCs were seeded on unmodified pεK gels, 60% cross-linked with decanedioic acid. ECFCs successfully attached, spread and grew on pεK hydrogels, showing potential as a xeno-free replacement of rat tail collagen I, and a suitable non-toxic, natural polymer surface for ECFCs to expand on.

To achieve controlled delivery of ECFCs to specific areas in the back of the eye for translation of cell replacement therapy to the clinic, pεK microparticles were provided from SpheriTech to trial this protocol. Having confirmed UCB-ECFCs were capable of incorporating into my novel, human, retina-specific co-culture model of the microvasculature (Chapter 3), pεK microparticles were assessed for cell attachment and delivery of ECFCs to the co-culture model, with the ultimate aim of ECFCs detaching in response to cell signalling stimulus to incorporate into the endothelium. To achieve this, a protocol was optimised to seed ECFCs onto pεK microparticles with or without peptide surface modification, then cell-laden beads were delivered to the healthy or diabetic co-culture model, to assess if cells could detach and incorporate into gaps in the hREC monolayer.

4.5.2 CURRENT PROTOCOL FOR *IN VITRO* EXPANSION OF ECFCs

Historically both human fibronectin and rat tail col I. have been used as a culture surface coating to isolate EPCs. However, it became clear over time that there were two distinct populations present in culture (CACs and ECFCs), and col I. performed better for expansion of the ECFC population[155]. Little work focused on the impact that the two different substrates had on the success of isolation and the expansion of ECFCs, until Colombo et al. concluded that ECFC isolation should take place using fibronectin, whilst col I. was best for expansion[173]. Both of these studies support rat tail col I. for expansion of ECFCs *in vitro*, however, steps

have already been taken to produce humanised ECFC-cultures for translational purposes, such as replacement of FBS with human platelet lysate[164]. Therefore, to progress to first in human trials, new xeno-free, GMP compliant substrate options for optimised ECFC expansion needs to be investigated. pεK hydrogels provide a highly controlled peptide surface with amine functionality to allow cell binding, and during production, the hydrogel properties can be tailored to best suit any particular cell-type.

4.5.3 pεK HYDROGELS SUPPORTED THE EXPANSION OF UBC-ECFCs

A common goal for stem cell therapy and regenerative medicine is facilitating the manufacture of products, or growth of cells, suitable for delivery into humans, whilst reducing the amount of undesirable or non-defined components[287]. For the current project, the aim was to maintain ECFC phenotype during expansion and replacing rat tail col I. coating with a xeno-free, non-toxic peptide hydrogel. The advantages of using a peptide hydrogel are that it can provide the chemical functionality of the col I. while being non-animal derived and consistently reproduced.

The peptide hydrogels were produced from poly-ε-lysine (pεK), a simple linear amino acid chain with around 28 residues per peptide. Once gelled this produces a surface rich in amine functionality. Sheets were cast in order to test their capability to support ECFC growth without dedifferentiation, using a xeno-free surface, to expand the number of undifferentiated ECFCs to levels that could be clinically useful[140]. pεK hydrogels were developed by SpheriTech using patent protected technology (EP2699620) to produce an antimicrobial corneal bandage lens. SpheriTech also have ongoing projects tailoring the pεK hydrogels for optimal expansion of various different types of cell *in vitro* (unpublished data). There is currently very little published data on the use of pεK hydrogels for cell expansion, however one study successfully grew HCT-E cells on pεK hydrogels cross-linked with 60% octanedioic acid, and these ECs expressed ZO-1, suggesting they had functional barrier properties[288]. In this study, the authors discuss the fact that pεK hydrogels can be optimised according to clinical need, and surface peptide modification means the pεK hydrogels can be tailored to become the optimal surface for attachment for multiple different types of cells, highlighting the huge potential of this polymer in regenerative medicine applications. In the present study, pεK hydrogels composed of 0.1g/ml and 0.13g/ml pεK, 60% cross-linked with decanedioic acid did support the expansion of UCB-ECFCs in both healthy and diabetic conditions for 21 days.

The number of ECFCs which initially attached appeared quite low (Figure 4.5, Figure 4.6), however by day 7, ECFC colonies were clearly visible on the pεK hydrogels and by day 14 ECFCs had filled the surface of the pεK hydrogels. Cells remained EC-like; small, cobble-stone, uniform-shaped, and maintained contacts with neighbouring cells when grown on pεK hydrogels, whereas a small number of ECFCs grown on col I. coated TC plastic expanded in size, suggesting either de-differentiation or senescence (Figure 4.5, Figure 4.7)[193]. The ECFCs grown on pεK hydrogels expressed EC-specific markers vWF, CD34, VE-Cad, CD31 and ZO-1, and there did not appear to be any senescent ECFCs present, assessed morphologically via the typical increase in size of the cell cytoplasm and nucleus. Similar to the HCE-T reported by Williams et al., the ECFCs seeded on pεK hydrogels of both densities expressed junctional proteins ZO-1, VE-Cad and CD31 at day 21 in healthy conditions (Figure 4.11, Figure 4.12)[288]. ECFCs grown in low oxygen (2%) or double insult of low oxygen and high glucose (2% O_2 and 33mM glucose) used in the diabetic model, expressed CD31 at day 21, and cells were present as a monolayer (Figure 4.13). ZO-1 was not assessed in stress conditions, due to the small sample size. Overall pεK hydrogels appear a very promising option for expansion of ECFCs, and the ECFCs demonstrated robustness against prolonged hypoxia and glucose insult as well as in healthy conditions on the pεK hydrogels.

4.5.4 ECFCs ATTACHED TO pεK MICROPARTICLES RANGING IN SIZE FROM 1000µm TO <150µm

pεK microparticles were developed and patented by SpheriTech (EP2699619) and were assessed in this project as a cell delivery platform, testing if ECFCs would initially adhere then detach when added to a model of injured ECs**.** ECFCs did not attach very well to pεK microparticles ranging in size from 1000µm to <150µm during initial optimisation. Despite initial poor attachment on unmodified pεK microparticles, after seeding at much higher cell density ($3.5x10^5$ cell/well rather than $2x10^4$ cells/well) ECFCs did attach to unmodified pεK microparticles, although they did not spread and remained rounded at all time points (Figure 4.14). In order to improve initial attachment, RGD was covalently bound to the surface of the pεK. The epsilon amino group in pεK is a good nucleophile at pH >8.0 and reacts with a variety of reagents to form stable, covalently attached ligands on the pεK substrate surface[289]. The RGD tripeptide sequence (Arg-Gly-Asp) is associated with ECM proteins such as fibronectin, laminin and collagen and has been grafted to many different kinds of biomaterials including polymers, metals and ceramics, to modulate cell adhesion[181,290]. After RGD was covalently bound to the pεK microparticles at ~10% coverage, ECFCs attached and spread onto the pεK (Figure 4.15). However, for the ultimate goal of cell delivery, loose attachment may in fact be

desirable, because if the ECFCs were attached too strongly to the pεK, any chemokine or cytokine migratory effect when added to the damaged hREC may not be sufficient to signal for the ECFCs to migrate off the microparticles. Therefore, unmodified pεK microparticles were used to deliver ECFCs to the retinal microvascular co-culture model.

4.5.5 ECFCs DELIVERED ON pεK MICROPARTICLES DID NOT INTEGRATE INTO THE hREC LAYER OF THE CO-CULTURE MODEL

ECFCs did not detach from the pεK microparticles when cell-laden pεK microparticles were added to either healthy or diabetic hREC monolayers, or when added to the diabetic co-culture model. No GFP-positive ECFCs could be detected in the hREC layer of any of the models, and after high resolution z-stack confocal microscopy was performed, ECFCs were detected still adhered to the pεK microparticles (

Figure 4.17). Therefore, although ECFCs appeared only loosely adhered to the pεK microparticles, due to their rounded shape, the adhesion to the pεK microparticle surface was able to withstand manual transfer of beads from the well using a metal scoop.

The optimised diabetic co-culture model conditions resulted in significant changes to the secretion of a number of proteins involved in angiogenesis, such as increase in secreted Ang-2 levels and decrease in secreted TIMP-2 levels (Figure 2.32). Ang-2 is a vascular growth factor which is increased in inflammatory and angiogenic environments [34] and TIMP-2 is a natural inhibitor of MMP-2, therefore, reduced TIMP-2 leads to increased MMP-2 activity and increased ECM remodelling. In combination, these two growth factors represent a pro-angiogenic environment. However, the growth factors present within the diabetic (or healthy) models did not cause migration of the ECFCs off the pεK microparticles in the present study.

4.5.6 ALTERNATIVES TO pεK

Hydrogels provide a biomimetic environment, with salient elements of native ECMs compared to protein coated TC plastic, and provide the opportunity to modify surfaces to best suit cell-specific needs[291]. There are different categories of hydrogels commonly used in cell culture, including naturally derived (collagen, fibrin and alginate), synthetically produced (polyacrylamide and polyethylene glycol) and hybrid (hyaluronic acid and polypeptide) hydrogels[292]. Each has positive and negative aspects and should be selected according to experimental application. Recombinant human ECM protein synthesis is an alternative xeno-free option, and collagen represents a successful model, however optimisation is still necessary within the different expression systems to improve productivity and bioactivity, as

well as cost and convenience[293]. With regards to stem cell expansion, soft polyacrylamide substrates have been shown to enable expansion of mouse embryonic stem cells which retain their pluripotency, highlighting that stiffness is involved in driving stem cell fate[294]. For clinical applications, it is important to be able to release cells from substrates in a controlled manner. A useful substrate for this task is thermo-responsive poly (N-isopropylacrylamide) (pNIPAAm), which is suitable for cell attachment and growth at 37°C, but at 20°C the pNIPAAm polymer chains hydrate and expand, which detaches the cells as a sheet[295]. For the present project, a hydrogel capable of expanding ECFCs and maintaining their progenitor phenotype *in vitro* was the main aim.

4.6 LIMITATIONS & FUTURE WORK

Modifications to the pεK microparticles to enable controlled release, such as pH-sensitive, temperature-sensitive or enzymatic release of ECFCs could be investigated. However, direct intraocular injection of ECFCs has been shown to result in successful incorporation in an OIR mouse model[153]. Using the same model, systemic injection of ECFCs through the common carotid artery also resulted in successful ECFC incorporation into the retinal vessels, although the numbers were lower than intravitreal delivery[170]. Therefore, ECFCs may not require a biomaterial for delivery purposes. An unexpected result from the co-culture model was no detectable secreted VEGF. Therefore addition of exogenous VEGF or any chemotactic molecule present in DR could be explored, to determine if ECFCs would migrate off the microparticles in the presence of a potent stimulator of EC migration. pεK gels could be cross-linked with other carboxylic acids, or the percentage cross-linkage adjusted, in order to assess the optimal pεK hydrogel composition to expand ECFCs in the future.

4.7 CONCLUSIONS

In the present study, for the first time, pεK cross-linked 60% with decanedioic acid has been shown to enable ECFC attachment and expansion, whilst maintaining phenotype for up to 21 days in both healthy and diabetic conditions. ECFCs also successfully adhered to pεK microparticles, although further modification of the surface chemistry of the pεK microparticles would be required to consider them for ECFC delivery to the back of the eye.

5 CHAPTER 5

5.1 DISCUSSION

The main aim of the work undertaken in this thesis was to develop a human primary cell model of the diabetic retinal microvasculature which could be used to assess the ability of ECFCs to integrate into the EC layer of the retinal capillaries, as a cell therapy option. Isolation and expansion techniques of ECFCs need to be further developed to become GMP compliant if they are to be used as a clinical cell therapy because the current method uses rat tail collagen I coated surfaces to expand ECFCs from the mononuclear fraction of blood. Non-toxic, pεK hydrogel surfaces were assessed for their capacity to expand ECFCs whilst retaining their endothelial progenitor properties, as a xeno-free replacement to rat tail collagen I.

The aim of chapter 2 was development of a novel human, primary co-culture model of the retinal vasculature to mimic diabetic retinopathy *in vitro.* Multiplex data from chapter 2 highlighted that the secretion pattern of angiogenic proteins was different when cells were co-cultured compared to grown individually. Human primary cells were challenging to expand *in vitro* and this may be why immortalised, non-human or large vessel cells have been used by others in previous studies, however, in the present study, it was possible to grow the two cell types in co-culture after extensive optimisation of culture conditions. Extending the culture period for up to 21 days was also very important because some angiogenic proteins were not secreted until beyond day 14, and considering the long onset of DR, some changes to cell behaviour may not be detected in short culture durations.

The aim of chapter 3 was to isolate, characterise and expand ECFCs from human UCB and APB and test their capability to incorporate into the healthy and diabetic human primary co-culture models of the retinal microvasculature. ECFCs were successfully isolated from APB and UCB, although higher numbers of ECFCs were expanded from UCB, and the ECFCs that did expand from APB grew slower and reached senescence earlier. GD-ECFCs showed no difference in expansion and integration capabilities compared to healthy UCB-ECFCs. Two subpopulations of EPCs can be isolated *in vitro*, therefore, stringent characterisation of putative ECFCs was carried out and data from chapter 3 confirmed that cells isolated using rat tail col I. coated TC surfaces and cultured in endothelial specific growth conditions for 2-6 weeks were true ECFCs. APB and UCB-ECFCs incorporated into hREC layers in mono- and co-culture models, in both healthy and diabetic conditions, confirming their potential as a future cell therapy to repair damaged vascular endothelium.

The aim of chapter 4 was to assess the capacity of pεK for ECFC attachment, viability and expansion without differentiation, and targeted delivery of ECFCs to an *in vitro* model of diabetic retinopathy. It was determined that pεK microparticles were not suitable as a delivery method of ECFCs, because cells remained attached to the microparticle rather than integrating into the hREC layer. However, long term culture of ECFCs on rat tail collagen I coated TC plastic surfaces lead to a heterogeneous population of cells, some of which expanded in size suggesting either differentiation or senescence. pεK hydrogels provided a xeno-free, highly reproducible, modifiable surface to expand ECFCs, and data in chapter 4 highlights that UCB-ECFCs cultured long term on pεK hydrogels in both healthy and diabetic conditions retained their EC morphology, expanded well, formed a TJ barrier when in a monolayer and remained a homogenous population. Therefore, pεK hydrogels may provide a replacement for rat tail collagen I as a surface with improved properties to expand ECFCs *in vitro* for potential clinical application.

5.2 CONCLUSIONS

- hREC and hRP survived low oxygen (2%) and high glucose (33mM) culture conditions for up to 21 days
- hREC and hRP grew on either side of a PET transwell insert seeded at 1:1 ratio to mimic the hRP coverage of the retinal capillary
- Diabetic conditions induced significant changes to the secretion profile of angiogenic proteins from hREC and hRP compared to healthy conditions
- hREC and hRP response to diabetic culture was different when the cells were co-cultured as opposed to cultured individually
- Fewer ECFCs were isolated from APB and they grew slower and reached senescence earlier than UCB-ECFCs
- Both APB, healthy and GD-UCB-ECFCs integrated into the hREC layer on PET membranes in healthy and diabetic conditions
- Healthy and GD-UCB-ECFCs integrated into the hREC of the co-culture model in both healthy and diabetic conditions
- UCB-ECFCs cultured for 21 days on pεK hydrogels retained their endothelial progenitor-specific phenotype
- UCB-ECFCs cultured for 21 days on rat tail col I. coated TC plastic began to differentiate or become senescent
- Even in low oxygen (2%) and high glucose (33mM) conditions UCB-ECFCs grown on pεK hydrogels remained a homogenous population expressing endothelial progenitor-specific markers
- pεK hydrogels are a promising alternative culture surface that is xeno-free, highly reproducible and modifiable to enable expansion of ECFCs *in vitro* whilst retaining their progenitor phenotype
- UCB-ECFCs adhered to unmodified pεK microparticles but did not detach when cell laden microparticles were delivered to the healthy or diabetic co-culture model

6 REFERENCES

1. Land, M. F. The Eye A Very Short Introduction. (OUP Oxford, 2014).
2. Dunn, K. C., Aotaki-Keen, A. E., Putkey, F. R. & Hjelmeland, L. M. ARPE-19, a human retinal pigment epithelial cell line with differentiated properties. **62**, 155–169 (1996).
3. WideRangeGalleries. Carlson Stock Art. Eye Anatomy 1 Illustration (2019). Available at: https://www.carlsonstockart.com/photo/human-eye-anatomy-illustration-1/. (Accessed: May, 2019).
4. The Retina Reference. The Retina Reference. Normal Retinal Anatomy (2019). Available at: www.retinareference.com/anatomy/. (Accessed: May, 2019).
5. Forrester, J., Dick, A., McMenamin, P., Roberts, F. & Pearlman, E. The Eye. (Saunders Ltd, 2015).
6. Encyclopaedia Britannica. Structure and function of photoreceptors (2019). Available at: https://www.britannica.com/science/photoreception/Structure-and-function-of-photoreceptors. (Accessed: May, 2019).
7. Kocaoglu, O. P., Liu, Z., Zhang, F., Kurokawa, K., Jonnal, R. S. & Miller, D. T. Photoreceptor disc shedding in the living human eye. *Biomed. Opt. Express.* **7**(11), 4554-4568 (2016).
8. Trinh, T. L. P., Li Calzi, S., Shaw, L., Yoder, M. & Grant, M. B. Promoting vascular repair in the retina: can stem/progenitor cells help? *Eye & Brain.* **8**, 113-122 (2016).
9. Lin, F. C., Zao, J. K., Tu, K. C., Wang, Y., Huang, Y. P., Chuang, C. W., Kuo, H. Y., Chien, Y. Y., Chou, C. C. & Jung, T. P. SNR analysis of high-frequency steady-state visual evoked potentials from the foveal and extrafoveal regions of Human Retina. *Proc. Annu. Int. Conf. IEEE Eng. Med. Biol. Soc.* 1810–1814 (2012).
10. Kiel, J. W. San Rafael (CA): The Ocular Circulation. (Morgan & Claypool Life Sciences, 2010). Available from: https://www.ncbi.nlm.nih.gov/books/NBK53323/. (Accessed: May, 2019)
11. Hayreh, S. S. Ischemic optic neuropathy. *Prog. Retin. Eye Res*. **28**, 34–62 (2009).
12. Levin, L. A., Nilsson, S. F. E., Ver Hoeve, J. V. & Wu, S. Alder's Physiology of the Eye. (Elsevier, 2011).
13. Yu, D. Y., Yu, P. K., Cringle, S. J., Kang, M. H. & Su, E. N. Functional and morphological characteristics of the retinal and choroidal vasculature. *Prog. Retin. Eye Res*. **40**, 53–93 (2014).
14. Craig, L. E., Spelman, J. P., Strandberg, J. D. & Zink, M. C. Endothelial Cells from Diverse Tissues Exhibit Differences in Growth and Morphology. *Microvascular Res*. **76**, 65–76 (1998).
15. Vecino, E., Rodriguez, F. D., Ruzafa, N., Pereiro, X. & Sharma, S. C. Glia-neuron interactions in the mammalian retina. *Prog. Retin. Eye Res*. **51**, 1–40 (2016).
16. Walshe, T. E., Ferguson, G., Connell, P., O'Brien, C. & Cahill, P. A. Pulsatile flow increases the expression of eNOS, ET-1, and prostacyclin in a novel in vitro coculture model of the retinal vasculature. *Investig. Ophthalmol. Vis. Sci.* **46**, 375–382 (2005).
17. Stitt, A. W., Curtis, T. M., Chen, M., Medina, R. J., McKay, G. J., Jenkins, A., Gardiner, T. A., Lyons, T. J., Hammes, H. P., Simó, R. & Lois, N. The progress in understanding and treatment of diabetic retinopathy. *Prog. Retin. Eye Res*. **51**, 156–186 (2016).
18. Hayreh, S. S. Ocular Vascular Occlusive Disorders. (Springer International Publishing, 2015).
19. Duh, E. J., Sun, J. K. & Stitt, A. W. Diabetic retinopathy: current understanding, mechanisms, and treatment strategies. *JCI Insight.* **2**, 1–13 (2017).
20. H, V. J. Types of Blood Vessels – Structure and Function of Arteries, Arterioles, Capillaries, Venules, And Veins. (2018). Available at: https://www.earthslab.com/physiology/types-blood-vessels-structure-function-arteries. (Accessed: May, 2019).
21. BCcampus. Structure and Function of Blood Vessels. Available at: https://opentextbc.ca/anatomyandphysiology/chapter/20-1-structure-and-function-of-blood-vessels/. (Accessed: May, 2019).
22. Jaffe, E. A., Nachman, R. L., Becker, C. G. & Minick, C. R. Culture of human endothelial cells derived from umbilical veins. Identification by morphologic and immunologic criteria. *J. Clin. Invest.* **52**, 2745–2756 (1973).
23. Bharadwaj, A. S., Appukuttan, B., Wilmarth, P. A., Pan, Y., Stempel, A. J., Chipps, T. J., Benedetti, E. E., Zamora, D. O., Choi, D., David, L. L. & Smith, J. R. Role of the retinal vascular endothelial cell in ocular disease. *Prog. Retin. Eye Res.* **32**, 102–180 (2013).

24. Deanfield, J. E., Halcox, J. P. & Rabelink, T. J. Endothelial Function and Dysfunction. *Circulation.* **115**, 1285–1295 (2018).
25. Díaz-Coránguez, M., Ramos, C. & Antonetti, D. A. The inner blood-retinal barrier: Cellular basis and development. *Vision Res*. **139**, 123–137 (2017).
26. Muller, W. A. PECAM-1 is required for trans-endothelial migration of leukocytes. *J. Exp. Med.* **178**, 449–460 (2004).
27. Ferrero, E., Elena, M., Pardi, R. & Raffaella, M. The platelet endothelial cell adhesion molecule-1 (PECAM1) contributes To Endothelial Barrier Function. *FEBS Letters*. **374**, 323–326 (1995).
28. Piali, L., Hammel, P., Uherek, C., Bachmann, F., Gisler, R. H., Dunon, D. & Imhof, B. A. CD31/PECAM-1 Is a Ligand for $\alpha_v\beta_3$ Integrin Involved in Adhesion of Leukocytes to Endothelium. *Cell.* **130**, 451–460 (2009).
29. DeLisser, H. M., Chilkotowsky, J., Yan, H. C., Daise, M. L., Buck, C. A. & Albelda, S. M. Deletions in the cytoplasmic domain of platelet-endothelial cell adhesion molecule-1 (PECAM-1, CD31) result in changes in ligand binding properties. *J. Cell Biol.* **124**, 195–203 (1994).
30. Buján, J., Gimeno, M. J., Prieto, A., Pascual, G., Bellón, J. M. & Alvarez-Mon, M. Modulation of PECAM-1 (CD31) expression in human endothelial cells: Effect of IFNγ and IL-10. J. *Vasc. Res.* **36**, 106–113 (1999).
31. Pu, F., Williams, R., Markkula, T. & Hunt, J. Expression of leukocyte–endothelial cell adhesion molecules on monocyte adhesion to human endothelial cells on plasma treated PET and PTFE in vitro. *Biomaterials.* **23**, 4705–4718 (2002).
32. Li, J.J., Huang Y. Q., Karpatkin, S. Thrombin induces the release of angiopoietin-1 from platelets. *Thromb Heamost*. **85**, 204–206 (2001).
33. Fiedler, U., Scharpfenecker, M., Koidl, S., Hegen, A., Grunow, V., Schmidt, J. M., Kriz, W., Thurston, G. & Augustin, H. G. The Tie-2 ligand Angiopoietin-2 is stored in and rapidly released upon stimulation from endothelial cell Weibel-Palade bodies. *Blood.* **103**, 4150–4156 (2004).
34. Thurston, G., Daly, C., Whitehead, K. J., Smith, M. C. P., Li, Y., Lampugnani, M. G., Landskroner-eiger, S. & Moneke, I. The Complex Role of Angiopoietin-2 in the Angiopoietin – Tie Signaling Pathway. *Cold Spring Harb Perspect Med*. **2**, 1–14 (2013).
35. Kim, I., Kim, J. H., Ryu, Y. S., Liu, M. & Koh, G. Y. Tumor necrosis factor-α upregulates angiopoietin-2 in human umbilical vein endothelial cells. *Biochem. Biophys. Res. Commun.* **269**, 361–365 (2000).
36. Mandriota, S.J. & Pepper, M.S., 1998. Regulation of angiopoietin-2 mRNA levels in bovine microvascular endothelial cells by cytokines and hypoxia. *Circ. Res.* **83**, 852-859.
37. Teichert, M., Milde, L., Holm, A., Stanicek, L., Gengenbacher, N., Savant, S., Ruckdeschel, T., Hasanov, Z., Srivastava, K., Hu, J., Hertel, S., Bartol, A., Schlereth, K. & Augustin, H. G. Pericyte-expressed Tie2 controls angiogenesis and vessel maturation. *Nat. Commun.* **8**, 1–12 (2017).
38. Kiran, M. S., Sameer Kumar, V. B., Viji, R. I. & Sudhakaran, P. R. Temporal relationship between MMP production and angiogenic process in HUVECs. *Cell Biol. Int.* **30**, 704–713 (2006).
39. Kiran, M. S., Viji, R., Kumar, S., Prabhakaran, A. & Sudhakaran, P. R. Changes in expression of VE-cadherin and MMPs in endothelial cells: Implications for angiogenesis. *Vasc. Cell.* **3**, 6 (2011).
40. Vestweber, D. VE-Cadherin The Major Endothelial Adhesion Molecule Controlling Cellular Junctions and Blood Vessel Formation. *Arterioscler. Thromb. Vasc. Biol.* **28**, 223–232 (2007).
41. Nolan, D. J., Ginsberg, M., Israely, E., Palikuqi, B., Poulos, M. G., James, D., Ding, B.-S., Schachterle, W., Liu, Y., Rosenwaks, Z., Butler, J. M., Xiang, J., Rafii, A., Shido, K., Rabbany, S. Y., Elemento, O. & Rafii, S. Molecular Signatures of Tissue-Specific Microvascular Endothelial Cell Heterogeneity in Organ Maintenance and Regeneration. *Dev. Cell*. **26**, 204–219 (2013).
42. Browning, A. C., Halligan, E. P., Stewart, E. A., Swan, D. C., Dove, R., Samaranayake, G. J. & Amoaku, W. M. Comparative gene expression profiling of human umbilical vein endothelial cells and ocular vascular endothelial cells. *Br. J. Ophthalmol.* **96**, 128–132 (2012).
43. Dejana, E., Hirschi, K. K. & Simons, M. The molecular basis of endothelial cell plasticity. *Nat. Commun.* **8**, 1–11 (2017).
44. Bergers, G. & Song, S. The role of pericytes in blood-vessel formation and maintenance. *Neuro. Oncol.* **7**, 452–464 (2005).
45. Ballabh, P., Braun, A. & Nedergaard, M. The blood-brain barrier: An overview: Structure, regulation, and clinical implications. *Neurobiol. Dis.* **16**, 1–13 (2004).

46. Tell, D. Von, Armulik, A. & Betsholtz, C. Pericytes and vascular stability. *Exp. Cell Res.* **312**, 623–629 (2006).
47. Berrone, E., Beltramo, E., Buttiglieri, S., Tarallo, S., Rosso, A., Hammes, H. & Porta, M. Establishment and characterization of a human retinal pericyte line: A novel tool for the study of diabetic retinopathy. *Int. J. Mol. Med.* **23**, 373–378 (2009).
48. Dore-duffy, P. & Cleary, K. Chapter 2 Morphology and Properties of Pericytes. *The Blood-Brain and Other Neural Barriers*. **686**, 49-68 (2011).
49. Tarallo, S., Beltramo, E., Berrone, E. & Porta, M. Human pericyte-endothelial cell interactions in co-culture models mimicking the diabetic retinal microvascular environment. *Acta Diabetol.* **49**, (2012).
50. Shepro, D. & Morel, N. M. Pericyte Physiology. *FASEB J.* **7**, 1031–1038 (1993).
51. Ribatti, D., Nico, B. & Crivellato, E. The role of pericytes in angiogenesis. *Int. J. Dev. Biol.* **55**, 261–268 (2011).
52. Motiejunaite, R. & Kazlauskas, A. Pericytes and ocular diseases. *Exp. Eye Res.* **86**, 171–177 (2008).
53. Hammes, H. P., Lin, J., Wagner, P., Feng, Y., Vom Hagen, F., Krzizok, T., Renner, O., Breier, G., Brownlee, M. & Deutsch, U. Angiopoietin-2 Causes Pericyte Dropout in the Normal Retina: Evidence for Involvement in Diabetic Retinopathy. *Diabetes.* **53**, 1104–1110 (2004).
54. Durham, J. T. & Herman, I. M. Microvascular Modifications in Diabetic Retinopathy. *Curr. Diab. Rep*. **11**, 253–264 (2011).
55. Kutcher, M. E. & Herman, I. M. The pericyte: Cellular regulator of microvascular blood flow. *Microvasc. Res.* **77**, 235–246 (2009).
56. Jiao, H., Wang, Z., Liu, Y., Wang, P. & Xue, Y. Specific role of tight junction proteins claudin-5, occludin, and ZO-1 of the blood-brain barrier in a focal cerebral ischemic insult. *J. Mol. Neurosci.* **44**, 130–139 (2011).
57. Klaassen, I., Noorden, C. J. F. Van & Schlingemann, R. O. Progress in Retinal and Eye Research Molecular basis of the inner blood-retinal barrier and its breakdown in diabetic macular edema and other pathological conditions. *Prog. Retin. Eye Res.* **34**, 19–48 (2013).
58. Rangasamy, S., Srinivasan, R., Maestas, J., McGuire, P. G. & Das, A. A potential role for angiopoietin 2 in the regulation of the blood-retinal barrier in diabetic retinopathy. *Investig. Ophthalmol. Vis. Sci.* **52**, 3784–3791 (2011).
59. Harris, E. S. & Nelson, W. J. VE-Cadherin: At the Front, Centre, and Sides of Endothelial Cell Organization and Function. *Curr. Opin. Cell Biol*. **22**, 651–658 (2011).
60. Tornavaca, O., Chia, M., Dufton, N., Almagro, L. O., Conway, D. E., Randi, A. M., Schwartz, M. A., Matter, K. & Balda, M. S. ZO-1 controls endothelial adherens junctions, cell-cell tension, angiogenesis, and barrier formation. *J. Cell Biol*. **208**, 821–838 (2015).
61. Noria, S., Cowan, D. B., Gotlieb, A. I. & Langille, B. L. Endothelial Cell Adherens Junctions. *Circ. Res*. 504–514 (1999).
62. Wisniewska-Kruk, J., Hoeben, K. a., Vogels, I. M. C., Gaillard, P. J., Van Noorden, C. J. F., Schlingemann, R. O. & Klaassen, I. A novel co-culture model of the blood-retinal barrier based on primary retinal endothelial cells, pericytes and astrocytes. *Exp. Eye Res.* **96**, 181–190 (2012).
63. Buchanan, C. F., Verbridge, S. S., Vlachos, P. P. & Rylander, M. N. Flow shear stress regulates endothelial barrier function and expression of angiogenic factors in a 3D microfluidic tumor vascular model. *Cell Adh. Migr.* **8**, 517–524 (2014).
64. Miao, H., Hu, Y. L., Shiu, Y. T., Yuan, S., Zhao, Y., Kaunas, R., Wang, Y., Jin, G., Usami, S. & Chien, S. Effects of flow patterns on the localization and expression of VE-cadherin at vascular endothelial cell junctions: In vivo and in vitro investigations. *J. Vasc. Res.* **42**, 77–89 (2005).
65. Holt, R. I. & Hanley, N. A. Essentials: Endocrinology and Diabetes. (John Wiley & Sons, 2011).
66. Diabetes UK. Diabetes: the basics. (2019). Available at: https://www.diabetes.org.uk/diabetes-the-basics. (Accessed: May, 2019).
67. Erem, C., Kuzu, U. B., Deger, O. & Can, G. Prevalence of gestational diabetes mellitus and associated risk factors in Turkish women: The Trabzon GDM Study. *Arch. Med. Sci*. **11**, 724–735 (2015).
68. Hod, M., Kapur, A., Sacks, D. A., Hadar, E., Agarwal, M., Di Renzo, G. C., Roura, L. C., McIntyre, H. D., Morris, J. L. & Divakar, H. New FIGO Guidelines on Gestational Diabetes. *Gynecol. Obstet*. **131**, S173-211 (2015).

69. Imam, K. Gestational Diabetes Mellitus. ADA. *Diabetes Care*. **27**, S88-S90 (2004).
70. National Institute for Health and Care Excellence (2015): Diabetes in pregnancy: management from preconception to the postnatal period (NG3). (2015).
71. Blue, E. K., Digiuseppe, R., Derr-Yellin, E., Acosta, J. C., Pay, S. L., Hanenberg, H., Schellinger, M. M., Quinney, S. K., Mund, J. A., Case, J. & Haneline, L. S. Gestational diabetes induces alterations in the function of neonatal endothelial colony-forming cells. *Pediatr. Res.* **75**, 266–272 (2014).
72. Ingram, D. A., Lien, I. Z., Mead, L. E., Estes, M., Prater, D. N., Derr-Yellin, E., DiMeglio, L. A. & Haneline, L. S. In vitro hyperglycemia or a diabetic intrauterine environment reduces neonatal endothelial colony-forming cell numbers and function. *Diabetes*. **57**, 724–731 (2008).
73. World Health Organization. 10 Facts on Diabetes. (2016). Available at: https://www.who.int/features/factfiles/diabetes/en/ (Accessed: May, 2019).
74. World Health Organization. Diabetes (2019). Available at: https://www.who.int/diabetes/en/, 2019. (Accessed: May, 2019).
75. Kourgalis, N. & Keller, H. Diabetic Retinopathy- silently blinding millions of people worldwide. IAPB Vision Altas (2019). Available at: http://atlas.iapb.org/vision-trends/diabetic-retinopathy/ (Accessed: May, 2019).
76. ADA. Statistics About Diabetes. (2018). Available at: http://www.diabetes.org/diabetes-basics/statistics/. (Accessed: May, 2019).
77. World Health Organization. Obesity and overweight. (2018). Available at: https://www.who.int/en/news-room/fact-sheets/detail/obesity-and-overweight. (Accessed: May, 2019).
78. Golay, A. & Ybarra, J. Link between obesity and type 2 diabetes. *Best Pract. Res. Clin. Endocrinol. Metab*. **19**, 649–663 (2005).
79. Farag, Y. M. K. & Gaballa, M. R. Diabesity: An overview of a rising epidemic. *Nephrol. Dial. Transplant*. **26**, 28–35 (2011).
80. Mokdad, A. H., Ford, E. S. & Bowman, B. A. Prevalence of obesity, diabetes, and obesity-related health risk factors. *J. Am. Med. Assoc.* **289**, 76–79 (2001).
81. Kusminski, C. M., Bickel, P. E. & Scherer, P. E. Targeting adipose tissue in the treatment of obesity-associated diabetes. *Nat. Rev. Drug Discov*. **15**, 639–660 (2016).
82. Chapman, D., Foxcroft, R., Dale-Harris, L., Ronte, H., Bidgoli, F. & Bellary, S. Insights for Care: The Healthcare Utilisation and Cost Impact of Managing Type 2 Diabetes-Associated Microvascular Complications. *Diabetes Ther*. **10**, 575–585 (2019).
83. Diabetes.co.uk. Cost of Diabetes. (2019). Available at: https://www.diabetes.co.uk/cost-of-diabetes.html. (Accessed: May, 2019).
84. Farzi, A., Hassan, A. M., Zenz, G. & Holzer, P. Diabesity and mood disorders: Multiple links through the microbiota-gut-brain axis. *Mol. Aspects Med*. 1-14 (2018).
85. Diabetes.co.uk. Diabetes and Amputation. (2019). Available at: https://www.diabetes.co.uk/diabetes-and-amputation.html. (Accessed: May, 2019).
86. Kusuhara, S., Fukushima, Y., Ogura, S., Inoue, N. & Uemura, A. Pathophysiology of diabetic retinopathy: The old and the new. *Diabetes Metab. J.* **42**, 364–376 (2018).
87. WHO - World Health Organization. Definition and Diagnosis of Diabetes Mellitus and Intermediate Hyperglycemia. *Who2*. **50,** (2006).
88. Diabetes.co.uk. Guide to HbA1c. (2019). Available at: https://www.diabetes.co.uk/what-is-hba1c.html. (Accessed: May, 2019).
89. Burrill, J. S., Long, E. K., Reilly, B., Deng, Y., Armitage, I. M., Scherer, P. E. & Bernlohr, D. A. Inflammation and ER Stress Regulate Branched Chain Amino Acid Uptake and Metabolism in Adipocytes. *Molecular Endocrinology.* 1–11 (2015).
90. Evans, J. L., Goldfine, I. D., Maddux, B. A. & Grodsky, G. M. Oxidative stress and stress-activated signaling pathways: A unifying hypothesis of type 2 diabetes. *Endocr. Rev.* **23**, 599–622 (2002).
91. Amirkhizi, F., Siassi, F., Minaie, S., Djalali, M., Rahimi, A. & Chamari, M. Is obesity associated with increased plasma lipid peroxidation and oxidative stress in women? ARYA Atheroscler. **2**, 189–192 (2007).
92. Ozata, M., Mergen, M., Oktenli, C., Aydin, A., Sanisoglu, S. Y., Bolu, E., Yilmaz, M. I., Sayal, A., Isimer, A. & Ozdemir, I. C. Increased oxidative stress and hypozincemia in male obesity. *Clin. Biochem.* **35**, 627–631 (2002).

93. Gilbert, R. E. Endothelial Loss and Repair in the Vascular Complications of Diabetes. *Circ. J*. **77**, 849–856 (2013).
94. Aoki, M., Nata, T., Morishita, R., Matsushita, H., Nakagami, H., Yamamoto, K., Yamazaki, K., Nakabayashi, M., Ogihara, T. & Kaneda, Y. Endothelial Apoptosis Induced by Oxidative Stress Through Activation of NF-κB. *Hypertension* **38**, 48–55 (2012).
95. Nakagami, H., Morishita, R., Yamamoto, K., Yoshimura, S., Taniyama, Y., Aoki, M., Matsubara, H., Kim, S., Kaneda, Y. & Ogihara, T. Kinase Downstream of Bax-Caspase-3 Pathway Leads to Cell Death Induced by High D-Glucose in Human Endothelial Cells. *Diabetes*. **50**, 1472–1481 (2001).
96. Marseglia, L., Manti, S., D'Angelo, G., Nicotera, A., Parisi, E., Di Rosa, G., Gitto, E. & Arrigo, T. Oxidative Stress in Obesity: A Critical Component in Human Diseases. *Int. J. Mol. Sci.* **16**, 378–400 (2014).
97. Piconi, L., Quagliaro, L., Assaloni, R., Giugliano, D. & Szabo, C. & Ceriello, A. Intermittent high glucose enhances ICAM-1 , VCAM-1 , E-selectin and interleukin-6 expression in human umbilical endothelial cells in culture : the role of poly(ADP-ribose) polymerase. *J. of Thromb. & Haem.* **2.** 1453–1459 (2004).
98. Funatsu, H., Yamashita, H., Ikeda, T., Mimura, T., Eguchi, S. & Hori, S. Vitreous levels of interleukin-6 and vascular endothelial growth factor are related to diabetic macular edema. *Ophthalmology*. **110**, 1690–1696 (2003).
99. Stewart, M. W. Future Treatments of Diabetic Retinopathy : Pharmacotherapeutic Products Under Development. *European Medical Journal Diabetes.* 93–103 (2017).
100. Singh, V. P., Bali, A., Singh, N. & Jaggi, A. S. Advanced glycation end products and diabetic complications. *Korean J. Physiol.* Pharmacol. **18**, 1–14 (2014).
101. Div. of Diabetes Translation, National Centre for Chronic Disease Prevention and Health Promotion, C. Public Health Focus: Prevention of Blindness Associated with Diabetic Retinopathy. (1993). Available at: https://www.cdc.gov/mmwr/preview/mmwrhtml/00019889.htm. (Accessed: May, 2019).
102. Baharivand, N., Zarghami, N., Panahi, F., Yazdan Dokht Ghafari, M., Fard, A. M. & Mohajeri, A. Relationship between vitreous and serum vascular endothelial growth factor levels, control of diabetes and microalbuminuria in proliferative diabetic retinopathy. *Clin. Ophthalmol.* **6**, 185–191 (2012).
103. Homme, R. P., Singh, M., Majumder, A., George, A. K., Nair, K., Sandhu, H. S., Tyagi, N., Lominadze, D. & Tyagi, S. C. Remodeling of retinal architecture in diabetic retinopathy: Disruption of ocular physiology and visual functions by inflammatory gene products and pyroptosis. *Front. Physiol.* **9**, 1–18 (2018).
104. Eshaq, R. S., Aldalati, A. M. Z., Alexander, J. S. & Harris, N. R. Diabetic retinopathy: Breaking the barrier. *Pathophysiology.* **24**, 229–241 (2017).
105. Wong-riley, M. Energy Metabolism of the Visual System. *Eye and Brain*. **2,** 99–116 (2010).
106. Hammes, H.-P., Lin, J., Renner, O., Shani, M., Lundqvist, A., Betsholtz, C., Brownlee, M. & Deutsch, U. Pericytes and the pathogenesis of diabetic retinopathy. *Diabetes.* **51**, 3107–3112 (2002).
107. Stitt, A. W., Li, Y. M., Gardiner, T. A., Bucala, R., Archer, D. B. & Vlassara, H. Advanced glycation end products (AGEs) co-localize with AGE receptors in the retinal vasculature of diabetic and of AGE-infused rats. *Am. J. Pathol.* **150**, 523–31 (1997).
108. Safi, S. Z., Qvist, R., Kumar, S., Batumalaie, K. & Ismail, I. S. Bin. Molecular mechanisms of diabetic retinopathy, general preventive strategies, and novel therapeutic targets. *Biomed Res. Int.* 2014, (2014).
109. NICE. Managing blood pressure in adults with type 2 diabetes. (2019). Available at: https://pathways.nice.org.uk/pathways/type-2-diabetes-in-adults#path=view%3A/pathways/type-2-diabetes-in-adults/managing-blood-pressure-in-adults-with-type-2-diabetes.xml&content=view-node%3Anodes-blood-pressure-measurement-and-targets. (Accessed: May, 2019).
110. Knowler, W. C., Barrett-Connor, E., Fowler, S. E., Hamman, R. F., Lachin, J. M., Walker, E. A. & Nathan, D. M. Reduction in the incidence of type 2 diabetes with lifestyle intervention or metformin. *N. Engl. J. Med.* **346**, 393 (2002).
111. Ting, R.-D., Keech, A. C., Drury, P. L., Donoghoe, M. W., Hedley, J., Jenkins, A. J., Davis, T. M. E.,

Lehto, S., Celermajer, D., Simes, R. J., Rajamani, K. & Stanton, K. Benefits and Safety of Long-Term Fenofibrate Therapy in People With Type 2 Diabetes and Renal Impairment: The FIELD Study. *Diabetes Care.* **35**, 218–225 (2012).

112. de Boer, I. H., Bangalore, S., Benetos, A., Davis, A. M., Michos, E. D., Muntner, P., Rossing, P., Zoungas, S. & Bakris, G. Diabetes and Hypertension: A Position Statement by the American Diabetes Association. Diabetes Care. **40**, 1273–1284 (2017).
113. Blasiak, J., Petrovski, G., Veréb, Z., Facskó, A. & Kaarniranta, K. Oxidative stress, hypoxia, and autophagy in the neovascular processes of age-related macular degeneration. *Biomed Res. Int.* 2014, (2014).
114. Maritim, A. C., Sanders, R. A. & Watkins, J. B. Diabetes, oxidative stress, and antioxidants: *A review. J. Biochem. Mol. Toxicol*. **17**, 24–38 (2003).
115. Kowluru, R. A, Engerman, R. L. & Kern, T. S. Abnormalities of retinal metabolism in diabetes or experimental galactosemia VIII. Prevention by aminoguanidine. *Curr Eye Res.* **21**, 814–819 (2000).
116. NHS England. What is Diabetic Eye Screening? (2019). Available at: https://www.nhs.uk/conditions/diabetic-eye-screening/. (Accessed: May, 2019).
117. Public Health England. NHS Diabetic Eye Screening Programme Grading definitions for referable disease. **16** (2017).
118. Medina, R. J., O'neill, C. L., O'doherty, T. M., Chambers, S. E. J., Guduric-Fuchs, J., Neisen, J., Waugh, D. J., Simpson, D. a. & Stitt, A. W. Ex vivo expansion of human outgrowth endothelial cells leads to IL-8-mediated replicative senescence and impaired vasoreparative function. *Stem Cells.* **31**, 1657–1668 (2013).
119. Simo, R. & Hernandez, C. Novel approaches for treating diabetic retinopathy based on recent pathogenic evidence. *Progress in Retinal and Eye Research*. **48**, 160–180 (2015).
120. Manchester Royal Eye Hospital, Retinal Services. Information for patients. Macular Laser. NHS. 1–2 (2018).
121. Shalaby, A. K., Lewis, K., Bush, K., Meredith, P. R., Di Simplicio, S. & Lockwood, A. J. Licence to save: a UK survey of anti-VEGF use for the eye in 2015. *Eye.* **30**, 1404–1406 (2016).
122. Reich, O., Schmid, M. K., Rapold, R., Bachmann, L. M. & Blozik, E. Injections frequency and health care costs in patients treated with aflibercept compared to ranibizumab: New real-life evidence from Switzerland. *BMC Ophthalmol*. **17**, 1–8 (2017).
123. Hollingworth, W., Jones, T., Reeves, B. C. & Peto, T. A longitudinal study to assess the frequency and cost of antivascular endothelial therapy, and inequalities in access, in England between 2005 and 2015. *BMJ Open.* **7**, 1–10 (2017).
124. Tsang, S. H. Stem Cell Biology and Regenerative Medicine in Ophthalmology. (Human Press, 2013).
125. McAllister, I. L., Vijayasekaran, S., Chen, S. D. & Yu, D. Y. Effect of Triamcinolone Acetonide on Vascular Endothelial Growth Factor and Occludin Levels in Branch Retinal Vein Occlusion. *Am. J. Ophthalmol*. **147**, 838-846.e2 (2009).
126. Ho, F. M., Liu, S. H., Liau, C. S., Huang, P. J. & Lin-Shiau, S. Y. High glucose-induced apoptosis in human endothelial cells is mediated by sequential activations of c-JUN NH2-terminal kinase and caspase-3. *Circulation*. **101**, 2618–2624 (2000).
127. Risso, A., Mercuri, F., Quagliaro, L., Damante, G. & Ceriello, A. Intermittent high glucose enhances apoptosis in human umbilical vein endothelial cells in culture. *Am. J. Physiol. Metab.* **281**, E924–E930 (2001).
128. Millipore, M. Millicell® inserts and plates. For microporous membrane-based cell culture (EMD Millipore Corporation, 2014).
129. Battiston, K. G., Cheung, J. W. C., Jain, D. & Santerre, J. P. Biomaterials Biomaterials in co-culture systems : Towards optimizing tissue integration and cell signaling within scaffolds. *Biomaterials*. **35**, 4465–4476 (2014).
130. Kumar, R., Harris-hooker, S., Kumar, R. & Sanford, G. Co-culture of Retinal and Endothelial Cells Results in the Modulation of Genes Critical to Retinal Neovascularization. *Vasc. Cell.* **3**, 27 (2011).
131. Tarallo, S., Beltramo, E., Berrone, E. & Porta, M. Human pericyte – endothelial cell interactions in co-culture models mimicking the diabetic retinal microvascular environment. *Acta Diabetol*. **49**, (2012).

132. Walshe, T. E., Connell, P., Cryan, L., Ferguson, G., Gardiner, T., Morrow, D., Redmond, E. M., O'Brien, C. & Cahill, P. A. Microvascular retinal endothelial and pericyte cell apoptosis in vitro: Role of hedgehog and notch signaling. *Investig. Ophthalmol. Vis. Sci.* **52**, 4472–4483 (2011).
133. Hatherell, K., Couraud, P. O., Romero, I. A., Weksler, B. & Pilkington, G. J. Development of a three-dimensional, all-human in vitro model of the blood-brain barrier using mono-, co-, and tri-cultivation Transwell models*. J. Neurosci. Methods*. **199**, 223–229 (2011).
134. Pan, C., Kumar, C., Bohl, S., Klingmueller, U. & Mann, M. Comparative Proteomic Phenotyping of Cell Lines and Primary Cells to Assess Preservation of Cell Type-specific Functions. *Mol. Cell. Proteomics*. **8**, 443–450 (2009).
135. Gaillard, P. J., Voorwinden, L. H., Nielsen, J. L., Ivanov, A., Atsumi, R., Engman, H., Ringbom, C., De Boer, A. G. & Breimer, D. D. Establishment and functional characterization of an in vitro model of the blood-brain barrier, comprising a co-culture of brain capillary endothelial cells and astrocytes. *Eur. J. Pharm. Sci*. **12**, 215–222 (2000).
136. Srinivasan, B., Kolli, A. R., Esch, M. B., Abaci, H. E., Shular, M. L. & Hickman, J. J. TEER measurement techniques for in vitro barrier model systems. *J Lab Autom.* **20**, 107–126 (2015).
137. Grainger, S. J. & Putnam, A. J. Assessing the permeability of engineered capillary networks in a 3D culture. *PLoS One.* **6**, (2011).
138. Asahara, T., Murohara, T., Sullivan, A., Silver, M., van Der Zee, R., Li, T., Witzenbichler, B., Schatteman, G. & Isner, J. M. Isolation of putative progenitor endothelial cells for angiogenesis. *Science.* **275**, 964–7 (1997).
139. Shantsila, E., Watson, T. & Lip, G. Y. H. Endothelial Progenitor Cells in Cardiovascular Disorders. *J. Am. Coll. Cardiol.* **49**, 741–752 (2007).
140. Neill, C. L. O., Mcloughlin, K. J., Chambers, S. E. J., Guduric-fuchs, J., Stitt, A. W. & Medina, R. J. The Vasoreparative Potential of Endothelial Colony Forming Cells : A Journey Through Pre-clinical Studies. *Front. Med.* **5**, 1–9 (2018).
141. Lin, Y., Weisdorf, D. J., Solovey, A. & Hebbel, R. P. Origins of circulating endothelial cells and endothelial outgrowth from blood.. *J Clin Invest.* **105**, 71–77 (2000).
142. Basile, D. P. & Yoder, M. C. Circulating and tissue resident endothelial progenitor cells. *J. Cell. Physiol.* **229**, 10–6 (2014).
143. Peichev, M., Naiyer, A. J., Pereira, D., Zhu, Z., Lane, W. J., Williams, M., Oz, C., Hicklin, D. J., Witte, L., Moore, M. A. S., Rafii, S. & Oz, M. C. Expression of VEGFR-2 and AC133 by circulating human CD34 + cells identifies a population of functional endothelial precursors. *Blood.***95,** 952–958 (2000).
144. Ingram, D. A, Mead, L. E., Tanaka, H., Meade, V., Fenoglio, A., Mortell, K., Pollok, K., Ferkowicz, M. J., Gilley, D., Yoder, M. C., Institutional, T., Board, R., Island, G. & Mesa, C. Identification of a novel hierarchy of endothelial progenitor cells using human peripheral and umbilical cord blood. *Blood.* **104**, 2752–2760 (2004).
145. Hofer-Warbinek, R., Sturtzel, C., Preisegger, K.-H. & Hofer, E. Endothelial Progenitor Cells Derived from Cord or Peripheral Blood and Their Potential for Regenerative Therapies. *Adult Pluripotent Stem Cells.* 37–51 (2014).
146. Yoder, M. C. Endothelial stem and progenitor cells (Stem cells): (2017 Grover Conference Series). *Pulm. Circ.* **8**, (2018).
147. Hill, J. M., Zalos, G., Halcox, J. P. J., Schenke, W. H., Waclawiw, M. A., Quyyumi, A. A. & Finkel, T. Circulating Endothelial Progenitor Cells, Vascular Function, and Cardiovascular Risk. *N. Engl. J. Med.* **348**, 593–600 (2003).
148. Gaillard, P. J., Voorwinden, L. H., Nielsen, J. L., Ivanov, A., Atsumi, R., Engman, H., Ringbom, C., De Boer, A. G. & Breimer, D. D. Establishment and functional characterization of an in vitro model of the blood-brain barrier, comprising a co-culture of brain capillary endothelial cells and astrocytes. *Eur. J. Pharm. Sci.* **12**, 215–222 (2001).
149. Ingram, D. A., Mead, L. E., Moore, D. B., Woodard, W., Fenoglio, A. & Yoder, M. C. Vessel wall–derived endothelial cells rapidly proliferate because they contain a complete hierarchy of endothelial progenitor cells. *Blood*. **105**, 2783–2786 (2005).
150. Yoder, M. C. Human endothelial progenitor cells. *Cold Spring Harb. Perspect. Med.* **2**, 1–14 (2012).
151. Fadini, G. P., Losordo, D. & Dimmeler, S. Critical re-evaluation of endothelial progenitor cell phenotypes for therapeutic and diagnostic use. *Circ. Res.* **110**, 624–637 (2012).

152. Hur, J., Yoon, C. H., Kim, H. S., Choi, J. H., Kang, H. J., Hwang, K. K., Oh, B. H., Lee, M. M. & Park, Y. B. Characterization of Two Types of Endothelial Progenitor Cells and Their Different Contributions to Neovasculogenesis. *Arterioscler. Thromb. Vasc. Biol*. **24**, 288–293 (2004).
153. Medina, R. J., O'Neill, C. L., Humphreys, M. W., Gardiner, T. a. & Stitt, A. W. Outgrowth endothelial cells: Characterization and their potential for reversing ischemic retinopathy. *Investig. Ophthalmol. Vis. Sci.* **51**, 5906–5913 (2010).
154. Yoder, M. C., Mead, L. E., Prater, D., Krier, T. R., Mroueh, K. N., Li, F., Temm, C. J., Prchal, J. T., Ingram, D. A., Dc, W. & Krasich, R. Redefining endothelial progenitor cells via clonal analysis and hematopoietic stem/progenitor cell principals. *Blood.* **109**, 1801–1809 (2007).
155. Medina, R. J., Barber, C. L., Sabatier, F., Dignat-George, F., Melero-Martin, J. M., Khosrotehrani, K., Ohneda, O., Randi, A. M., Chan, J. K., Yamaguchi, T., van Hinsbergh, V. W. M., Yoder, M. C. & Stitt, A. W. Endothelial Progenitors : A Consensus Statement on Nomenclature. *Stem Cells Transl. Med.* **6**, 1316–1320 (2017).
156. Fadini, G. P., Miorin, M., Facco, M., Bonamico, S., Baesso, I., Grego, F., Menegolo, M., de Kreutzenberg, S. V., Tiengo, A., Agostini, C. & Avogaro, A. Circulating endothelial progenitor cells are reduced in peripheral vascular complications of type 2 diabetes mellitus. *J. Am. Coll. Cardiol.* **45**, 1449–57 (2005).
157. Lois, N., McCarter, R. V., O'Neill, C., Medina, R. J. & Stitt, A. W. Endothelial Progenitor Cells in Diabetic Retinopathy. *Front. Endocrinol.* **5**, 1–11 (2014).
158. Massa, M., Rosti, V., Ferrario, M., Campanelli, R., Ramajoli, I., Rosso, R., De Ferrari, G. M., Ferlini, M., Goffredo, L., Bertoletti, A., Klersy, C., Pecci, A., Moratti, R. & Tavazzi, L. Increased circulating hematopoietic and endothelial progenitor cells in the early phase of acute myocardial infarction. *Blood*. **105**, 199–206 (2005).
159. Heeschen, C., Lehmann, R., Honold, J., Assmus, B., Aicher, A., Walter, D. H., Martin, H., Zeiher, A. M. & Dimmeler, S. Profoundly Reduced Neovascularization Capacity of Bone Marrow Mononuclear Cells Derived from Patients with Chronic Ischemic Heart Disease. *Circulation.* **109**, 1615–1622 (2004).
160. Banerjee, M. N., Bolli, R. & Hare, J. M. Clinical studies of cell therapy in cardiovascular medicine recent developments and future directions. *Circ. Res.* **123**, 266–287 (2018).
161. Lucas, T., Abraham, D., Untergasser, G., Zins, K., Hofer, E., Gunsilius, E. & Aharinejad, S. Adenoviral-mediated endothelial precursor cell delivery of soluble CD115 suppresses human prostate cancer xenograft growth in mice. *Stem Cells.* **27**, 2342–2352 (2009).
162. Hendrickx, B., Verdonck, K., Van Den Berge, S., Dickens, S., Eriksson, E., Vranckx, J. J. & Luttun, A. Integration of blood outgrowth endothelial cells in dermal fibroblast sheets promotes full thickness wound healing. *Stem Cells*. **28**, 1165–1177 (2010).
163. Banno, K. & Yoder, M. C. Tissue regeneration using endothelial colony-forming cells: Promising cells for vascular repair. *Pediatr. Res*. 1–8 (2017).
164. Schallmoser, K., Bartmann, C., Rohde, E., Reinisch, A. & Kashofer, K. Human platelet lysate can replace fetal bovine serum for clinical-scale expansion of functional mesenchymal stromal cells. *Transplantation & Cellular Engineering*. **47**, 1436–1446 (2007).
165. Ferratge, S., Ha, G., Carpentier, G., Arouche, N., Bascetin, R., Muller, L., Germain, S. & Uzan, G. Initial clonogenic potential of human endothelial progenitor cells is predictive of their further properties and establishes a functional hierarchy related to immaturity. *Stem Cell Res*. **21**, 148–159 (2017).
166. He, T., Peterson, T. E., Holmuhamedov, E. L., Terzic, A., Caplice, N. M., Oberley, L. W. & Katusic, Z. S. Human endothelial progenitor cells tolerate oxidative stress due to intrinsically high expression of manganese superoxide dismutase. *Arterioscler. Thromb. Vasc. Biol.* **24**, 2021–2027 (2004).
167. O'Neill, C. L., O'Doherty, M. T., Wilson, S. E., Rana, A. A., Hirst, C. E., Stitt, A. W. & Medina, R. J. Therapeutic revascularisation of ischaemic tissue: The opportunities and challenges for therapy using vascular stem/progenitor cells. *Stem Cell Res. Ther.* **3**, 1–7 (2012).
168. Stitt, A., O'Neill, C. & O'Doherty, M. Vascular stem cells and ischaemic retinopathies. *Prog. Retin.* **30**, 149–166 (2011).
169. Hookham, M. B., Ali, I. H. A., O'Neill, C. L., Hackett, E., Lambe, M. H., Schmidt, T., Medina, R. J., Chamney, S., Rao, B., McLoone, E., Sweet, D., Stitt, A. W. & Brazil, D. P. Hypoxia-induced responses by endothelial colony-forming cells are modulated by placental growth factor. *Stem*

Cell Res. Ther. **7**, 1–12 (2016).
170. Reid, E., Guduric-Fuchs, J., O'Neill, C. L., Allen, L. D., Chambers, S. E. J., Stitt, A. W. & Medina, R. J. Preclinical Evaluation and Optimization of a Cell Therapy Using Human Cord Blood-Derived Endothelial Colony-Forming Cells for Ischemic Retinopathies. *Stem Cells Transl. Med.* **7**, 59–67 (2018).
171. O'Neill, K. M. Campbell, D. C., Edgar, K. S., Gill, E. K., Moez, A., McLoughlin, K. J., O-Neill, C. L., Dellett,. M., Hargey, C. J., Abudola, R. A., O'Hare, M., Doyle, P., Toh, T., Khoo, J., Wong, J., McCrudden, C. M., Meloni, M., Brunssen, C., Morawietz, H., Yoder, M. C., McDonald, D. M., Watson, C. J., Stitt, A. W., Margarita,A., Medina, R. J. & Grieve, D. J. NOX4 is a major regulator of cord blood-derived endothelial colony-forming cells which promotes post-ischaemic revascularization. *Cardiovasc. Res.* **44**, (2019).
172. Medina, R. J., O'Neill, C. L., O'Doherty, T. M., Wilson, S. E. J. & Stitt, A. W. Endothelial Progenitors as Tools to Study Vascular Disease. *Stem Cells Int.* **2012**, 1–5 (2012).
173. Colombo, E., Calcaterra, F., Cappelletti, M., Mavilio, D. & Della Bella, S. Comparison of Fibronectin and Collagen in Supporting the Isolation and Expansion of Endothelial Progenitor Cells from Human Adult Peripheral Blood. *PLoS One.* **8**, (2013).
174. Shih, I. L., Shen, M. H. & Van, Y. T. Microbial synthesis of poly(ε-lysine) and its various applications. *Bioresour. Technol.* **97**, 1148–1159 (2006).
175. Shima, S. & Sakai, H. Department of Agricultural Chemistry, College of Agriculture, University of Osaka Prefecture, Sakai, Japan. *Communication.* **41**, 1807–1809 (1977).
176. Nishikawa, M. & Ogawa, K. Inhibition of epsilon-poly-L-lysine biosynthesis in Streptomycetaceae bacteria by short-chain polyols. *Appl. Environ. Microbiol.* **72**, 2306–2312 (2006).
177. Chheda, A. H. & Vernekar, M. R. A natural preservative ε-poly-L-lysine: Fermentative production and applications in food industry. *Int. Food Res. J.* **22**, 23–30 (2015).
178. Wen, Q. & Dong, Y. *Gels Handbook- Fundamental, Properties and Applications. Volume 1: Fundamentals of Hydrogels*. (World Scientific, 2016).
179. Gallagher, A. G., Alorabi, J. A., Wellings, D. A., Lace, R., Horsburgh, M. J. & Williams, R. L. A Novel Peptide Hydrogel for an Antimicrobial Bandage Contact Lens. *Adv. Healthc. Mater.* **5**, 2013–2018 (2016).
180. Pierschbacher, M. D. & Ruoslahti, E.Cell Attachment Activity of Fibronectin Can Be Duplicated By Small Synthetic Fragments of the Molecule. *Nature.* **309**, 3–6 (1984).
181. D'Souza, S. E., Ginsberg, M. H. & Plow, E. F. Arginyl-glycyl-aspartic acid (RGD): a cell adhesion motif. *Trends Biochem. Sci.* **16**, 246–250 (1991).
182. Ruoslahti, E. RGD and other recognition sequences for integrins. *Annu. Rev. Cell Dev. Biol.* **12**, 697–715 (1996).
183. Hersel, U., Dahmen, C. & Kessler, H. RGD modified polymers : biomaterials for stimulated cell adhesion and beyond. *Biomaterials*. **24**, 4385–4415 (2003).
184. Chollet, C., Chanseau, C., Remy, M., Guignandon, A., Bareille, R., Labrugère, C., Bordenave, L. & Durrieu, M. C. The effect of RGD density on osteoblast and endothelial cell behavior on RGD-grafted polyethylene terephthalate surfaces. *Biomaterials* **30**, 711–720 (2009).
185. Seeto, W. J., Tian, Y. & Lipke, E. A. Peptide-grafted poly(ethylene glycol) hydrogels support dynamic adhesion of endothelial progenitor cells. *Acta Biomater.* **9**, 8279–8289 (2013).
186. Bota, P. C. S., Collie, A. M. B., Puolakkainen, P., Vernon, R. B., Sage, H. S., Ratne, B. D. & Stayton, P. S. Biomaterial Topography Alters Healing In Vivo and Monocyte/ Macrophage Activation In Vitro. *J Biomed Mater Res A.* **95**, 649–657 (2010).
187. Lace, R., Murray-Dunning, C. & Williams, R. Biomaterials for ocular reconstruction. *J. Mater. Sci.* **50**, 1523–1534 (2014).
188. Gallagher, A. G., McLean, K., Stewart, R. M. K., Wellings, D. A., Allison, H. E. & Williams, R. L. Development of a poly-ε-lysine contact lens as a drug delivery device for the treatment of fungal keratitis. *Investig. Ophthalmol. Vis. Sci.* **58**, 4499–4505 (2017).
189. SpheriTech. Polymeric Microspheres For Peptide Synthesis And Immobilisation. (2018). Available at: https://spheritech.com/polymeric-microspheres-synthesis-immobilisation/. (Accessed: May, 2019).
190. Park, T. I. H., Feisst, V., Brooks, A. E. S., Rustenhoven, J., Monzo, H. J., Feng, S. X., Mee, E. W., Bergin, P. S., Oldfield, R., Graham, E. S., Curtis, M. A., Faull, R. L. M., Dunbar, P. R. & Dragunow,

M. Cultured pericytes from human brain show phenotypic and functional differences associated with differential CD90 expression. *Sci. Rep.* **6**, 1–17 (2016).
191. Kashyap, M. V, Ranjan, A. P., Shankardas, J. & Vishwanatha, J. K. Establishment of Human Retinal Microvascular Endothelial Cells with Extended Life-span. *In Vivo*. **27**, 685–694 (2013).
192. Bonkowski, D., Katyshev, V., Balabanov, R. D., Borisov, A. & Dore-duffy, P. The CNS microvascular pericyte : pericyte-astrocyte crosstalk in the regulation of tissue survival. *Fluids & Barriers of the CNS.* **8**, 1–12 (2011).
193. Rodier, F. & Campisi, J. Four faces of cellular senescence. *J. Cell Biol*. **192**, 547–556 (2011).
194. Nachman, R. L. & Jaffe, E. A. Endothelial cell culture: Beginnings of modern vascular biology. *J. Clin. Invest*. **114**, 1037–1040 (2004).
195. Solomon, I., O-Reilly, M., Ionescu, L., Alphonse, Rajesh, S., Rajabali, S., Zhong, S., Vadivel, A., Shelley, C. W., Yoder, M. C. & Thebaud, B. Functional Differences Between Placental Micro- and Macrovascular Endothelial Colony-Forming Cells. *Transl. Med.* **5**, 291–300 (2016).
196. Folkman, J., Haudenschild, C. C. & Zetter, B. R. Long-term culture of capillary endothelial cells. *Proc. Natl. Acad. Sci.* **76**, 5217–5221 (2006).
197. Cao, Y., Feng, B., Chen, S., Chu, Y. & Chakrabarti, S. Mechanisms of endothelial to mesenchymal transition in the retina in diabetes. *Investig. Ophthalmol. Vis. Sci.* **55**, 7321–7331 (2014).
198. Coll-Bonfill, N., Musri, M. M., Ivo, V., Barberà, J. A. & Tura-Ceide, O. Trans-differentiation of endothelial cells to smooth muscle cells play an important role in vascular remodelling. *Am. J. Stem Cells.* **4**, 13–21 (2015).
199. Hayashi, K., Nakao, S., Nakaoke, R., Nakagawa, S., Kitagawa, N. & Niwa, M. Effects of hypoxia on endothelial/pericytic co-culture model of the blood-brain barrier. *Regul. Pept.* **123**, 77–83 (2004).
200. Nakagawa, S., Deli, M. A., Nakao, S., Honda, M., Hayashi, K., Nakaoke, R., Niwa, M. & Kataoka, Y. Pericytes from Brain Microvessels Strengthen the Barrier Integrity in Primary Cultures of Rat Brain Endothelial Cells. *Cell. Mol. Neurobiol.* **27**, 687–694 (2007).
201. Armulik, A., Genove, G. & Betsholtz, C. Pericytes : Developmental, Physiological, and Pathological Perspectives, Problems, and Promises. *Dev. Cell.* **21**, 193–215 (2011).
202. Verbeek, M. M., Otte-Holler, I., Wesseling, P., Ruiter, D. J. & de Waal, R. M. Induction of alpha-smooth muscle actin expression in cultured human brain pericytes by transforming growth factor-beta 1. *Am. J. Pathol*. **144**, 372–382 (1994).
203. Chen, J., Luo, Y., Hui, H., Cai, T., Huang, H., Yang, F., Feng, J., Zhang, J. & Yan, X. CD146 coordinates brain endothelial cell–pericyte communication for blood–brain barrier development. *Proc. Natl. Acad. Sci.* **114**, E7622–E7631 (2017).
204. Blocki, A., Wang, Y., Koch, M., Peh, P., Beyer, S., Law, P., Hui, J. & Raghunath, M. Not All MSCs Can Act as Pericytes: Functional In Vitro Assays to Distinguish Pericytes from Other Mesenchymal Stem Cells in Angiogenesis. *Stem Cells Dev*. **22**, 2347–2355 (2013).
205. Pfister, F., Przybyt, E. & Harmsen, M. C. Pericytes in the eye. *Eur J Physiol.* **465**. 789–796 (2013).
206. Stratman, A. N., Malotte, K. M., Mahan, R. D., Davis, M. J. & Davis, G. E. Pericyte recruitment during vasculogenic tube assembly stimulates endothelial basement membrane matrix formation. *Blood.* **114**, 5091–5102 (2009).
207. Zouani, O. F., Lei, Y. & Durrieu, M. Pericytes, Stem-Cell-Like Cells, but not Mesenchymal Stem Cells are Recruited to Support Microvascular Tube Stabilization. *Small.* **9**, 3070-3075 (2013).
208. Urich, E., Patsch, C., Aigner, S., Graf, M., Iacone, R. & Freskgård, P. O. Multicellular self-assembled spheroidal model of the blood brain barrier. *Sci. Rep.* **3**, (2013).
209. Hall, C. N., Reynell, C., Gesslein, B., Hamilton, N. B., Mishra, A., Sutherland, B. A., O' Farrell, F. M., Buchan, A. M., Lauritzen, M. & Attwell, D. Capillary pericytes regulate cerebral blood flow in health and disease. *Nature.* **508**, 55–60 (2014).
210. NICE Guidelines. Type 2 diabetes in adults: management. (2017). Available at: https://www.nice.org.uk/guidance/ng28. (Accessed: May, 2019).
211. Nyengaard, J. R., Ido, Y., Kilo, C. & Williamson, J. R. Interactions Between Hyperglycaemia and Hypoxia- Implications for Diabetic Retinopathy. *Diabetes.* **53**, 2931–2938 (2004).
212. Amano, S., Yamagishi, S., Inagaki, Y. & Nakamura, K. Pigment epithelium-derived factor inhibits oxidative stress-induced apoptosis and dysfunction of cultured retinal pericytes. *Microvascular Res*. **69**, 45–55 (2005).
213. Trudeau, K., Molina, A. J. A. & Roy, S. High Glucose Induces Mitochondrial Morphology and

Metabolic Changes in Retinal Pericytes. *Invest. Ophthalmol. Vis. Sci.* **52**, 8657–8664 (2011).
214. Giebel, S. J., Menicucci, G., McGuire, P. G. & Das, A. Matrix metalloproteinases in early diabetic retinopathy and their role in alternation of the blood-retinal barrier. *Lab. Investig.* **85**, 597–607 (2005).
215. Romeo, G., Liu, W., Asnaghi, V., Kern, T. S. & Lorenzi, M. Activation of Nuclear Factor-kB Induced by Diabetes and High Glucose Regulates a Proapoptotic Program in Retinal Pericytes. *Diabetes*. **51**, 2241-2248 (2002).
216. Zhong, Y., Wang, J. J. & Zhang, S. X. Intermittent But Not Constant High Glucose Induces ER Stress and Infl ammation in Human Retinal Pericytes. *Retinal Degenerative Diseases*. 285–292 (2012).
217. Ivanovic, Z. Hypoxia or in situ normoxia: The stem cell paradigm. *J. Cell. Physiol.* **219**, 271–275 (2009).
218. Li, S.-Y., Fu, Z. J. & Lo, A. C. Y. Hypoxia-Induced Oxidative Stress in Ischemic Retinopathy. *Oxid. Med. Cell. Longev*. **2012**, 1–10 (2012).
219. Antonetti, D. A., Barber, A. J., Bronson, S. K., Freeman, W. M., Gardner, T. W., Jefferson, L. S., Kester, M., Kimball, S. R., Krady, J. K., LaNoue, K. F., Norbury, C. C., Quinn, P. G., Sandirasegarane, L. & Simpson, I. A. Diabetic Retinopathy: Seeing Beyond Glucose-Induced Microvascular Disease. *Diabetes.* **55**, 2401–2411 (2006).
220. Packer, L. & Fuehr, K. Low oxygen concentration extends the lifespan of cultured human diploid cells. *Nature.* **267**, 423–425 (1977).
221. Jagannathan, L., Cuddapah, S. & Costa, M. Oxidative Stress Under Ambient and Physiological Oxygen Tension in Tissue Culture. *Curr. Pharmacol. Reports.* **2**, 64–72 (2016).
222. Grzelak, A., Rychlik, B. & Bartosz, G. Reactive oxygen species are formed in cell culture media. *Acta Biochim*. **47**, 1197–1198 (2000).
223. Carreau, A., Hafny-Rahbi, B. El, Matejuk, A., Grillon, C. & Kieda, C. Why is the partial oxygen pressure of human tissues a crucial parameter? Small molecules and hypoxia. *J. Cell. Mol. Med.* **15**, 1239–1253 (2011).
224. Semenza, G. L. Hypoxia-inducible factor 1: Master regulator of O2 homeostasis. *Curr. Opin. Genet. Dev.* **8**, 588–594 (1998).
225. Zelko, I. N., Mariani, T. J. & Folz, R. J. superoxide dismutase multigene family: a comparison of the CuZn-SOD (SOD1), Mn-SOD (SOD2), and EC-SOD (SOD3) gene structures, evolution, and expression. *Free Radic. Biol. Med.* **33**, 337–349 (2002).
226. Kowluru, R. A., Kowluru, V., Xiong, Y. & Ho, Y. S. Overexpression of mitochondrial superoxide dismutase in mice protects the retina from diabetes-induced oxidative stress. *Free Radic. Biol. Med.* **41**, 1191–1196 (2006).
227. Roy, S., Jiang, J. X., Li, A. F. & Kim, D. Connexin channel and its role in diabetic retinopathy. *Prog. Retin. Eye Res.* **61**, 35–59 (2017).
228. Janssen-Beinhold, U., Dermietzel, R. & Weiler, R. Distribution of Connexin43 Immunoreactivity in the Retinas. *J. Comp. Neurol.* **396**, 310–321 (1998).
229. Roy, S., Kim, D. & Lim, R. Cell-cell communication in diabetic retinopathy. *Vision Res.* **139**, 115–122 (2017).
230. Gardner, T. W., Lieth, E., Khin, S. A., Barber, A. J., Bonsall, D. J., Lesher, T., Rice, K. & Brennan, W. A. Astrocytes increase barrier properties and ZO-1 expression in retinal vascular endothelial cells. *Investig. Ophthalmol. Vis. Sci*. **38**, 2423–2427 (1997).
231. Dohgu, S., Takata, F., Yamauchi, A., Nakagawa, S., Egawa, T., Naito, M., Tsuruo, T., Sawada, Y., Niwa, M. & Kataoka, Y. Brain pericytes contribute to the induction and up-regulation of blood-brain barrier functions through transforming growth factor-β production. *Brain Res*. **1038**, 208–215 (2005).
232. Beaulieu Leclerc, V., Roy, O., Santerre, K. & Proulx, S. TGF-β1 promotes cell barrier function upon maturation of corneal endothelial cells. *Sci. Rep*. **8**, 1–15 (2018).
233. Neng, L., Zhang, F., Kachelmeier, A. & Shi, X. Endothelial cell, pericyte, and perivascular resident macrophage-type melanocyte interactions regulate cochlear intrastrial fluid-blood barrier permeability. *JARO - J. Assoc. Res. Otolaryngol*. **14**, 175–185 (2013).
234. Goers, L., Freemont, P. & Polizzi, K. M. Co-culture systems and technologies: taking synthetic biology to the next level. *J. R. Soc. Interface.* **11**, 1–13 (2014).
235. Busik, J. V., Mohr, S. & Grant, M. B. Hyperglycaemia-Induced reactive oxygen species toxicity

to endothelial cells is dependent on paracrine mediators. *Diabetes.* **57**, 1952–1965 (2008).
236. Campochiaro, P. A. & Peters, K. G. Targeting Tie-2 for Treatment of Diabetic Retinopathy and Diabetic Macular Edema. *Curr. Diab. Rep.* **16**, (2016).
237. Park, S. W., Yun, J., Kim, J. H., Kim, K., Cho, C. & Kim, J. H. Angiopoietin 2 Induces Pericyte Apoptosis via α3β1 Integrin Signalling in Diabetic Retinopathy. *Diabetes*. **63**, 3057–3068 (2014).
238. Balaban, Y. H., Sumer, H., Simsek, H., Us, D. & Tatar, G. Metabolic syndrome, non-alcoholic steatohepatitis (NASH), and hepatocyte growth factor (HGF). *Ann Hepatol.* **5**, 109–114 (2006).
239. Oliveira, A. G., Araújo, T. G., Carvalho, B. de M., Rocha, G. Z., Santos, A. & Saad, M. J. A. The Role of Hepatocyte Growth Factor (HGF) in Insulin Resistance and Diabetes. *Front. Endocrinol.* **9**, 1–10 (2018).
240. Cai, W., Rook, S. L., Jiang, Z. Y., Takahara, N. & Aiello, L. P. Mechanisms of Hepatocyte Growth Factor – Induced Retinal Endothelial Cell Migration and Growth. *IOVS.* **41**, 1885–1893 (2000).
241. Hiratsuka, A., Adachi, H., Fujiura, Y., Yamagishi, S. I., Hirai, Y., Enomoto, M., Satoh, A., Hino, A., Furuki, K. & Imaizumi, T. Strong association between serum hepatocyte growth factor and metabolic syndrome. *J. Clin. Endocrinol. Metab.* **90**, 2927–2931 (2005).
242. Nishimura, M., Ikeda, T., Ushiyama, M., Nanbu, A., Kinoshita, S. & Yoshimura, M. Increased vitreous concentrations of human hepatocyte growth factor in proliferative diabetic retinopathy. *J. Clin. Endocrinol. Metab.* **84**, 659–662 (1999).
243. Baggiolini, M., Clark-lcwisb, I. & Iturirtrrr, T. A chemotactic and inflammatory. *Fed. Eur. Biochem. Soc.* **307**, 97–101 (1992).
244. Cimini, F. A., Barchetta, I., Porzia, A., Mainiero, F., Costantino, C., Bertoccini, L., Ceccarelli, V., Morini, S., Baroni, M. G., Lenzi, A. & Cavallo, M. G. Circulating IL-8 levels are increased in patients with type 2 diabetes and associated with worse inflammatory and cardiometabolic profile. *Acta Diabetol.* **54**, 961–967 (2017).
245. Lan, C. C. E., Wu, C. S., Huang, S. M., Wu, I. H. & Chen, G. S. High-Glucose environment enhanced oxidative stress and increased interleukin-8 secretion from keratinocytes. *Diabetes.* **62**, 2530–2538 (2013).
246. Castruita-De la Rosa, C., Garza-Veloz, I., Cardenas-Vargas, E., Castaneda-Miranda, R., Solis-Sanchez, L. O., Ortiz-Rodriguez, J. M., Vega-Carrillo, H. R., Martinez-Blanco, M. R., Fllores-Morales, V., Hernandez-Delgadillo, G. P., Badillo-Almaraz, J. I. & Martinez-Fierro, M. L. Biological Activity and Implications of the Metalloproteinases in Diabetic Foot Ulcers. *Intech open.* 169-190 (2017).
247. Roy, S., Ha, J., Trudeau, K. & Beglova, E. Vascular basement membrane thickening in diabetic retinopathy. *Curr. Eye Res.* **35**, 1045–1056 (2010).
248. Vranes, D., Cooper, M. E. & Dilley, R. J. Cellular mechanisms of diabetic vascular hypertrophy. *Microvasc. Res.* **57**, 8–18 (1999).
249. Ayuk, S. M., Abrahamse, H. & Houreld, N. N. The Role of Matrix Metalloproteinases in Diabetic Wound Healing in relation to Photobiomodulation. *J. Diabetes Res.* **2016**, 1–9 (2016).
250. Murphy, A. N., Unsworth, E. J. & Stetler-Stevenson, W. G. Tissue inhibitor of metalloproteinases-2 inhibits bFGF-induced human microvascular endothelial cell proliferation. *J. Cell. Physiol.* **157**, 351–358 (1993).
251. Derosa, G., D'Angelo, A., Tinelli, C., Devangelio, E., Consoli, A., Miccoli, R., Penno, G., Del Prato, S., Paniga, S. & Cicero, A. F. G. Evaluation of metalloproteinase 2 and 9 levels and their inhibitors in diabetic and healthy subjects. *Diabetes Metab.* **33**, 129–134 (2007).
252. Lobmann, R., Ambrosch, A., Schultz, G., Waldmann, K., Schiweck, S. & Lehnert, H. Expression of matrix-metalloproteinases and their inhibitors in the wounds of diabetic and non-diabetic patients. *Diabetologia* **45**, 1011–1016 (2002).
253. Jayashree, K., Yasir, M., Senthilkumar, G. P., Ramesh Babu, K., Mehalingam, V. & Mohanraj, P. S. Circulating matrix modulators (MMP-9 and TIMP-1) and their association with severity of diabetic retinopathy. *Diabetes Metab. Syndr. Clin. Res. Rev.* **12**, 869–873 (2018).
254. Yuen, D. A., Zhang, Y., Thai, K., Spring, C., Chan, L., Guo, X., Advani, A., Sivak, J. M. & Gilbert, R. E. Angiogenic Dysfunction in Bone Marrow-Derived Early Outgrowth Cells from Diabetic Animals Is Attenuated by SIRT1 Activation. *Stem Cells Transl. Med.* **1**, 921–926 (2012).
255. Meleth, A. D., Agrón, E., Chan, C. C., Reed, G. F., Arora, K., Byrnes, G., Csaky, K. G., Ferris, F. L. & Chew, E. Y. Serum inflammatory markers in diabetic retinopathy. *Investig. Ophthalmol. Vis.*

Sci. **46**, 4295–4301 (2005).
256. Scheller, J., Chalaris, A., Schmidt-Arras, D. & Rose-John, S. The pro- and anti-inflammatory properties of the cytokine interleukin-6. *Biochim. Biophys. Acta.* **1813**, 878–88 (2011).
257. Donath, M. Y. & Shoelson, S. E. Type 2 diabetes as an inflammatory disease. *Nat. Rev. Immunol.* **11**, 98–107 (2011).
258. Goksen, S., Balabanli, B. & Coskun-Cevher, S. Application of platelet derived growth factor-BB and diabetic wound healing: the relationship with oxidative events. *Free Radic. Res.* **51**, 498–505 (2017).
259. Wang, Q. Y., Guan, Q. H. & Chen, F. Q. The changes of platelet-derived growth factor-BB (PDGF-BB) in T2DM and its clinical significance for early diagnosis of diabetic nephropathy. *Diabetes Res. Clin. Pract.* **85**, 166–170 (2009).
260. Praidou, A., Klangas, I., Papakonstantinou, E., Androudi, S., Georgiadis, N., Karakiulakis, G. & Dimitrakos, S. Vitreous and serum levels of platelet-derived growth factor and their correlation in patients with proliferative diabetic retinopathy. *Curr. Eye Res.* **34**, 152–161 (2009).
261. Aiello, L. P. Avery, R. L., Arrigg, P. G., Keyt, B. A., Jampel, H. D., Shah, S. T., Pasquale, L. R., Thieme, H., Iwamoto, M. A., Park, J. E., Nguyen., H. V., Aiello, L. M., Ferrara, N., & King G. L. Vascular endothelial growth factor in ocular fluid of patients with diabetic retinopathy and other retinal disorders. *J. Med.* **331**, 417–424 (1994).
262. Naldini, L., Blomer, U., Gallay, P., Ory, D., Mulligan, R., Gage, F. H. & Verma, I. M.Trono, D. In Vivo Gene Delivery and Stable Transduction of Non-dividing Cells by a Lentiviral Vector. *Science.* **272**, 263–267 (2006).
263. Williamson, K., Stringer, S. E. & Alexander, M. Y. Endothelial progenitor cells enter the aging arena. *Frontiers in Pysiology.* **3**, 1–7 (2012).
264. Patel, J., Wong, H. Y., Wang, W., Alexis, J., Shafiee, A., Stevenson, A. J., Gabrielli, B., Fisk, N. M. & Khosrotehrani, K. Self-Renewal and High Proliferative Colony Forming Capacity of Late-Outgrowth Endothelial Progenitors is Regulated by Cyclin-Dependent Kinase Inhibitors Driven by Notch Signaling. *Stem Cells.* **34**, 902–912 (2016).
265. Smith, G., McLeod, D., Foreman, D. & Boulton, M. Immunolocalisation of the VEGF receptors FLT-1, KDR, and FLT-4 in diabetic retinopathy. *Br. J. Ophthalmol.* **83**, 486–494 (1999).
266. Ding, J., Zhao, Z., Wang, C., Wang, C. X., Li, P. C., Qian, C. & Teng, G. J. Bioluminescence imaging of transplanted human endothelial colony-forming cells in an ischemic mouse model. *Brain Res.* **1642**, 209–218 (2016).
267. He, T., Peterson, T. E., Holmuhamedov, E. L., Terzic, A., Caplice, N. M., Oberley, L. W. & Katusic, Z. S. Human endothelial progenitor cells tolerate oxidative stress due to intrinsically high expression of manganese superoxide dismutase. *Arterioscler. Thromb. Vasc. Biol.* **24**, 2021–2027 (2004).
268. Fan, J., Cai, H., Yang, S., Yan, L. & Tan, W. S. Comparison between the effects of normoxia and hypoxia on antioxidant enzymes and glutathione redox state in ex vivo culture of CD34+ cells. *Comp. Biochem. Physiol. - B Biochem. Mol. Biol.* **151**, 153–158 (2008).
269. Sidney, L. E., Branch, M. J., Dunphy, S. E., Dua, H. S. & Hopkinson, A. Concise review: Evidence for CD34 as a common marker for diverse progenitors. *Stem Cells.* **32**, 1380–1389 (2014).
270. Fina, B. L., Molgaard, H. V, Robertson, D., Bradley, N. J., Monaghan, P., Delia, D., Sutherland, D. R., Baker, M. a & Greaves, M. F. the CD34 Gene. *Breast.* **75**, 2417–2426 (1990).
271. Lanza, F., Healy, L. & Sutherland, D. R. Structural and functional features of the CD34 antigen: An update. *J. Biol. Regul. Homeost. Agents.* **15**, 1–13 (2001).
272. Tasev, D., Konijnenberg, L. S. F., Amado-Azevedo, J., van Wijhe, M. H., Koolwijk, P. & van Hinsbergh, V. W. M. CD34 expression modulates tube-forming capacity and barrier properties of peripheral blood-derived endothelial colony-forming cells (ECFCs). *Angiogenesi.s* **19**, 325–338 (2016).
273. Nishikawa, T., Edelstein, D., Du, X. L., Yamagishi, S., Matsumura, T., Kaneda, Y., Yorek, M. A., Beebe, D., Oates, P. J., Hammes, H.-P., Giardino, I. & Brownlee, M. Normalizing mitochondrial superoxide production blocks three pathways of hyperglycaemic damage. *Nature.* **404**, 787–790 (2000).
274. Nuzzolo, E. R., Capodimonti, S., Martini, M., Iachininoto, M. G., Bianchi, M., Cocomazzi, A., Zini, G., Leone, G., Larocca, L. M. & Teofili, L. Adult and cord blood endothelial progenitor cells have different gene expression profiles and immunogenic potential. *Blood Transfus.* **12**, (2014).

275. Ziello, J. E., Jovin, I. S. & Huang, Y. Hypoxia-Inducible Factor (HIF)-1 regulatory pathway and its potential for therapeutic intervention in malignancy and ischemia. *Yale J. Biol. Med.* **80**, 51–60 (2007).
276. Nguyen, L. K., Cavadas, M. A. S., Scholz, C. C., Fitzpatrick, S. F., Bruning, U., Cummins, E. P., Tambuwala, M. M., Manresa, M. C., Kholodenko, B. N., Taylor, C. T. & Cheong, A. A dynamic model of the hypoxia-inducible factor 1a (HIF-1a) network. *J. Cell Sci.* **128**, 422–422 (2015).
277. Jiang, Y. Z., Li, Y., Wang, K., Dai, C. F., Huang, S. A., Chen, D. B. & Zheng, J. Distinct roles of HIF1A in endothelial adaptations to physiological and ambient oxygen. *Mol. Cell. Endocrinol.* **391**, 60–67 (2014).
278. Leicht, S. F., Schwarz, T. M., Hermann, P. C., Seissler, J., Aicher, A. & Heeschen, C. Adiponectin pre-treatment counteracts the detrimental effect of a diabetic environment on endothelial progenitors. *Diabetes.* **60**, 652–661 (2011).
279. Tepper, O. M., Galiano, R. D., Capla, J. M., Kalka, C., Gagne, P. J., Jacobowitz, G. R., Levine, J. P. & Gurtner, G. C. Human Endothelial Progenitor Cells From Type II Diabetics Exhibit Impaired Proliferation, Adhesion, and Incorporation Into Vascular Structures. *Circulation.* **106**, 2781–2786 (2002).
280. Bhatwadekar, A. D., Glenn, J. V., Curtis, T. M., Grant, M. B., Stitt, A. W. & Gardiner, T. A. Retinal endothelial cell apoptosis stimulates recruitment of endothelial progenitor cells. *Investig. Ophthalmol. Vis. Sci.* **50**, 4967–4973 (2009).
281. Schwarz, T. M., Leicht, S. F., Radic, T., Rodriguez-Araboalaza, I., Hermann, P. C., Berger, F., Saif, J., Böcker, W., Ellwart, J. W., Aicher, A. & Heeschen, C. Vascular incorporation of endothelial colony-forming cells is essential for functional recovery of murine ischemic tissue following cell therapy. *Arterioscler. Thromb. Vasc. Biol.* **32**, 13–21 (2012).
282. Stitt, A. W., Lois, N., Medina, R. J., Adamson, P. & Curtis, T. M. Advances in our understanding of diabetic retinopathy. *Clin Sci.* **125**, 1–17 (2013).
283. Hackett, S. F., Ozaki, H., Strauss, R. W., Wahlin, K., Suri, C., Maisonpierre, P., Yancopoulos, G. & Campochiaro, P. A. Angiopoietin 2 expression in the retina: Upregulation during physiologic and pathologic neovascularization. *J. Cell. Physiol.* **184**, 275–284 (2000).
284. Caldwell, R. B., Bartoli, M., Behzadian, M. A., El-Remessy, A. E. B., Al-Shabrawey, M., Platt, D. H. & Caldwell, R. W. Vascular endothelial growth factor and diabetic retinopathy: Pathophysiological mechanisms and treatment perspectives. *Diabetes. Metab. Res. Rev.* **19**, 442–455 (2003).
285. Anand-apte, B. Dysfunction of Circulating Endothelial Progenitor Cells in Diabetic Retinopathy. Chapter 25, 517–528. (2012).
286. Hadarits, O., Zoka, A., Barna, G., Al-Aissa, Z., Rosta, K., Rigo Jr., J., Kautzky-Willer, A., Somogyi, A. & Firneisz, G. Increased proportion of hematopoietic stem and progenitor cell population in cord blood of neonates born to mothers with gestational diabetes mellitus. *Stem Cells Dev.* 1-16 (2015).
287. Hagbard, L., Cameron, K., August, P., Penton, C., Parmar, M., Hay, D. C. & Kallur, T. Developing defined substrates for stem cell culture and differentiation. *Philos. Trans. R. Soc. B Biol. Sci.* **373**, (2018).
288. Williams, R., Lace, R., Kennedy, S., Doherty, K. & Levis, H. Biomaterials for Regenerative Medicine Approaches for the Anterior Segment of the Eye. *Adv. Healthc. Mater.* **7**, 1-13 (2018).
289. Shukla, S. C., Singh, A., Pandey, A. K. & Mishra, A. Review on production and medical applications of ε-polylysine. *Biochem. Eng. J.* **65**, 70–81 (2012).
290. Lei, Y., Zouani, O. F., Rémy, M., Ayela, C. & Durrieu, M.-C. Geometrical microfeature cues for directing tubulogenesis of endothelial cells. *PLoS One.* **7**, 1-14(2012).
291. Abidian, M. R., Gurkan, U. A. & Edalat, F. *Gels Handbook- Fundamentals, Properties & Applications*. (2016).
292. Caliari, S. R. & Burdick, J. A. A practical guide to hydrogels for cell culture. *Nat. Methods.* **13**, 405–414 (2016).
293. Ruggiero, F. & Koch, M. Making recombinant extracellular matrix proteins. *Methods.* **45**, 75–85 (2008).
294. Chowdhury, F., Li, Y., Poh, Y. C., Yokohama-Tamaki, T., Wang, N. & Tanaka, T. S. Soft substrates promote homogeneous self-renewal of embryonic stem cells via downregulating cell-matrix tractions. *PLoS One.* **5**, 1-10 (2010).

295. Tang, Z., Akiyama, Y. & Okano, T. Temperature-responsive polymer modified surface for cell sheet engineering. *Polymers.* **4**, 1478–1498 (2012).